UCSF
UC San Francisco Electronic Theses and Dissertations

Title

Dissecting IL-2 Signaling Dynamics with an Irreversible JAK3 Inhibitor

Permalink

https://escholarship.org/uc/item/8h12g25z

Author

Smith, Geoffrey Alexander

Publication Date

2017

Peer reviewed|Thesis/dissertation

Dissecting IL-2 Signaling Dynamics with an Irreversible JAK3
Inhibitor

by

Geoffrey Alexander Smith

DISSERTATION

Submitted in partial satisfaction of the requirements for the degree of

DOCTOR OF PHILOSOPHY

in

Chemistry and Chemical Biology

in the

GRADUATE DIVISION

of the

UNIVERSITY OF CALIFORNIA, SAN FRANCISCO

Acknowledgements

A PhD dissertation does not come together without the help of many people. First, I would like to thank both of my advisers, Jack Taunton and Art Weiss. Jack welcomed me into the lab before it was even clear I was going to do a PhD and gave me a new project to start. I am indebted to his advocacy on my behalf when I did commit to completing the PhD. Jack taught me the high standards that rigorous science demands and inspired me always to push for greater understanding and the best experiment. As I leave the lab, I will miss the many "short chats" Jack and I had about my project and science in general. It was in these chats that I learned not just how to design and execute a project, but how to think about science. I hope they will continue even when I am no longer a student.

I am equally thankful to Art Weiss. In his many years at UCSF, Art had never taken a joint student, but when this chemist strolled into his office and proposed a jointly mentored PhD, he took a chance on me. I thought Art's early skepticism about the project was unique to me, but I have since learned that skepticism is what focuses all projects in his lab on impactful questions. Art taught me always to know the answer to "so what" when thinking about a result or a potential experiment and that advice will guide my career going forward. I am grateful for all of Art's mentorship and look forward to it continuing, even as the "last" student.

Both labs were amazing environments to train in not just because of the advisors but also because of the people. In Jack's lab, Kenji Uchida and Adolfo Cuesta helped me immensely with the medicinal chemistry part of this project, synthesizing many compounds between them. Many post docs and students, past and present, provided constructive discussion, criticism and support when needed: Rand Miller, Jordan Carelli, Becca Maglathlin, Nathan Gushwa, Shyam Krishnan, Ville Paavilainen, Jesse McFarland, Jonathan Choy, Pat Sharp, Steve Sethofer, Sumit Prakash and Julia Rumpf. In the Weiss lab, I am particularly grateful to Byron AuYeung and Haopeng Wang, who together taught me everything I know about immunology. I similarly benefited from the advice and support of many others in the

To Mom, Dad, Sarah and Jordan

Abstract

The common γ-chain cytokines (IL-2, 4, 7, 9, 15 and 21) play an essential role in lymphocyte development and function. Their signals are transduced through receptor complexes comprised of the IL-2Rγ (γ_c) and one or two private subunits. These subunits lack intrinsic kinase activity and thus require the cytoplasmic kinases JAK1 and JAK3 for signal transduction. Cytokine binding induces a conformational change that activates JAK1 and JAK3, which in turn phosphorylate key tyrosines within one of the receptor subunits. These phosphorylated tyrosines recruit downstream signaling molecules, principally the STAT transcription factor family members. It is unknown what the precise non-redundant roles are for JAK1 and JAK3 in the signaling complex. Furthermore, although it is known that proliferation or differentiation requires hours to days of continuous cytokine exposure, how the signaling dynamics change over time has not been studied.

To address both the specific role of JAK3 and the requirements for JAK3 catalytic activity over time, we identified a potent and highly selective JAK3 inhibitor with in vivo activity. We took advantage of a cysteine found in JAK3 (Cys909 human/Cys905 mouse) but not in other JAK kinases to design selective inhibitors based on three different scaffolds, ultimately identifying JAK3i. By monitoring STAT5 phosphorylation over 20 hours in IL-2-stimulated CD4+ T cells, we document a previously unappreciated second wave of signaling that is much more sensitive to JAK3i than the first wave. Selective inhibition of this second wave is sufficient to block cyclin expression and S-phase entry.

Finally, we extended this study of IL-2 signaling dynamics to the closely related CD8+ T cell, which has an earlier and greater proliferative response to IL-2. When STAT5 phosphorylation was followed over time, CD8 T cells sustained this signaling throughout a 6-hour time course, in contrast to the biphasic CD4 response. A 50% knockdown of the IL-2Rβ receptor chain converted CD8 T-cells to a CD4-like signaling pattern and reduced early S-phase

entry. This cell type variability in IL-2Rβ expression appears to tune responses, potentially

preventing extensive, autoimmune expansion of CD4 T-cells while still enabling sufficient CD8

expansion to control viral infections.

Table of Contents

List of Figures

List of Tables

Chapter 1   Introduction

1.1 The Common γ-chain Family of Cytokines

The common γ-chain family cytokines play an essential role in lymphocyte development and function. Over the past 30+ years, study of this crucial system has both furthered our understanding of basic immunology and presented opportunities for therapeutic intervention. Seven cytokines (IL-2, 4, 7, 9, 15 and 21) signal through receptor complexes containing an IL-2Rγ and a private chain. In humans, IL-2Rγ deficiency results in X-linked Severe Combined Immunodeficiency (SCID)[1]. These patients lack T cells and NK cells and have present, but dysfunctional B cells (T⁻B⁺NK⁻ SCID). Patients lacking the IL-2Rγ associated kinase JAK3 present with an identical phenotype[2,3], confirming a crucial role for this kinase and this family of cytokines in the development and function of the immune system.

Mouse models largely confirm these striking human genetics, albeit with some small differences, and help dissect the role of individual γ-chain cytokines in lymphocyte development. Like humans, mice deficient in IL-2Rγ lack NK cells. Yet, unlike humans, they have very few B cells and diminished, but still present T cells[4]. Two reports of JAK3 deficient mice confirm the same phenotype (T⁺B⁻NK⁻ SCID), and a third shows that IL2Rγ⁻/⁻ and JAK3⁻/⁻ are completely equivalent in mice[5]. Based on mouse models[6], the developmental defects in the B and T cell compartment appear to be due to a loss of IL-7 signaling[7], while the NK cell defects can be attributed to loss of IL-15 signaling[8].

Individually, these cytokines play a wide range of roles in lymphocyte function beyond development, which complicate potential therapeutic interventions (reviewed in Table 1-1). The canonical γc-cytokine IL-2 exemplifies the diverse and seemingly contradictory functions of γc family members. Originally identified as a T cell growth factor[9,10], the predominant phenotype in IL-2 deficient mice[11], as well as mice deficient in the private IL-2 chains IL-2Rα[12] and IL-2Rβ[13], is not immunodeficiency but rather autoimmunity. This paradoxical result can be explained by the essential role of IL-2 in the survival of regulatory T cells (Treg)[14]. While autoimmunity is the

dominant phenotype of knockout animals, other studies indicate that IL-2 does play important roles in a physiologic immune response in both CD4 and CD8 T cells. In addition to promoting CD4 proliferation in vitro, in vivo IL-2 contributes to CD4 differentiation to Th1[15] and Th2[16] cells, and opposes differentiation into Th17 cells[17]. The recall response of memory CD8 T cells depends on IL-2 during the priming infection[18], and IL-2 enables CD8 T cells to respond to weaker antigen stimulation[19]. Given the pleotropic effects of this one cytokine, it is puzzle to rationalize the net therapeutic effects of exogenous IL-2 in disease settings, such as melanoma or renal cancer[20]. Understanding which of these phenotypes contribute to physiologic and pathologic responses remains an important question for the field and likely necessitates careful in vivo study with a variety of tools.

Cytokine	Function	Genetic Models
IL-2	Promote CD4 and CD8 proliferation[9], Treg survival and function[14], CD4 subset differentiation[15-17], CD8 memory priming[18], CD8 activation[19]	IL2[-/-(21)], IL2RA[-/-(12)], IL2RB[-/-(13)]
IL-4	B-cell proliferation and Ig class switching, Th2 differentiation	IL4[-/-(22)]
IL-7	Development & survival of T and B Cells	IL7RA[-/-(7)], IL7[-/-(23)]
IL-9	Promote mucus production and mast cell proliferation	IL9[-/-(24)]
IL-15	Development of NK cells & survival of CD8, NKT and $\gamma\delta$-T cells, support antitumor responses	IL15RA[-/-(8)]
IL-21	Immunoglobulin production, plasma cell differentiation, Th17 differentiation, support antitumor responses	IL21R[-/-(25)]

Table 1-1 Function of Common y-chain Cytokines

1.2   Signaling via the Common γ-chain

The seven γ_c-cytokines signal through complexes comprised of IL-2Rγ and one or two private, cytokine specific chains (Figure 1-1). The receptor chains lack intrinsic kinase activity and thus require the cytoplasmic kinases JAK1 and JAK3 for signal transduction (discussed in more detail below). In addition to the IL-2Rγ, each complex has a signaling chain that constitutively recruits JAK1 and contains 1-3 tyrosines essential for downstream signals. In the

3

case of IL-2 and IL-15, there is a third, much smaller receptor chain that has no direct signaling

function but increases affinity of the receptor complex. For IL-2, this IL-2Rα chain generally

presents IL-2 in cis to receptor complexes on the same cell, although there are reports of trans

presentation[26]. By contrast, IL-15Rα presents IL-15 almost exclusively in trans to CD8, NK, NKT

and CD8αα Intraepithelial lymphocytes[27].
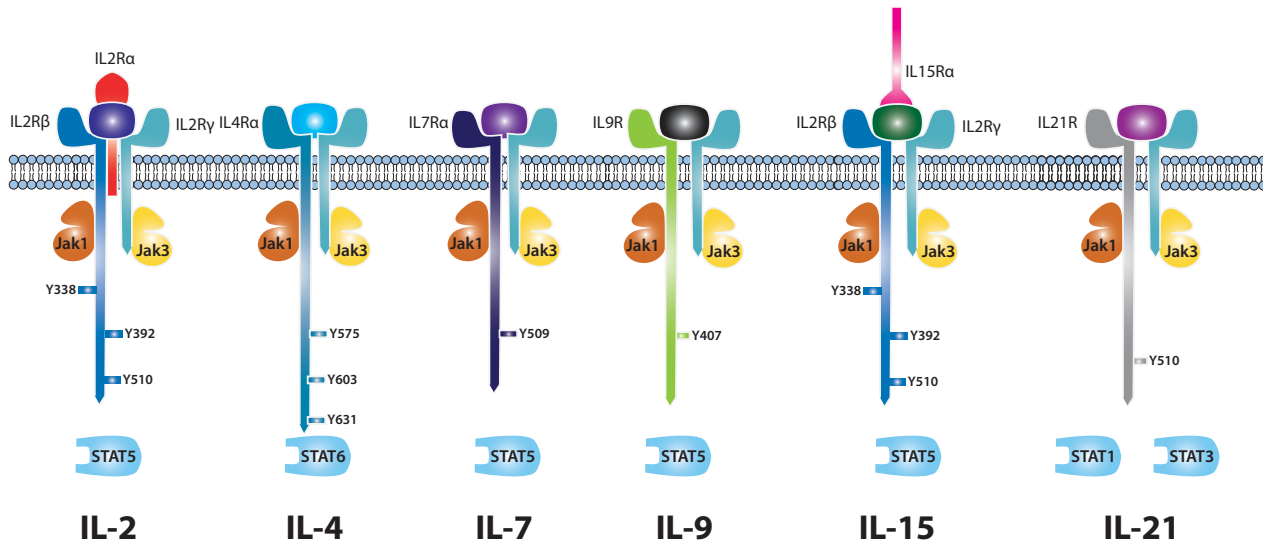
Figure 1-1 Common γ-chain Cytokines, Receptor Complexes and Associated STATs

The IL-2 signaling pathway is the archetypal γ_c-cytokine signaling cascade (Figure 1-2).

IL-2 first binds to either IL-2Rα[28,29] or a complex of IL-2Rα/IL-2Rβ[30,31], and then to IL-2Rγ to

initiate signaling. Due to a lack of specific IL-2/IL-2Rγ contacts[28], IL-2 has no detectable affinity

for IL-2Rγ[32], which may explain how IL-2Rγ can be shared across the family of cytokines. A

conformational change in the receptor then activates JAK1 and JAK3, which are constitutively

associated with the IL-2Rβ and IL-2Rγ respectively[33,34].
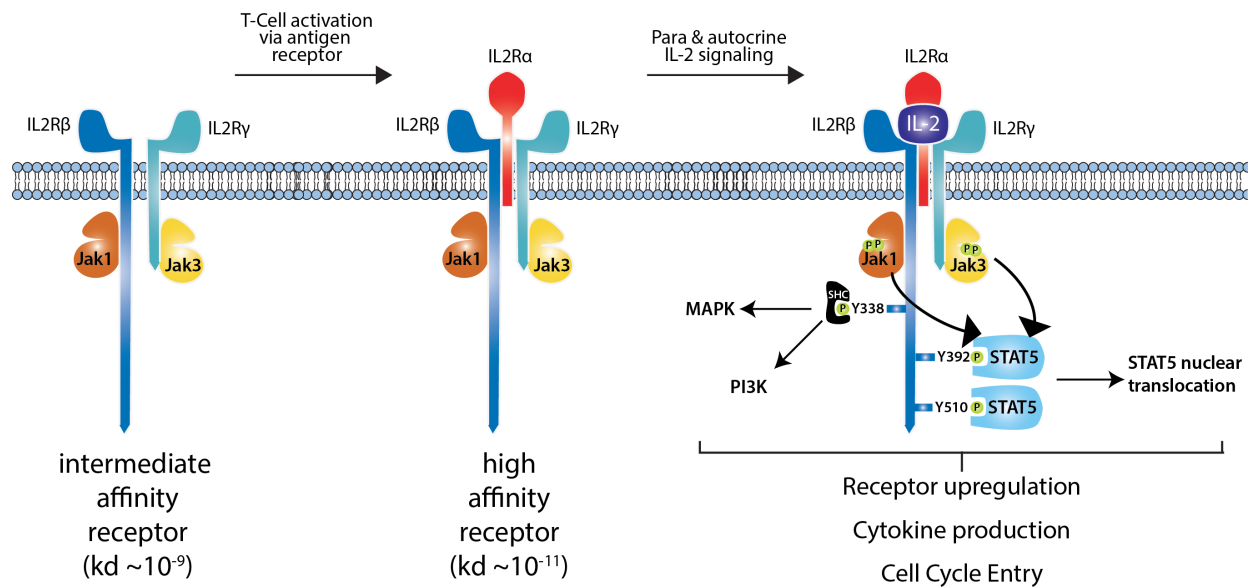
Figure 1-2 IL-2 Signaling Pathway

Upon IL-2 stimulation, JAK1[33] and JAK3[35] rapidly become tyrosine phosphorylated. The activation loop of each kinase contains two sequential tyrosines important in the regulation of catalytic activity: Y1033 and Y1034 in JAK1 and Y980 and Y981 in JAK3[36]. Mutagenesis studies in vitro and in cell lines show that Y1033 is essential for JAK1 activity[36], while Y980 positively regulates and Y981 negatively regulates JAK3 activity[37]. It has not been conclusively demonstrated whether these sites are phosphorylated in trans or are autophosphorylated. In vitro, both are capable of autophosphorylation[33]. Recent evidence from the related growth hormone receptor / JAK2 signaling system would favor trans phosphorylation of one JAK by the other JAK following a conformational change in the receptor complex[38]. Prior biochemical work suggests that JAK3 is capable of transphosphorylating JAK1 but not vice versa[39]. This suggests a hierarchy of JAK activation, whereby JAK3 becomes at least minimally active and phosphorylates JAK1, which triggers further downstream phosphorylation. However, this model does not explain how JAK3 becomes phosphorylated. Further work is necessary to elucidate many of these mechanistic details of activation and will likely require both better reagents for

5

detecting JAK activation loop phosphorylation and highly specific inhibitors to probe catalytic function in parallel with genetic manipulations.

Following JAK activation, three key tyrosines (Y338, Y392 and Y510) in the IL-2Rβ are phosphorylated[40]. It remains unclear whether one or both of the JAKs are responsible phosphorylating the IL-2Rβ. JAK1 can phosphorylate these tyrosines when overexpressed in COS-7[40], but JAK3 can also form specific interactions with the cytoplasmic tail of IL-2Rβ [41], suggesting it may also be in close enough proximity to phosphorylate these sites as well. Once phosphorylated, these tyrosines serve to recruit and activate three key downstream signaling pathways.

The transcription factor STAT5 localizes to the phosphorylated IL-2Rβ via Src-homology 2 (SH2) domain mediated binding to either Y392 or Y510. Both tyrosines are required for maximal IL-2 driven proliferation[40]. After binding, STAT5 is phosphorylated at Y694 by one or possibly both of the JAKs[36,42]. STAT5 is essential for almost all IL-2 induced responses. Complete, homozygous knockouts of all paralogs of STAT5 (A&B) have severely impaired signaling resulting in decreased T cell (especially IL-2-dependent Treg) survival[43], which was also seen in mice with only one of the 4 STAT5 alleles (STAT5a$^{-/+}$/STAT5b$^{-/-}$)[44]. After tyrosine phosphorylation, STAT5 homodimerizes and translocates to the nucleus, where it induces significant changes in over 5000 mRNAs[45]. STAT5 can also form a homotetramer and almost 10% of the IL-2 regulated genes require STAT5 tetramerization[45,46].

Beyond STAT5, IL-2 can activate the canonical PI3K/mTOR and RAS/MAPK pathways. The adapter protein Shc binds to phosphorylated Y338 of the IL-2Rβ and serves as the key scaffold for both of these pathways[47,48]. Tyrosine phosphorylated Shc subsequently recruits the adapter Grb2 and induces phosphorylation of the Grb2 associated protein 2 (GAB2)[49,50]. Phospho-GAB2 co-immunoprecipitiates with PI3K and this ultimately leads to activation of the p110α PI3K catalytic unit[51]. Although this Shc/Grb2/GAB2 complex is sufficient for immediate

PI3K and AKT activation, it appears sustained activation requires at least low level STAT5 activation via Y392 and Y510[52]. Full, sustained activation of PI3K signaling is essential for IL-2 stimulated S-phase entry in T-cells[53].

The Shc/Grb2 complex also recruits SOS to the IL-2R complex, leading to RAS and subsequent MAPK cascade activation[48]. There are conflicting reports as to whether IL-2 stimulation culminates in ERK activation[54,55]. The answer may depend on the cell type and state of the cells stimulated, as activated T cells express strong negative regulators of ERK activity, including PAC-1[56,57]. In B cell lines transformed with JAK1 activating mutations, ERK is strongly activated but the same mutations only weakly activate ERK in T cell derived lines[58], consistent with the PAC-1 expression.

Although not as well studied, three mechanisms appear to contribute to the termination of IL-2 signaling. First, a number of constitutively active phosphatases negatively regulate key tyrosines in the pathway. The T-Cell Protein Tyrosine Phosphatase (TCPTP) dephosphorylates both JAK1 and JAK3, and TCPTP deficient cells show prolonged STAT5 phosphorylation[59]. STAT5 Y694 is a substrate for the phosphatase SHP2[60], although its net effect on IL-2 signaling is more complicated[61]. The tyrosine phosphatase for IL-2Rβ has not yet been identified. Second, IL-2 bound receptors are rapidly internalized ($t_{1/2}$ ~15 minutes), and the IL-2Rβ and IL-2Rγ are degraded, terminating new signaling generation[62,63]. Finally, IL-2 signaling triggers a classic negative feedback loop by induction of the Suppressor of Cytokine Signaling (SOCS) family of proteins, especially SOCS1[64] and CISH[65]. Both of these proteins function primarily as kinase inhibitors, binding to the JAK1/IL-2Rβ complex and inserting a kinase inhibitory region into the substrate-binding pocket. Interestingly, both SOCS1 and CISH have no inhibitory activity towards JAK3[66-68]. These results raise the possibility that JAK1 inhibition is sufficient to terminate signaling and support the model of hierarchical JAK activation discussed above.

1.3   JAK3 in γ-chain Signaling

JAK1 and JAK3 are part of the Janus Kinase family of cytoplasmic tyrosine kinases, along with JAK2 and TYK2. Renamed[*] for the two-faced Roman god of transitions[69], Janus, these kinases are characterized by the presence of both a kinase and pseudokinase domain (Figure 1-3). The JH2 pseudokinase domain lacks the aspartate of the canonical Histidine-Arginine-Asparate (HRD) motif found in almost all kinases, rendering it a weak binder of ATP with minimal or no catalytic activity[70,71]. Activating mutations within the pseudokinase domain suggest that it functions to negatively regulate catalytic activity[71]. The JAKs interact with their receptor chains via the 4.1, erzin, radixin, moesin (FERM) domain spanning JH6 and JH7[72]. All JAKs also have an SH2-like domain in the JH3 and JH7 regions, but mutations to this region had no effect on JAK1 receptor binding or function, raising questions as to its functional significance[73].
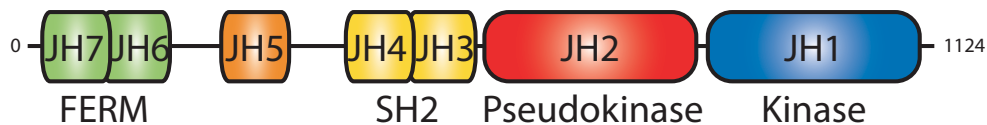
Figure 1-3 JAK3 Domain Structure

Both JAK1 and JAK3 are essential for γ_c-signaling. T-cells or thymocytes from mice deficient in JAK1 or JAK3 fail to proliferate in response to γ_c-cytokines [74,75]. These observations, coupled with the druggability of kinases, make both potential targets for new immunosuppressive agents. While JAK1 is ubiquitously expressed and used by many cytokines, JAK3 expression is largely restricted to the hematopoietic system and is involved only in γ_c-cytokine signaling[76]. Given this selective expression, and the perinatal lethal phenotype of JAK1 deficiency[74], JAK3 inhibition should in principle enable pathway blockade with fewer on target

---

[*] Interestingly, the kinases were originally named Just Another Kinase. Upon discovery of the second kinase domain, they were renamed the Janus Kinases[69].

toxicities. Human JAK3 mutations in the pseudokinase [77] and kinase[78] domains that abolish catalytic activity but preserve protein expression and receptor binding can cause JAK3 SCID. The heterozygous parents of these children are unaffected. These observations suggest that partial JAK3 inhibition could modulate the immune response, potentially in the setting of transplantation or autoimmunity.

Recent work has challenged the importance of JAK3 catalytic activity in γ_c-signaling. Working with a highly selective small molecule inhibitor (see Chapter 2)[79], Haan and colleagues see little effect of JAK3 inhibition on IL-2 induced STAT5 phosphorylation in both the Kit225 T-cell leukemia line and human peripheral blood lymphocytes[80]. Yet, as predicted by human genetics, siRNA knockdown of JAK1 or JAK3 in Kit225 cells completely blocks IL-2 induced STAT5 phosphorylation. To address this genetic and pharmacological discrepancy, Haan et al. introduced kinase dead, constitutively active, or analogue sensitive JAK1 and JAK3 alleles into the U4C human fibrosarcoma cell line. Cells expressing JAK1 kinase dead and analogue sensitive alleles treated with inhibitor do not phosphorylate STAT5 in response to IL-2. However, cells expressing JAK3 kinase dead and analogue sensitive alleles are still able to phosphorylate STAT5, albeit to a lesser degree with kinase dead JAK3. Haan et al. propose that JAK3 is a scaffolding protein in the γ_c-signaling complex and that its catalytic activity is largely dispensable. Instead, JAK1 is the dominant kinase and its activity is essential for downstream signal transduction[80].

One important implication of the Haan et al. study is that catalytic inhibitors of JAK3 will fail to block γ_c-signaling, and, by extension, will not have the desired immunosuppressive effect. This conclusion is surprising in light of the human genetic evidence discussed above and the failure of JAK3-kinase dead alleles to rescue the phenotype of JAK3 deficient mice[75]. In an effort to resolve this controversy and understand what, if any, non-redundant roles for JAK1 and JAK3 exist, we aimed to develop a highly selective, covalent JAK3 inhibitor (Chapter 2). This

tool enabled us to uncover an important temporal dimension to IL-2 signaling in CD4 T cells that had previously been overlooked (Chapter 3). Finally, we extended our study of signaling kinetics to CD8 and regulatory T cells, revealing multiple patterns of IL-2R signaling dynamics (Chapter 4).

1.4 References

1. Noguchi, M. *et al.* Interleukin-2 receptor gamma chain mutation results in X-linked severe combined immunodeficiency in humans. *Cell* **73,** 147–157 (1993).

2. Macchi, P. *et al.* Mutations of Jak-3 gene in patients with autosomal severe combined immune deficiency (SCID). *Nature* **377,** 65–68 (1995).

3. Russell, S. M. *et al.* Mutation of Jak3 in a Patient with SCID: Essential Role of Jak3 in Lymphoid Development. *Science* **270,** 797–800 (1995).

4. Cao, X. *et al.* Defective lymphoid development in mice lacking expression of the common cytokine receptor γ chain. *Immunity* **2,** 223–238 (1995).

5. Suzuki, K. *et al.* Janus kinase 3 (Jak3) is essential for common cytokine receptor gamma chain (gamma(c))-dependent signaling: comparative analysis of gamma(c), Jak3, and gamma(c) and Jak3 double-deficient mice. *Int Immunol* **12,** 123–132 (2000).

6. Park, S. Y. *et al.* Developmental defects of lymphoid cells in Jak3 kinase-deficient mice. *Immunity* **3,** 771–782 (1995).

7. Peschon, J. J. Early lymphocyte expansion is severely impaired in Interleukin 7 receptor-deficient mice. *Journal of Experimental Medicine* **180,** 1955–1960 (1994).

8. Lodolce, J. P. *et al.* IL-15 receptor maintains lymphoid homeostasis by supporting lymphocyte homing and proliferation. *Immunity* **9,** 669–676 (1998).

9. Cantrell, D. A. & Smith, K. A. The Interleukin-2 T-cell system: a new cell growth model. *Science* **224,** 1312–1316 (1984).

10. Smith, K. A. & Cantrell, D. A. Interleukin 2 regulates its own receptors. *Proc. Natl Acad. Sci. USA* **82,** 864–868 (1985).

11. Sadlack, B. *et al.* Generalized autoimmune disease in Interleukin-2-deficient mice is triggered by an uncontrolled activation and proliferation of CD4+ T cells. *Eur. J. Immunol.* **25,** 3053–3059 (1995).

12. Willerford, D. M. *et al.* Interleukin-2 receptor α chain regulates the size and content of the

peripheral lymphoid compartment. *Immunity* **3,** 521–530 (1995).

13.   Suzuki, H. *et al.* Deregulated T cell activation and autoimmunity in mice lacking

Interleukin-2 receptor beta. *Science* **268,** 1472–1476 (1995).

14.   Fontenot, J. D., Rasmussen, J. P., Gavin, M. A. & Rudensky, A. Y. A function for

Interleukin 2 in Foxp3-expressing regulatory T cells. *Nature Immunol.* **6,** 1142–1151

(2005).

15.   Liao, W., Lin, J.-X., Wang, L., Li, P. & Leonard, W. J. Modulation of cytokine receptors by

IL-2 broadly regulates differentiation into helper T cell lineages. *Nature Immunol.* **12,**

551–559 (2011).

16.   Cote-Sierra, J. *et al.* Interleukin 2 plays a central role in Th2 differentiation. *Proc. Natl*

Acad. Sci. USA **101,** 3880–3885 (2004).

17.   Laurence, A. *et al.* Interleukin-2 Signaling via STAT5 Constrains T Helper 17 Cell

Generation. *Immunity* **26,** 371–381 (2007).

18.   Williams, M. A., Tyznik, A. J. & Bevan, M. J. Interleukin-2 signals during priming are

required for secondary expansion of CD8+ memory T cells. *Nature* **441,** 890–893 (2006).

19.   Au-Yeung, B. B. *et al.* IL-2 Modulates the TCR Signaling Threshold for CD8 but Not CD4

T Cell Proliferation on a Single-Cell Level. *J. Immunol.* 1601453 (2017).

doi:10.4049/jimmunol.1601453

20.   Rosenberg, S. A. IL-2: The First Effective Immunotherapy for Human Cancer. *J. Immunol.*

192, 5451–5458 (2014).

21.   Kündig, T. M. *et al.* Immune responses in Interleukin-2-deficient mice. *Science* **262,**

1059–1061 (1993).

22.   Kühn, R., Rajewsky, K. & Müller, W. Generation and analysis of Interleukin-4 deficient

mice. *Science* **254,** 707–710 (1991).

23.   Freeden-Jeffry, von, U. *et al.* Lymphopenia in Interleukin (IL)-7 gene-deleted mice

identifies IL-7 as a nonredundant cytokine. *J. Exp. Med.* **181,** 1519–1526 (1995).

24. Townsend, M. J. *et al.* IL-9-Deficient Mice Establish Fundamental Roles for IL-9 in Pulmonary Mastocytosis and Goblet Cell Hyperplasia but Not T Cell Development. *Immunity* **13,** 573–583 (2000).

25. Ozaki, K. *et al.* A critical role for IL-21 in regulating immunoglobulin production. *Science* **298,** 1630–1634 (2002).

26. Wuest, S. C. *et al.* A role for Interleukin-2 trans-presentation in dendritic cell–mediated T cell activation in humans, as revealed by daclizumab therapy. *Nat Med* **17,** 604–609 (2011).

27. Stonier, S. W. & Schluns, K. S. Trans-presentation: a novel mechanism regulating IL-15 delivery and responses. *Immunology Letters* **127,** 85–92 (2010).

28. Wang, X., Rickert, M. & Garcia, K. C. Structure of the quaternary complex of Interleukin-2 with its alpha, beta, and gammac receptors. *Science* **310,** 1159–1163 (2005).

29. Stauber, D. J. Crystal structure of the IL-2 signaling complex: Paradigm for a heterotrimeric cytokine receptor. *Proc. Natl Acad. Sci. USA* **103,** 2788–2793 (2006).

30. Wu, Z., Johnson, K. W., Choi, Y. & Ciardelli, T. L. Ligand binding analysis of soluble Interleukin-2 receptor complexes by surface plasmon resonance. *J. Biol. Chem.* **270,** 16045–16051 (1995).

31. Stefano F Liparoto *et al.* Analysis of the Role of the Interleukin-2 Receptor γ Chain in Ligand Binding†. *Biochemistry* **41,** 2543–2551 (2002).

32. Rickert, M., Boulanger, M. J., Goriatcheva, N. & Garcia, K. C. Compensatory Energetic Mechanisms Mediating the Assembly of Signaling Complexes Between Interleukin-2 and its α, β, and γc Receptors. *J. Mol. Biol.* **339,** 1115–1128 (2004).

33. Miyazaki, T. *et al.* Functional activation of Jak1 and Jak3 by selective association with IL-2 receptor subunits. *Science* **266,** 1045–1047 (1994).

34. Russell, S. M. *et al.* Interaction of IL-2R beta and gamma c chains with Jak1 and Jak3: implications for XSCID and XCID. *Science* **266,** 1042–1045 (1994).

35. Johnston, J. A. *et al.* Phosphorylation and activation of the Jak-3 Janus kinase in response to Interleukin-2. *Nature* **370,** 151–153 (1994).

36. Liu, K. D., Gaffen, S. L., Goldsmith, M. A. & Greene, W. C. Janus kinases in Interleukin-2-mediated signaling: JAK1 and JAK3 are differentially regulated by tyrosine phosphorylation. *Current Biology* **7,** 817–826 (1997).

37. Zhou, Y. J. *et al.* Distinct tyrosine phosphorylation sites in JAK3 kinase domain positively and negatively regulate its enzymatic activity. *Proc. Natl Acad. Sci. USA* **94,** 13850–13855 (1997).

38. Brooks, A. J. *et al.* Mechanism of Activation of Protein Kinase JAK2 by the Growth Hormone Receptor. *Science* **344,** 1249783 (2014).

39. Witthuhn, B. A., Williams, M. D., Kerawalla, H. & Uckun, F. M. Differential substrate recognition capabilities of Janus family protein tyrosine kinases within the Interleukin 2 receptor (IL2R) system: Jak3 as a potential molecular target for treatment of leukemias with a hyperactive Jak-Stat signaling machinery. *Leuk Lymphoma* **32,** 289–297 (1999).

40. Friedmann, M. C., Migone, T. S., Russell, S. M. & Leonard, W. J. Different Interleukin 2 receptor beta-chain tyrosines couple to at least two signaling pathways and synergistically mediate Interleukin 2-induced proliferation. *Proc. Natl Acad. Sci. USA* **93,** 2077–2082 (1996).

41. Zhu, M. H., Berry, J. A., Russell, S. M. & Leonard, W. J. Delineation of the regions of Interleukin-2 (IL-2) receptor beta chain important for association of Jak1 and Jak3. Jak1-independent functional recruitment of Jak3 to Il-2Rbeta. *J. Biol. Chem.* **273,** 10719–10725 (1998).

42. Lin, J. X., Mietz, J., Modi, W. S., John, S. & Leonard, W. J. Cloning of human Stat5B. Reconstitution of Interleukin-2-induced Stat5A and Stat5B DNA binding activity in COS-7 cells. *J. Biol. Chem.* **271,** 10738–10744 (1996).

43. Yao, Z. *et al.* Stat5a/b are essential for normal lymphoid development and differentiation.

Proc. Natl Acad. Sci. USA **103,** 1000–1005 (2006).

44.   Villarino, A. *et al.* Signal transducer and activator of transcription 5 (STAT5) paralog dose governs T cell effector and regulatory functions. *eLife* **5,** 847 (2016).

45.   Lin, J.-X. *et al.* Critical Role of STAT5 transcription factor tetramerization for cytokine responses and normal immune function. *Immunity* **36,** 586–599 (2012).

46.   Villarino, A. V., Kanno, Y., Ferdinand, J. R. & O'shea, J. J. Mechanisms of Jak/STAT Signaling in Immunity and Disease. *J. Immunol.* **194,** 21–27 (2014).

47.   Burns, L. A., Karnitz, L. M., Sutor, S. L. & Abraham, R. T. Interleukin-2-induced tyrosine phosphorylation of p52shc in T lymphocytes. *J. Biol. Chem.* **268,** 17659–17661 (1993).

48.   Ravichandran, K. S. & Burakoff, S. J. The adapter protein Shc interacts with the Interleukin-2 (IL-2) receptor upon IL-2 stimulation. *J. Biol. Chem.* **269,** 1599–1602 (1994).

49.   Gadina, M., Sudarshan, C. & O'shea, J. J. IL-2, but not IL-4 and other cytokines, induces phosphorylation of a 98-kDa protein associated with SHP-2, phosphatidylinositol 3'-kinase, and Grb2. *J. Immunol.* **162,** 2081–2086 (1999).

50.   Gadina, M. *et al.* The docking molecule gab2 is induced by lymphocyte activation and is involved in signaling by Interleukin-2 and Interleukin-15 but not other common gamma chain-using cytokines. *J. Biol. Chem.* **275,** 26959–26966 (2000).

51.   Gu, H. *et al.* New Role for Shc in Activation of the Phosphatidylinositol 3-Kinase/Akt Pathway. *Molecular and Cellular Biology* **20,** 7109–7120 (2000).

52.   Lockyer, H. M., Tran, E. & Nelson, B. H. STAT5 is essential for Akt/p70S6 kinase activity during IL-2-induced lymphocyte proliferation. *J. Immunol.* **179,** 5301–5308 (2007).

53.   Brennan, P. *et al.* Phosphatidylinositol 3-Kinase Couples the Interleukin-2 Receptor to the Cell Cycle Regulator E2F. *Immunity* **7,** 679–689 (1997).

54.   Kuo, C. J. *et al.* Rapamycin selectively inhibits Interleukin-2 activation of p70 S6 kinase. *Nature* **358,** 70–73 (1992).

55.   Perkins, G. R. Interleukin 2 activates extracellular signal-regulated protein kinase 2.

Journal of Experimental Medicine **178,** 1429–1434 (1993).

56.   Ward, Y. *et al.* Control of MAP kinase activation by the mitogen-induced threonine/tyrosine phosphatase PAC1. *Nature* **367,** 651–654 (1994).

57.   Pastor, M. I., Reif, K. & Cantrell, D. The regulation and function of p21ras during T-cell activation and growth. *Immunology Today* **16,** 159–164 (1995).

58.   Kleppe, M., Mentens, N., Tousseyn, T., Wlodarska, I. & Cools, J. MOHITO, a novel mouse cytokine-dependent T-cell line, enables studies of oncogenic signaling in the T-cell context. *Haematologica* **96,** 779–783 (2011).

59.   Simoncic, P. D., Lee-Loy, A., Barber, D. L., Tremblay, M. L. & McGlade, C. J. The T Cell Protein Tyrosine Phosphatase Is a Negative Regulator of Janus Family Kinases 1 and 3. *Current Biology* **12,** 446–453 (2002).

60.   Chen, Y. *et al.* Identification of Shp-2 as a Stat5A Phosphatase. *J. Biol. Chem.* **278,** 16520–16527 (2003).

61.   Xu, D. & Qu, C.-K. Protein tyrosine phosphatases in the JAK/STAT pathway. *Front. Biosci.* **13,** 4925–4932 (2008).

62.   Hémar, A. *et al.* Endocytosis of Interleukin 2 receptors in human T lymphocytes: distinct intracellular localization and fate of the receptor alpha, beta, and gamma chains. *J Cell Biol* **129,** 55–64 (1995).

63.   Lamaze, C. *et al.* Interleukin 2 Receptors and Detergent-Resistant Membrane Domains Define a Clathrin-Independent Endocytic Pathway. *Mol Cell* **7,** 661–671 (2001).

64.   Sporri, B., Kovanen, P. E., Sasaki, A., Yoshimura, A. & Leonard, W. J. JAB/SOCS1/SSI-1 is an Interleukin-2-induced inhibitor of IL-2 signaling. *Blood* **97,** 221–226 (2001).

65.   Yang, X. O. *et al.* The signaling suppressor CIS controls proallergic T cell development and allergic airway inflammation. *Nature Immunol.* **14,** 732–740 (2013).

66.   Babon, J. J. *et al.* Suppression of Cytokine Signaling by SOCS3: Characterization of the Mode of Inhibition and the Basis of Its Specificity. *Immunity* **36,** 239–250 (2012).

67.   Kershaw, N. J. *et al.* SOCS3 binds specific receptor–JAK complexes to control cytokine signaling by direct kinase inhibition. *Nature Structural & Molecular Biology* **20,** 469–476 (2013).

68.   Delconte, R. B. *et al.* CIS is a potent checkpoint in NK cell-mediated tumor immunity. *Nature Immunol.* **17,** 816–824 (2016).

69.   Rane, S. G. & Reddy, E. P. Janus kinases: components of multiple signaling pathways. *Oncogene* **19,** 5662–5679 (2000).

70.   Eyers, P. A. & Murphy, J. M. Exploring Kinomes: Pseudokinases and Beyond. *Biochem. Soc. Trans* (2013).

71.   Constantinescu, S. N., Leroy, E., Gryshkova, V., Pecquet, C. & Dusa, A. Activating Janus kinase pseudokinase domain mutations in myeloproliferative and other blood cancers. *Biochem. Soc. Trans* **41,** 1048–1054 (2013).

72.   Zhou, Y.-J. *et al.* Unexpected Effects of FERM Domain Mutations on Catalytic Activity of Jak3. *Mol Cell* **8,** 959–969 (2001).

73.   Radtke, S. *et al.* The Jak1 SH2 domain does not fulfill a classical SH2 function in Jak/STAT signaling but plays a structural role for receptor interaction and up-regulation of receptor surface expression. *J. Biol. Chem.* **280,** 25760–25768 (2005).

74.   Rodig, S. J. *et al.* Disruption of the Jak1 Gene Demonstrates Obligatory and Nonredundant Roles of the Jaks in Cytokine-Induced Biologic Responses. *Cell* **93,** 373–383 (1998).

75.   Thomis, D. C. & Berg, L. J. Peripheral expression of Jak3 is required to maintain T lymphocyte function. *J. Exp. Med.* **185,** 197–206 (1997).

76.   Kawamura, M. *et al.* Molecular cloning of L-JAK, a Janus family protein-tyrosine kinase expressed in natural killer cells and activated leukocytes. *Proc. Natl Acad. Sci. USA* **91,** 6374–6378 (1994).

77.   Chen, M. *et al.* Complex Effects of Naturally Occurring Mutations in the JAK3

Pseudokinase Domain: Evidence for Interactions between the Kinase and Pseudokinase Domains. *Molecular and cellular biology* **20,** 947–956 (2000).

78. Notarangelo, L. D. *et al.* Mutations in severe combined immune deficiency (SCID) due to JAK3 deficiency. *Hum. Mutat.* **18,** 255–263 (2001).

79. Thoma, G. *et al.* Identification of a Potent Janus Kinase 3 Inhibitor with High Selectivity within the Janus Kinase Family. *J. Med. Chem.* **54,** 284–288 (2010).

80. Haan, C. *et al.* Jak1 Has a Dominant Role over Jak3 in Signal Transduction through γc-Containing Cytokine Receptors. *Chem. Biol.* **18,** 314–323 (2011).

Chapter 2   Identification of a selective, irreversible JAK3 Inhibitor

2.1 Abstract

Development of selective JAK3 inhibitors to probe JAK3 biology and clinical applications has been complicated by high sequence identity within the ATP binding pocket of closely related kinases. Here, we design inhibitors to target the unique Cysteine 909 found in JAK3. A series of maleimide-based inhibitors derived from the reversible JAK3 inhibitor NIBR3049 were irreversible biochemical inhibitors of JAK3 and showed improved cellular potency, but could not sustain inhibition after washout from cell culture. We next explored a promiscuous pyrimidine scaffold that inhibited many cysteine-containing kinases and tuned selectivity to yield a potent and selective dual ITK-JAK3 inhibitor. Finally, we characterized pyrrolopyrimidine **30** (JAK3i), which was a highly potent and selective compound that was active in vivo. Compound **30** prolonged survival in a model of acute graft versus host disease, which motivates further exploration of JAK3 inhibition in transplantation and autoimmunity. Additionally, two clickable JAK3 occupancy probes were described, which will help understand the degree of target engagement needed for efficacy.

2.2 Introduction

For almost 20 years, medicinal chemists have pursued a selective JAK3 inhibitor, lured by the potential of a next-generation oral immunosuppressive with few side effects[1]. High sequence identity within the ATP binding pocket has stymied most efforts to date. JAK1, JAK2 and TYK2 have 84%, 87% and 80% sequence identity, respectively, with the JAK3 ATP binding pocket[2]. Early inhibitors, such as AG490 (**1**), "JAK Inhibitor 1" (**2**), and WHI-P131 (**3**) lacked cell potency and selectivity, both within the Janus Kinase family and across the kinome (Figure 2-1)[3,4]. In 2003, Pfizer reported the first "selective" JAK3 inhibitor, tofacitinib (then CP-690,550)[5]. Based on in vitro kinase assays, tofacitinib was then reported to have 20 and 112-fold selectivity for JAK3 over JAK2 and JAK1 respectively. However, subsequent work from Pfizer and others has shown that, in fact, tofacitinib exhibits little isoform selectivity between JAK1, JAK2 and

JAK3, especially when assayed at physiologic ATP concentrations or in cellular assays[4,6].

Clinically, although approved for use in rheumatoid arthritis, tofacitinib has toxicities consistent

with inhibiting JAK1- and JAK2-dependent cytokines, underscoring the potential benefit of a

selective JAK3 inhibitor[7].

Two reversible JAK3 inhibitors have been reported with improved selectivity relative to

tofacitinib. WYE-151650 (**5**) is a purinone scaffold with moderate biochemical selectivity (14-36

fold) and good cellular selectivity (>500-fold vs IL-6 (JAK1/JAK2) and 34-fold vs GM-CSF

(JAK2)). Notably, this compound is efficacious in the collagen-induced arthritis model at doses

that had little or no effect on JAK1/JAK2-dependent IL-6 and EPO signaling, which suggests

that JAK3 inhibition may be sufficient in some autoimmune settings[8]. However, it remains

possible that **5** targets JAK1 downstream of γ_c-cytokines, since its selectivity was never tested

biochemically with physiological ATP and the cellular assays can be misleading. In contrast to

the results with WYE-151650, data from NIBR3049 (**6**) are more equivocal on the potential for a

selective JAK3 inhibitor[9]. Despite excellent in vitro potency (8 nM) and selectivity (>100-fold vs

all JAKs), NIBR3049 is poorly active in all cellular assays, leading Novartis to conclude that

JAK3 activity is largely dispensable for common γ-chain signaling[4]. The conflicting results with

WYE-151650 and NIBR3049 suggest that JAK3 requires further validation.
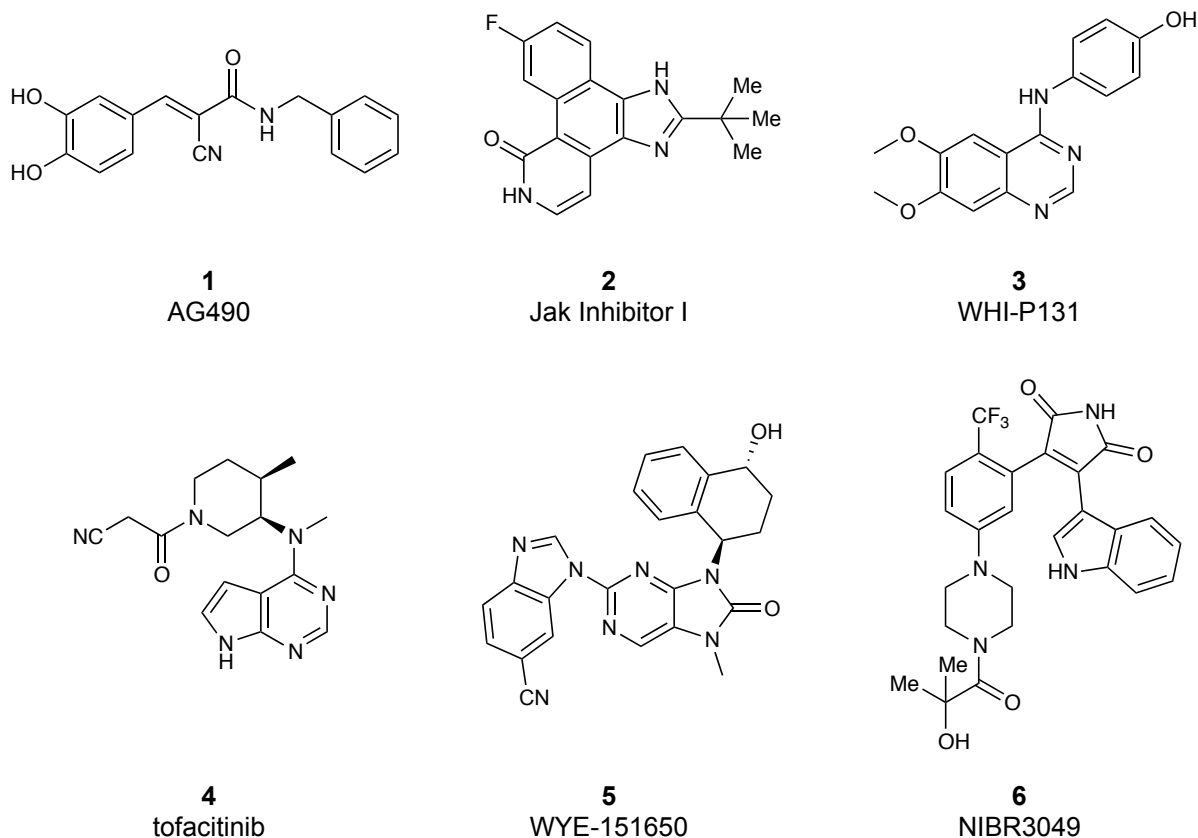
Figure 2-1 Representative JAK Inhibitors Circa 2011

To resolve the discrepancies between the Wyeth and Novartis compounds, we sought a highly selective and cell-active probe whose specificity could be genetically validated. Within the JAK family, only JAK3 has a cysteine near the gatekeeper residue in the ATP binding pocket (Figure 2-2). The Taunton lab has taken advantage of similar cysteines to generate highly selective inhibitors of the kinases RSK1/2, NEK2, MSK1, and BTK[10-13]. Since these compounds require the cysteine for covalent binding, this strategy enabled us to genetically validate JAK3 specific effects by mutating Cys[905] to the drug-resistant serine found in other JAK3 family members. Ultimately, we hoped to create a chemical-genetic toolbox that could address the controversies of JAK3 biology.

```
                              Gatekeeper
JAK1  953  LIMEFLPSGSLKEYLPK  969
JAK2  927  LIMEYLPYGSLRDYLQK  943
JAK3  896  LVMEYLPSGCLRDFLQR  912
TYK2  969  LVMEYVPLGSLRDYLPR  985
```

Figure 2-2 Sequence alignment of JAK Family Members (mus musculus)

In order to generate an irreversible JAK3 inhibitor, we pursued three strategies. First, we synthesized acrylamide derivatives of the NIBR3049 scaffold in order to improve cell potency. Next, we began with a broadly cysteine-reactive pyrimidine and generated more selective derivatives. Finally, we turned to the patent literature and characterized a series of pyrrolopyrimidine acrylamides in vitro and in vivo. From this, we identified compound **30**, which was highly selective in cell-based assays and showed efficacy in a murine graft-versus-host disease model.

2.3   Results

Maleimide Irreversible JAK3 Inhibitors

To generate a selective irreversible inhibitor, we first began with the maleimide scaffold from NIBR3049 (**6**), which we reasoned would provide substantial reversible affinity for the ATP binding pocket, and incorporated a cysteine-reactive acrylamide. Using the published crystal structure of compound **6** bound to JAK3, we replaced the 2-hydroxy-2-methylpropanamide with an acrylamide *in silico* to build a rough model of a potential inhibitor[9]. This model placed the acrylamide β-carbon approximately 3 Å from Cys[905] (Figure 2-3). To optimize the distance and geometry of the acrylamide relative to Cys[905], we also replaced piperazine with either a 1,4-diazapene (compound **9**), a 4-amino-piperidine (compound **11**) or a (*S*)-3-amino-piperdine (compound **13**). Finally, propionamide variants of 3 of the acrylamides were generated as control compounds (Figure 2-4, see Methods for synthetic scheme).
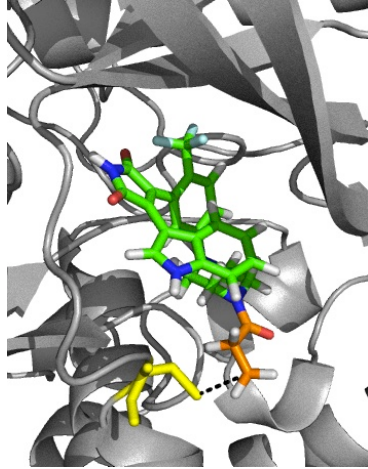
Figure 2-3 Model of Compound 7 bound to JAK3
Based on 3PJC structure of NIBR3049
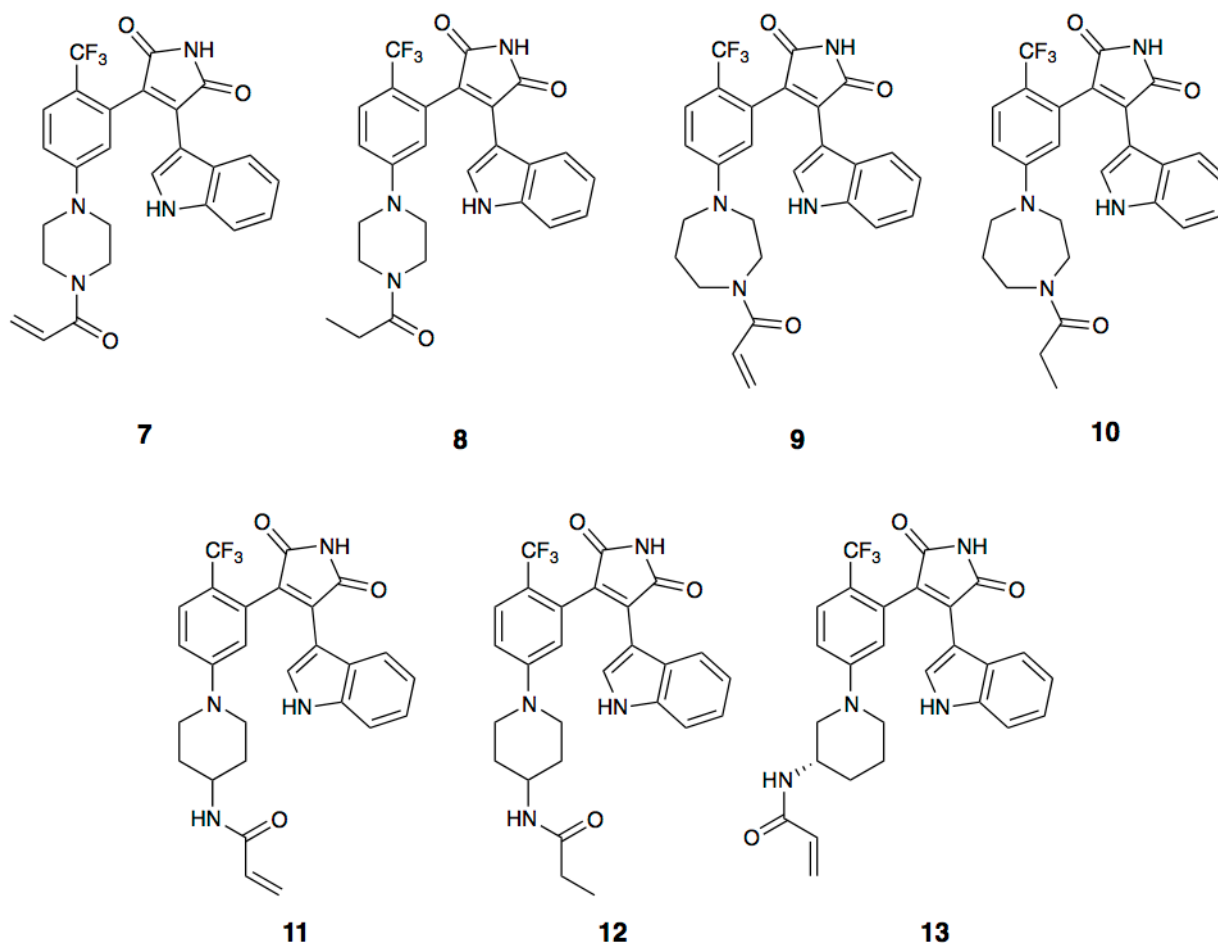
Figure 2-4 Structure of Maleimide Series

Initially, compounds **7**-**13** were assessed in biochemical assays with purified JAK3 kinase domain relative to NIBR3049 (**6**) and tofacitinib (**4**) (Table 2-1). Kinase and compound were pre-incubated for 30 minutes prior to adding substrate and radioactive ATP. All of the acrylamides were less potent than the parent compound, suggesting a loss of reversible affinity by removing the 2-hydroxy-2-methylpropionamide. For compounds **7**, **9**, **11**, the loss of potency was 10-30 fold, while compound **13** was greater than 500-fold less potent than **6**. Despite this loss of biochemical potency, acrylamides **7, 9**, and **11** were 2-3-fold more potent than the parent compound in a proliferation assay of IL-2 stimulated murine CD4+ T cell blasts. Interestingly, the potency of **7, 9,** and **11** in a JAK1 kinase assay was largely unchanged from the parent compound (<2-fold change), suggesting a loss of in vitro selectivity with these new derivatives.

Compound	JAK3 (nM)	JAK1 (nM)	IL-2 Proliferation (nM)
Tofacitinib (**4**)	3.1	2.7	13.5
NIBR3049 (**6**)	2	957	224
7	57	658	87
8	389	536	176
9	24	1530	140
10	82	1090	348
11	28	1820	101
12	612	4184	4184
13	1050	18300	n.d.

Table 2-1 Activity and selectivity of Maleimide Series.
JAK3 and JAK1 in vitro kinase assays conducted with 100 mM ATP. Proliferation of murine CD4 T-cell blasts in response to IL-2 assessed by 3H-thymidine incorporation. Values are IC50 in nanomolar.

The acrylamides were designed to form irreversible, covalent bonds with JAK3. Consistent with this design, the propionamide variants of **7**, **9**, and **11** (compounds **8**, **10**, and **12**) were 6.8, 3.4, and 22-fold less potent respectively. Especially for **7/8** and **9/10**, these shifts were somewhat smaller than expected given literature reports with EGFR[14]. This could be explained by high reversible affinity for JAK3 and/or by favorable interactions formed with the propionamide. To conclusively demonstrate irreversible inhibition, purified JAK3 was incubated with compound for 2 hours and then free compound was removed by dialysis. After 2 days of dialysis, JAK3 incubated with acrylamides **7**, **9** and **11** had recovered less than 10% kinase activity relative to DMSO. By contrast, JAK3 treated with tofacitinib (**4**), NIBR3049 or the propionamide **8** had recovered 70-100% of the DMSO kinase activity. Together, these data indicated that the new acrylamides were irreversible inhibitors in biochemical assays.
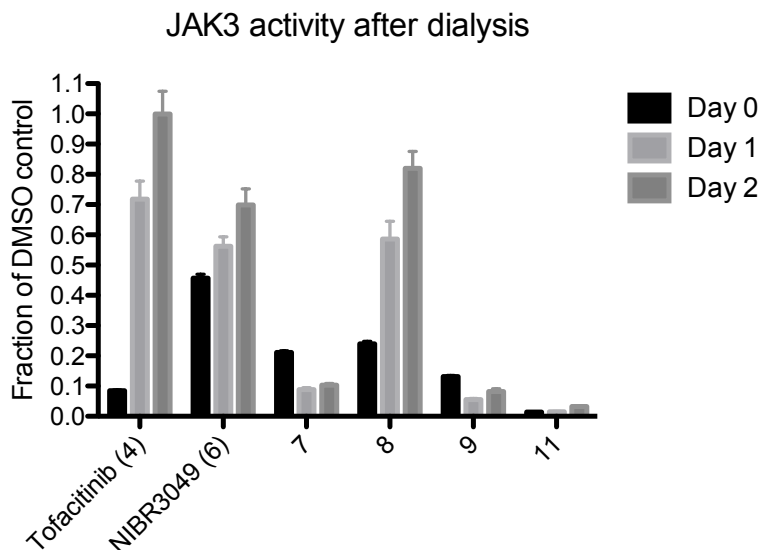
Figure 2-5 JAK3 activity after dialysis.
Purified JAK3 kinase domain was incubated with the indicated compound (100 nM) for 2 hours. After removing an initial time point, the protein was then dialyzed for 1 or 2 days and then kinase activity was assayed by ^{32}P-ATP labeling. The resulting activity was normalized to DMSO control samples from the same day. Plotted as mean +/- SEM of technical triplicates.

Data from IL-2 proliferation assays provided evidence that acrylamides **7, 8**, and **9** were cell active, but also that the corresponding propionamides were only 2-fold less potent for compounds **7** and **8**. These results implied that covalency was not essential for cellular potency and raised the possibility that the compounds were not acting as irreversible inhibitors in cells. To test this, we assessed sustained inhibition after washout in a cell line model. In RAMOS B cells, IL-4 triggered STAT6 phosphorylation is JAK1/JAK3 dependent[15]. Treatment with 2 μM of compounds 4, 6, 7, 8 and 11 completely abrogated pSTAT6 (Figure 2-6). To assess sustained inhibition in cells, pre-treated cells were subjected to a strenuous washout protocol (see methods). As expected, pSTAT6 recovered completely after washing out the reversible compounds **4**, and **6.** However, acrylamide **7** washed out just as well as the corresponding propionamide **8**, indicating no sustained inhibition. Acrylamide **11** showed substantial, if

incomplete, recovery after washout, suggesting that little of the JAK3 was irreversibly bound (Figure 2-6).
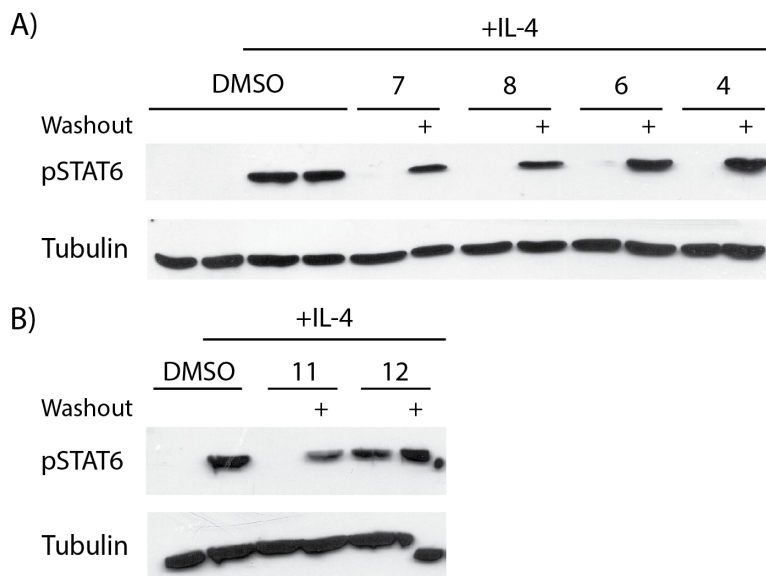
Figure 2-6 Cellular Washout Studies.
A) and B) RAMOS B cells were incubated with DMSO or 2 μM of the indicated compound for 2 hours. Compound was left or washed out and then cells were stimulated with IL-4 for 30 minutes prior to cell lysis and western analysis.

Ultimately, these maleimide acrylamides offered a small but consistent improvement in cellular potency relative to the parent compound NIBR3049. However, they were still not as potent as tofacitinib (Table 2-1). Furthermore, while they were biochemically irreversible, they did not sustain inhibition after washout in cells, limiting their utility as part of a chemical genetic toolbox targeting Cys[905].

Pyrimidine Scaffold

Our next strategy was to identify a scaffold with broad activity against kinases with a similar cysteine and tune its reversible interactions to optimize JAK3 selectivity. Across the kinome, 10 kinases share a similar cysteine, including EGFR and BTK, which have been the focus of significant drug discovery efforts. An Avila patent described compound **14**, which was designed as BTK inhibitor but was shown to covalently modify JAK3 in vitro (Figure 2-7)[16]. In the process of developing an EGFR T790M irreversible inhibitor, Nathanael Gray's group generated compound **15**, which had significant activity against JAK3 in the Ambit screen[17]. We resynthesized both of these compounds and confirmed their activity in vitro versus JAK3 (IC_{50} 1.6 nM and 4.8 nM respectively).

14 **15**
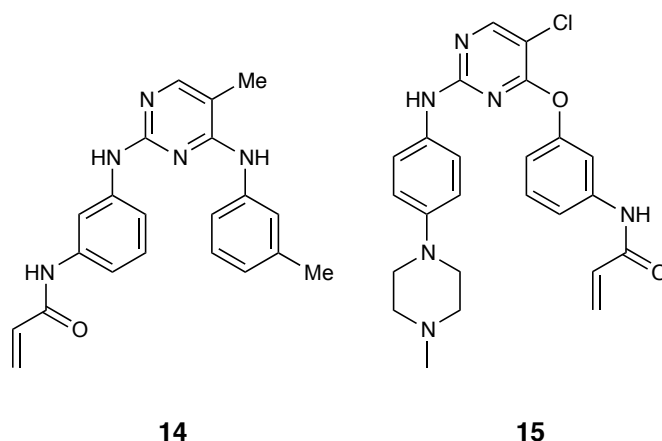
Figure 2-7 Pyrimidine Starting Scaffolds

Since the maleimide-derived acrylamides failed to show sustained inhibition in cells, we next assessed the resistance of **14** and **15** to washout using the IL-4/RAMOS model. After a 2-hour incubation and strenuous washout, there was no or little recovery of pSTAT6 following IL-4 stimulation for acrylamides **14** and **15** respectively (Figure 2-8 A). When the same cells were instead stimulated with IFNα (a JAK1/JAK2 dependent cytokine), compound **14** inhibited pSTAT1 but recovered substantially after washout (Figure 2-8 B). This was expected because although acrylamide **14** inhibited JAK1 in vitro (IC_{50} 1.3 nM), JAK1 lacks the cysteine to form an

irreversible interaction. Compound **15** had little effect on IFNα/pSTAT1 in either continuous or washout treatments (Figure 2-8 B). This selectivity for JAK3 over JAK1 was confirmed with a broad dose titration. Both compounds inhibited IL-4/pSTAT6 completely in the 100-200 nM range (Figure 2-8 C). Compound **14** completely blocked IFNα/pSTAT1 at 50-100 nM, while compound **15** largely spared IFNα pSTAT1 up to 5 μM (Figure 2-8 D), which led us to pursue **15** scaffold for further optimization.
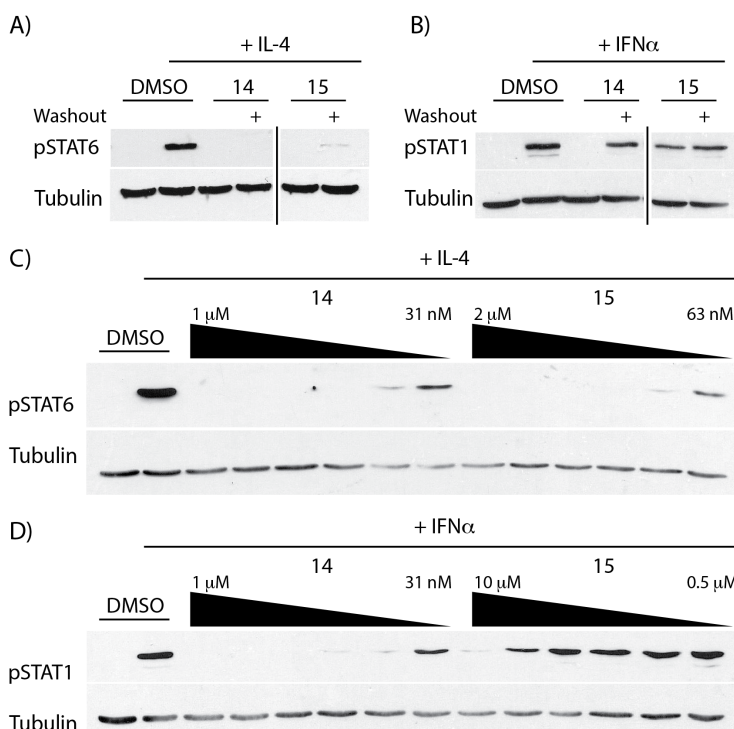
Figure 2-8 Cellular Activity of Compounds 14 & 15.
A) and B) RAMOS B cells were treated with compound for 2 hours followed by strenuous washout. Cells were then stimulated with IL-4 (5 ng/mL, A) for 30 minutes or IFNα (1 ng/mL, B) for 15 minutes, lysed and blotted for pSTAT6 (A) or pSTAT1 (B). C) and D) Dose titration of RAMOS B cells treated with the indicated concentrations of inhibitor and then stimulated with IL-4 (C) or IFNα for 30 or 15 minutes, respectively. Representative of two independent experiments. In A) and B), vertical line indicates blot was digitally cropped to remove unrelated compound.

Biologically, we were initially interested in studying the requirements for JAK3 in CD4+ T cells. Acrylamide **15** potently blocked JAK3 IL-2 driven proliferation in CD4 T cell blasts (IC$_{50}$ 36 nM, Figure 2-9). Among the 10 kinases with an equivalent cysteine, the TEC family members ITK and RLK are highly expressed in T cells and are important in the T cell receptor (TCR) signaling pathway[18]. To assess acrylamide **15**'s cellular activity against both ITK and RLK, we

stimulated naïve CD4+ T cells via their TCR and assessed production of IL-2. Acrylamide **15** potently inhibited IL-2 production (IC$_{50}$ 9 nM, Figure 2-9). This inhibition of ITK/RLK-dependent IL-2 production limited the utility of compound **15** as a JAK3 probe to settings without concurrent TCR stimulation.
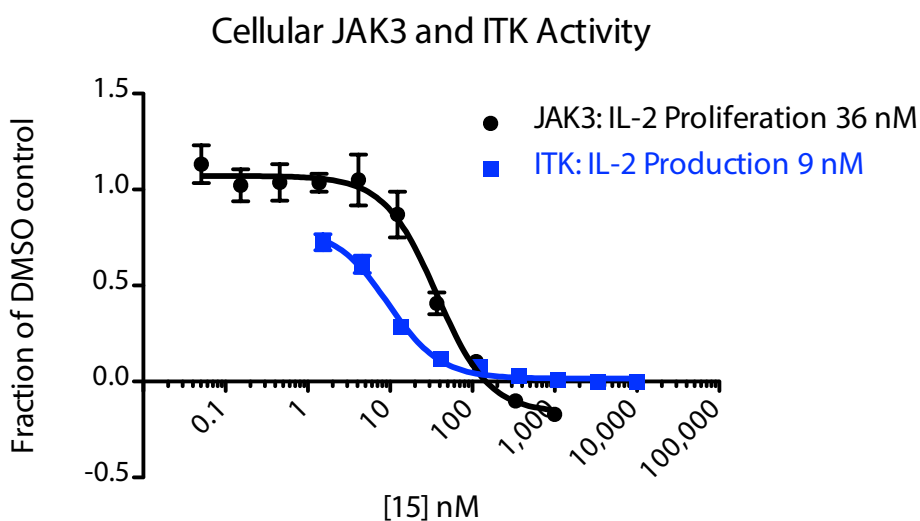
Figure 2-9 Cellular Selectivity Profile of 15.
Dose titration of compound 15 in naïve murine CD4+ T cells (IL-2 production) or CD4+ T cell blasts (IL-2 proliferation). IL-2 production was assessed by ELISA and IL-2 proliferation was assessed by ^{3}H-thymidine incorporation.

T cells rarely encounter IL-2 without concurrent or recent TCR stimulation in physiological settings, so we pursued a JAK3-selective variant of compound **15**. Since JAK3, ITK and RLK share a similar cysteine, we attempted to tune the reversible interactions via a number of approaches. Based on a patent report of potential JAK3 inhibitors[19], the ether linkage was replaced with a thioether linkage (**16** and **18**, Figure 2-10), which reduced potency (Table 2-2). Alternate tail groups (**19**) and cysteine reactive groups (**20**) also reduced potency (Table 2-2). Varying the orientation of the electrophile gave mixed results: Although *para*-substituted compound **22** was significantly less potent than **15**, the para substitution pattern was generally preferred when the 5-position of the pyrimidine was not chlorine. We varied the size and polarity of the 5-substituent in an attempt to differentiate between the Phe gatekeeper residue in

31

ITK and the smaller Met in JAK3 (**17, 23-26, 29**). In this series, JAK3 potency was largely retained, and the bromo-substituted compound **23** had deceased potency vs. ITK, yielding a compound with equivalent cellular potency vs. JAK3 and ITK (Table 2-2). In vitro, compound **23** was 4-fold selective for JAK3 over ITK (IC$_{50}$s with 1 mM ATP: JAK3 6.6 nM, ITK 26.1 nM, BTK 137 nM, EGFR >10 μM). Replacing the acrylamide with a propionamide (**21**) led to a ~7-fold loss of potency, consistent with a role for covalent binding. Adding a *meta*-methoxy substituent (**27**) yielded the best selectivity within the series.
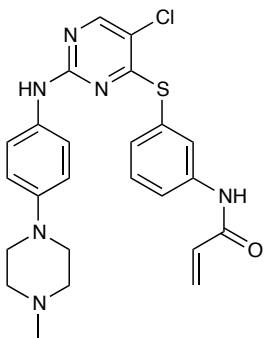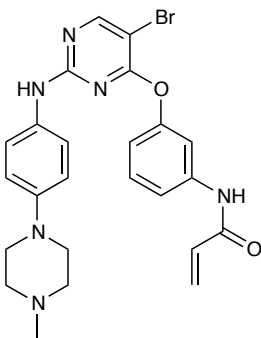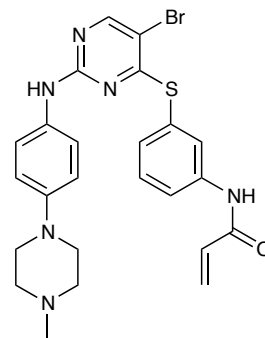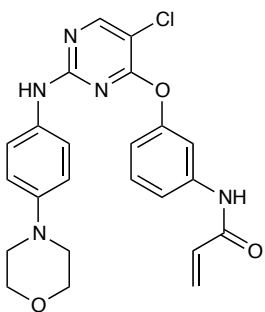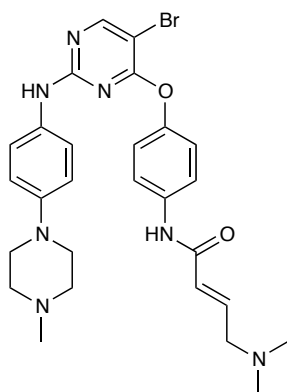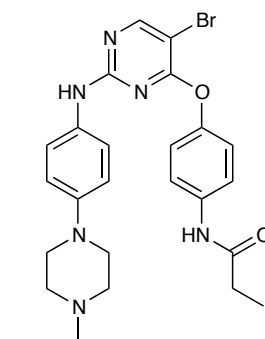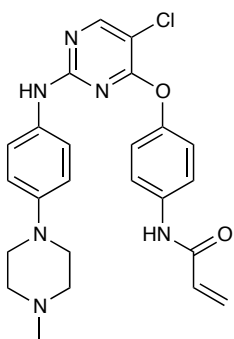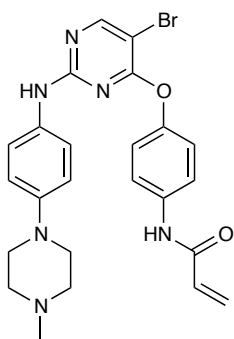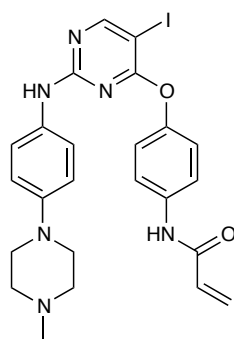
16 **17** **18** **19** **20** **21** **22** **23** **24** **25** **26** **27** **28** **29**
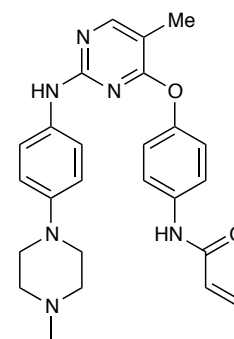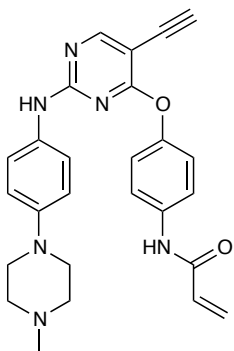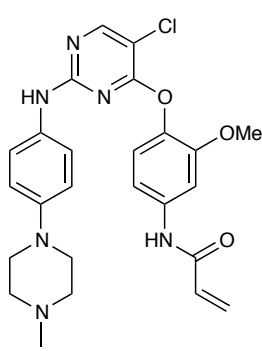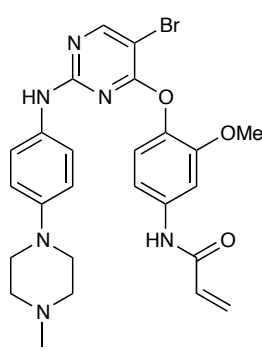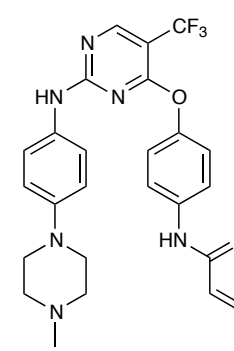
Figure 2-10 Pyrimidine Derivatives

33

Compound	IL-2 proliferation (JAK3) nM	IL-2 Production (ITK) nM
15	36	9.4
16	436	n.d.
17	70	n.d.
18	409	n.d.
19	297	n.d.
20	269	n.d.
21	223	n.d.
22	379	n.d.
23	33	38
24	27	16
25	93	77
26	73	12
27	44	118
28	43	66
29	28	40

Table 2-2 Cellular Activity of Pyrimidine Series.
IL-2 proliferation and IL-2 production assays as described in Figure 2-9.

This structure-activity relationship study culminated in compound **27**, which reversed the selectivity of the original compound **15** for ITK over JAK3. However, this selectivity was insufficient to specifically probe JAK3's roles in physiological T cell activation settings. Some of these compounds, particularly compound **23,** may be useful as dual JAK3/ITK inhibitors, but for the purpose of investigating JAK3 biology, a different scaffold was needed.

Pyrrolopyrimidines

In 2013, Merck disclosed a series of pyrrolopyrimidines described as Janus Kinase inhibitors[20]. Some of these compounds featured electrophiles, leading us to believe that they could be covalent JAK3 inhibitors. We synthesized a series of compounds reported in the patent, along with closely realted variants (Figure 2-11). Compound **30** and its isomer **31** were nanomolar inhibitors of JAK3-dependent IL-2 proliferation (Table 2-3). This activity absolutely required the acrylamide (see compound **32**, IC50 >5 μM). Furthermore, compounds **30** and **31** were highly selective for JAK3 over ITK in cellular assays (~300-fold). α-Methyl substituted acrylamides are less reactive than unsubstituted acrylamides and thus may require higher non-covalent affinity for efficient covalent bond formation[21]. This offers a strategy to potentially improve selectivity over other kinases containing a similar cysteine but that make suboptimal reversible contacts with the scaffold. Compounds **33** and **34** had slightly decreased cellular potency at JAK3 (49 and 14 nM respectively), but compound **34** had improved selectivity over ITK (IC50 9.0 μM, >600-fold selective). Since the electronics of the aryl ring can impact reactivity of aniline-based acrylamides[21], in addition to non-covalent binding affinity, we synthesized chloro-substituted derivatives **35** and **36**, which were slightly less potent than **30** with roughly similar selectivity over ITK. Replacing the ethyl ester on the pyrrolopyrimidine with a trifluoromethyl group (**37** and **38**) resulted in a significant loss of potency, suggesting that this ester is important for non-covalent interactions with JAK3. Cyanoacrylamides are reversible, covalent cysteine reactive groups that offer the benefits of covalent inhibition with less potential for haptenization[22]. We attempted to replace the acrylamide with a substituted cyanoacrylamide (**39**), but this resulted in a loss of cellular activity. Finally, to design a probe compatible with click chemistry (see next section), we replaced the ethyl ester on the pyrrolopyrimidine core with a propynyl ester (**40**), which was well tolerated.

In this pyrrolopyrimidine series, we identified highly selective and potent JAK3 inhibitors. Based on the initial cellular studies, compound **30** (later referred to as JAK3i) was synthesized on gram scale for future use in vitro and in vivo.
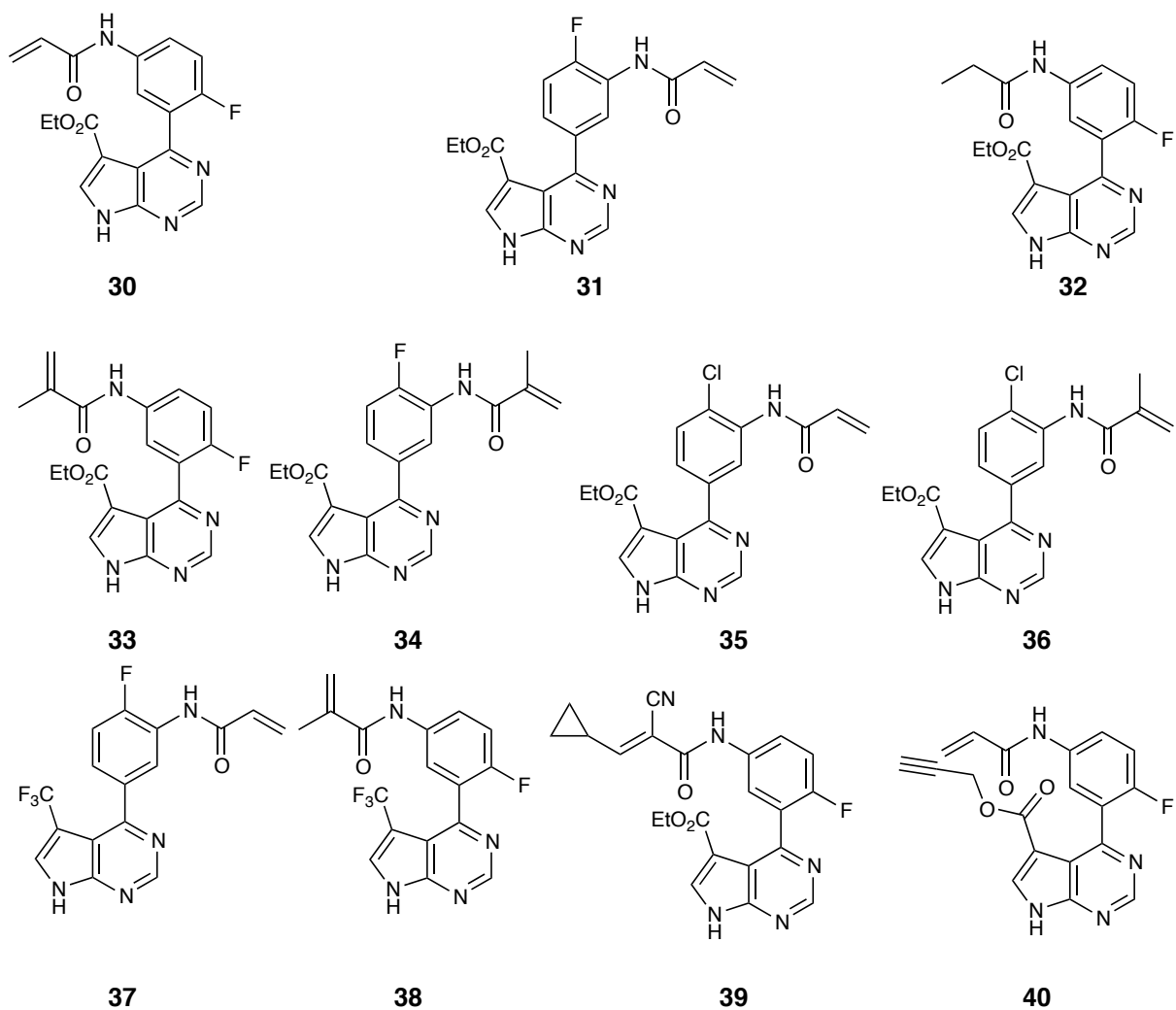
Figure 2-11 Pyrrolopyrimidine Derivatives

Compound	IL-2 proliferation (JAK3) nM	IL-2 Production (ITK) μM
30	3.7	1.12
31	3.9	1.08
32	5132	n.d.
33	49	n.d.
34	14	9.01
35	8.0	0.997
36	11	4.63
37	6038	n.d.
38	>10,000	n.d.
39	5655	n.d.
40	14	2.43

Table 2-3 Cellular Activity of Pyrrolopyrimidine Series

Toward a Clickable Occupancy Probe

To validate a drug target and discover new biology with a chemical probe, ideally one would demonstrate target engagement in cells and in vivo [23]. One pproach to demonstrate target engagement is to develop an occupancy probe that can measure free target after treatment with an inhibitor[23,24]. To this end, pyrimidine **26** and pyrrolopyrimidine **40** incorporated alkyne groups compatible with click chemistry to enable ligation to a fluorophore for in-gel fluorescence or biotin for western analysis. Neither **26** nor **40** could detect JAK3 when clicked to TAMRA-N_3, presumably due to its low cellular abundance (data not shown). However, when clicked to biotin, enriched with streptavidin, eluted and run on a gel for western detection of JAK3, both probes were able to detect JAK3 in cells. Pretreatment with a high dose of compound **30** abrogated subsequent labeling of JAK3 by probe **26** and **40** (Figure 2-12). Further work is needed to refine the methodology for consistent application of these probes, but they provide proof of concept for the development of JAK3 occupancy probes.

A)   30   +   B)   30   +
           26   +   +   40   +   +
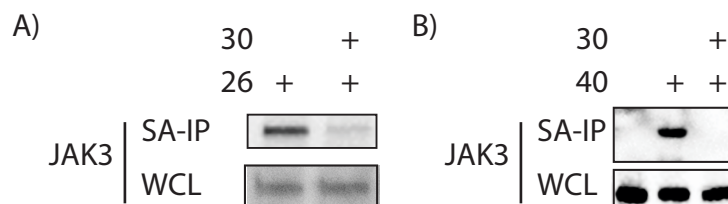
Figure 2-12 Clickable JAK3 Occupancy Probes.
A) ACK Lysed murine splencoytes were pretreated with compound 30 (1 μM) for 1 hour at 37 °C and then incubated with probe 26 (1 μM) for 1 hour at 37. Cells were lysed, precleared and the alkyne was clicked to biotin azide for subsequent immunoprecipitation and blotting for JAK3. B) EL4 cells were pretreated with compound 30 (1 μM) for 1 hour at 37 and then incubated with probe 39 (1 μM) for 1 hour at 37. Samples were processed as in A). SA-IP – Streptavidin Immunoprecipitation; WCL – Whole Cell Lysate.

Evaluation of JAK3i (compound 30) In Vivo

Optimally, a JAK3 probe would be able to not just address biological questions in cell culture but probe the requirements for JAK3 in physiologic and pathologic responses in vivo. Many immunological questions must be addressed in vivo to account for the complex interactions between signaling networks in multiple cell types. Based on promising early in vitro studies of compound **30** (henceforth JAK3i), we did a series of in vivo pilot studies.

First, we measured plasma concentrations of JAK3i after dosing mice. After assessing a number of formulations, we dissolved JAK3i in a mixture of DMSO and solutol (10% DMSO in 30% solutol in saline). One hour after dosing by intraperitoneal (IP) injection, JAK3i plasma concentrations ranged from several hundred to several thousand nanomolar depending on the dose (Figure 2-13A). The compound was rapidly cleared, with less than 100 nM left 6 hours after 40 mg/kg IP ($t_{1/2}$!50 minutes) (Figure 2-13B). While this short half-life would be concerning for a reversible inhibitor, this was tolerable for an irreversible inhibitor, which has the potential to confer prolonged inhibition after the compound is cleared.

A) 1 hr IP

B) 6 hr IP
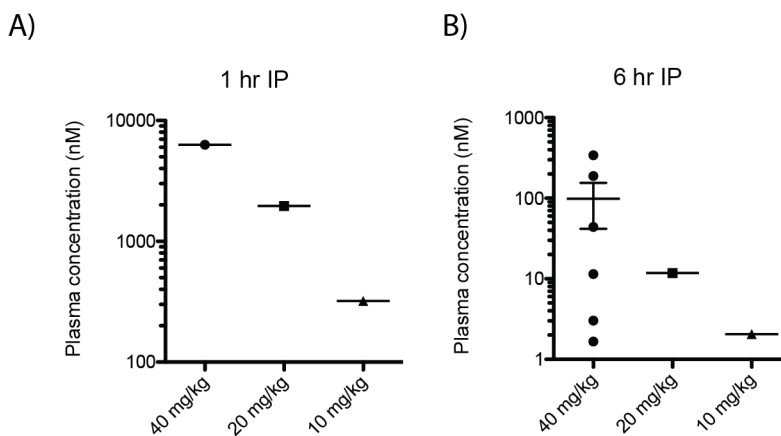
Figure 2-13 Plasma Concentration of Compound 30.
Compound **30** was dosed by intraperitoneal injection to C57BL/6J mice in 10% DMSO / 90% Solution (30% solution in normal saline). After 1 (A) or 6 hours (B), animals were sacrificed, blood collected via cardiac puncture, plasma isolated and concentration quantified by LC-MS/MS analysis relative to standard curve.

In parallel with the pilot pharmacokinetic studies, we developed a pharmacodynamic assay assessing the IL-2 response of cells from drug-treated animals ex vivo. Tregs respond to IL-2 without any pre-activation and are among the first to respond following TCR activation in vivo [25], making them an ideal cell type to study rapidly ex vivo. Stimulation of splenic Tregs from vehicle-treated mice with IL-2 ex vivo gave a strong induction of STAT5 phosphorylation (pSTAT5) (Figure 2-14). This signal was significantly reduced by treatment with 500 nM JAK3i ex vivo. In vivo treatment with JAK3i inhibited pSTAT5 in a dose-dependent fashion, with the 40 mg/kg dose yielding complete inhibition (Figure 2-14). It is unlikely that this potent inhibition can be explained by reversible drug binding in culture, as the spleen was diluted greater than 75-fold (based on an average splenic volume of 0.07 mL[26]). Based on the PK data above, this would yield a concentration of <85 nM in the ex vivo stimulation, substantially less than the 500 nM in vivo that had a partial effect. Thus, JAK3i dosing in vivo could inhibit JAK3 sufficiently to block the response of an IL-2 sensitive cell type ex vivo.
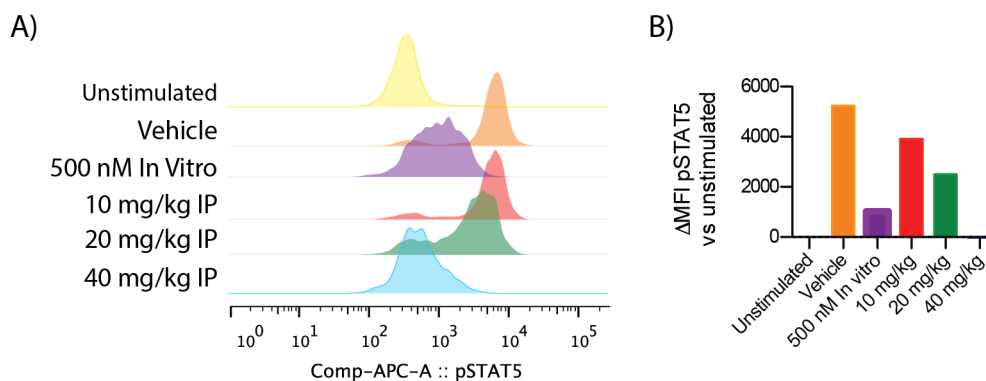
Figure 2-14 Pharmacodynamic Assessment of Compound 30.
C57BL/6J mice were treated with compound 30 IP as in Figure 2-13. After 1 hour, animals were sacrificed, splenocytes rapidly isolated and stimulated with 50 units/mL rhIL-2 for 15 minutes prior to fixation and analysis by phosphoflow. A) Histograms of pSTAT5. B) Quantification of pSTAT5 mean fluorescence intensity relative to unstimulated vehicle.

To test where JAK3i could reveal potential clinical applications for a pure JAK3 inhibitor, we sought a model that met three criteria: 1) previous genetic or pharmacological evidence for the importance of γ_c-cytokines; 2) a rapid and simple readout; 3) published efficacy of another JAK inhibitor. Acute graft-versus-host disease following a mismatched bone marrow transplant met all of these criteria: a prior report showed efficacy of an antibody against IL-2Rγ[27]; survival was less than 20 days without intervention[28,29]; and ruxolitinib (JAK1/JAK2 inhibitor) was efficacious in the model[30]. We pre-treated recipient C57BL/6-Ly5.1 mice with JAK3i for 1 day, then transferred MHC-mismatched BALB/c bone marrow and CD4+ T-cells to the irradiated recipients. All of the vehicle-treated mice died by day 18 (median survival 12 days), while only one of the JAK3i treated mice died by the end of the 24 day study (median survival not reached, p<0.02 Log-rank Test) (Figure 2-15A). Interestingly, weight among drug treated and vehicle treated animals was not significantly different throughout the study (unlike with ruxolitinib treatment[30]). This may reflect a potential toxicity of either the formulation or the compound that merits further exploration. Regardless, this model provided an initial proof of concept of selective JAK3 inhibition in a model of autoimmune disease.
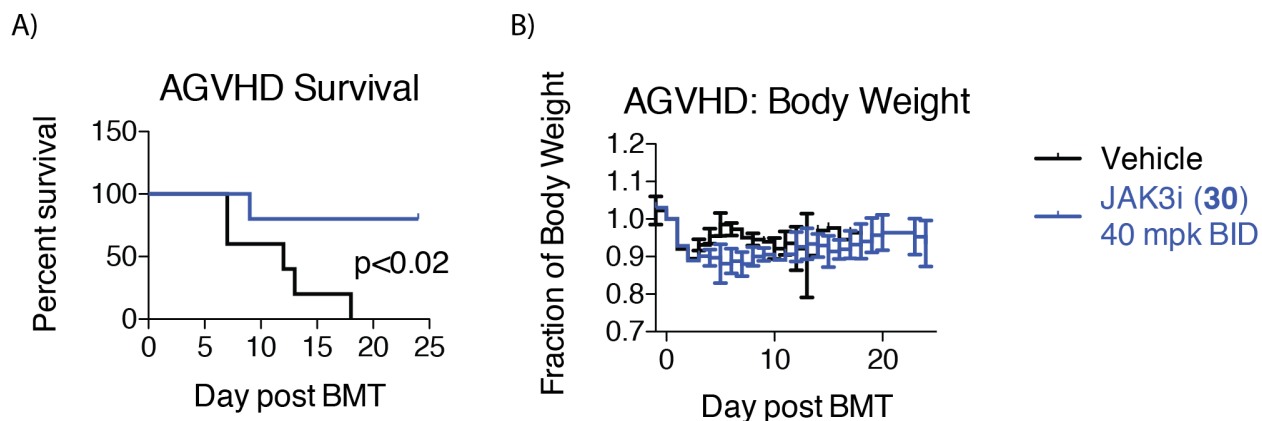
Figure 2-15 JAK3 Inhibition in Acute Graft Versus Host Disease (AGVHD).
Bone marrow and CD4+ T Cells from BALB/c mice were transferred into irradiated C57BL/6-Ly5.1 hosts. Recipients were treated twice daily with vehicle or JAK3i (30) formulated in 5% ethanol/95% Captex 355 at 40 mg/kg. A) Survival Curve. Significance assessed by Log-rank test. B) Change in body weight from beginning of study. N=5 mice per group.

2.4   Discussion

Since the initiation of this project in 2011, there have been many changes in the JAK3 inhibitor landscape. To date, a non-covalent JAK3 inhibitor remains elusive. Vertex disclosed decernotinib (VX-509, **41**), a supposedly JAK3 selective, non-covalent inhibitor (Figure 2-16)[31]. Data from Clark et al. suggests that this compound is approximately equally potent at JAK1 (IC_{50} 112 nM) and JAK3 (74.4 nM) when assayed at physiological ATP, and is more potent at JAK1-dependent IL-6 signaling than JAK3-dependent IL-15 signaling in whole blood[6]. This is consistent with the clinical results[32], which show efficacy in rheumatoid arthritis but also show the lipid abnormalities associated with blockade of IL-6 signaling[33].
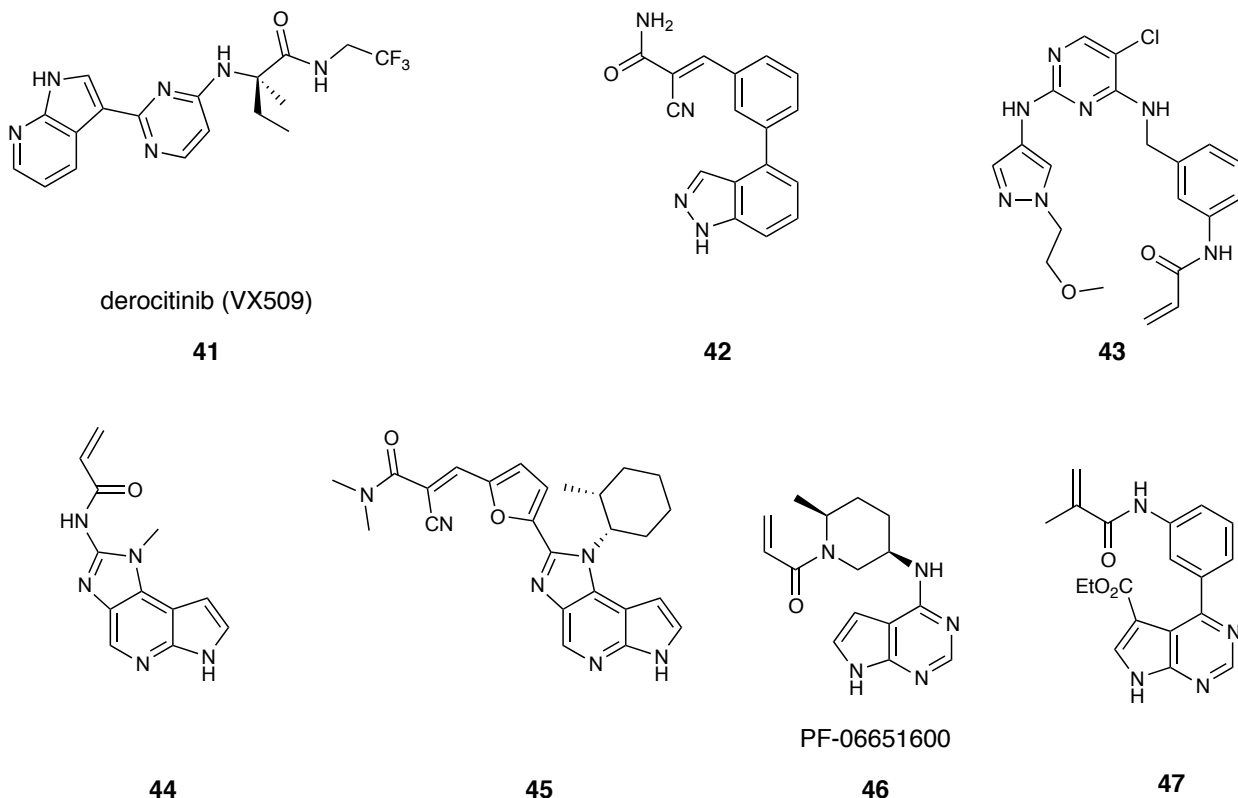
Figure 2-16 Published JAK3 inhibitors as of March 2017

Many groups have found the development of cysteine-targeted JAK3 inhibitors to be much more successful. Our lab described a series of computationally designed cyanoacrylamides (exemplified by indazole **42**, Figure 2-16), which are very selective in biochemical assays for JAK3 over JAK1, but lack cellular activity[34]. Li et al. disclosed acrylamide **43**, which is related to the pyrimidine series described above (compounds **16-29**)[35]. Significantly, compound **43** has reasonable pharmacokinetics, although there has been no application to in vivo biology. The tricyclic acrylamide **44** was described by Abbvie and is the first covalent JAK3 inhibitor to show complete inhibition of acute, IL-2 stimulated STAT5 phosphorylation in human T cells while sparing JAK1[2]. Building off the tofacitinib scaffold, Forster et al. identified the first cell-active reversible, covalent JAK3 inhibitor (cyanoacrylamide **45**), and provided crystallographic evidence of covalent binding. This compound, like compounds **42**-**44**, was not tested in animal models of autoimmune disease.

Our medicinal chemistry efforts culminated in the first example of *in vivo* JAK3 inhibition (see Chapter 3). JAK3i showed a reasonable half-life, ex vivo pharmacodynamic activity and efficacy in the AGVHD model, which is known to be dependent on γ_c-cytokines. Subsequent to our publication, Thorarensen and colleagues described the discovery of PF-06651600 (compound **46**), Pfizer's clinical JAK3 covalent inhibitor[37]. Acrylamide **46** is highly selective for JAK3, has a longer half-life than JAK3i (mice 1.3 hr, predicted 1.8 hr in humans)[37], and is efficacious in the rat adjuvant-induced arthritis model[38]. Finally, Merck recently described a pyrrolopyrimidine similar to JAK3i (compound **47**)[39]. The α-methyl substituted acrylamide is highly selective for JAK3 and supposedly is more selective for JAK3 over BTK in biochemical assays (in our hands, JAK3i has no effect on BTK signaling up to 10 μM in cells, see Chapter 3). Surprisingly, this compound appears to require much greater doses in vivo (300-600 mg/kg for efficacy in the collagen arthritis model). Lower doses are effective if administered simultaneously with a CYP inhibitor, suggesting that this compound has significant metabolic liabilities[39]. Based on the published data from all three compounds, it appears that PF-06651600 (**46**) and JAK3i (**30**) are the most appropriate tools for future study of JAK3 in vivo. PF-06651600 has a few advantages that may make it the most preferred (slightly longer half-life, greater selectivity profiling data, and commercial availability). Given the wisdom of using multiple inhibitors to validate pharmacology[23], JAK3i remains a valuable tool for the study of JAK3 biology.

One important question for the future of covalent JAK3 inhibitors is the turnover of JAK3 in human cells. Especially since many of these inhibitors have relatively short half-lives, the duration of action will be determined by new protein synthesis rate and not clearance of the compound. The best-published evidence suggests that the half-life of JAK3 in human T cells is between 3 and 4 hours[38]. Depending on the degree of JAK3 occupancy required for efficacy, this might necessitate frequent dosing or ultimately become a barrier to efficacy. Ongoing phase

II clinical trials studying PF-06651600 in rheumatoid arthritis (NCT02969044), alopecia areata (NCT02974868) and ulcerative colitis (NCT02958865) will hopefully address the clinical relevance of JAK3 inhibition. Given the range of γ_c-cytokines and cell types potentially involved, a successful clinical trial will raise many mechanistic questions. The combination of multiple covalent JAK3 inhibitors, such as PF-06651600 and JAK3i, and a drug resistant mutant (C905S) is a powerful toolkit to probe the underlying biology.

2.5   Materials and Methods

In vitro kinase assays: Purified JAK1 (9.4 nM), JAK2 (1.15 nM) or JAK3 (3.13 nM) kinase (all Invitrogen) were preincubated with compound and 100 μM ATP for 30 minutes in manufacturer prescribed buffer. Reactions were run for 30 minutes at 23 °C with γ-^{32}P ATP (16.7 nM, Perkin Elmer) and the appropriate substrate: JAK1 - IRS1 (0.06 mg/mL, Enzo Life Sciences); JAK2 - PDKTide (0.19 mg/mL, EMD Millipore); JAK3 - JAK3tide (0.0325 mg/mL, EMD-Millipore). ITK (3.13 nM, Invitrogen) was performed similarly except using 1 mM ATP and Myelin Basic Protein substrate (Sigma). Kinase assays with BTK, EGFR, JAK3 (all with 1 mM ATP), and TYK2 (100 μM ATP) were performed by Nanosyn.

RAMOS Signaling Assays: RAMOS B Cells were incubated with indicated concentrations of compound for 2 hours in low serum (1%) RPMI. In washout studies, cells were diluted with 10x volume media, spun down, washed 3 x 15 minutes in RPMI (10% serum) at 37 °C on a bacterial shaker in 5x original volume, and then resuspended in the original volume of RPMI (1% serum). Cells were then stimulated with IL-4 (5 ng/mL, R&D Systems) for 30 minutes or IFNα for 15 minutes at 37 °C. Cells were then spun down, washed in 1 mL of cold PBS, spun again and lysed in Cell Lytic M (Sigma-Aldrich). Protein was normalized by bicinchoninic acid assay,

separated on 7.5% acrylamide gels and transferred to nitrocellulose. Blots were probed for tubulin (DM1a, Sigma Aldirch), and either pSTAT1 Tyr701 (Cell Signaling #9172) or pSTAT6 Tyr641 (Cell Signaling #9361).

T-Cell Proliferation and Production Assays: See Chapter 3 Methods for detailed description of mice, cell isolation and assays.

JAK3 Occupancy: ACK Lysed murine splenocytes or EL4 murine T-cells were pretreated with compound **30** for 1 hour at 37 °C and then treated with probe **26** or probe **39** for 1 hr at 37 °C. Cells were spun down, washed with PBS, and then lysed in 250 uL of NP40 lysis buffer (no EDTA added). Lysates were clarified and protein quantified by BCA. Equal amounts were then precleared overnight with 50 uL of high capacity Streptavidin resin (Life Technologies). Beads were removed, an input sample removed and frozen, and the remaining lysate was clicked biotin azide (1 hr, RT, 1% SDS, 50 μM biotin ester azide, 1 mM TCEP, 85 μM TBTA ligand, 1 mM $CuSO_4$), and protein precipitated by ice cold acetone (1 mL) overnight at -20 °C. The precipitated proteins were pelleted for 30 minutes at 4 °C at maximum speed in a tabletop centrifuge, washed acetone (1 mL), washed methanol (1 mL) and the pellet air dried. The protein was resuspend in 1% SDS, 100 mM Tris (400 uL) and then diluted with 600 uL of 1% NP40. Samples were then gel filtered (NAP-10 columns). To the eluate was added streptavidin magnetic beads (150 uL, Pierce) and the tube was rotated overnight at 4 °C. The next morning, beads were washed 2 x 1 mL 1% NP-40/0.1% SDS in PBS and then boiled in 30 uL of 1x sample buffer (10 min 95 °C). Samples were separated on 7.5% acrylamide gels, transferred to PVDF and probed for JAK3 (D7B12, Cell Signaling #8863).

Plasma JAK3i Concentration: Animals were injected intraperitoneally with JAK3i formulated in 10% DMSO / 90% Solutol HS-15 (30% w/w in saline, Sigma). After the indicated time, animals were sacrificed by CO2 asphyxiation and cervical dislocation. Blood was collected by cardiac puncture into heparin coated tubes and spun down 14,000 RPM x 10 minutes at 4 °C on a tabletop centrifuge. Protein was precipitated by addition of 200 μL of ice-cold acetonitrile for every 50 μL of plasma. Samples were spun 14,000 RPM x 10 minutes at 4 °C on a tabletop centrifuge and the clarified samples were stored at -80 °C until analysis. Samples were quantified relative to a standard curve in vehicle treated plasma by multiple reaction monitoring LC-MS/MS on a Waters Acquity LCT UPLC equipped with a TUV detector (monitored at 254 nm) and a Waters Acquity UPLC 1.7 μm C-18 column, eluting at 0.6 mL/min with a 2.5 or 5 minute water:MeCN (with 0.1% formic acid) gradient method.

Ex-vivo Pharmacodynamics: Animals were treated with JAK3i as in the plasma concentration assay for 1 hour prior to euthanasia. Spleens were rapidly isolated, crushed through cell strainers into cold PBS, spun down and red blood cells lysed in ACK lysis buffer (5 mL) for 2 minutes. Samples were diluted with cold PBS, spun down and resuspended in RPMI complete media (500 uL) at 37 °C. Samples were stimulated with 50 u/mL rhIL-2 (Roche) for 15 minutes at RT and fixed by addition of an equal volume of 4% paraformaldehyde in PBS for 10 minutes at RT. Samples were spun down, surface stained for CD4, CD8 and CD25, refixed, permeabilized with methanol, bar coded (Pacific Blue / Pacific Orange NHS-ester, see Chapter 3), and stained for pSTAT5 Y694 (AF647 conjugated BD Cat#612599). FACS data were collected on a BD LSR Fortessa Special Order Research Instrument and analyzed in FlowJo (TreeStar Inc).

Acute Graft Versus Host Disease Model: B6-Ly5 mice (BoyCR, Charles River) were treated with vehicle or JAK3i (40 mg/kg twice daily, formulated in 5% ethanol / 95% Captex 355 (ABITech)[†]) for 1 day. Mice were then irradiated 2 x 550 rads (separated by 4 hours). After 1 hour, 5×10^6 BALB/c bone marrow cells and 1×10^6 purified CD4+ T cells from BALB/c were injected in 200 uL of warm PBS into the lateral tail vein of each mouse. Twice daily dosing resumed. Mice were weighed daily and body condition score recorded until BCS≤2 or weight <80% of original weight, at which point animals were euthanized.

[†] Formulation was changed due to toxicity associated with repeated dosing of DMSO/Solutol formulation

Synthetic Methods

All purchased chemicals were used as received without further purification. Solvents were dried

by passage through columns (either alumina or activated molecular sieves) on a Glass Contour

solvent system. NMR spectra were obtained on a Varian Inova 400 MHz or Bruker 500 MHz

spectrometer and referenced to the residual solvent peak. LC-MS analysis was performed on a

Waters Acquity LCT UPLC equipped with a TUV detector (monitored at 254 nm) and a Waters

Acquity UPLC 1.7 µm C-18 column, eluting at 0.6 mL/min with a 2.5 or 5 minute water:MeCN

(with 0.1% formic acid) gradient method.

Maleimide Series

General Synthetic Scheme
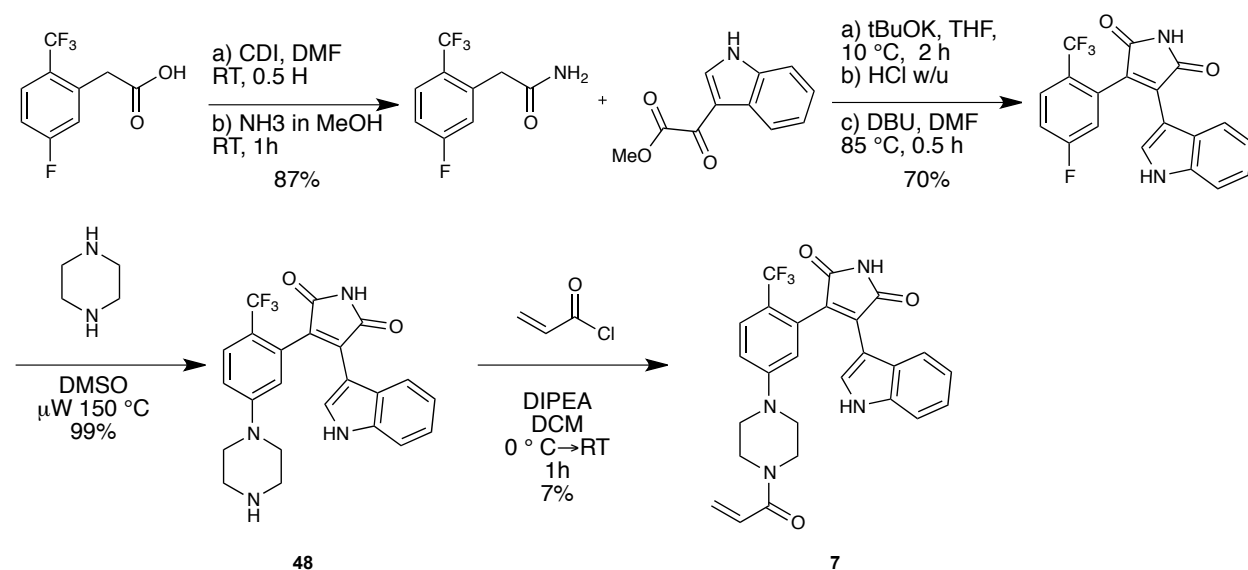
Synthesis and Characterization of Assayed Compounds
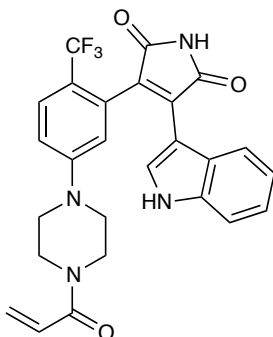
(7) 3-(5-(4-acryloylpiperazin-1-yl)-2-(trifluoromethyl)phenyl)-4-(1H-indol-3-yl)-1H-pyrrole-2,5-dione.

To a stirred suspension of amine **48** (42 mg, 0.095 mmol) in dichloromethane in an ice bath was added diisopropylethylamine (17 μL, 0.097 mmol) and stirred. After 10 minutes, acryloyl chloride (9 mL, 0.11 mmol) was added and the reaction monitored by LCMS. After 10 minutes, the reaction was complete by LCMS and was warmed to RT prior to quenching with 0.3 M HCl, washing with saturated sodium bicarbonate, brine, drying over sodium sulfate and concentrating to give 62 mg of a yellow oil. The oil was purified by preparative HPLC (5-95% acetonitrile in water) to give 3.2 mg of a yellow solid (7%). ^{1}H NMR (400 MHz, DMSO-d_6): 11.83 (s, 1H), 11.06 (s, 1H), 7.92 (s, 1H), 7.62 (d, J = 9.0 Hz, 1H), 7.35 (d, J = 7.8 Hz, 1H), 7.13 (s, 1H), 7.01 (t, J = 7.5 Hz, 1H), 6.93 (s, 1H), 6.80 – 6.67 (m, 2H), 6.63 (d, J = 7.9 Hz, 1H), 6.16 – 6.01 (m, 1H), 5.72 – 5.59 (m, 1H), 3.62 – 3.46 (m, 4H), 3.21 (s, 4H). ESI-MS: 495.2 (M+H$^+$), 492.9 (M-H$^+$).
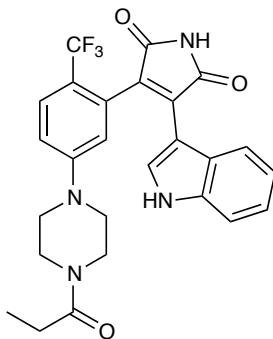
(8) 3-(1H-indol-3-yl)-4-(5-(4-propionylpiperazin-1-yl)-2-(trifluoromethyl)phenyl)-1H-pyrrole-2,5-dione.

Prepared as per **7** except propionyl chloride (0.098 mmol, 1.1 eq) was added, yielding 4.8 mg of a yellow solid (11%). ^{1}H NMR (400 MHz, DMSO-d_6): 11.83 (s, 1H), 11.05 (s, 1H), 7.92 (s, 1H), 7.62 (d, J = 8.9 Hz, 1H), 7.35 (d, J = 8.1 Hz, 1H), 7.11 (d, J = 8.7 Hz, 1H), 7.05 – 6.97 (m, 1H), 6.91 (s, 1H), 6.78 – 6.65 (m, 1H), 6.62 (d, J = 8.3 Hz, 1H), 3.41 (s, 4H), 3.23 – 3.12 (m, 4H), 2.27 (dd, J = 14.8, 7.6 Hz, 2H), 1.08 (d, J = 1.0 Hz, 1H), 0.94 (t, J = 7.4 Hz, 3H).. ESI MS: 497.4 (M+H)
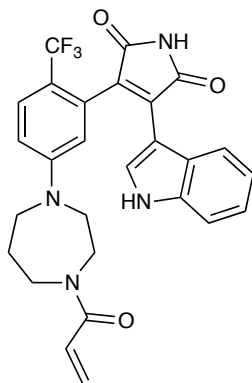
(9) 3-(5-(4-acryloyl-1,4-diazepan-1-yl)-2-(trifluoromethyl)phenyl)-4-(1H-indol-3-yl)-1H-pyrrole-2,5-dione.

Prepared as per protocol for **7**. Isolated 21.6 mg (21%) of a yellow solid. ^{1}H NMR (400 MHz, DMSO-d_6): 11.84 (s, 1H), 11.01 (s, 1H) 7.99 (d, 1H), 7.56 (d, 1H), 7.36 (d, 1H), 7.00 (t, 1H), 6.92

(t, 1H), 6.60 (m, 4H), 6.04 (ddd, 1H), 5.58 (ddd, 1H), 3.61-3.39 (m, 5 H), 3.23 (m, 1H), 2.93 (m, 2H), 1.61 (m, 1H), 1.32 (m, 1H). ESI MS: 509.2 (M+H)
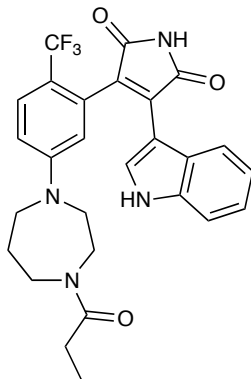
(10) 3-(1H-indol-3-yl)-4-(5-(4-propionyl-1,4-diazepan-1-yl)-2-(trifluoromethyl)phenyl)-1H-pyrrole-2,5-dione.

Prepared as per **8**. Isolated 31 mg (32%). ^{1}H NMR (400 MHz, DMSO-d$_6$): 11.87 (s, 1H), 11.03 (s, 1H), 8.02 (dd, 1H), 7.58 (dd, 1H), 7.38 (dd, 1H), 7.03 (t, 1H), 6.94 (d, 1H), 6.69 (t, 1H), 6.63 (s, 1H), 6.52 (dd, 1H), 3.68-3.21 (m, 6H), 2.86 (m, 2H), 2.18 (m, 2H), 1.63 (m, 1H), 1.35 (m, 1H), 0.90 (m, 3H). ESI-MS: 511.2 (M+H).
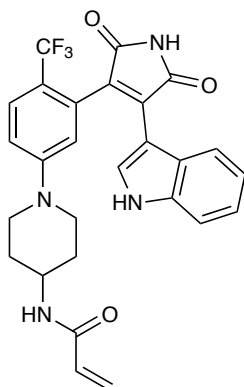
(11) N-(1-(3-(4-(1H-indol-3-yl)-2,5-dioxo-2,5-dihydro-1H-pyrrol-3-yl)-4-(trifluoromethyl)phenyl)piperidin-4-yl)acrylamide.

Prepared as per **7**. Isolated 3.3 mg (7%) of a yellow solid. ^{1}H NMR (400 MHz, (CD$_3$)$_2$CO): 11.14 (s, 1H), 9.84 (s, 1H), 8.09 (s, 1H), 7.63 (d, 1H), 7.43 (d, 1H), 7.14 (d, 1H), 7.09 (m, 1H), 6.95 (d, 1H), 6.79 (m, 1H), 6.26-6.12 (m, 2H), 5.53 (dd, 1H), 3.82 (m, 1H), 3.78 (m, 1H), 2.96 (m, 1H), 1.75 (m, 1H), 1.29 (m, 5H), 0.86 (m, 2H). ESI-MS: 509.2 (M+H).
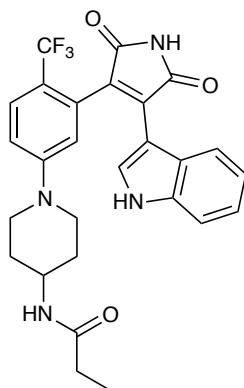
(12) N-(1-(3-(4-(1H-indol-3-yl)-2,5-dioxo-2,5-dihydro-1H-pyrrol-3-yl)-4-(trifluoromethyl)phenyl)piperidin-4-yl)propionamide.

Prepared as per **8**. Isolated was 1.5 mg (2%) of a yellow solid. ^{1}H NMR (400 MHz, DMSO-d$_6$): 11.13 (s, 1H), 9.84 (s, 1H), 8.10 (d, 1 H), 8.00 (s, 1H), 7.73 (m, 1H), 7.63 (d, 1H), 7.43 (d, 1H), 7.08 (m, 1H), 6.93 (m, 1H), 6.78 (m, 1H), aliphatic heavily masked by solvent. ESI-MS: 511.3 (M+H).
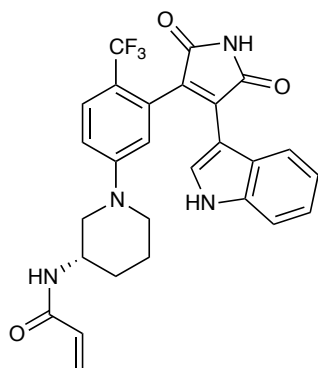
(13) (*S*)-*N*-(1-(3-(4-(1*H*-indol-3-yl)-2,5-dioxo-2,5-dihydro-1*H*-pyrrol-3-yl)-4-(trifluoromethyl)phenyl)piperidin-3-yl)acrylamide.

Prepared as per **7.** Isolated was 1.0 mg (2%) of a yellow solid ^{1}H NMR (400 MHz, DMSO-d_d): 11.86 (s, 1H), 11.04 (s, 1H), 8.08 (dd, *J* = 9.2, 2.3 Hz, 1H), 7.95 (dd, *J* = 28.8, 3.2 Hz, 1H), 7.69 (m, 1H), 7.37 (d, *J* = 8.5 Hz, 1H), 7.14 (dd, *J* = 6.3, 3.8 Hz, 1H), 7.08-7.01 (m, 1H), 6.93 (d, *J* = 24.7 Hz, 1H), 6.57-6.68 (m, 1H), 6.58 (d, *J* = 8.7 Hz, 1H), 6.21 (dd, *J* = 17.3, 9.3 Hz, 1H), 6.16-6.00 (m, 1H), 5.58 (d, *J* = 11.1 Hz, 1H), 3.92-3.54 (m, 2H), 2.82 (m, 1H), 2.66 (m, 1H), 1.87-1.60 (m, 2H), 1.46 (ddd, *J* = 18.6, 15.2, 5.6 Hz, 2H), 1.29-1.08 (m, 1H). ESI-MS: 509.2 (M+H).

Pyrimidine Series

General Synthetic Scheme
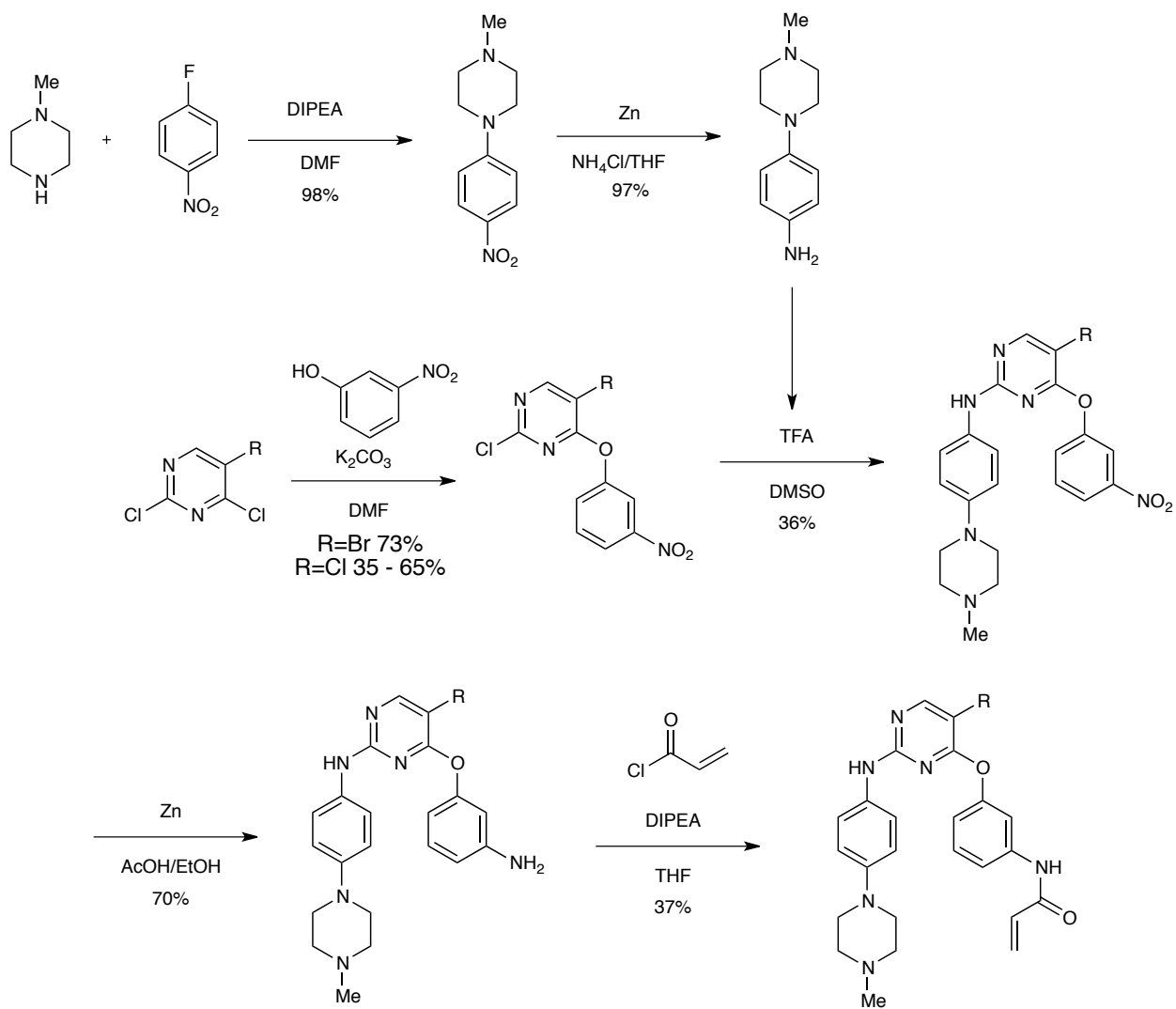
Synthesis and Characterization of Assayed Compounds
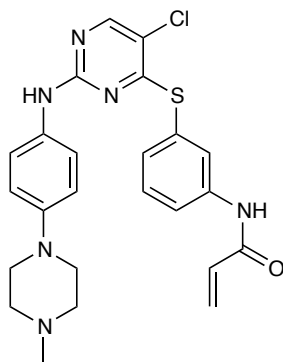
(16) N-(3-((5-chloro-2-((4-(4-methylpiperazin-1-yl)phenyl)amino)pyrimidin-4-yl)thio)phenyl)acrylamide.

To a stirred suspension of the aniline in THF was add diisopropylethylamine (DIPEA, 4.0 eq), and the reaction was stirred at 0 °C. Acryloyl chloride (1.0 eq) was added dropwise and the reaction was stirred for 30 minutes. A second equivalent of acryloyl chloride was added to push the reaction to completion. The reaction was quenched with saturated sodium bicarbonate, extracted with ethyl acetate, dried over magnesium sulfate, concentrated in vacuo and triturated with benzene to give 2 mg (12%) of an off white solid. ^{1}H NMR (600 MHz, DMSO-d$_6$): 10.46 (s, 1H), 9.52 (s, 1H), 8.27 (s, 1H), 8.17 (d, J = 7.3 Hz, 1H), 7.87 (s, 1H), 7.52 (t, J = 8.0 Hz, 1H), 7.34 ? 7.32 (m, 1H), 6.99 (s, 2H), 6.53 (d, J = 8.1 Hz, 2H), 6.43 (dd, J = 16.9, 10.2 Hz, 1H), 6.27 (dd, J = 17.0, 1.9 Hz, 1H), 5.78 (dd, J = 10.1, 1.9 Hz, 1H), 3.02 (s, 4H), 2.62 (s, J = 1.8 Hz, 4H), 2.44 - 2.32 (m, 3H). ESI-MS: 481.2 (M+H), 479.2 (M-H).
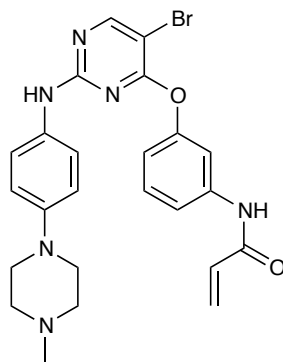
(17) N-(3-((5-bromo-2-((4-(4-methylpiperazin-1-yl)phenyl)amino)pyrimidin-4-yl)oxy)phenyl)acrylamide.

Synthesized as per **16** except purified by prep-HPLC (5-45% ACN in H2O w/0.1% TFA) to give 8.5 mg (35%). ^{1}H NMR (600 MHz, DMSO-d_6): 10.36 (s, 1H), 8.45 (s, 1H), 7.63 (s, 1H), 7.44 (t, J=8.0 Hz, 1H), 7.21 (s, 1H), 6.69 (s, 1H), 6.62 (s, 1H), 6.44 (dd, J=16.9, 10.2 Hz, 1H), 6.26 (d, J=16.9 Hz, 1H), 5.77 (d, J=10.1 Hz, 1H), 2.96 (s, 4H), 2.44-2.38 (m, 4H), 2.20 (s, 3H). ESI-MS: 509.2 (M+H), 507.2 (M-H).
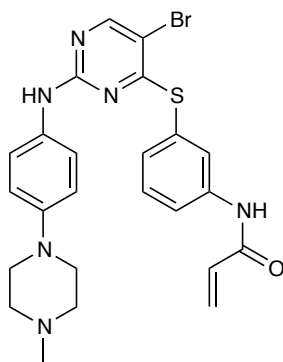
(18) N-(3-((5-bromo-2-((4-(4-methylpiperazin-1-yl)phenyl)amino)pyrimidin-4-yl)thio)phenyl)acrylamide.

Synthesized as per **16** except triturated with toluene to give 6 mg of a white solid (24%). ^{1}H NMR (400 MHz, DMSO-d_6): 10.54 (s, 1H), 9.54 (s, 2H), 8.39 ? 8.26 (m, 1H), 8.23 - 8.13 (m, 1H), 8.05 - 7.92 (m, 1H), 7.89 (d, *J* = 6.5 Hz, 1H), 7.59 - 7.44 (m, 1H), 7.40 - 7.24 (m, 1H), 6.98 (d, *J*

= 7.2 Hz, 1H), 6.67 - 6.45 (m, 2H), 6.27 (dd, *J* = 16.9, 2.0 Hz, 1H), 5.83 - 5.67 (m, 1H), 3.60 (s, 4H), 3.10 (dt, *J* = 14.6, 9.1 Hz, 4H), 2.88 (s, 3H).

(19) N-(3-((5-chloro-2-((4-morpholinophenyl)amino)pyrimidin-4-yl)oxy)phenyl)acrylamide.

Synthesized as per **16** to yield 1.1 mg (8%) of a solid. ESI-MS: 452.2 (M+H).
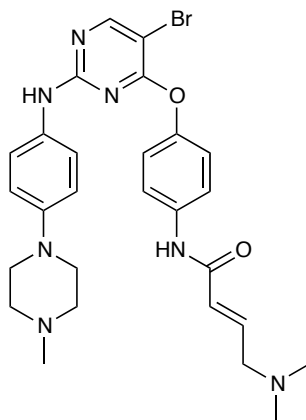
(20) (E)-N-(4-((5-bromo-2-((4-(4-methylpiperazin-1-yl)phenyl)amino)pyrimidin-4-yl)oxy)phenyl)-4-(dimethylamino)but-2-enamide.

To a solution of the aniline (0.14 mmoL) in DMF (1.5 mL) was added 4-(dimethylamino)-2-butenoic acid hydrochloride (26 mg, 0.15 mmoL) and triethylamine (100 μL). The reaction was cooled to 0 C and HATU was added. The reaction was warmed to RT and stirred for 1 hour prior to dilution with ethyl acetate, washing with saturated sodium bicarbonate solution, 5 x H2O, brine and dried over magnesium sulfate prior to HPLC purification and lyophilization, yielding 1 mg (1%) of white powder. ESI-MS: 565.2 (M+H).
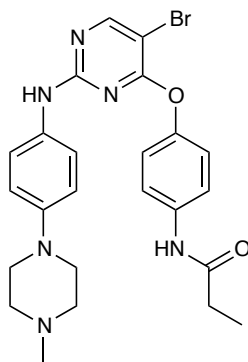
(21) N-(4-((5-bromo-2-((4-(4-methylpiperazin-1-yl)phenyl)amino)pyrimidin-4-yl)oxy)phenyl)propionamide.

To the chloropyrimidine intermediate with the propionamide installed stirred in trifluoroethanol was added 4-(4-Methyl)piperazinoaniline (1.2 eq) and TFA (0.05 mL). The reaction was heated to reflux for 24 hours, concentrated in vacuo and purified by HPLC to yield 7 mg (14%) of a yellow solid. ^{1}H NMR (400 MHz, DMSO-d$_6$): 10.01 (s, 1H), 9.48 (s, 1H), 8.42 (s, 1H), 7.68 (d, J=8.9 Hz, 2H), 7.21-7.09 (M, 4H), 6.62 (s, 2H), 3.02-2.93 (m, 4H), 2.44-2.39 (m, 4H), 2.35 (q, J=7.5 Hz, 2H), 2.20 (s, 3H), 1.12 (t, J=7.6 Hz, 3H). ESI-MS: 511.2 (M+H), 509.1 (M-H).
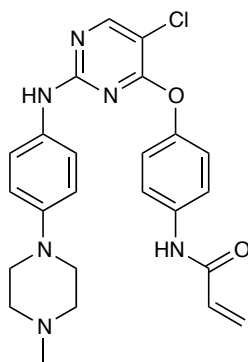
(22) N-(4-((5-chloro-2-((4-(4-methylpiperazin-1-yl)phenyl)amino)pyrimidin-4-yl)oxy)phenyl)acrylamide.

Synthesized as per **16**, yielding 20 mg (37%) of a solid. ^{1}H NMR (400 MHz, CDCl$_3$): 8.21 (s, 1H), 7.66 (d, J = 9.9 Hz, 2H), 7.35 (s, 1H), 7.16 (m, 3H), 6.82-6.75 (m, 3H), 6.48 (dd, J = 16.8, 1.3 Hz, 1H), 6.28 (dd, J = 16.8, 10.2 Hz, 1H), 5.82 (dd, J = 10.2, 1.3 Hz, 1H), 3.11 (m, J = 5.9, 3.9 Hz, 4H), 2.57-2.53 (m, 4H), 2.34 (s, 3H). ESI-MS:
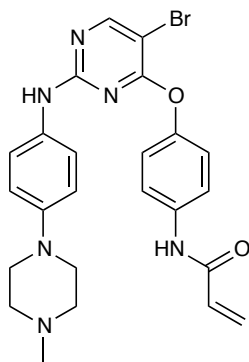
(23) N-(4-((5-bromo-2-((4-(4-methylpiperazin-1-yl)phenyl)amino)pyrimidin-4-yl)oxy)phenyl)acrylamide.

Synthesized as per **16** yielding 21 mg (42%) of a white solid. ^{1}H NMR (400 MHz, CDCl$_3$): 8.30 (s, 1H), 7.66 (d, J=8.3 Hz, 2H), 7.49 (s, 1H), 7.19-7.08 (m, 4H), 6.84 (s, 1H), 6.76 (s, J=8.6 Hz, 2H), 6.48 (dd, J=16.8 Hz, 1.3 Hz, 1H), 6.30 (dd, J=16.9, 10.2 Hz, 1H), 5.81 (dd, J=10.2 Hz, 1.3 Hz), 3.18-3.09 (m, 4H), 2.66-2.57 (m, 4H, 2.38 (s, 3H). ESI-MS: 510.1 (M+H).
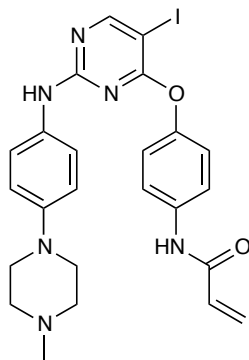
(24) N-(4-((5-iodo-2-((4-(4-methylpiperazin-1-yl)phenyl)amino)pyrimidin-4-yl)oxy)phenyl)acrylamide.

To a white suspension of chloro-pyrimidine acrylamide precursor was added a purple suspension of aniline and the reaction was stirred overnight at 80 °C. The reaction was cooled to RT, concentrated in vacuo, quenched with saturated bicarbonate, extracted with chloroform, dried over sodium sulfate, and purified by SGFC to give 139 mg (13%) of a yellow solid: ^{1}H

NMR (400 MHz, CDCl₃): 10.55 (s, 1H), 8.49 (d, 1H), 7.76 (m, 2H), 7.19-7.10 (m, 4H), 6.8-6.5 (m, 4H), 6.26 (d, 1H), 5.77 (d, 1H), 2.93 (m, 4H), 2.37 (m, 4H), 2.18 (s, 3H). ESI-MS: 557.2 (M+H).

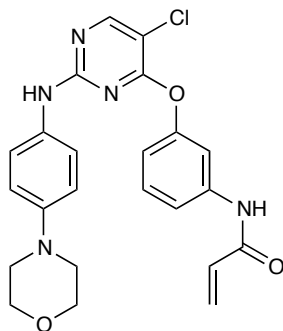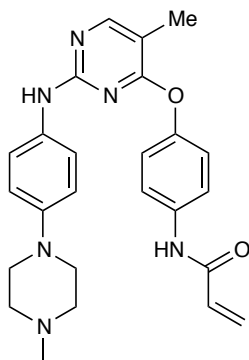**(25) N-(4-((5-methyl-2-((4-(4-methylpiperazin-1-yl)phenyl)amino)pyrimidin-4-yl)oxy)phenyl)acrylamide.**

Synthesized as per **16** except for HPLC purification (5-55%) to yield 1.0 mg of a white solid (10%).
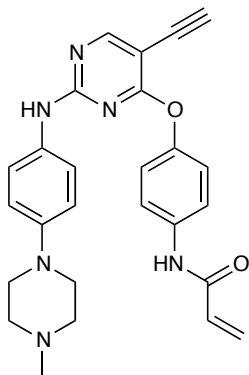
(26) N-(4-((5-ethynyl-2-((4-(4-methylpiperazin-1-yl)phenyl)amino)pyrimidin-4-yl)oxy)phenyl)acrylamide.

The TMS-protected alkyne was dissolved in methanol, potassium carbonate was added and the reaction was stirred for 1 hr at RT. The mixture was evaporated and purified by SGFC (CHCl3:MeOH 95:5 → 90:10) to give 24 mg (34%) of a yellow solid. ^{1}H NMR (400 MHz, DMSO-d₆): 10.29 (s, 1H), 9.4 (s, br, 1H), 8.42 (s, 1H), 7.76 (d, 2H), 7.20 (m, 2H), 7.15 (m, 2H), 6.6 (m,

3H), 6.46-6.26 (m, 2H), 5.82 (dd, 1H), 4.39 (s, 1H), 2.95 (m, 4H), 2.39 (m, 4H), 2.20 (s, 3H).

ESI-MS: 455.1 (M+H).
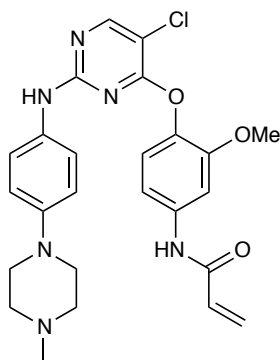
(27) N-(4-((5-chloro-2-((4-(4-methylpiperazin-1-yl)phenyl)amino)pyrimidin-4-yl)oxy)-3-methoxyphenyl)acrylamide.

To the precursor aniline stirred in acetone was added potassium carbonate (1.5 equiv) and the reaction was cooled to 0 C prior to adding acryloyl chloride. After 30 minutes the reaction was concentrated in vacuo and purified by HPLC (5-55% ACN in H2O w/0.1% FA), giving 5 mg (16%) of a white power after lyophylization from benzene. Purity and identity confirmed by LC/MS. ESI-MS: 495.3 (M+H), 493.2 (M-H).
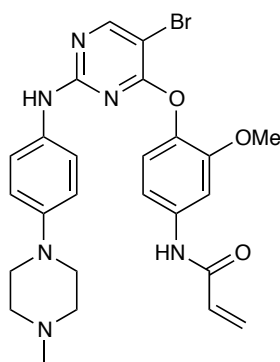
(28) N-(4-((5-bromo-2-((4-(4-methylpiperazin-1-yl)phenyl)amino)pyrimidin-4-yl)oxy)-3-methoxyphenyl)acrylamide.

Synthesized as per **27**, yielding <1 mg (<1%). Purity and identity confirmed by LC/MS. ESI-MS: M+H 539.1 (M+H).
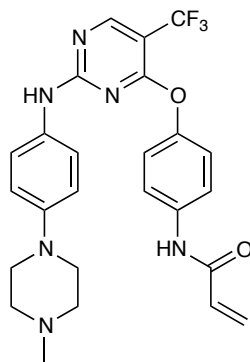
(29) N-(3-methoxy-4-((2-((4-(4-methylpiperazin-1-yl)phenyl)amino)-5-(trifluoromethyl)pyrimidin-4-yl)oxy)phenyl)acrylamide.

Synthesized as per **16**. Isolated was 15.1 mg (21%) of a pale yellow solid. ^{1}H NMR (400 MHz, DMSO-d$_6$): 10.70 (s, 1h), 10.10 (s, 1H), 8.7 (s, 1H), 7.55 (m, 2H), 7.26 (d, 2H), 7.15 (m, 2H), 6.65-6.5 (m, 3H), 6.35 (d, 1H), 5.8 (d, 1H), 2.95 (m, 4H), 2.4 (m, 4H), 2.19 (s, 3H). ESI-MS: 499.1 (M+H).

Pyrrolopyrimidines

Synthetic Scheme
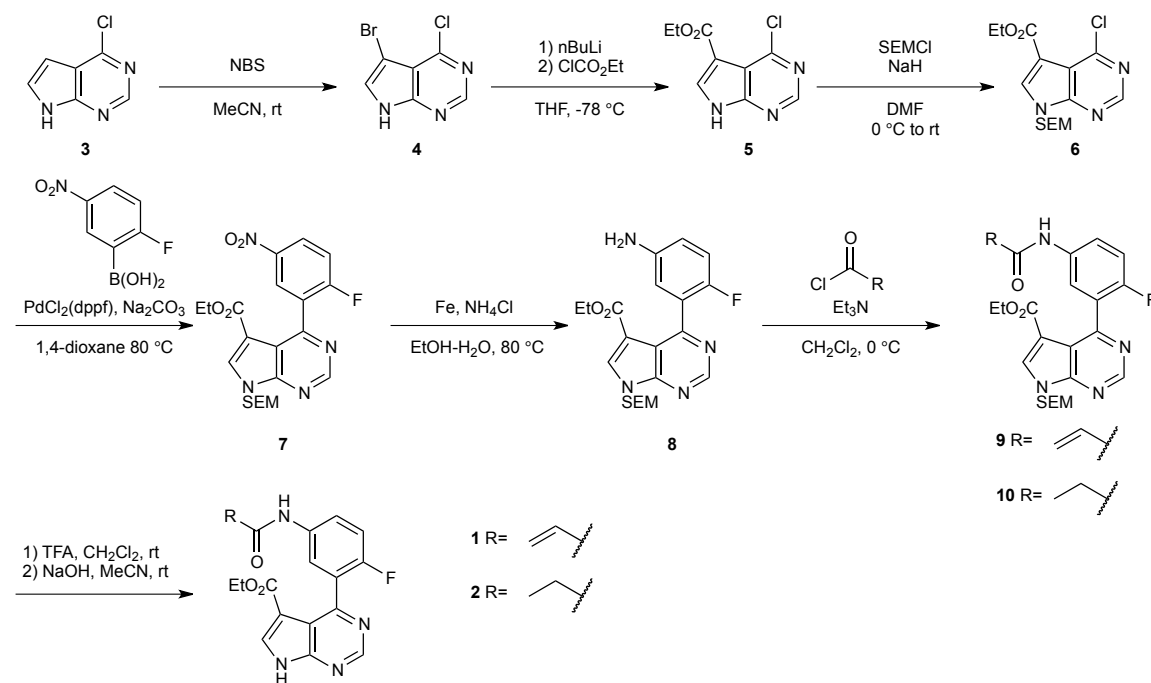
Synthesis and Characterization of Assayed Compounds
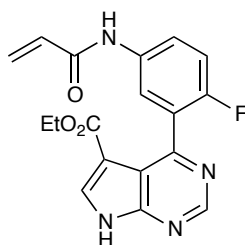
(30) ethyl 4-(5-acrylamido-2-fluorophenyl)-7H-pyrrolo[2,3-d]pyrimidine-5-carboxylate.

See Chapter 3.
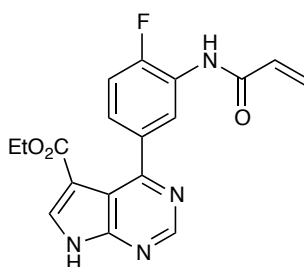
(31) ethyl 4-(3-acrylamido-4-fluorophenyl)-7H-pyrrolo[2,3-d]pyrimidine-5-carboxylate.

Synthesized as per **30** to give 41 mg (80% of a yellow solid. ^{1}H NMR (400 MHz, DMSO): 10.05 (s, 1H), 8.91 (s, 1H), 8.39 (d, *J* = 6.9 Hz, 1H), 8.31 (d, *J* = 2.5 Hz, 1H), 7.39 (dd, *J* = 17.4, 6.4 Hz, 2H), 6.65 (dd, *J* = 16.9, 10.0 Hz, 1H), 6.27 (d, *J* = 17.1 Hz, 1H), 5.78 (d, *J* = 10.2 Hz, 1H), 3.91 (q, *J* = 7.1 Hz, 2H), 0.91 (t, *J* = 7.1 Hz, 3H). ESI-MS: 355.3 (M+H).
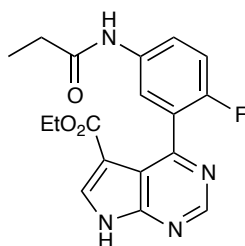
(32) ethyl 4-(2-fluoro-5-propionamidophenyl)-7H-pyrrolo[2,3-d]pyrimidine-5-carboxylate.

See Chapter 3.
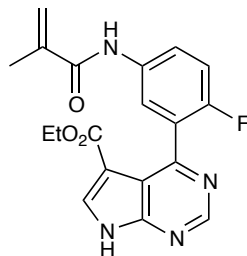
(33) ethyl 4-(2-fluoro-5-methacrylamidophenyl)-7H-pyrrolo[2,3-d]pyrimidine-5-carboxylate

As per **30**. Isolated 70 mg (80%) of a yellow solid. ^{1}H NMR (400 MHz, DMSO-d_6): 9.95 (s, 1h), 8.96 (s, 1H), 8.33 (s, 1H), 8.06 (dd, 1H), 7.85 (dd, 1H), 7.2 (m, 1H), 5.85 (s, 1H), 5.53 (s,1H), 3.92 (s, br, 2H), 1.96 (s, 3H), 0.96 (t, 3H). ESI-MS: 369.0 (M+H).
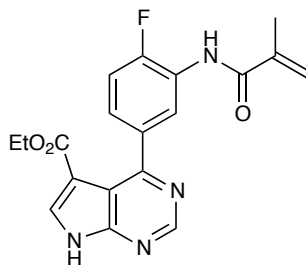
(34) ethyl 4-(4-fluoro-3-methacrylamidophenyl)-7H-pyrrolo[2,3-d]pyrimidine-5-carboxylate.

Deprotected as per **30** yielding 30 mg (79%) of a white solid. ^{1}H NMR (400 MHz, DMSO-d_6): 9.66 (s, 1H), 8.88 (s, 1H), 8.30 (s 1H), 7.88 (dd, 1H), 7.43 (m, 1H), 7.34 (m, 1H), 5.87 (s, 1H), 5.54 (s, 1H), 3.92 (q, 2H), 1.94 (s, 3H), 0.90 (t, 3 H). ESI-MS: 369.3 (M+H).
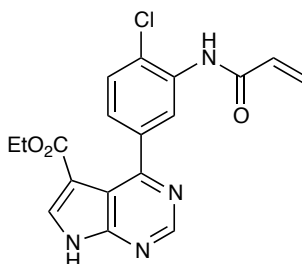
(35) ethyl 4-(3-acrylamido-4-chlorophenyl)-7H-pyrrolo[2,3-d]pyrimidine-5-carboxylate.

Deprotected as per **30** yielding 34 mg (91%) of a white solid. ^{1}H NMR (400 MHz, DMSO-d$_6$):

9.78 (s, 1H), 8.91 (s, 1H), 8.12 (s, 1H), 7.60 (d, 1H), 7.44 (dd, 1H), 6.64 (dd, 1H), 6.25 (d, 1H),

5.77 (dd, 1H), 3.91 (q, 2H), 0.89 (t, 3H). ESI-mS: 371.3 (M+H).
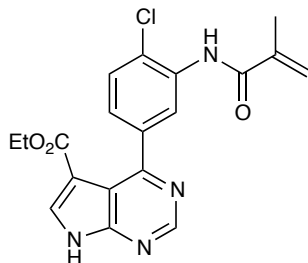
(36) ethyl 4-(4-chloro-3-methacrylamidophenyl)-7H-pyrrolo[2,3-d]pyrimidine-5-carboxylate.

Deprotected as per **30** yielding 42 mg (89%) of a white solid. ^{1}H NMR (400 MHz, DMSO-d$_6$):

9.53 (s, 1H), 8.92 (s, 1H), 8.34 (s, 1H), 7.91 (d, 1H), 7.61 (d, 1H), 7.46 (dd, 1H), 5.92 (d, 1H),

5.56 (m, 1H), 3.94 (q, 2H), 1.97 (m, 3H), 0.93 (t, 3H). ESI-MS: 385.3 (M+H).
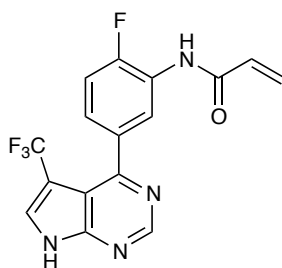
(37) N-(2-fluoro-5-(5-(trifluoromethyl)-7H-pyrrolo[2,3-d]pyrimidin-4-yl)phenyl)acrylamide.

Deprotected as per **30** to give 29 mg (95%) of a white solid. ^{1}H NMR (400 MHz, DMSO-d$_6$):

10.20 (s, 1H), 9.01 (s, 1H), 8.94 (d, *J* = 7.5 Hz, 1H), 8.06 – 7.98 (m, 1H), 7.50 (dd, *J* = 10.8, 8.6

Hz, 2H), 6.68 (dd, *J* = 17.1, 10.1 Hz, 1H), 6.34 (dd, *J* = 17.0, 1.8 Hz, 1H), 5.83 (dd, *J* = 10.2, 1.7

Hz, 1H). ESI-MS: 351.3 (M+H).
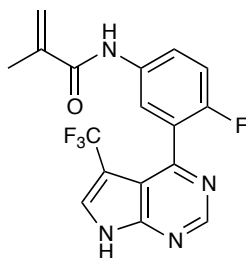
(38) N-(4-fluoro-3-(5-(trifluoromethyl)-7H-pyrrolo[2,3-d]pyrimidin-4-yl)phenyl)methacrylamide.

Deprotected as per **30** to yield 20 mg (87%) of a white solid. ^{1}H NMR (400 MHz, DMSO-d$_6$): 9.80 (s, 1H), 9.02 (s, 1H), 8.44 (dd, J = 7.4, 2.1 Hz, 1H), 8.19 – 8.01 (m, 1H), 7.50 (dd, J = 19.3, 9.2 Hz, 2H), 5.94 (s, 1H), 5.60 (s, 2H), 1.99 (s, 3H). ESI-MS: 365.3 (M+H).
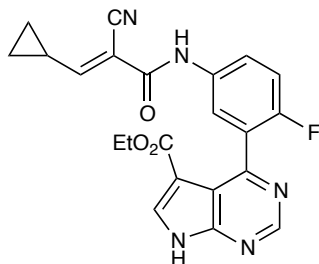
(39) (E)-ethyl 4-(5-(2-cyano-3-cyclopropylacrylamido)-2-fluorophenyl)-7H-pyrrolo[2,3-d]pyrimidine-5-carboxylate.

Deprotected as per **30** to yield 5.0 mg (60%) of a solid. ^{1}H NMR (400 MHz, DMSO-d$_6$): 10.22 (s, 1H), 8.96 (s, 1H), 8.39 – 8.29 (m, 1H), 7.97 (dd, J = 6.5, 2.8 Hz, 1H), 7.85 – 7.74 (m, 1H), 7.29 – 7.19 (m, 1H), 7.12 (d, J = 11.0 Hz, 1H), 2.03 – 1.92 (m, 1H), 1.26 (dt, J = 42.4, 13.4 Hz, 4H), 0.95 (t, J = 7.1 Hz, 3H). ESI-MS: 420.3 (M+H).
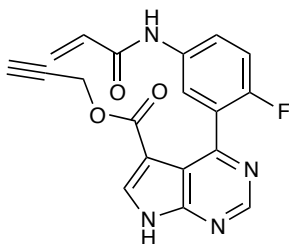
(40) prop-2-yn-1-yl 4-(5-acrylamido-2-fluorophenyl)-7H-pyrrolo[2,3-d]pyrimidine-5-carboxylate.

Deprotected as per **30** to yield 9.3 mg (79%) of a pale yellow solid. ^{1}H NMR (400 MHz, DMSO-d$_6$): 10.31 (s, 1H), 8.98 (s, 1H), 8.41 (d, J = 2.4 Hz, 1H), 8.03 (s, 1H), 7.80 (s, 1H), 7.25 – 7.15 (m, 1H), 6.44 (dd, J = 16.9, 10.2 Hz, 1H), 6.27 (d, J = 15.6 Hz, 1H), 5.78 (d, J = 10.0 Hz, 1H), 4.58 (s, 1H), 3.50 – 3.36 (m, 2H). ESI-MS: 365.0 (M+H).

2.6 Acknowledgements

Compounds 19, 22 and 25 were synthesized and biochemically characterized by Adolfo Cuesta.

Kenji Uchida synthesized compounds 29-39.

2.7 References

1. O'Shea, J. J., Pesu, M., Borie, D. C. & Changelian, P. S. A new modality for immunosuppression: targeting the JAK/STAT pathway. *Nat. Rev. Drug Discov.* **3,** 555–564 (2004).

2. Goedken, E. R. *et al.* Tricyclic covalent inhibitors selectively target Jak3 through an active site thiol. *J. Biol. Chem.* **290,** 4573–4589 (2015).

3. Changelian, P. S. *et al.* The specificity of JAK3 kinase inhibitors. *Blood* **111,** 2155–2157 (2008).

4. Haan, C. *et al.* Jak1 Has a Dominant Role over Jak3 in Signal Transduction through γc-Containing Cytokine Receptors. *Chem. Biol.* **18,** 314–323 (2011).

5. Changelian, P. S. *et al.* Prevention of organ allograft rejection by a specific Janus kinase 3 inhibitor. *Science* **302,** 875–878 (2003).

6. Clark, J. D., Flanagan, M. E. & Telliez, J.-B. Discovery and development of Janus kinase (JAK) inhibitors for inflammatory diseases. *J. Med. Chem.* **57,** 5023–5038 (2014).

7. Cutolo, M. & Marianna meroni. Clinical utility of the oral JAK inhibitor tofacitinib in the treatment of rheumatoid arthritis. *JIR* 129 (2013). doi:10.2147/JIR.S35901

8. Lin, T. H. *et al.* Selective functional inhibition of JAK-3 is sufficient for efficacy in collagen-induced arthritis in mice. *Arthritis & Rheumatism* **62,** 2283–2293 (2010).

9. Thoma, G. *et al.* Identification of a Potent Janus Kinase 3 Inhibitor with High Selectivity within the Janus Kinase Family. *J. Med. Chem.* **54,** 284–288 (2010).

10. Cohen, M. S., Zhang, C., Shokat, K. M. & taunton, J. Structural Bioinformatics-Based Design of Selective, Irreversible Kinase Inhibitors. *Science* **308,** 1318 (2005).

11. Henise, J. C. & Taunton, J. Irreversible Nek2 Kinase Inhibitors with Cellular Activity. *J. Med. Chem.* 110531114757055 (2011). doi:10.1021/jm200222m

12. Miller, R. M., Paavilainen, V. O., Krishnan, S., Serafimova, I. M. & Taunton, J. Electrophilic Fragment-Based Design of Reversible Covalent Kinase Inhibitors. *JACS* 130329160430004 (2013). doi:10.1021/ja401221b

13. Bradshaw, J. M. *et al.* Prolonged and tunable residence time using reversible covalent kinase inhibitors. *Nat. Chem. Bio.* **11,** 525–531 (2015).

14. Schwartz, P. A. *et al.* Covalent EGFR inhibitor analysis reveals importance of reversible interactions to potency and mechanisms of drug resistance. *Proc. Natl Acad. Sci. USA* **111,** 173–178 (2014).

15. Kim, S.-H. & Lee, C.-E. Counter-regulation mechanism of IL-4 and IFN-α signal transduction through cytosolic retention of the pY-STAT6:pY-STAT2:p48 complex. *Eur. J. Immunol.* **41,** 461–472 (2010).

16. Kluge, A. F. *et al.* Heteroaryl compounds and uses thereof. WIPO Patent WO158571/A1 (2009).

17. Zhou, W. *et al.* Novel mutant-selective EGFR kinase inhibitors against EGFR T790M. *Nature* **462,** 1070–1074 (2009).

18. Schaeffer, E. M. *et al.* Requirement for Tec kinases Rlk and Itk in T cell receptor signaling and immunity. *Science* **284,** 638–641 (1999).

19. Bourke, D. G. *et al.* Thiopyrimidine-Based Compounds and uses thereof. WIPO WO092199A1 (2008).

20. Ahearn, S. P. *et al.* Pyrrolopyrimidines as Janus Kinase Inhibitors. 1–212 (2013).

21. Ward, R. A. *et al.* Structure- and reactivity-based development of covalent inhibitors of the activating and gatekeeper mutant forms of the epidermal growth factor receptor (EGFR). *J. Med. Chem.* **56,** 7025–7048 (2013).

22. Serafimova, I. M. *et al.* Reversible targeting of noncatalytic cysteines with chemically

tuned electrophiles. *Nat. Chem. Bio.* **8,** 471–476 (2012).

23. Bunnage, M. E., Chekler, E. L. P. & Jones, L. H. Target validation using chemical probes. *Nat. Chem. Bio.* **9,** 195–199 (2013).

24. Miller, R. M. & Taunton, J. *Methods in Enzymology* **548,** 93–116 (2014).

25. O'Gorman, W. E. *et al.* The Initial Phase of an Immune Response Functions to Activate Regulatory T Cells. *J. Immunol.* **183,** 332–339 (2009).

26. Economopoulos, V., Noad, J. C., Krishnamoorthy, S., Rutt, B. K. & Foster, P. J. Comparing the MRI Appearance of the Lymph Nodes and Spleen in Wild-Type and Immuno-Deficient Mouse Strains. *PLoS ONE* **6,** e27508 (2011).

27. Hechinger, A.-K. *et al.* Therapeutic activity of multiple common γ-chain cytokine inhibition in acute and chronic GVHD. *Blood* **125,** 570–580 (2015).

28. Schroeder, M. A. & DiPersio, J. F. Mouse models of graft-versus-host disease: advances and limitations. *Disease Models & Mechanisms* **4,** 318–333 (2011).

29. Hakim, F., Fowler, D. H., Shearer, G. M. & Gress, R. E. in *Current Protocols in Immunology* (John Wiley & Sons, Inc., 1998). doi:10.1002/0471142735.im0403s27

30. Spoerl, S. *et al.* Activity of therapeutic JAK 1/2 blockade in graft-versus-host disease. *Blood* **123,** 3832–3842 (2014).

31. Farmer, L. J. *et al.* Discovery of VX-509 (Decernotinib): A Potent and Selective Janus Kinase 3 Inhibitor for the Treatment of Autoimmune Diseases. *J. Med. Chem.* **58,** 7195–7216 (2015).

32. Fleischmann, R. M. *et al.* A randomized, double-blind, placebo-controlled, twelve-week, dose-ranging study of decernotinib, an oral selective JAK-3 inhibitor, as monotherapy in patients with active rheumatoid arthritis. *Arthritis Rheumatol* **67,** 334–343 (2015).

33. Souto, A. *et al.* Lipid profile changes in patients with chronic inflammatory arthritis treated with biologic agents and tofacitinib in randomized clinical trials: a systematic review and meta-analysis. *Arthritis Rheumatol* **67,** 117–127 (2015).

34.   London, N. *et al.* Covalent docking of large libraries for the discovery of chemical probes. *Nat. Chem. Bio.* **10,** 1066–1072 (2014).

35.   Tan, L. *et al.* Development of Selective Covalent Janus Kinase 3 Inhibitors. *J. Med. Chem.* **58,** 6589–6606 (2015).

36.   Smith, G. A., Uchida, K., Weiss, A. & Taunton, J. Essential biphasic role for JAK3 catalytic activity in IL-2 receptor signaling. *Nat. Chem. Bio.* **12,** 373–379 (2016).

37.   Thorarensen, A. *et al.* Design of a Janus Kinase 3 (JAK3) Specific Inhibitor 1-((2S,5R)-5-((7H-Pyrrolo[2,3-d]pyrimidin-4-yl)amino)-2-methylpiperidin-1-yl)prop-2-en-1-one (PF-06651600) Allowing for the Interrogation of JAK3 Signaling in Humans. *J. Med. Chem.* **60,** 1971–1993 (2017).

38.   Telliez, J.-B. *et al.* Discovery of a JAK3-Selective Inhibitor: Functional Differentiation of JAK3-Selective Inhibition over pan-JAK or JAK1-Selective Inhibition. *ACS Chem. Biol.* **11,** 3442–3451 (2016).

39.   Elwood, F. *et al.* Evaluation of JAK3 biology in autoimmune disease using a highly selective, irreversible JAK3 inhibitor. *J. Pharmacol. Exp. Ther.* (2017). doi:10.1124/jpet.116.239723 (ASAP).

Chapter 3   Essential Biphasic Role for JAK3 Catalytic Activity in IL-2 Signaling

3.1 Abstract

To drive lymphocyte proliferation and differentiation, common g-chain (gc) cytokine receptors require hours to days of sustained stimulation. While JAK1 and JAK3 kinases are found together in all gc-receptor complexes, it is not known how their respective catalytic activities contribute to signaling over time. Here, we dissect the temporal requirements for JAK3 kinase activity with a selective covalent inhibitor (JAK3i). By monitoring STAT5 phosphorylation over 20 hours in IL-2-stimulated CD4+ T cells, we document a previously unappreciated second wave of signaling that is much more sensitive to JAK3i than the first wave. Selective inhibition of this second wave is sufficient to block cyclin expression and S-phase entry. An inhibitor-resistant JAK3 mutant (Cys905Ser) rescued all effects of JAK3i in isolated T cells and in mice. Our chemical genetic toolkit elucidates a biphasic requirement for JAK3 kinase activity in IL-2-driven T-cell proliferation and will find broad utility in studies of gc-receptor signaling.

3.2   Introduction

The common gamma chain (γ_c) receptor cytokines (IL-2, 4, 7, 9, 15 and 21) are essential for lymphocyte development, survival, differentiation and proliferation[1]. All six of these cytokines signal by engaging a receptor complex comprising the common gamma chain (IL-2Rγ, CD132) and one or two additional chains. These receptors have no intrinsic kinase activity. Hence, the tightly associated cytoplasmic kinases, JAK1 (bound to IL-2Rβ and others) and JAK3 (bound to IL-2Rγ)[2], are required for signal transduction and are clinically validated targets for the treatment of autoimmune diseases[1,3]. In the prototypical case of IL-2, ligand binding rapidly triggers the phosphorylation of 3 tyrosines within the IL-2Rβ cytoplasmic tail (Y341, Y395, Y498) and the subsequent recruitment, phosphorylation, and activation of the transcription factor STAT5. In addition, IL-2 receptor ligation activates the PI3K/AKT and MEK/ERK pathways via the recruited adapter protein Shc[4]. Genetic studies indicate that among these downstream signaling events, STAT5 activation is especially critical, enabling full lymphocyte expansion *in vitro* and *in vivo* as well as immune regulation by CD4+ regulatory T-cells[5-8].

Loss of JAK3 in mice and humans results in severely compromised T-cell function[9,10]. Nevertheless, the requirement for JAK3 kinase activity downstream of IL-2R and other γ_c cytokine receptors remains controversial. Critical tyrosines on IL-2Rβ and STAT5 are likely phosphorylated by JAK1 and/or JAK3, but none of these phosphorylation events have been uniquely attributed to either kinase[11]. Interestingly, a recent study concluded that JAK1 kinase activity is necessary and sufficient for IL-2-stimulated STAT5 phosphorylation, whereas JAK3 kinase activity is dispensable[12]. Instead, JAK3 was proposed to play an essential scaffolding role. These conclusions were based primarily on experiments in cell lines expressing combinations of kinase-dead and analog-sensitive JAK1/3 mutants. Moreover, and of particular relevance to the work presented here, signaling events were only followed for one hour after IL-2 stimulation.

The temporal requirements for JAK3 kinase activity in driving cytokine-induced cell proliferation are completely unknown. Is a transient pulse of JAK3 activity sufficient to drive quiescent T cells into S-phase (DNA synthesis), or is sustained JAK3 signaling required? As is true for other γ_c cytokine-driven processes[13-16], T-cell proliferation requires at least 6 hours of continuous exposure to IL-2[17]. Yet, receptor-proximal signaling events (e.g., IL-2Rβ and STAT5 phosphorylation) are most often assessed at early time points (< 1 hr) after receptor stimulation. The relative contributions of JAK1 and JAK3 kinase activity to cell proliferation, and how they evolve over time, is a central unanswered question in JAK-STAT signaling.

To define the temporal requirements for JAK3 kinase activity in a manner not achievable with genetic knockout approaches, we employed a highly selective inhibitor, JAK3i. Like other recently reported JAK3-selective inhibitors[18-20], JAK3i forms a covalent bond with a cysteine found in JAK3, but not the closely related kinase domains in JAK1, JAK2, or TYK2. We exploited the nonessential nature of this cysteine to generate an inhibitor-resistant JAK3 mutant (Cys905Ser). This combined chemical and genetic toolkit revealed new insights into JAK3 signaling requirements in the context of IL-2-stimulated primary CD4+ T cells. Contrary to the report described above[12], we find that JAK3 kinase activity is absolutely essential for STAT5 phosphorylation. Through detailed time-course experiments, we characterize a previously unreported second wave of STAT5 phosphorylation that is sustained for at least 10 hours after IL-2 addition. This second, more prolonged wave of signaling is exquisitely sensitive to JAK3 inhibition and is essential for T-cell proliferation. Finally, we demonstrate that JAK3i abolishes IL-2-driven T-cell proliferation in mice, a phenotype that is completely rescued by C905S JAK3.

3.3   Results

JAK3i is selective for JAK3 over closely related kinases

To dissect the role of JAK3 in γ_c-receptor signaling, we sought a highly selective chemical probe that would allow us to study signaling with temporal control and without perturbing lymphocyte development. However, the discovery of JAK3-selective inhibitors has proven challenging due to the nearly identical ATP binding sites shared between all JAK-family kinase domains[21]. Although we recently identified reversible covalent JAK3 inhibitors with selectivity over other JAK-family kinases by targeting a cysteine unique to JAK3 (Figure 3-1 **a**)[18], these compounds were not sufficiently potent for cellular studies and lacked selectivity toward other cysteine-containing kinases such as ITK, a critical T-cell kinase[22]. As an alternative, we identified a series of acrylamide-containing pyrrolopyrimidines, exemplified by JAK3i (Figure 3-1 **b**), in a patent application[23]. Although compounds related to JAK3i were reported to inhibit JAK3 with subnanomolar potency in biochemical assays, no data were provided on the activity of these compounds in cells or animals.

a

```
              Gatekeeper
JAK1 953 LIMEFLPSGSLKEYLPK 969
JAK2 927 LIMEYLPYGSLRDYLQK 943
JAK3 896 LVMEYLPSGCLRDFLQR 912
TYK2 969 LVMEYVPLGSLRDYLPR 985
```

b

JAK3i (1)

c   In Vitro Selectivity within JAK Family

Kinase	IC_{50} (nM)
JAK1	1,520
JAK2	8,680
JAK3	0.43
TYK2	>10,000

(100 µM ATP)

d In Vitro Selectivity vs. kinases containing similar cysteine

Kinase	IC_{50} (nM)
JAK3	7.43
BTK	363
ITK	4630
EGFR	>10,000

(1 mM ATP)

Figure 3-1 In Vitro Selectivity.
a) JAK Family Sequence Alignment. b) Structure of JAK3i. c) In vitro selectivity profile among JAK-family (100 mM ATP). d) In vitro selectivity profile among kinases with similar cysteine (1 mM ATP).

JAK3i was highly selective in biochemical kinase assays, with >3,000-fold selectivity for JAK3 over the closely related kinases JAK1, JAK2, and TYK2 (Figure 3-1 **c**). In addition to JAK3, 9 other kinases share a structurally equivalent cysteine. They include the TEC-family kinases, which play an important role in antigen receptor signaling[22]. When tested against a small panel of these kinases in the presence of physiological ATP, JAK3i was also highly selective for JAK3: 1,300-fold vs. EGFR, 600-fold vs. ITK and 50-fold vs. BTK (Figure 3-1 **d**).

JAK3i differentially affects IL-2 signaling events

The high selectivity of JAK3i within the JAK family enabled us to elucidate the specific requirements for JAK3 catalytic activity in γ_c-receptor signaling. For these experiments, we isolated primary murine CD4+ T cells and activated them via plate-bound αCD3 and αCD28 to induce expression of the high-affinity IL-2 receptor. We then monitored IL-2-stimulated STAT5 phosphorylation by FACS. Contrary to an earlier chemical genetic study[12], we found that JAK3 kinase activity was absolutely required for STAT5 phosphorylation (pSTAT5) after 15 minutes of IL-2 stimulation (IC_{50} 47 nM, Figure 3-2 **a-b**). Our finding is consistent with a recently published report in which a structurally distinct, irreversible JAK3 inhibitor was found to block STAT5 phosphorylation at early time points[19]. The effect of JAK3-selective inhibitors on later IL-2-driven signaling events has not been reported and is the primary focus of our study.
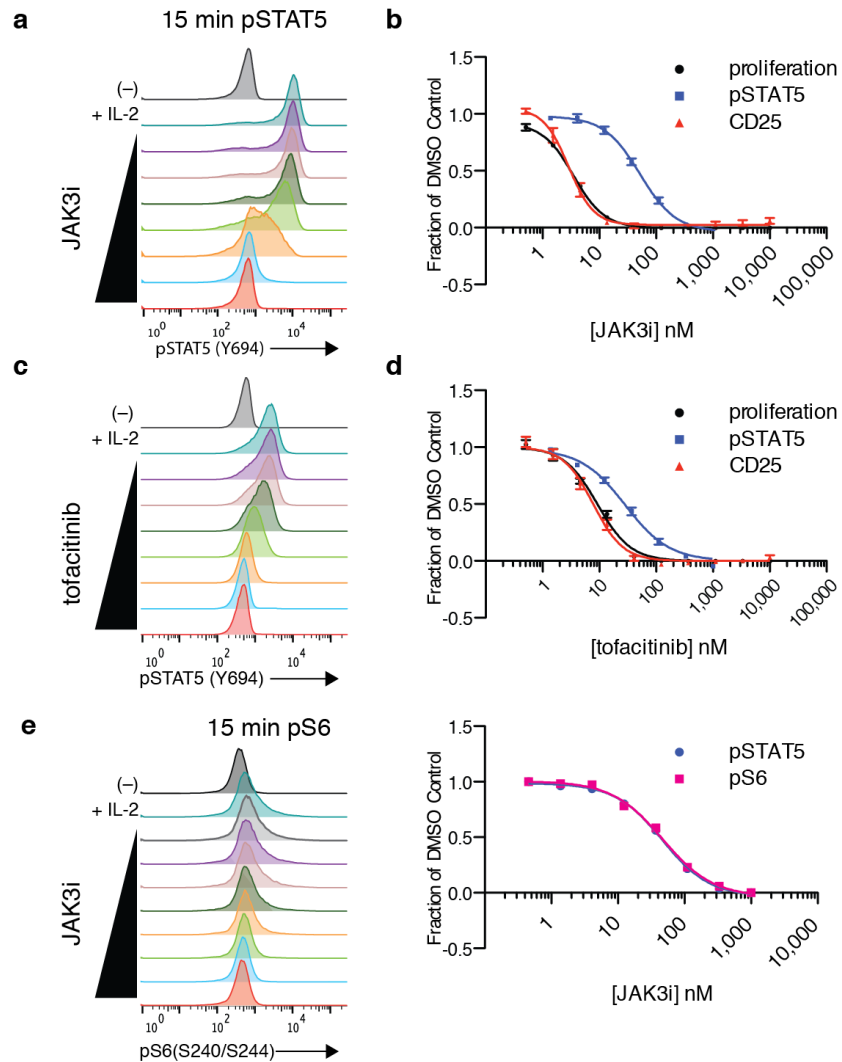
Figure 3-2 Early and late signaling events are differential affected by JAK3i.
CD4+ T-cell blasts were pretreated for 2 hrs with indicated dose of JAK3i (a–b, e) or tofacitinib (c–d) and stimulated with IL-2 (50 u/mL). (a & c) STAT5 phosphorylation was monitored by phosphoflow 15 min after IL-2 stimulation. (c & d) Dose-response curves comparing effects on pSTAT5, proliferation, and CD25 upregulation. Proliferation was assessed by ^{3}H-thymidine uptake after 24-48 hrs. CD25 (IL-2Ra) upregulation was quantified by FACS after 24 hrs (see Figure 3-1 for FACS histograms). e) S6 phosphorylation (Ser240/244) was monitored by phosphoflow in parallel with pSTAT5 after 15 minutes of IL-2 stimulation. See Figure 3-5 **c** for corresponding pSTAT5 histograms. Data in a,c & e are representative of 5, 8 and 2 independent experiments. Data in b are cumulative of 6 (proliferation) and 4 (pSTAT5 & CD25) independent experiments, plotted as mean ± SEM. Data in c are cumulative of 3 (proliferation), 7 (pSTAT5) and 5 (CD25) independent experiments, plotted as mean ± SEM. See **Table 3-1** average IC$_{50}$ values from all experiments.

Table 3-1 Cellular effects of JAK3i and tofacitinib.

	JAK3i	Tofacitinib (pan-JAKi)
pSTAT5 (15 min)	47.2 ± 4.5 (n=5)	24.7 ± 5.7 (n=8)
CD25	3.1 ± 0.9 (n=7)	7.7 ± 4.9 (n=7)
proliferation	3.7 ± 1.6 (n=9)	12.5 ± 5.6 (n=13)
		IC_{50} in nM

Average IC_{50} values ± S.D. from all experiments assessing effects of JAK3i and tofacitinib on 15 min pSTAT5, CD25 upregulation and proliferation as described in Figure 3-2. n refers to the number of independent experiments, which were each 10-pt, 3-fold titrations from 10 µM to 0.51 nM or 1 µM to 0.05 nM (CD25 and proliferation), or 7-pt, 3 fold titrations from 1 µM to 1.37 nM (pSTAT5). Each proliferation experiment was conducted in technical triplicate.

a 24h CD25

b IL-2 stimulated IFN-γ production
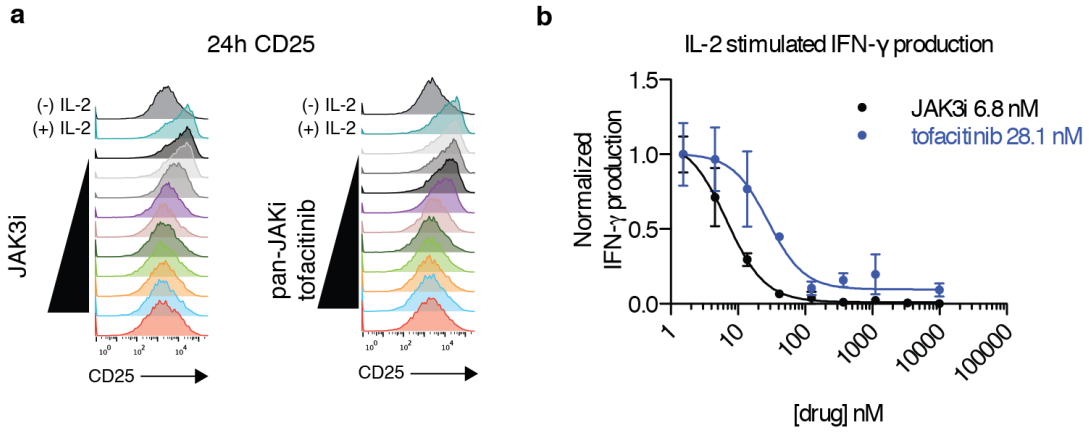
Figure 3-3 Role of JAK3 in downstream readouts.
(a) FACS Histograms of CD25 upregulation after 24 hours of IL-2 stimulation in the presence of JAK3i or tofacitinib, as graphed in **Fig. 2 b,d**. (b) JAK3i potently inhibits IL-2 stimulated IFN-γ production, measured by ELISA after 24 hours. Plotted as mean ± SEM of triplicates. Data are representative of 7 (a) and 2 (b) independent experiments.

To our surprise, three downstream readouts of IL-2 signaling, all measured at 24-48 hours after stimulation, were much more sensitive to JAK3i (IC_{50} 3-7 nM), with significant inhibition occurring at concentrations that had no effect on pSTAT5: (1) upregulation of IL-2Rα (CD25) at 24 hours (IC_{50} 3.1 nM, Figure 3-3 **a** and Figure 3-2 **b**); (2) proliferation, quantified by ^{3}H-thymidine uptake from 24-48 hours (IC_{50} 3.7 nM, Figure 3-2 **b**); (3) IFN-γ production at 24 hours (IC_{50} 6.8 nM, Figure 3-3 **b**). This disconnect between early and late signaling readouts was less pronounced with the pan-JAK inhibitor tofacitinib[21]. Rather, tofacitinib's concentration-dependent effects on early pSTAT5 more closely mirrored its effects on CD25 upregulation, T-cell proliferation, and IFN-γ production (Figure 3-2 **c-d** and Figure 3-3 **b**), as expected given that all three processes require STAT5-mediated transcription. Thus, in contrast to tofacitinib, a JAK3-selective inhibitor can prevent critical STAT5-dependent processes (e.g., T-cell proliferation) in the absence of any effect on early STAT5 phosphorylation. This suggests that the requirements for JAK3 (and possibly, JAK1) catalytic activity change over time, a possibility we address in greater detail below.

The apparent disconnect between JAK3i effects on early pSTAT5 and downstream readouts could potentially be explained by inhibition of MEK/ERK or PI3K/mTOR pathways, both of which are canonically activated by IL-2[4]. In our primary CD4+ T-cell blasts, we detected very little phospho-ERK (Figure 3-4 **a**), and MEK/ERK signaling was dispensable for proliferation (Figure 3-4 **b**). By contrast, inhibition of PI3K, AKT or mTOR was sufficient to abolish IL-2-stimulated proliferation (Figure 3-5 **a**), consistent with prior studies in human T-cell lines[24]. Upon stimulation with IL-2 for 15 minutes, we consistently detected a small induction of phosphorylated ribosomal protein S6 (a p70S6K substrate and proxy for PI3K and mTOR signaling[25]) by phosphoflow (Figure 3-5 **b**). This induction was blocked by JAK3i, but with an equivalent IC_{50} to pSTAT5 (Figure 3-2 **e**), suggesting that these two processes have similar requirements for JAK3 catalytic activity.
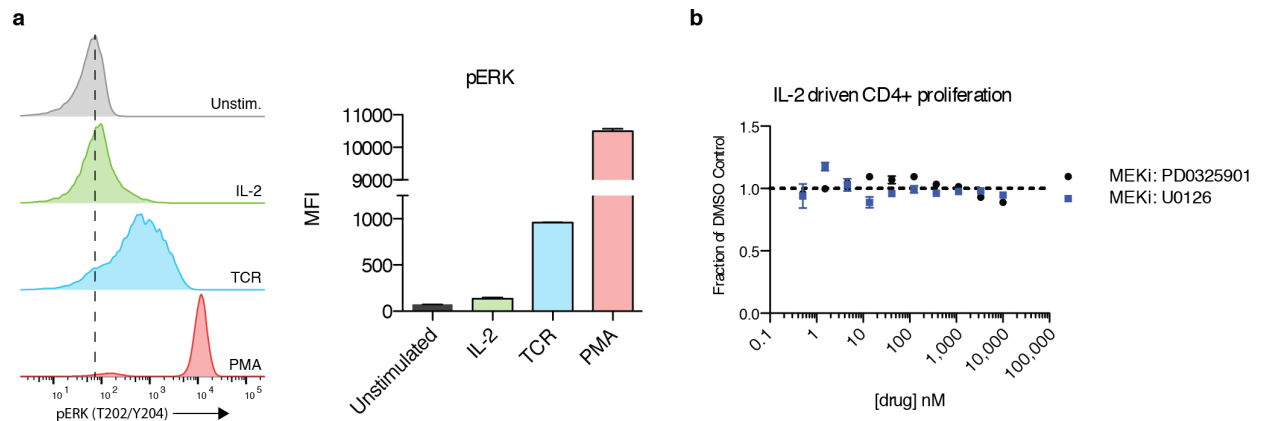
Figure 3-4 MEK/ERK Signaling is dispensable for IL-2-driven T-cell proliferation.
(a) CD4+ T-cell blasts were stimulated with IL-2 (50 U/mL) or PMA (50 ng/mL) for 15 minutes or αCD3 (10 mg/mL) crosslinking for 5 minutes and pERK was monitored by phosphoflow. Results quantified at right, MFI ± SEM of pooled results from three independent experiments. (b) Titration of MEK inhibitors PD0325901 and U0126 in 3H-thymidine proliferation assay. Plotted as mean ± SEM of technical triplicates. Representative of 3 independent experiments.
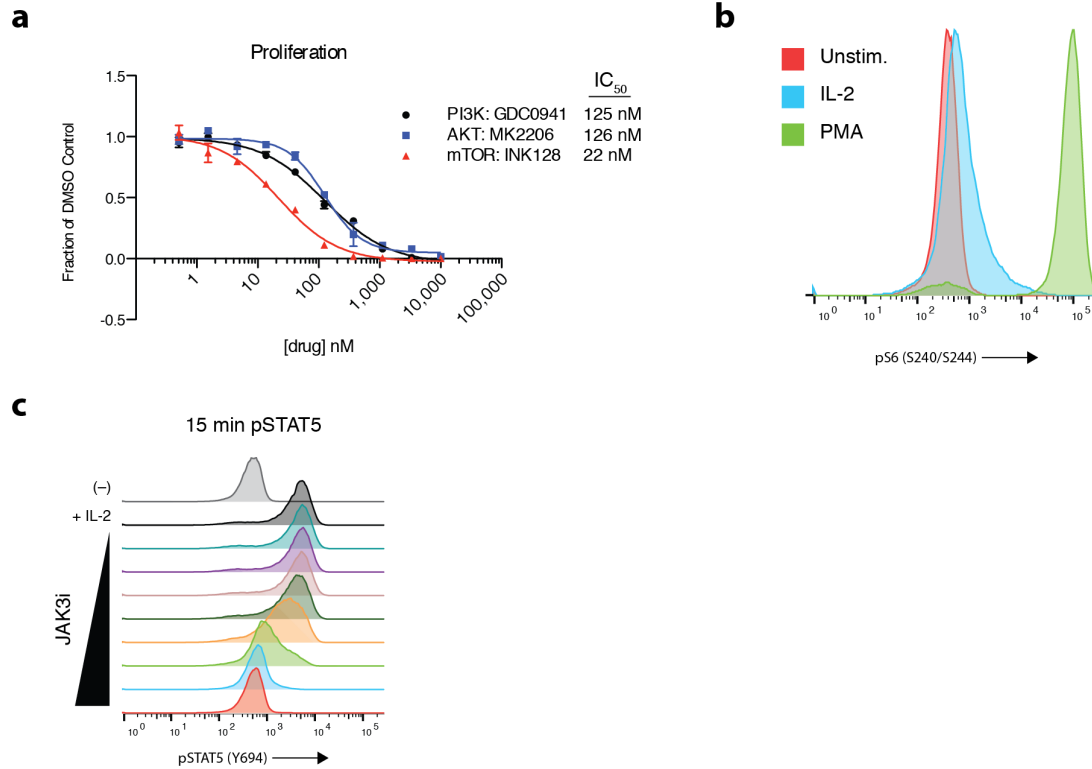
Figure 3-5 PI3K, AKT, and mTOR are required for IL-2-driven T-cell proliferation.
(a) Titration of PI3K (GDC0941), AKT (MK2206) or mTOR (INK128) inhibitors in the 3H-thymidine proliferation assay, plotted as mean ± SEM of three replicates. Representative of 4 (GDC0941), 3 (MK2206), or 2 (INK128) independent experiments. (b) Phosphorylation of ribosomal protein S6 Ser240/244 after stimulation with IL-2 (50 U/mL) or PMA (50 ng/mL) for 15 minutes. (c) pSTAT5 histograms from cells costained with pS6 (see Fig. 2e). (b) and (c) are representative data from 2 independent experiments.

C905S JAK3 mutant rescues JAK3i effects

Before pursuing additional mechanistic studies, we sought to ensure that all phenotypes induced by JAK3i were indeed the result of JAK3 kinase inhibition. We established this through multiple independent approaches. Compound **2**, which lacks cysteine reactivity but is otherwise structurally identical to JAK3i, is >200-fold less potent in all biochemical and cellular assays (Figure 3-6). To address the possibility that JAK3i acts by targeting an alternative cysteine-containing kinase (e.g., ITK or RLK, both expressed in T cells) or any other protein besides JAK3, we retrovirally overexpressed a JAK3 mutant lacking the key cysteine (C905S) (Figure 3-7 **a**). Relative to the empty vector, overexpression of wild-type JAK3 in mouse CD4+ T-cell blasts caused a slight reduction in JAK3i sensitivity in the IL-2 proliferation assay (IC_{50} 23 nM, Figure 3-8 **a**), consistent with the large increase in cellular JAK3 levels (Figure 3-7 **b**). In contrast to WT JAK3, overexpression of C905S JAK3 completely prevented JAK3i effects on T-cell proliferation at relevant concentrations, resulting in an apparent 1,000-fold shift in potency (IC_{50} > 4,000 nM). STAT5 phosphorylation and CD25 upregulation were similarly rescued by C905S JAK3 (Figure 3-8 **b and** Figure 3-7 **c**). These genetic perturbations had no effect on tofacitinib sensitivity (Figure 3-7 **d-e**). JAK3i thus provides a powerful tool for inactivating JAK3 catalytic activity in an acute, selective, and graded manner. The C905S JAK3 mutant, which is resistant to JAK3i, completes the chemical genetic toolkit by enabling genetic rescue experiments to rigorously control for potential off-target effects.

We obtained additional evidence supporting the selectivity of JAK3i from cellular assays dependent on JAK or TEC-family kinases: IFN-γ-stimulated STAT1 phosphorylation (JAK1 and JAK2), TCR-stimulated IL-2 production (ITK and TXK/RLK[27]), and BCR-stimulated CD69 expression (BTK). Consistent with the results from biochemical kinase assays, JAK3i had no significant effect on these potentially confounding pathways (IC_{50} > 1,100 nM**,** Figure 3-8 **c,** Table 3-2) at concentrations that abolished IL-2-driven proliferation and STAT5 phosphorylation (Figure 3-2**b** and Figure 3-8 **a**,**b**).
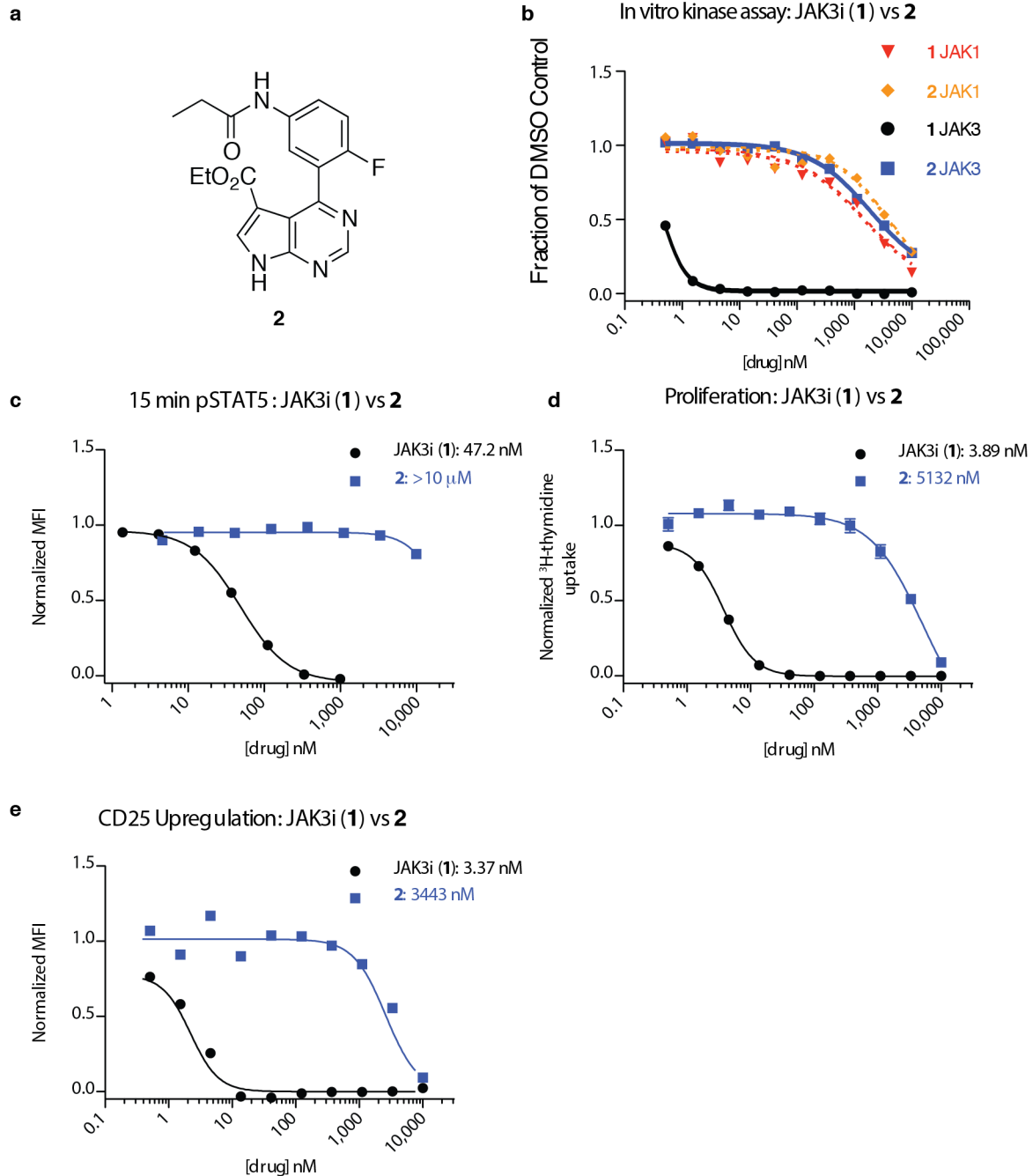
Figure 3-6 Propionamide 2 is much less potent than JAK3i.
(a) Structure of propionamide **2.** (b) In vitro kinase assays with JAK1 and JAK3**.** (c-e) IL-2-stimulated STAT5 phosphorylation (15 min, c), proliferation (d), and CD25 upregulation (e) (EC_{50} values shown for **1** and **2**). Proliferation data (d) are plotted as mean ± SEM of triplicates. Panels are representative of one (b) or two (c-e) independent experiments.
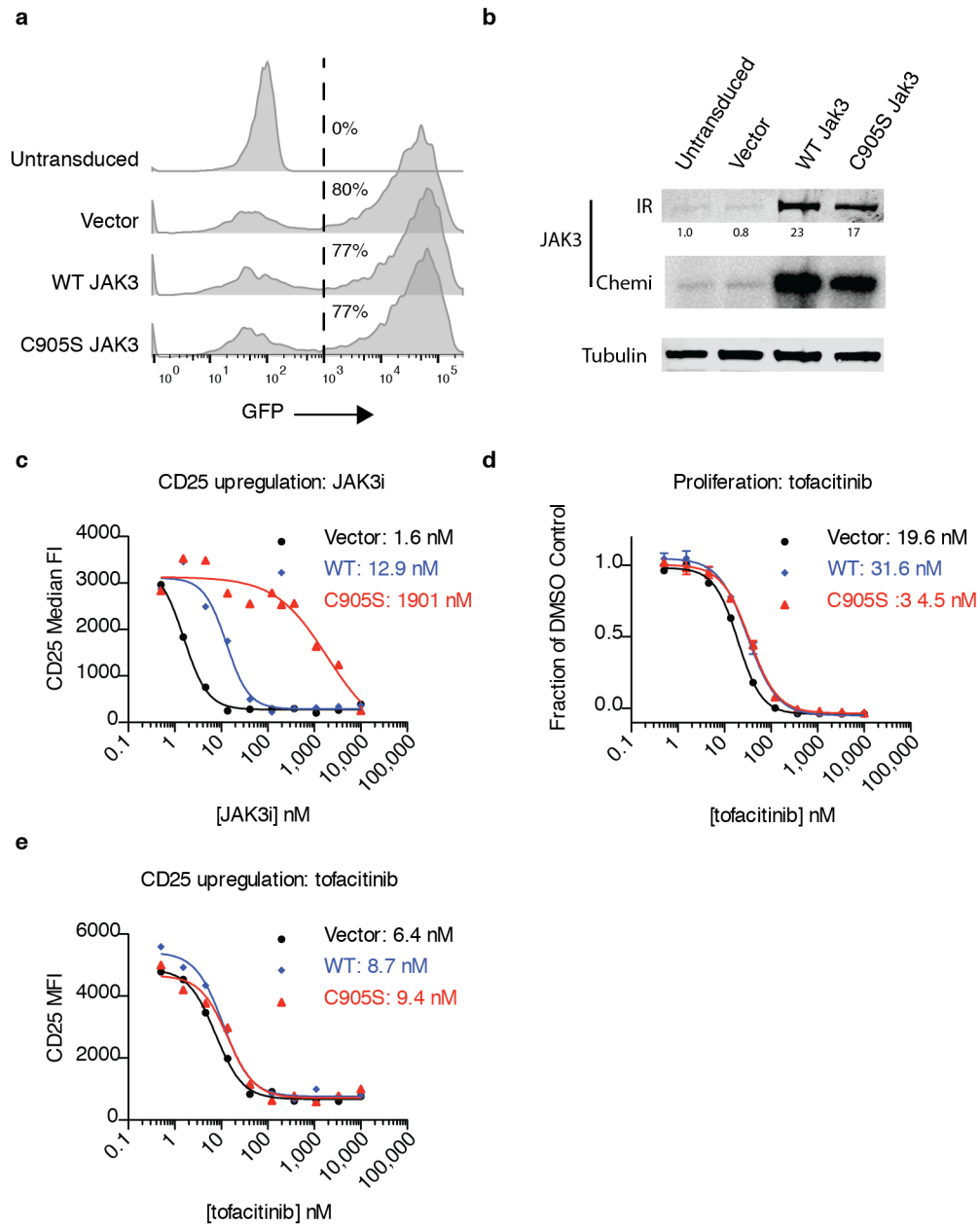
Figure 3-7 C905S JAK3 Mutant Rescue.
(a) Transduction efficiency of primary CD4+ T cells used without sorting in proliferation assays (Fig. 3a). (b) Overexpression of JAK3 in unsorted cells detected by Western blotting. Quantification from Licor data (IR), normalized to tubulin and relative to untransduced cells, is indicated below. For comparison, overexposed blots with chemiluminescence detection (Chemi) are shown. (c) CD25 upregulation after 24 hours of IL-2 stimulation in GFP+ cells transduced with WT JAK3, C905S JAK3 or empty vector. (d-e) Tofacitinib inhibition of IL-2-driven proliferation (c) and CD25 upregulation (d) is unaffected by C905S JAK3. Proliferation results (d) are plotted as the mean ± SEM of three replicates. All data are representative of two independent experiments.
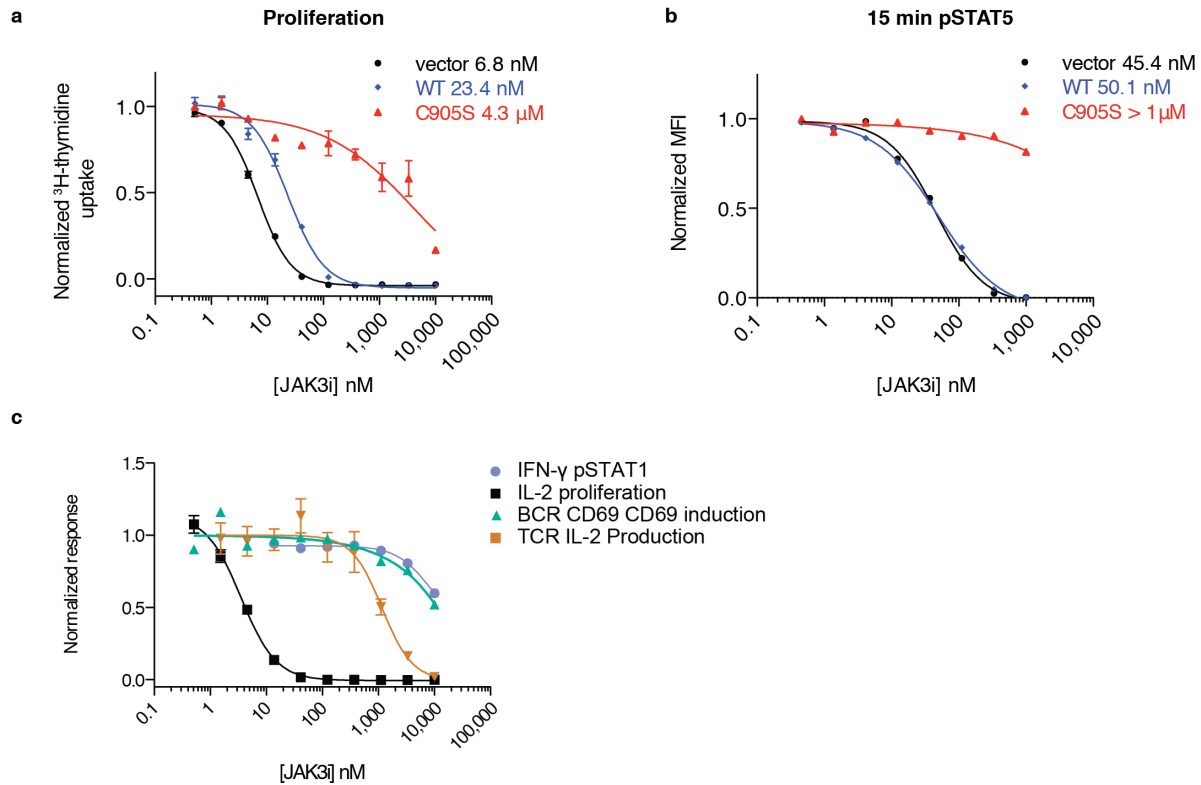
Figure 3-8 C905S JAK3 mutant rescues JAK3i effects in primary CD4+ T cells.
Rescue of JAK3i-mediated inhibition of (a) proliferation in unsorted CD4+ cells and (b) pSTAT5 (t = 15 min) in CD4+GFP+ cells. Cells were retrovirally transduced with empty vector, WT JAK3, or C905S JAK3, treated with JAK3i for 2 hrs, and stimulated with 50 units/mL rhIL-2. See Supplementary Fig. 6a for transduction efficiency. (a) and (b) are representative of two independent experiments. (c) Cellular selectivity of JAK3i in primary murine immune cells. IFN-γ-stimulated pSTAT1 (JAK1/JAK2 dependent), measured by phosphoflow, and IL-2-driven proliferation (JAK1/JAK3 dependent), measured by 3H-thymidine uptake, were assessed in CD4+ T-cell blasts. T-cell receptor (TCR)-driven IL-2 production (ITK/RLK dependent) was assessed by ELISA in naïve CD4+ T cells. Activation of naïve B cells (BTK dependent) by B-cell receptor (BCR) stimulation (α-IgM) was determined by FACS measurement of CD69 upregulation. Data are representative of 2 (IFN-γ, BCR), 9 (IL-2), or 3 (TCR) independent experiments. See Table 3-2 for IC50 values from all cellular selectivity experiments. Proliferation (a, c) and IL-2 ELISA (c) data are plotted as mean ± SEM of triplicates.

Table 3-2 Cellular Selectivity of JAK3i

Cellular Assay	Kinases	IC_{50}
IFN-γ pSTAT1	JAK1/2	>10 µM (n=2)
IL-2 proliferation	JAK1/3	3.7 ± 1.6 nM (n=9)
α-IgM CD69 induction	BTK	>10 µM (n=2)
TCR IL-2 production	ITK/RLK	1.12 ± 0.5 µM (n=3)

Average IC_{50} values (± SD when n ≥ 3) of JAK3i in indicated cellular assays of potential off target kinases. n indicates number of independent experiments. See Figure 3-8 for details.

Two waves of IL-2 signaling

The inability of JAK3i to inhibit STAT5 phosphorylation at concentrations that blocked proliferation, CD25 induction, and IFN-γ production was initially puzzling, since these processes are known to be STAT5-dependent[5]. However, by monitoring the dynamics of STAT5 phosphorylation over 20 hours, we discovered a second wave of signaling that, to our knowledge, has not been characterized previously. STAT5 phosphorylation peaked initially at 15 minutes and then declined to an intermediate level by one hour. In a majority of cells, pSTAT5 intensity rapidly returned to the original peak level and remained at this level for at least 10 hours (Figure 3-9 **a,b**). Signaling through the PI3K/mTOR pathway, while detected at early time points, was most prominent 2-6 hours after stimulation (Figure 3-10).
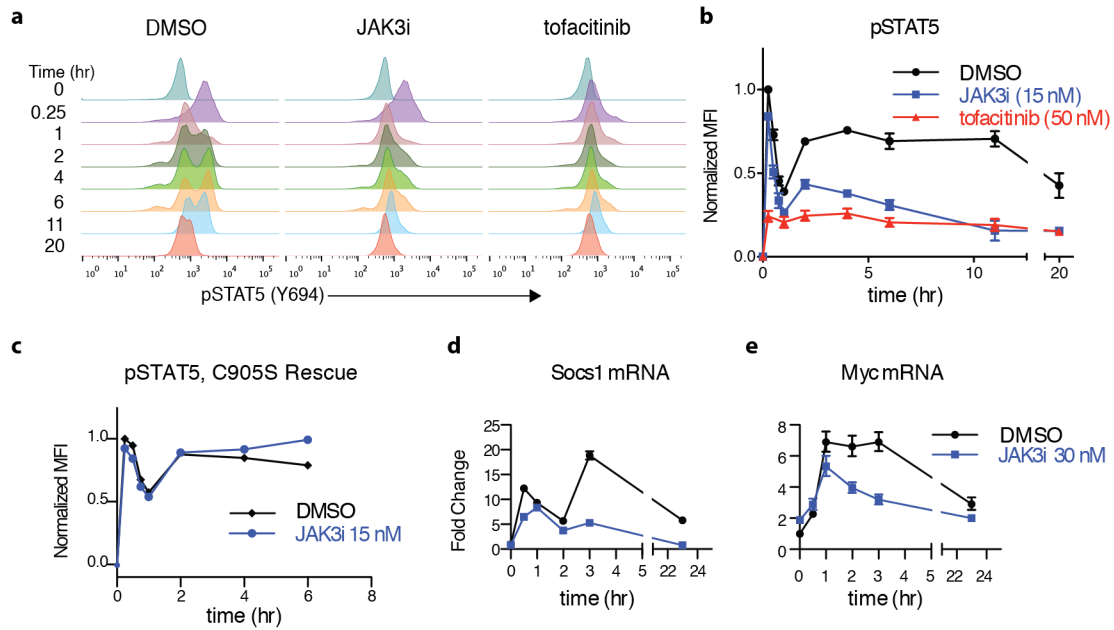
Figure 3-9 A second wave of STAT5 signaling is highly sensitive to JAK3 inhibition.
(a) CD4+ T-cell blasts were pretreated with inhibitors at the EC_{90} dose for blocking T-cell proliferation (JAK3i 15 nM, tofacitinib 50 nM) for 2 hrs and then stimulated with IL-2 (50 u/mL). pSTAT5 was monitored by phosphoflow at the indicated times. (b) pSTAT5 time course from (a), quantified by mean fluorescence intensity (MFI), normalized to the maximum value (t = 15 min, DMSO) and plotted ± SEM of 10 independent experiments. (c) Time course showing C905S JAK3 rescue of pSTAT5 inhibition by JAK3i. (d–e) Cells were pretreated with JAK3i (30 nM) and stimulated with IL-2. mRNA levels were monitored by qPCR at the indicated times. Plotted as mean fold-induction with 95% confidence intervals. Data are representative of 10 (a), 2 (c) or 3 (d–e) independent experiments.
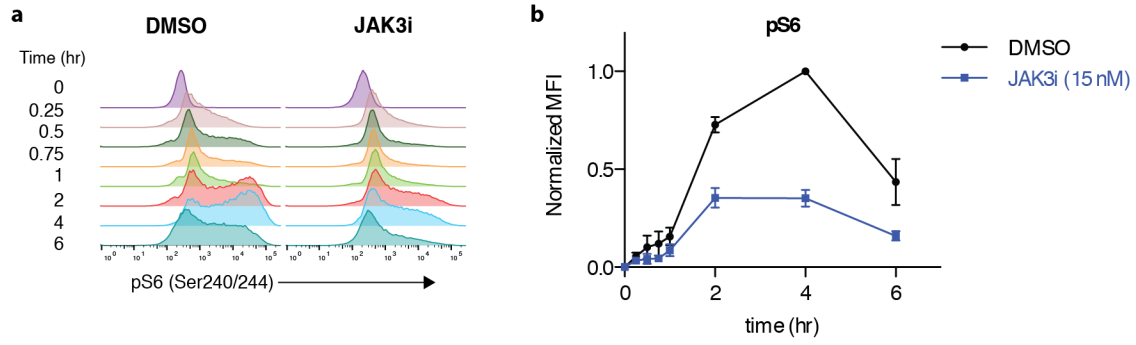
Figure 3-10 Time course of S6 phosphorylation.
(a) pS6 (Ser240/244) was followed by phosphoflow in the presence of DMSO or JAK3i (15 nM) over 6 hours in IL-2-stimulated CD4+ T cells. Representative of three independent experiments. (b) cumulative quantification of all three experiments, plotted as mean ± SEM.

Washout experiments have shown that continuous exposure to IL-2 over a period at least 6 hours is required to drive T-cell blasts into S phase[17]. Based on this precedent and our observation of a second wave of signaling, we surmised that JAK3 catalytic activity might be especially critical during the second wave, potentially accounting for the potent effects of JAK3i on T-cell proliferation. To test this, we treated cells with a concentration of JAK3i sufficient to block IL-2-driven proliferation by 90% (EC_{90} 15 nM) and monitored pSTAT5 levels over time. Although it had little effect on the first wave, JAK3i at 15 nM knocked down pSTAT5 and pS6 levels by >50% in a sustained manner throughout the second wave (Figure 3-9 **a-b**, Figure 3-10). As expected, this inhibitory effect was completely prevented in cells expressing the JAK3i-resistant allele, C905S JAK3 (Figure 3-9 **c** and Figure 3-11). The pan-JAK inhibitor tofacitinib had a completely different profile from JAK3i, reducing pSTAT5 to a similar extent during the first and second waves when tested at its EC_{90} for T-cell proliferation (50 nM). Importantly, the remaining levels of second-wave pSTAT5 were nearly identical in cells treated with JAK3i and tofacitinib (Figure 3-9 **a-b**). Hence, with both JAK3i and tofacitinib, a sustained yet partial reduction (>50%) in pSTAT5 levels during the second wave correlates with a nearly complete block in T-cell proliferation. Moreover, this second wave of STAT5 phosphorylation is much more sensitive to selective JAK3 inhibition than the first wave, whereas both waves are equally sensitive to pan-JAK inhibition.
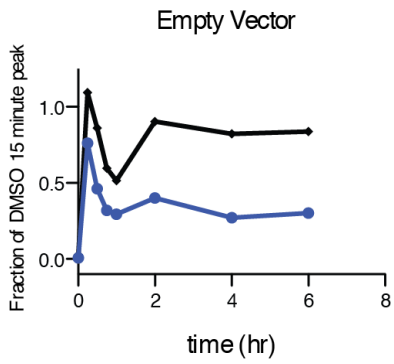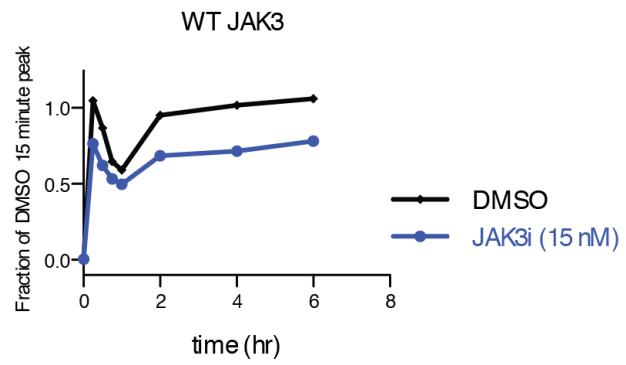
Figure 3-11 Signaling time course in overexpression controls.
STAT5 phosphorylation was monitored over 6 hours in cells transduced with an empty vector (a) or WT JAK3 (b) and treated with or without 15 nM JAK3i. Data are representative of two independent experiments.

To test whether the effects of JAK3i on pSTAT5 correlate with effects on transcription, we analyzed a panel of STAT5-dependent genes implicated in T-cell proliferation, survival, and cytokine production. Based on their temporal expression patterns, these genes can be divided into three groups: first, a biphasic pattern exemplified by *Socs1* (a negative regulator of JAK-STAT signaling) and *Fos* (Figure 3-9 **d** and Figure 3-12 **a**); second, early and sustained induction, exemplified by *Myc* and *Ifng* (Figure 3-9 **e** and Figure 3-12 **b**); and third, delayed induction, roughly coinciding with the second wave of pSTAT5 and exemplified by *Bcl2* and *Il2ra* (Figure 3-12 **c**). In all cases, pretreatment with JAK3i had little effect during the first 1-2 hours following IL-2 stimulation, yet profoundly reduced mRNA levels at later time points, consistent with more potent effects on pSTAT5 during the second wave.

a Biphasic Induction
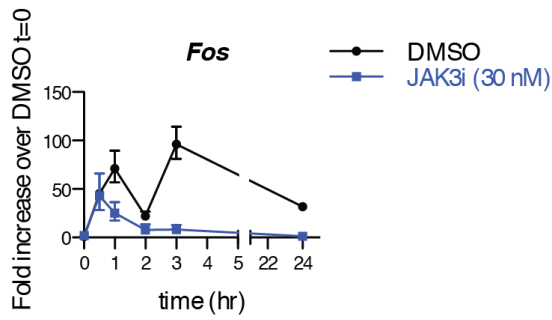
b Early and Sustained Induction
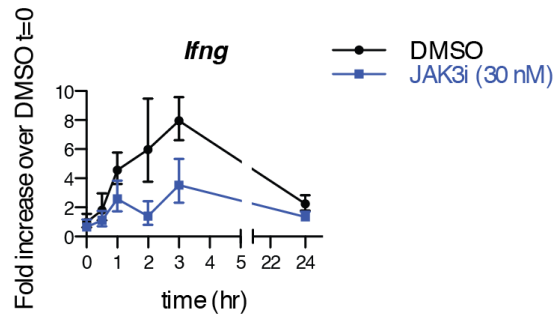
c Delayed Induction
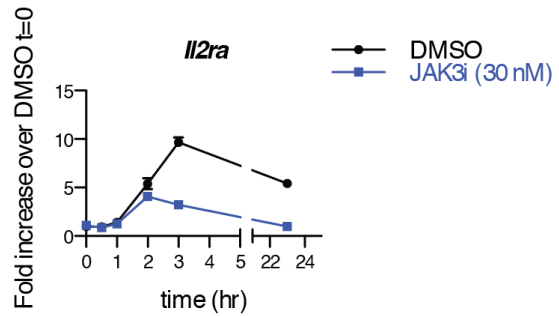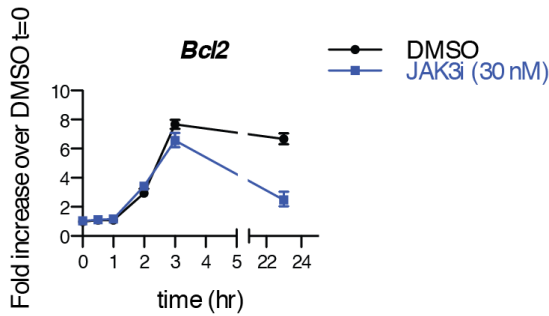
Figure 3-12 Transcriptional time course.
qPCR analysis of genes induced by IL-2 stimulation, grouped by pattern (mean of 3 replicates with 95% confidence interval): (a) biphasic, (b) early and sustained, and (c) delayed induction. Data are representative of three independent experiments.

94

Cell cycle progression requires continuous JAK3 activity

The above results demonstrate a correlation between JAK3i's effects on late IL-2 signaling events and T-cell proliferation. To test directly whether JAK3 inhibition during the second wave is sufficient to prevent cell cycle progression, we added JAK3i to IL-2-stimulated cells after the initial peak of pSTAT5 had subsided. Treatment with JAK3i at the onset of the second wave induced rapid (within 30 min) and sustained reduction of both pSTAT5 and pS6 levels, similar to pretreating cells before IL-2 stimulation (Figure 3-13 **a,** Figure 3-14 **a**). Moreover, adding JAK3i with or 2 hours after IL-2 stimulation similarly inhibited S-phase entry (Figure 3-13), as assessed by labeling cells with 5-ethynyl-2'-deoxyuridine (EdU) for one hour at the onset of S phase (t = 24 hrs, Figure 3-14 **b**). Addition of 15 nM JAK3i at later time points during the second wave led to a progressive increase in the fraction of cells incorporating EdU. However, even an 8-hour delay in JAK3i treatment prevented more than half the cells from entering S phase (Figure 3-13 **b**). Strikingly, late addition of 100 nM JAK3i, a higher but still selective dose (Figure 3-8), up to 8 hours after IL-2 stimulation inhibited S-phase entry by 95% (Figure 3-13 **c**); a minority of cells (~30%) managed to escape when this higher dose was delayed for 12 hours. These experiments establish a minimal requirement of 8-12 hours of sustained JAK3 catalytic activity for T cells to progress from G1 to S phase in response to IL-2.
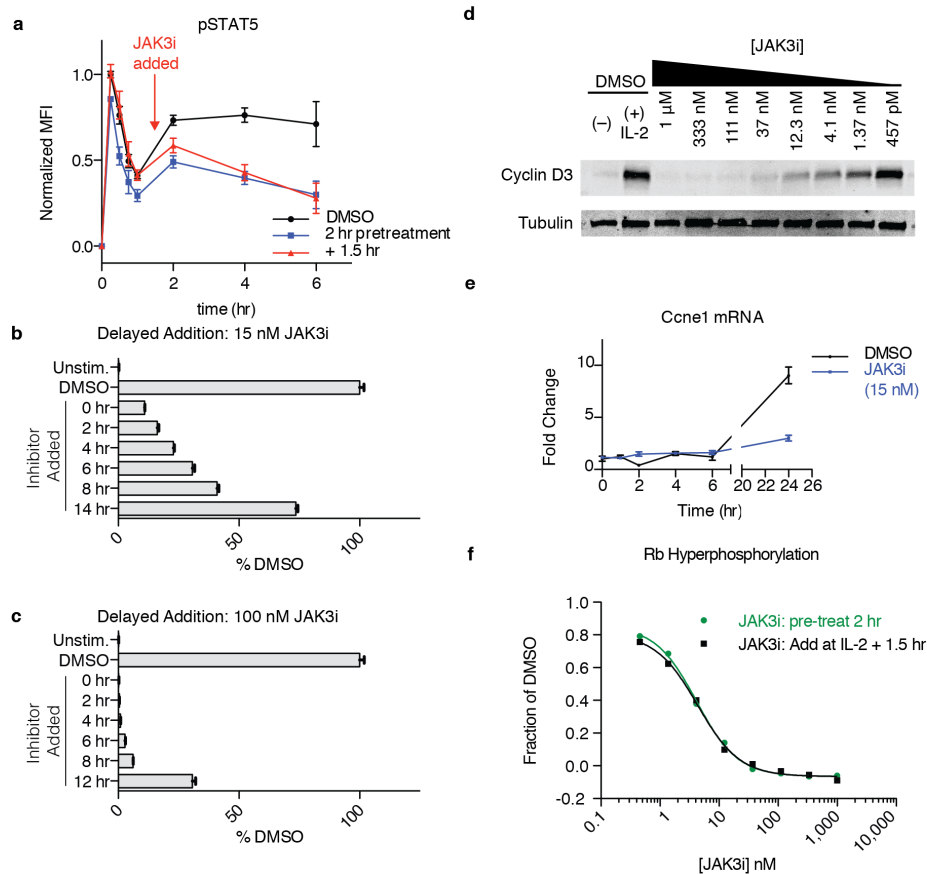
Figure 3-13 Sustained JAK3 activity is required for S-phase entry.
(a) pSTAT5 levels were monitored over time in T cells treated with JAK3i (15 nM) either 2 hrs before or 90 min after IL-2 stimulation. Data are normalized the maximum value (t=15 min DMSO) and plotted as mean ± SEM of 4 independent experiments. (b–c) JAK3i was added at a concentration of 15 nM (b) or 100 nM (d) at the indicated times after IL-2 stimulation. After 24 hrs, cells were labeled with EdU for 1 hr, and the percentage of EdU+ cells was measured by FACS and normalized to DMSO (± SEM of replicates, n = 3). Typically, 35-45% of cells were in S-phase 24-25 hours after stimulation. (d) Cyclin D3 was monitored by immunoblot 24 hrs after IL-2 stimulation in the presence of indicated concentrations of JAK3i. For full gel, see **Supplementary Fig. 12**. (e) Cells were pretreated with 15 nM JAK3i, and cyclin E1 mRNA was quantified by qPCR at the indicated times after IL-2 stimulation. (f) T cells were treated with JAK3i 2 hrs before or 1.5 hrs after IL-2 stimulation. After 24 hrs, phosphorylation of the retinoblastoma protein (Rb) at S800/S804 was quantified by FACS. Original histograms are shown in Figure 3-14 **d**. Data are representative of 4 (d), 3 (b, e) or 2 (c, f) independent experiments.
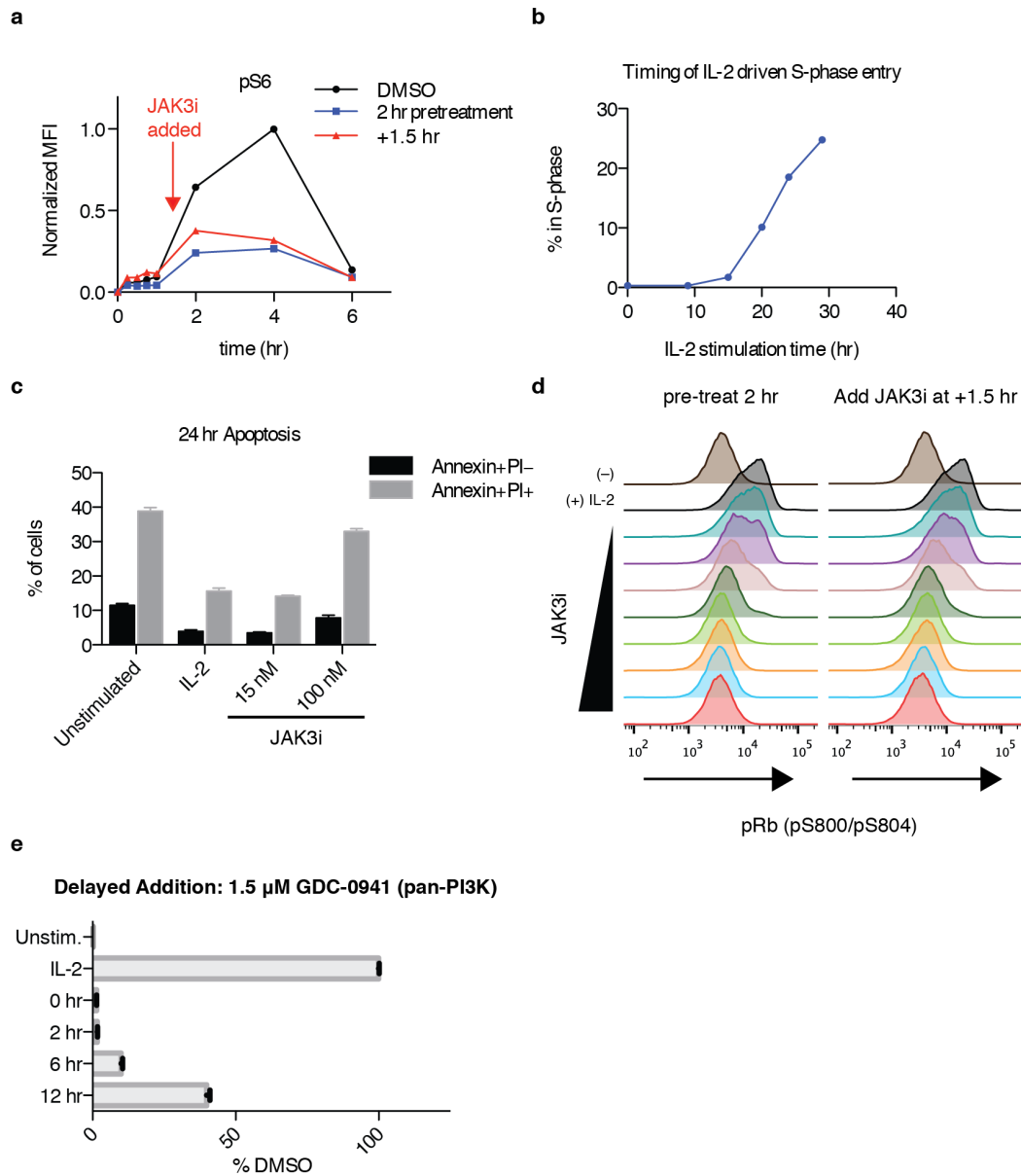
Figure 3-14 Delayed addition studies.
(a) pS6 (Ser240/244) levels were monitored over time in T cells treated with JAK3i (15 nM) either 2 hours before or 90 min after IL-2 stimulation, as in Fig. 5a. (b) Kinetics of IL-2 stimulated S-phase entry was assessed by 1-hour pulse of EdU at the indicated times. (c) T cells were treated with 15 nM or 100 nM JAK3i, stimulated with IL-2, and incubated for 24 hours before staining with Annexin and PI to mark cells undergoing apoptosis (Annexin+PI-) and dead cells (Annexin+PI+). Plotted as mean ± SEM of triplicates. (d) FACS histograms of pRB (pS800/p804) after 24 hours of IL-2 stimulation, with an 8-point JAK3i titration series added 2 hours before or 90 minutes after stimulation. MFI plotted in Fig. 5f. (e) PI3K inhibitor GDC-0941 was added at the indicated times after IL-2 stimulation (1.5 µM, EC90 for blocking proliferation, Supplementary Fig. 3a). After 24 hrs, cells were labeled with EdU for 1 hr, and the percentage of EdU+ cells was measured by FACS and normalized to DMSO (± SEM, n = 3). Data from all panels are representative of two independent experiments.

Since treatment with low-dose JAK3i blocked proliferation without inducing apoptosis (Figure 3-14 **c**), we next focused on the mechanism of the observed G0/G1 arrest. In T cells, progression into S phase requires phosphorylation of the retinoblastoma protein (Rb) by CDK4/6 and CDK2 kinases[28]. IL-2 regulates these kinases, in part, via STAT5-mediated induction of cyclin D3 and E1[28]. We asked whether this pathway was particularly sensitive to JAK3 kinase inactivation. Indeed, JAK3i potently blocked IL-2-stimulated induction of cyclin D3 (Figure 3-13 **d**) and cyclin E1 (Figure 3-13 **e**, detected by qPCR due to a lack of suitable antibodies). Consistent with its effects on cyclin induction, JAK3i abolished Rb phosphorylation at Ser800 and Ser804, assessed by flow cytometry 24 hours after IL-2 stimulation. Importantly, pRb inhibition occurred with identical potency whether JAK3i was added 2 hours before or 90 minutes after IL-2 stimulation (Figure 3-13 **f**). Thus, JAK3 kinase activity is required during a critical window – between 2 and 8 hours after IL-2 stimulation – to upregulate G1 and S-phase cyclins, which in turn promote Rb hyperphosphorylation and DNA replication. It is likely that additional JAK3- and STAT5-dependent processes (e.g. mTOR signaling, Figure 3-10, *Myc* induction, Figure 3-9 **e**) contribute to timely cell cycle progression. Indeed, addition of the PI3K inhibitor GDC0941 – even 12 hours after IL-2 stimulation – prevented the majority of cells from entering S-phase, suggesting a similar requirement for sustained PI3K activity in cell cycle progression (Figure 3-14 **e**). Thus, JAK3i's antiproliferative effects likely reflect partial suppression of both STAT5 and PI3K activities during this crucial second wave of IL-2 signaling.

JAK3i blocks IL-2-driven T-cell proliferation in vivo

Whereas *in vitro* experiments enabled careful dissection of JAK3-dependent signaling dynamics in primary T cells, the cells were necessarily isolated from the milieu of cytokines, growth factors, and other cell types that contribute to T-cell functions *in vivo*. To test whether JAK3 activity is required for IL-2 proliferation in this environment and assess the utility of JAK3i as an *in vivo* tool compound, we devised a proliferation assay similar to our in vitro system using

adoptively transferred T-cell blasts. *Ex vivo*-activated CD4+ T-cell blasts were labeled with carboxyfluorescein succinimidyl ester (CFSE) and injected into congenically marked (CD45.1+) hosts. The mice were then dosed with JAK3i twice daily and stimulated over two days with thrice-daily injections of IL-2 (Figure 3-15 **a**). Cell division was monitored by CFSE dilution 50 hours after the first IL-2 injection, which yielded 2–4 divisions for most cells in the control mice (Figure 3-15 **b**). JAK3i strongly inhibited T-cell proliferation *in vivo*, with a nearly complete block at 40 mg/kg and substantial reduction at 10 mg/kg (Figure 3-15 **c**).

To rule out off-target effects, we developed an assay that allowed the simultaneous assessment of T cells expressing either WT or C905S JAK3 in the same mouse (Figure 3-15 **d**). Two congenic markers were used to distinguish host cells (CD45.1/CD90.2) from donor cells transduced *ex vivo* with WT JAK3 (CD45.2/CD90.2) or C905S JAK3 (CD45.2/CD90.1) (Figure 3-15 **e**). Upon IL-2 stimulation as described above, T cells transduced with WT or C905S JAK3 proliferated to the same extent in vehicle-treated mice (Figure 3-15 **f**,**g**). By contrast, in mice dosed with JAK3i, T-cells expressing WT JAK3 failed to proliferate, whereas T-cells expressing C905S JAK3 proliferated normally in the exact same animals. These results strongly implicate JAK3 as the relevant *in vivo* target of JAK3i, even at relatively high doses (40 mg/kg, twice daily).
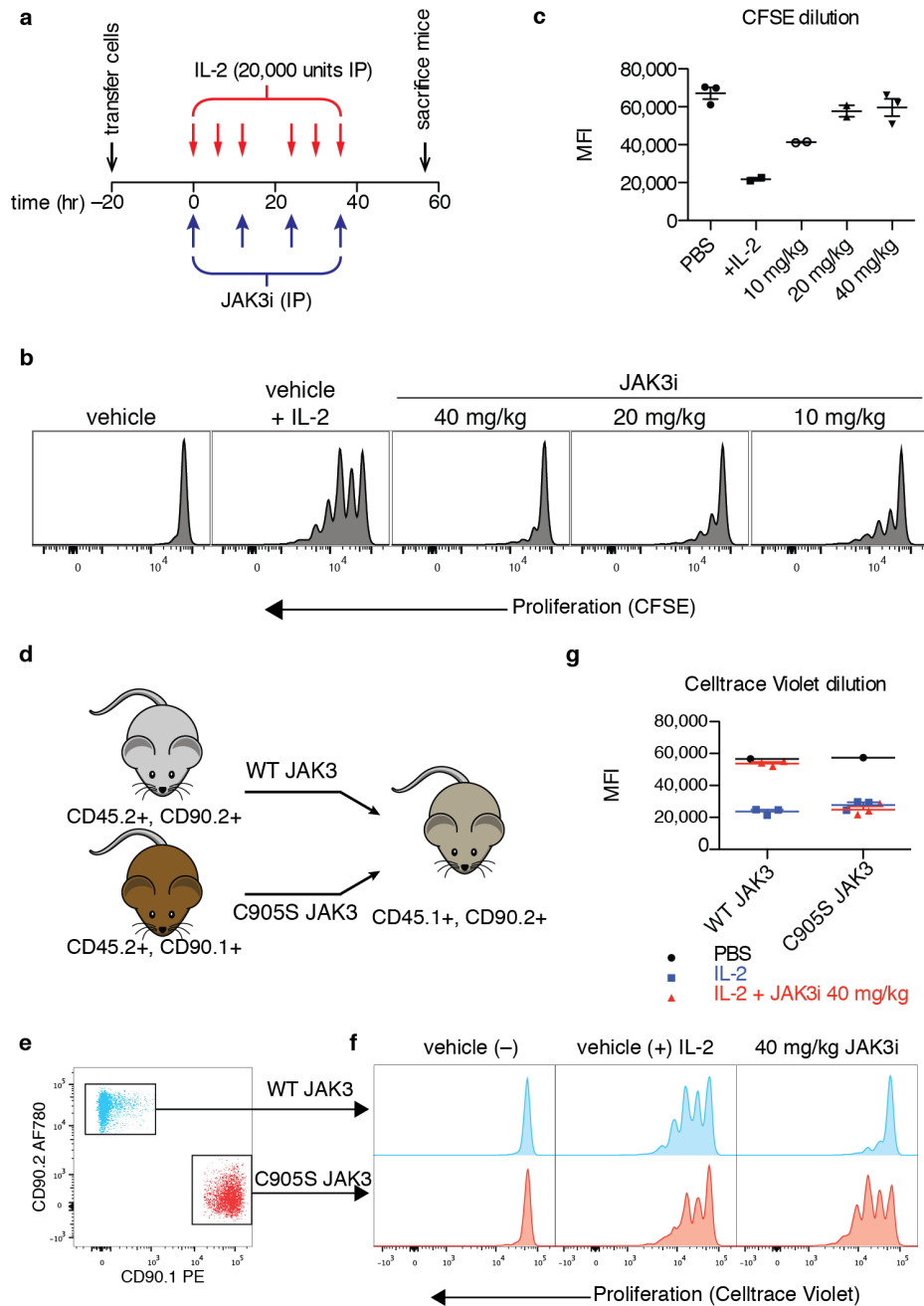
Figure 3-15 JAK3 inhibition blocks IL-2-driven proliferation *in vivo*.
(a) Experimental timeline, showing adoptive transfer of CD4+ T-cell blasts (5×10^6) labeled with carboxyfluorescein succinimidyl ester (CFSE), twice-daily dosing with JAK3i, and thrice-daily injections of IL-2 (20,000 units). (b) Representative CFSE dilution histograms for the indicated treatments. (c) Median CFSE intensity (plotted ± SEM for n>2) for the indicated treatments, 2–3 mice per group as indicated. (d) Congenic marking and transfer scheme for *in vivo* proliferation and rescue experiment. A 1:1 mixture of WT and C905S T-cells (total 5×10^6) was transferred to each mouse. (e) FACS identification of WT and C905S JAK3-transduced cells from the same mouse (see complete gating in Figure 3-16). (f) Representative Celltrace Violet dilution profiles. Each column depicts cells from the same mouse. (g) Median Celltrace Violet intensity for the indicated treatments and JAK3 overexpression construct (n = 3 mice per IL-2-stimulated treatment condition, n = 1 mouse for the unstimulated control). Data in a-c are pooled from two independenet experiments and data in d-g are from one experiment with indicated numbers of mice.
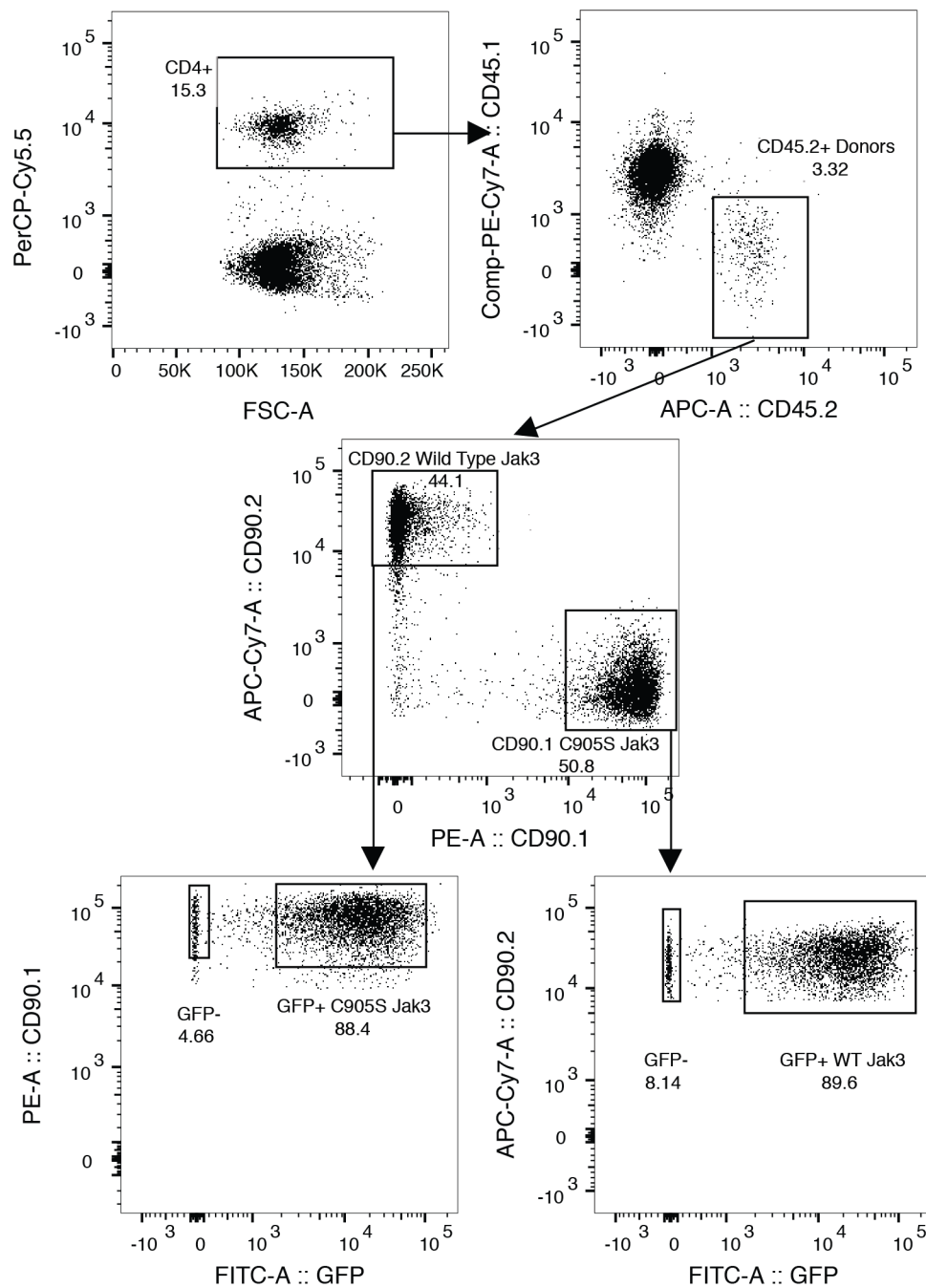
Figure 3-16 In vivo rescue experiment gating scheme.
Splenocytes were gated on FSC/SSC lymphocyte profile and single cells (not shown), then on CD4+ cells.
CD45.1-CD45.2+ identified adoptively transferred donor cells. CD90.1 and CD90.2 staining distinguished cells
transduced with C905S JAK3 and WT JAK3, respectively. Finally, cells were gated on GFP+ to confirm viral
transduction.

3.4   Discussion

In this study, we elucidated a previously unknown requirement for JAK3 catalytic activity in sustaining a second wave of STAT5 phosphorylation in IL-2-stimulated CD4+ T cells. Although JAK3 activity is also required for the initial wave of pSTAT5 that peaks within 15 minutes of IL-2 stimulation, the second, more prolonged wave shows greater sensitivity to acute inhibition by JAK3i. This increased sensitivity accounts for the potent effects of JAK3i on STAT5-dependent processes occurring many hours after IL-2 stimulation, which include transcriptional activation of genes required for cell cycle progression. Sustained activation of the PI3K/mTOR pathway was also more sensitive to JAK3i and essential for cell cycle progression, suggesting a general requirement for second-wave JAK3 activity in multiple signaling pathways downstream of the IL-2 receptor.

What determines this biphasic pattern of STAT5 phosphorylation? In IL-6-stimulated macrophages, STAT3 phosphorylation shows a similar biphasic pattern. Here, the initial decrease in pSTAT3 is ablated in cells lacking the Suppressor of Cytokine Signaling-3 (*Socs3*)[29]. Based on this precedent, we speculate that induction of one or more SOCS proteins could promote the rapid decrease in pSTAT5 that occurs within one hour of IL-2 stimulation (Figure 3-9). The SOCS-family genes, *Socs1, Socs3*, and *Cish*, are all transcriptionally induced by IL-2[5]. Moreover, *Socs1*-deficient T-cells are hyper-responsive to IL-2 at the level of both STAT5 phosphorylation and proliferation[30]. Finally, in IL-2-stimulated T cells lacking *Cish*, the temporal pattern of STAT5 phosphorylation and dephosphorylation is altered[31]. Hence, SOCS-family proteins likely play complex and partially overlapping roles in tuning the dynamics of IL-2 signaling. Induction of SOCS1 or SOCS3 is expected to shift the balance of JAK kinase dependency toward JAK3, since both proteins bind and directly inhibit JAK1 but not JAK3 kinase domains[32]. Induction of SOCS1 or SOCS3 could therefore lead to diminished JAK1 activity during the second wave, and hence, a greater reliance on JAK3 activity.

High levels of pSTAT5 were sustained for at least 12 hours after IL-2 stimulation, suggesting that acute JAK3 inhibition during the second wave might be sufficient to block IL-2-stimulated T-cell proliferation. Consistent with this prediction, delayed addition of 100 nM JAK3i 8 hours after IL-2 stimulation completely prevented almost all cells from entering S phase. In patients, tofacitinib inhibits JAK1/3 activity for less than half the time between each dose and yet still exerts a clinically beneficial effect[33]. Extrapolating from our in vitro studies, tofacitinib may work by preventing the sustained activation of STATs required for committed cellular responses. An inhibitor that selectively blocks JAK3 activity for short periods of time may show similar efficacy to pan-JAK or JAK1-selective inhibitors, but without the side effects resulting from inhibition of JAK1/2-dependent cytokines.

The combination of JAK3i and the C905S JAK3 mutant provides a powerful toolkit to decipher the function of JAK3. Tofacitinib sensitivity is often cited as evidence for JAK3 dependence (see, for example, recent work on alopecia areata[34]). However, many of tofacitinib's effects result from blockade of JAK3-independent cytokines[35]. It remains unclear whether blocking γ_c cytokines is sufficient to achieve therapeutic efficacy in the setting of autoimmune disease, or whether it is instead necessary to block additional cytokines (e.g., IL-6), as observed with tofacitinib. Together with the inhibitor-resistant C905S JAK3 mutant, JAK3i will enable future preclinical studies to address this important question.

3.5   Methods

Mice. C57BL/6J mice, B6.Cg-*Gpi1*[a]*Thy1*[a]*Igh*[a]/J and B6.SJL-*Ptprc*[a] *Pepc*[b]/BoyJ (Jackson) used in this study were housed in the specific pathogen–free facilities at the University of California, San Francisco, and were treated according to protocols approved by the Institutional Animal Care and Use Committee in accordance with US National Institutes of Health guidelines. Both male and female mice were used as a source of primary CD4+ T-cells, all aged 6-12 weeks.

Reagents. pan-Jak inhibitor tofacitinib (CP-690,550), MEK inhibitor PD0325901 and AKT inhibitor MK2206 were purchased from Selleck Chemicals and MEK inhibitor U0126 was purchased from Cell Signaling Technologies. JAK3i **1** and inactive analogue **2** were synthesized as described in the **Supplementary Note.** pan-PI3K inhibitor GDC-0941 and mTOR inhibitor INK128 were a gift of K. Shokat (UCSF). Recombinant human IL-2 was from the NIH AIDS Reagent Program, Division of AIDS, National Institute of Allergy and Infectious Diseases, NIH: Maurice Gately (Hoffmann-La Roche). Recombinant mouse IFN-γ was a gift of R. Locksley.

In vitro kinase assays: Purified JAK1 (9.4 nM), JAK2 (1.15 nM) or JAK3 (3.13 nM) kinase (all Invitrogen) were preincubated with compound and 100 μM ATP for 30 minutes in manufacturer prescribed buffer. Reactions were run for 30 minutes at 23 °C with γ-^{32}P ATP (16.7 nM, Perkin Elmer) and the appropriate substrate: JAK1 - IRS1 (0.06 mg/mL, Enzo Life Sciences); JAK2 - PDKTide (0.19 mg/mL, EMD Millipore); JAK3 - JAK3tide (0.0325 mg/mL, EMD-Millipore). ITK (3.13 nM, Invitrogen) was performed similarly except using 1 mM ATP and Myelin Basic Protein substrate (Sigma). Kinase assays with BTK, EGFR, JAK3 (all with 1 mM ATP), and TYK2 (100 μM ATP) were performed by Nanosyn.

Primary T-Cell Culture. T cells were purified from single-cell suspensions of spleen and lymph nodes from male and female mice aged 6-12 weeks by negative selection with biotinylated antibodies (CD8, CD19, B220, CD11b, CD11c, DX5, Ter119 and CD24, UCSF Monoclonal Antibody Core) and magnetic anti-Biotin beads (MACSi Beads, Miltenyi Biotec). For IL-2 stimulation, purified T cells were pre-activated on 96-well plates coated with anti-CD3 (2C11) and anti-CD28 (37.51) for 72 hours, removed and cultured with rhIL-2 (100 u/mL, Roche) for 36 hours, and then cultured without rhIL-2 for the 36 hours prior to all experiments.

T-Cell Proliferation. Pre-activated T cells were cultured in 96-well plates with titrations of inhibitor or DMSO (0.1%) for 2 hours prior to stimulation with rhIL-2 (50 u/mL). After 18 hours, cells were pulsed with [Methyl-^{3}H]-thymidine (1 μCi/well, Perkin Elmer) and incubated for 24 hours. Cells were harvested onto glass fiber filtermats, dried, and counted on a Microbeta 1450 Trilux Liquid Scintillation Counter (Wallac). Alternatively, T cells were grown in 24-well plates for 10-30 hours and pulsed with 10 μM 5-ethynyl-2'-deoxyuridine for 1 hour and assayed per the manufacturer's procedure (Click-IT Plus EdU, Life Technologies).

IFN-γ production. CD4+ T cells, purified and pre-activated as described above, were cultured in 96-well plates with titrations of inhibitor or DMSO for 2 hours and then stimulated with rhIL-2 (50 u/mL). After 24 hours, the plate was spun down and the media was carefully removed. Media was diluted 1:1 in assay diluent and assayed for IFN-γ content as per the manufacture's procedure (BD OptEIA Set Mouse IFN-γ, Cat# 555138).

Cellular Selectivity. ITK and RLK inhibition:IL-2 production was assessed by culturing purified naive CD4+ T cells on anti-CD3 anti-CD28-coated 96-well plates in the presence of inhibitors and measuring IL-2 in the media after 24 hours by ELISA (BD OptEIA Mouse IL-2 ELISA Set

#555148). JAK1/JAK2: CD4+ T-cell blasts prepared as above were stimulated with 100 u/mL IFN-γ for 30 minutes, fixed and analyzed by FACS as described below. BTK: Freshly isolated mouse splenocytes were stimulated and assayed for CD69 expression as previously described[33].

Flow Cytometry. Cells were live/dead stained using the Live/Dead Fixable Near IR Dead Cell Stain Kit (Life Technologies). For surface stains, cells were stained for 30 minutes on ice with indicated antibodies. Clones, sources & dilutions can be found in the **Supplementary Table 5**. For intracellular stains, samples were fixed at the indicated time after stimulation in 2% paraformaldehyde, surface stained with CD25-biotin and CD4-BUV395, fixed again and permeabilized with ice cold 90% methanol at -20 °C overnight. Samples were then barcoded using Pacific Orange-NHS ester (0.33 or 5 μg/mL), Pacific Blue-NHS Ester (0.67 or 10 μg/mL), and AlexaFluor (AF) 488-NHS Ester (0.26 or 2 μg/mL) (Life Technologies), as previously described[36]. Intracellular antigens were then stained for 30 minutes at 23 °C with antibodies indicated in **Supplementary Table 5**. Samples were acquired on a BD LSR Fortessa and analyzed in FlowJo (Tree Star).

Apoptosis Assay: CD4+ T-cells, pre-activated and rested as described above, were initially stained with Live/Dead Fixable Near IR (Life Tech) to identify any dead cells at beginning of the assay, and then cultured with either 15 or 100 nM JAK3i in the presence of 50 u/mL IL-2 for 24 hours. Cells were then stained with Annexin V FITC and PI as per manufacture's protocol (BD) and acquired on a BD LSR Fortessa. Using FlowJo (Tree Star), results were first gated on cells that were live at the beginning of the assay (~90%) and then as live (Annexin V-PI-), undergoing apoptosis (Annexin V+PI-) or dead (Annexin V+PI+). These gates were determined by reference to cells cultured in PBS or in media without IL-2 for 24 hours.

Retroviral Overexpression: Murine JAK3 (plasmid provided by L. Berg) was cloned into a pMIG-derived vector (MSCV-IRES-GFP) via Gibson cloning and the C905S mutant was generated by site-directed mutagenesis. Retrovirus was generated in Phoenix cells co-transfected with pCL-Eco. CD4+ T-cells were isolated and activated as described above. After 24 hours of T-cell receptor stimulation, cells were spin transduced for 1 hr with fresh viral supernatant in the presence of Lipofectamine 2000 (Life Technologies) and 100 u/mL rhIL-2. Cells were left on coated plates for 48 hours and then expanded and rested as described above. Transduction efficiency was >75% and cells were used unsorted for proliferation assays. In CD25 and pSTAT5 assays, cells were gated on GFP expression.

qPCR: RNA was isolated from $1\text{-}2 \times 10^6$ CD4+ T-cell blasts per condition using RNAeasy kit (Qiagen) and cDNA was synthesized using qScript (Quanta Biosciences). mRNA was detected by Primetime (IDT) or Taqman (Life Technologies) predesigned qPCR assays. Primer & probe sequences can be found in **Supplementary Table 6**. Data are from 3 replicates collected on a QuantStudio 12k (Life Technologies), plotted with 95% confidence intervals as calculated by Quantstudio (Life Technologies).

Western Blots: $5\text{-}10 \times 10^6$ cells were lysed in 50 μL RIPA buffer with 500 mM NaCl, clarified, and protein normalized by bicinchoninic acid assay (Pierce). Proteins (20-30 μg) were resolved by 7.5% or 10% SDS-PAGE, transferred to a polyvinylidene fluoride membrane and blocked with Odyssey Block (LI-COR Biosciences). Blots were probed for Cyclin D3 (DCS22, 1:1000) or JAK3 (D7B12, 1:1000) (Cell Signaling Technologies), normalized to tubulin (DM1A, 1:5000, Sigma-Aldrich) and detected with fluorescent secondary antibodies on an Odyssey Scanner (LI-COR Biosciences). Alternatively, blots were probed with HRP-linked goat-anti-rabbit secondary

(Southern Biotech, Birmingham AL), developed with Western Lightening Plus ECL (Pierce) and detected on a ChemiDocMP (Biorad).

In vivo proliferation: Prior to transfer, mice were marked by ear punch, assigned a number and then randomized to treatment group without blinding. Pilot experiments demonstrated that the effect size was large enough to use 2 mice per dose group. CD4+ T-cell blasts from C57BL/6J mice were labeled with carboxyfluorescein diacetate succinimidyl ester (CFSE, Life Technologies), and 5×10^6 cells were adoptively transferred into 8-week old B6.SJL-*Ptprc^a Pepc^b*/BoyJ male mice via lateral tail vein injection. After 12 hours, mice were treated with JAK3i or vehicle by intraperitoneal injection twice a day and stimulated 3 times a day with 20,000 units rhIL-2 IP for 2 days. On day 3, mice were sacrificed, spleens isolated, and proliferation of adoptively transferred cells was assessed by FACS as described above. For in vivo proliferation with cells overexpressing either WT or C905S JAK3, isolated CD4+ T cells from C57BL/6J were transduced with WT JAK3 and CD4+ T-cells from B6.Cg-*Gpi1^{a}Thy1^{a}Igh^a*/J mice were transduced with C950S JAK3, then mixed 1:1 and labeled with Celltrace Violet (Life Technologies) prior to transfer of 5×10^6 cells (2.5×10^6 each of WT and C905S) into 8-week old B6.SJL-*Ptprc^a Pepc^b*/BoyJ male mice via lateral tail vein injection. Mice were treated with vehicle + IL-2 (3) or JAK3i + IL-2 (3) or vehicle only (1) and proliferation assessed as described above.

Statistical Analysis: Prism (Graphpad Software) was used to calculate mean and standard error of the mean for all graphs except qPCR data. Relative gene expression is plotted as mean with 95% confidence intervals calculated by Quantstudio software.

Synthetic Methods

All purchased chemicals were used as received without further purification. Solvents were dried by passage through columns (either alumina or activated molecular sieves) on a Glass Contour solvent system. NMR spectra were obtained on a Varian Inova 400 MHz spectrometer and referenced to the residual solvent peak. LC-MS analysis was performed on a Waters Acquity LCT UPLC equipped with a TUV detector (monitored at 254 nm) and a Waters Acquity UPLC 1.7 µm C-18 column, eluting at 0.6 mL/min with a 2.5 or 5 minute water:MeCN (with 0.1% formic acid) gradient method.

Synthetic Scheme
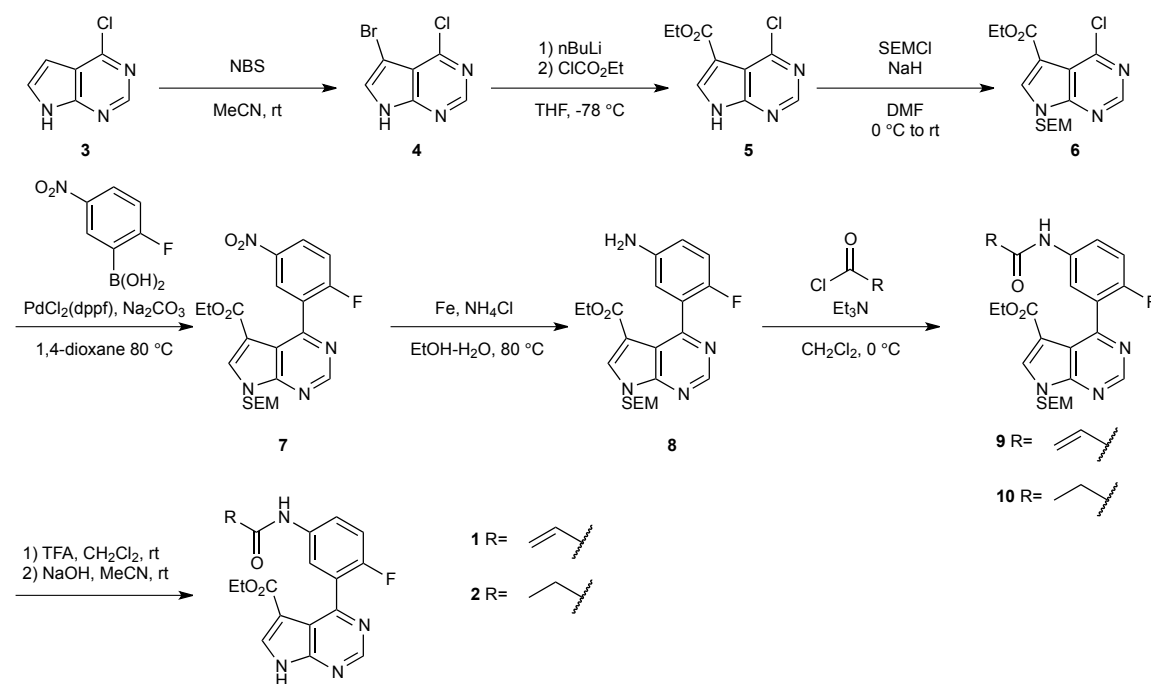
Synthetic protocols for 3-6 were previously reported[1].
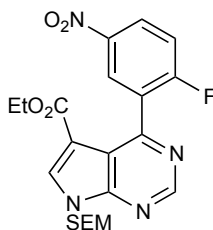
(**7**) **ethyl 4-(2-fluoro-5-nitrophenyl)-7-((2-(trimethylsilyl)ethyoxy)methyl)-7*H*-pyrrolo[2,3-d]pyrimidine-5-carboxylate**

Ethyl 4-chloro-7-{[2-(trimethylsilyl)ethoxy]methyl}-7*H*-pyrrolo[2,3-*d*]pyrimidine-5-carboxylate (**6**, 500 mg, 1.40 mmol), 2-fluoro-5-nitrophenylboronic acid (390 mg, 2.11 mmol) and [1,1'-Bis(diphenylphosphino)ferrocene]dichloropalladium(II), complex with dichloromethane (172 mg, 0.211 mmol) were suspended in 1,4-dioxane (10 mL). 2M sodium carbonate solution (2.11 mL, 4.21 mmol) was added and the mixture was degassed, and then stirred at 80 ºC for 3 hours. The mixture was cooled to room temperature, then saturated ammonium chloride solution was added and the mixture was extracted with ethyl acetate. The organic layer was washed with brine, dried over sodium sulfate, filtered and evaporated. The residue was purified by silica gel column chromatography (hexane/ethyl acetate: 90/10 – 70:30) to afford **7** (539 mg, 84%) as a pale yellow oil. ^{1}H NMR (400 MHz, CDCl$_3$): 9.10 (s, 1H), 8.70 (dd, *J* = 3.0, 6.1 Hz, 1H), 8.41 (ddd, *J* = 3.0, 4.2, 9.0 Hz, 1H), 8.18 (s, 1H), 7.28 (dd, *J* = 9.0, 9.0 Hz, 1H), 5.77 (s, 2H), 4.14 (br s, 2H), 3.64 (t, *J* = 8.4 Hz, 2H), 1.19 (t, *J* = 7.2 Hz, 3H), 0.97 (t, *J* = 8.4 Hz, 2H), –0.01 (s, 9H). ^{13}C NMR (100 MHz, CDCl$_3$): 164.1 (*J* = 259 Hz), 162.5, 152.9 (*J* = 13.7 Hz), 152.3, 144.0, 135.9, 133.3, 128.9 (*J* = 17.6 Hz), 127.1 (*J* = 5.5 Hz), 126.6 (*J* = 10.7 Hz), 116.1 (*J* = 24.4 Hz), 115.1, 108.9 (*J* = 2.3 Hz), 73.4, 67.3, 60.4, 17.7, 14.1, –1.5. ESI-MS: 461.2 (M+H$^+$).
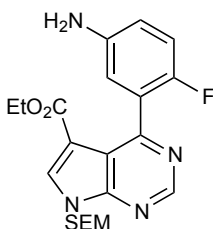
(8) ethyl 4-(5-amino-2-fluorophenyl)-7-{[2-(trimethylsilyl)ethoxy]methyl}-7*H*-pyrrolo[2,3-d]pyrimidine-5-carboxylate

Intermediate **7** (535 mg, 1.16 mmol) was dissolved in ethanol (8.0 mL) and water (2.0 mL). Iron powder (195 mg, 3.49 mmol) and ammonium chloride (195 mg, 3.49 mmol) were added and the mixture was stirred at 80 ºC for 6 hours. The mixture was cooled to room temperature, filtered through pad of celite and evaporated. The residue was diluted with ethyl acetate, washed with brine, dried over sodium sulfate, filtered and evaporated. The residue was purified by silica gel column chromatography (hexane/ethyl acetate: 70/30 – 30/70) to afford **8** (468 mg, 94%) as a pale yellow oil. ^{1}H NMR (400 MHz, CDCl$_3$): 9.03 (s, 1H), 8.10 (s, 1H), 7.12 (dd, *J* = 2.7, 5.9 Hz, 1H), 6.92 (dd, *J* = 9.0, 9.0 Hz, 1H), 6.82-6.75 (m, 1H), 5.73 (s, 2H), 4.11 (br s, 2H), 3.67 (br s, 2H), 3.61 (t, *J* = 8.2 Hz, 2H), 1.09 (t, *J* = 7.2 Hz, 3H), 0.96 (t, *J* = 8.2 Hz, 2H), –0.02 (s, 9H). ^{13}C NMR (100 MHz, CDCl$_3$): 163.0, 155.3, 154.0 (*J* = 239 Hz), 152.5, 151.9, 142.5, 134.7, 127.3 (*J* = 15.3 Hz), 117.4 (*J* = 7.6 Hz), 116.4 (*J* = 3.1 Hz), 115.2 (*J* = 22.9 Hz), 114.6, 109.7 (*J* = 3.1 Hz), 73.1, 66.9, 60.2, 17.5, 13.7, –1.6. ESI-MS: 431.0 (M+H^{+}).
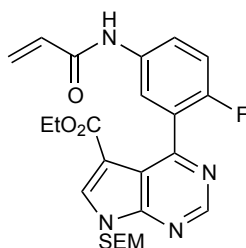
(9) ethyl 4-(5-acrylamido-2-fluorophenyl)-7-((2-(trimethylsilyl)ethoxy)methyl)-7*H*-pyrrolo[2,3-*d*]pyrimidine-5-carboxylate

Intermediate **8** (56.9 mg, 0.132 mmol) was dissolved in dichloromethane (1.5 mL) and the mixture was cooled to 0 ºC. Acryloyl chloride (12.9 mL, 0.159 mmol) and triethylamine (27.6 mL, 0.198 mmol) were added and the mixture was stirred at 0 ºC for 10 minutes. Saturated ammonium chloride solution was added and the mixture was extracted with dichloromethane. The organic layer was dried over sodium sulfate, filtered and evaporated. The residue was

purified by preparative thin-layer chromatography (hexane/ethyl acetate: 40/60) to afford **9a**

(49.0 mg, 77%) as a pale yellow oil. ^{1}H NMR (400 MHz, CDCl$_3$): 8.96 (s, 1H), 8.13 (s, 1H), 8.07

(br s, 1H), 7.97-7.89 (m, 1H), 7.81-7.75 (m, 1H), 7.04 (dd, J = 9.0, 9.0 Hz, 1H), 6.39 (d, J = 16.8

Hz, 1H), 6.17 (dd, J = 10.2, 16.8 Hz, 1H), 5.73 (s, 2H), 5.69 (d, J = 10.2 Hz, 1H), 4.11 (br s, 2H),

3.63 (t, J = 8.2 Hz, 2H), 1.11 (t, J = 7.2 Hz, 3H), 0.96 (t, J = 8.2 Hz, 2H), −0.02 (s, 9H). ^{13}C NMR

(100 MHz, CDCl$_3$): 163.4, 163.1, 157.1 (J = 243 Hz), 154.7, 152.7, 152.0, 135.3, 134.2, 130.1,

127.6, 127.4 (J = 15.3 Hz), 122.9 (J = 8.1 Hz), 122.0, 115.3 (J = 22.9 Hz), 114.9, 109.6 (J = 2.0

Hz), 73.3, 67.3, 60.5, 17.7, 14.0, −1.5. ESI-MS: 485.4 (M+H$^+$).
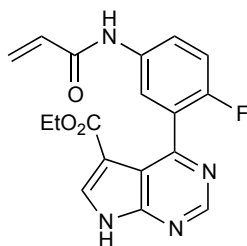
(1) ethyl 4-(5-acrylamido-2-fluorophenyl)-7H-pyrrolo[2,3-d]pyrimidine-5-carboxylate

Intermediate **9** (47.0 mg, 0.0990 mmol) was dissolved in dichloromethane (1.5 mL).

Trifluoroacetic acid (1.5 mL) was added and the mixture was stirred at room temperature for 14

hours. The mixture was concentrated and the residue was suspended in acetonitrile (1.5 mL),

and then the mixture was cooled to 0 ºC. 1M Sodium hydroxide solution (1.5 mL) was added

and the mixture was stirred at 0 ºC for 5 minutes. Saturated ammonium chloride solution was

added and the mixture was extracted with ethyl acetate. The organic layer was washed with

brine, dried over sodium sulfate, filtered and evaporated. The residue was purified by

preparative thin-layer chromatography (ethyl acetate) to afford JAK3i **1** (33.9 mg, 97%) as a

white solid. ^{1}H NMR (400 MHz, DMSO): 13.04 (br s, 1H), 10.33 (s, 1H), 8.97 (s, 1H), 8.33 (s,

1H), 8.06 (dd, J = 2.7, 6.6 Hz, 1H), 7.83 (ddd, J = 2.7, 4.7, 9.0 Hz, 1H), 7.23 (dd, J = 9.0, 9.0 Hz,

1H), 6.44 (dd, J = 10.2, 16.8 Hz, 1H), 6.28 (dd, J = 2.0, 16.8 Hz, 1H), 5.77 (dd, J = 2.0, 10.2 Hz,

1H), 4.01 (br s, 1H), 3.88 (br s, 1H), 0.94 (t, *J* = 7.4 Hz, 3H). ^{13}C NMR (100 MHz, DMSO): 163.1, 162.8, 156.1 (*J* = 243 Hz), 153.6, 153.0, 151.6, 135.0 (*J* = 2.3 Hz), 134.6, 131.7, 127.5 (*J* = 15.3 Hz), 127.0, 121.8 (*J* = 8.4 Hz), 121.5 (*J* = 3.1 Hz), 115.2 (*J* = 23.7 Hz), 113.8, 107.7 (*J* = 3.1 Hz), 59.5, 13.7. ESI-MS: 355.4 (M+H$^+$).
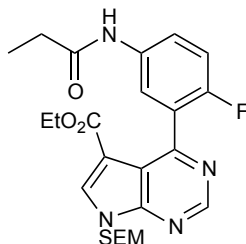
(**10**) **ethyl 4-(2-fluoro-5-propionamidophenyl)-7-((2-(trimethylsilyl)ethoxy)methyl)-7*H*-pyrrolo[2,3-*d*]pyrimidine-5-carboxylate**

Intermediate **8** (31.4 mg, 0.0729 mmol) was dissolved in dichloromethane (1.0 mL) and the mixture was cooled to 0 ºC. Propionyl chloride (7.6 mL, 0.0875 mmol) and triethylamine (15.2 mL, 0.109 mmol) were added and the mixture was stirred at 0 ºC for 10 minutes. Saturated ammonium chloride solution was added and the mixture was extracted with dichloromethane. The organic layer was dried over sodium sulfate, filtered and evaporated. The residue was purified by preparative thin-layer chromatography (hexane/ethyl acetate: 50/50) to afford **9b** (32.3 mg, 91%) as a pale yellow oil. ^{1}H NMR (400 MHz, CDCl$_3$): 8.95 (s, 1H), 8.11 (s, 1H), 7.96 (br s, 1H), 7.89-7.82 (m, 1H), 7.74 (dd, *J* = 2.8, 6.2 Hz, 1H), 7.00 (dd, *J* = 9.2, 9.2 Hz, 1H), 5.72 (s, 2H), 4.10 (br s, 2H), 3.62 (t, *J* = 8.2 Hz, 2H), 2.29 (q, *J* = 7.6 Hz, 2H), 1.17 (t, *J* = 7.6 Hz, 3H), 1.10 (t, *J* = 7.2 Hz, 3H), 0.95 (t, *J* = 8.2 Hz, 2H), –0.03 (s, 9H). ^{13}C NMR (100 MHz, CDCl$_3$): 172.1, 163.0, 156.8 (*J* = 248 Hz), 154.8, 152.6, 151.9, 135.2, 134.5 (*J* = 3.1 Hz), 127.1 (*J* = 15.3 Hz), 122.6 (*J* = 7.6 Hz), 121.7 (*J* = 2.3 Hz), 115.1 (*J* = 22.9 Hz), 114.8, 109.6 (*J* = 2.3 Hz), 73.3, 67.2, 60.5, 30.4, 17.7, 13.9, 9.6, –1.5. ESI-MS: 487.1 (M+H$^+$).
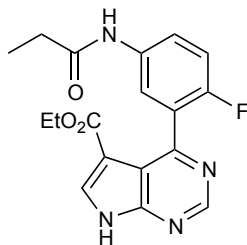
(2) ethyl 4-(2-fluoro-5-propionamidophenyl)-7*H*-pyrrolo[2,3-*d*]pyrimidine-5-carboxylate

Intermediate **10** (32.0 mg, 0.0658 mmol) was dissolved in dichloromethane (1.0 mL).

Trifluoroacetic acid (0.5 mL) was added and the mixture was stirred at room temperature for 3

hours. The mixture was concentrated and the residue was suspended in acetonitrile (1.5 mL).

20% ammonia solution (1.0 mL) was added and the mixture was stirred at room temperature for

overnight. The mixture was concentrated and purified by preparative thin-layer chromatography

(ethyl acetate) to afford **2** (18.8 mg, 97%) as a pale yellow solid. ^{1}H NMR (400 MHz, DMSO):

13.01 (br s, 1H), 10.02 (s, 1H), 8.95 (s, 1H), 8.32 (s, 1H), 7.98 (dd, *J* = 2.7, 6.6 Hz, 1H), 7.73

(ddd, *J* = 2.7, 4.4, 9.0 Hz, 1H), 7.18 (dd, *J* = 9.0, 9.0 Hz, 1H), 4.00 (br s, 1H), 3.88 (br s, 1H),

2.33 (q, *J* = 7.8 Hz, 2H), 1.09 (t, *J* = 7.8 Hz, 3H), 0.94 (t, *J* = 7.0 Hz, 3H). ^{13}C NMR (100 MHz,

DMSO): 171.9, 162.7, 155.7 (*J* = 242 Hz), 153.7, 152.9, 151.6,135.3 (*J* = 2.3 Hz), 134.5, 127.3

(*J* = 15.3 Hz), 121.4 (*J* = 7.6 Hz), 121.2 (*J* = 3.1 Hz), 114.9 (*J* = 22.9 Hz), 113.7, 107.7 (*J* = 3.1

Hz), 59.5, 29.5, 13.7, 9.6. ESI-MS: 357.1 (M+H$^+$).

3.6   References

1.   Rochman, Y., Spolski, R. & Leonard, W. J. New insights into the regulation of T cells by gc family cytokines. *Nat. Rev. Immunol.* **9,** 480–490 (2009).

2.   Miyazaki, T. *et al.* Functional activation of Jak1 and Jak3 by selective association with IL-2 receptor subunits. *Science* **266,** 1045–1047 (1994).

3.   Ghoreschi, K., Laurence, A. & O'shea, J. J. Janus kinases in immune cell signaling. *Immunol. Rev.* **228,** 273–287 (2009).

4.   Liao, W., Lin, J.-X. & Leonard, W. J. Interleukin-2 at the Crossroads of Effector Responses, Tolerance, and Immunotherapy. *Immunity* **38,** 13–25 (2013).

5.   Lin, J.-X. *et al.* Critical Role of STAT5 transcription factor tetramerization for cytokine responses and normal immune function. *Immunity* **36,** 586–599 (2012).

6.   Laurence, A. *et al.* Interleukin-2 Signaling via STAT5 Constrains T Helper 17 Cell Generation. *Immunity* **26,** 371–381 (2007).

7.   Lockyer, H. M., Tran, E. & Nelson, B. H. STAT5 is essential for Akt/p70S6 kinase activity during IL-2-induced lymphocyte proliferation. *J. Immunol.* **179,** 5301–5308 (2007).

8.   Yao, Z. *et al.* Stat5a/b are essential for normal lymphoid development and differentiation. *Proc. Natl Acad. Sci. USA* **103,** 1000–1005 (2006).

9.   Thomis, D. C., Gurniak, C. B., Tivol, E., Sharpe, A. H. & Berg, L. J. Defects in B lymphocyte maturation and T lymphocyte activation in mice lacking Jak3. *Science* **270,** 794–797 (1995).

10.   Thomis, D. C. & Berg, L. J. Peripheral expression of Jak3 is required to maintain T lymphocyte function. *J. Exp. Med.* **185,** 197–206 (1997).

11.   Witthuhn, B. A., Williams, M. D., Kerawalla, H. & Uckun, F. M. Differential substrate recognition capabilities of Janus family protein tyrosine kinases within the Interleukin 2 receptor (IL2R) system. *Leuk Lymphoma* **32,** 289–297 (1999).

12.   Haan, C. *et al.* Jak1 Has a Dominant Role over Jak3 in Signal Transduction through gc-Containing Cytokine Receptors. *Chem. Biol.* **18,** 314–323 (2011).

13.   Perona-Wright, G., Mohrs, K. & Mohrs, M. Sustained signaling by canonical helper T cell cytokines throughout the reactive lymph node. *Nature Immunol.* **11,** 520–526 (2010).

14.   Swainson, L. *et al.* IL-7-induced proliferation of recent thymic emigrants requires activation of the PI3K pathway. *Blood* **109,** 1034–1042 (2006).

15.   Liao, W. *et al.* Opposing actions of IL-2 and IL-21 on Th9 differentiation correlate with their differential regulation of BCL6 expression. *Proc. Natl Acad. Sci. USA* **111,** 3508–3513 (2014).

16.   Arneja, A., Johnson, H., Gabrovsek, L., Lauffenburger, D. A. & White, F. M. Qualitatively Different T Cell Phenotypic Responses to IL-2 versus IL-15 Are Unified by Identical Dependences on Receptor Signal Strength and Duration. *J. Immunol.* **192,** 123–135 (2014).

17.   Cantrell, D. A. & Smith, K. A. The Interleukin-2 T-cell system: a new cell growth model. *Science* **224,** 1312–1316 (1984).

18.   London, N. *et al.* Covalent docking of large libraries for the discovery of chemical probes. *Nat. Chem. Bio.* **10,** 1066–1072 (2014).

19.   Goedken, E. R. *et al.* Tricyclic covalent inhibitors selectively target Jak3 through an active site thiol. *J. Biol. Chem.* **290,** 4573–4589 (2015).

20.   Tan, L. *et al.* Development of Selective Covalent Janus Kinase 3 Inhibitors. *J. Med. Chem.* **58,** 6589–6606 (2015).

21.   Clark, J. D., Flanagan, M. E. & Telliez, J.-B. Discovery and development of Janus kinase (JAK) inhibitors for inflammatory diseases. *J. Med. Chem.* **57,** 5023–5038 (2014).

22.   Readinger, J. A., Mueller, K. L., Venegas, A. M., Horai, R. & Schwartzberg, P. L. Tec kinases regulate T-lymphocyte development and function: new insights into the roles of Itk and Rlk/Txk. *Immunol. Rev.* **228,** 93–114 (2009).

23.   Ahearn, S. P. *et al.* Pyrrolopyrimidines as Janus Kinase Inhibitors. WO085802 A1 (2013).

24.   Brennan, P. *et al.* Phosphatidylinositol 3-Kinase Couples the Interleukin-2 Receptor to the Cell Cycle Regulator E2F. *Immunity* **7,** 679–689 (1997).

25.   Cornish, G. H., Sinclair, L. V. & Cantrell, D. A. Differential regulation of T-cell growth by IL-2 and IL-15. *Blood* **108,** 600–608 (2006).

26.   Lanning, B. R. *et al.* A road map to evaluate the proteome-wide selectivity of covalent kinase inhibitors. *Nat. Chem. Bio.* **10**, 760-767 (2014).

27.   Schaeffer, E. M. *et al.* Requirement for Tec kinases Rlk and Itk in T cell receptor signaling and immunity. *Science* **284,** 638–641 (1999).

28.   Rowell, E. A. & Wells, A. D. The role of cyclin-dependent kinases in T-cell development, proliferation, and function. *Crit. Rev. Immunol.* **26,** 189–212 (2006).

29.   Wormald, S. *et al.* The Comparative Roles of Suppressor of Cytokine Signaling-1 and -3 in the Inhibition and Desensitization of Cytokine Signaling. *J. Biol. Chem.* **281,** 11135–11143 (2006).

30.   Cornish, A. L. *et al.* Suppressor of Cytokine Signaling-1 Regulates Signaling in Response to Interleukin-2 and Other g_c-dependent Cytokines in Peripheral T Cells. *J. Biol. Chem.* **278,** 22755–22761 (2003).

31.   Yang, X. O. *et al.* The signaling suppressor CIS controls proallergic T cell development and allergic airway inflammation. *Nature Immunol.* **14,** 732–740 (2013).

32.   Babon, J. J. *et al.* Suppression of Cytokine Signaling by SOCS3: Characterization of the Mode of Inhibition and the Basis of Its Specificity. *Immunity* **36,** 239–250 (2012).

33.   Dowty, M. E. *et al.* Preclinical to Clinical Translation of Tofacitinib, a Janus Kinase Inhibitor, in Rheumatoid Arthritis. *J. Pharmacol. Exp. Ther.* **348,** 165–173 (2014).

34.   Xing, L. *et al.* Alopecia areata is driven by cytotoxic T lymphocytes and is reversed by JAK inhibition. *Nat Med* (2014). doi:10.1038/nm.3645

35.   Ghoreschi, K. *et al.* Modulation of innate and adaptive immune responses by tofacitinib

(CP-690,550). *J. Immunol.* **186,** 4234–4243 (2011).

36.   Krutzik, P. O. & Nolan, G. P. Fluorescent cell barcoding in flow cytometry allows high-

throughput drug screening and signaling profiling. *Nat Meth* **3,** 361–368 (2006).

Chapter 4   IL-2Rβ Abundance Tunes T Cell IL-2 Signaling Dynamics

4.1 Abstract

The cytokine IL-2 drives both activated CD4 and CD8 T cells to proliferate. On a molecular level, both cell types signal through an identical receptor complex and show the same IL-2 dose-dependent phosphorylation of the canonical transcription factor STAT5. Despite this, CD8 T cells enter S-phase sooner and proliferate to a greater overall degree in response to IL-2. Here, we identify distinct IL-2 signaling dynamics in CD4 and CD8 T-cell blasts. When STAT5 phosphorylation was followed over time, CD8 T cells sustained this signaling throughout a 6-hour time course, while CD4 T cells had a biphasic response, with maxima at 15 minutes and 2-4 hours. Two components of the IL-2R, IL-2Rβ and IL-2Rγ, were twice as abundant on the surface and within CD8 T cells. A 50% knockdown of the IL-2Rβ receptor chain converted CD8 T cells to a CD4-like signaling pattern and reduced early S-phase entry. These results suggest that a large pool of IL-2Rβ in CD8 T-cells sustains strong IL-2 signaling over time and contributes to the quantitatively greater IL-2 proliferative response relative to CD4 T cells. This cell type variability in IL-2Rβ expression appears to tune responses, potentially preventing extensive, autoimmune expansion of CD4 T cells while still enabling sufficient CD8 expansion to control viral infections.

120

4.2   Introduction

The common γ-chain cytokine IL-2 plays an essential role in the development, expansion, and function of many lymphocyte subsets, including T and NK cells [1]. IL-2 induces signals by binding to a receptor complex minimally comprised of the IL-2Rβ and IL-2Rγ subunits. Binding induces a conformational change that activates the associated cytoplasmic kinases JAK1 and JAK3, which in turn phosphorylate three tyrosines on the IL-2Rβ chain. Phospho-Tyr[392] and -Tyr[510] recruit the transcription factor STAT5, which is rapidly phosphorylated and alters transcription of IL-2 dependent genes [2]. Phospho-Tyr[338] recruits the adapter protein Shc, which can activate PI3K signaling and, in some cell types, MAPK signaling. Depending on the cell type and physiologic context, these signals combine to trigger proliferation, production of effector molecules or differentiation into distinct T-cell subsets, such as regulatory (Treg) or memory T cells.

IL-2 driven cell fate changes require hours to days of sustained signaling. Differentiation into Tregs requires up to 3 days of IL-2 exposure [3], and S-phase entry by effector T cells requires 8-12 hours of continuous IL-2 [4,5]. Despite this, most studies of IL-2 signaling have focused on events immediately following stimulation. In our previous work in activated CD4 T cells, we examined IL-2 signaling throughout this critical 8-12 hour period prior to S-phase entry and found that there are two waves of STAT5 phosphorylation (pSTAT5) following stimulation: an initial strong rapid induction of pSTAT5 that peaks within 15 minutes and decays by approximately an hour and a second wave, which appears between 2 and 12 hours after initial stimulation. Abolishing the second wave of pSTAT5 was sufficient to prevent S-phase entry [5]. This unique signaling pattern, coupled with the importance of sustained IL-2 signaling, raises the question of how signaling dynamics vary by cell type or cytokine and how this impacts cell fate decisions.

At physiologic doses, IL-2 signals through the 'high affinity' (K_d ~10 pM) receptor complex composed of IL-2Rα (CD25), IL-2Rβ (CD122) and IL-2Rγ (CD132)[6]. This trimeric architecture enables regulation of T-cell IL-2 responsiveness at multiple levels. While all T cells express IL-2Rγ, resting, naïve T cells do not express IL-2Rα and are unresponsive to physiologic doses of IL-2[7]. Upon activation via the T-cell receptor (TCR), IL-2Rα is induced to very high abundance, at least 10-fold higher than IL-2Rβ or IL-2Rγ[8-10], and cells become sensitive to IL-2. Additionally, naïve CD4 T cells surface IL-2Rβ is at or below the limit of detection, rendering these cells minimally responsive to IL-2 until at least 24 hours after TCR activation, despite the rapid induction of IL-2Rα[11]. By contrast, naïve CD8 T cells have small, but detectable quantity of IL-2Rβ chains and can respond to high dose IL-2 through the 'intermediate affinity' (K_d~ 1 nM) receptor [6,12]. Similar to CD4 T cells, activation induces higher IL-2Rβ abundance Upon IL-2 binding, receptor complexes are rapidly internalized (surface $t_{1/2}$ ~15 minutes) and the majority of IL-2Rβ and IL-2Rγ subunits are degraded ($t_{1/2}$~50-70 minutes) while IL-2Rα is recycled to the surface ($t_{1/2}$ >>6 hours) [13,14]. The precise number and subcellular localization of inidivdual IL-2 receptor subunits is a potentially important regulatory mechanism given the requirement for sustained IL-2 signaling and the short half-life of IL-2-bound receptor complexes [15].

Here, we compared the IL-2 signaling dynamics of CD4 and CD8 T cells. As others have reported [16], we found that IL-2 triggered quantitatively stronger proliferation in CD8 compared CD4 T cells. At the signaling level, unlike the biphasic response seen in CD4 T cells, CD8 T cells had a very different signaling pattern: a strong and sustained induction of pSTAT5. We compared the abundance of IL-2R subunits and found that CD8 T cells express approximately twice as much IL-2Rβ and IL-2Rγ as CD4 T cells. By examining the dynamics of other γ_c-cytokines, we identified IL-2Rβ as a limiting receptor component in CD4 T cells. A 50% reduction of IL-2Rβ abundance in CD8 T cells converted the signaling dynamics to a CD4-like

phenotype and greatly blunted their proliferative response. Finally, we found that Tregs express

similar amounts of IL-2Rβ to CD8 T cells and also have a strong and sustained pattern of IL-2

signaling. These results suggest a model whereby IL-2Rβ abundance across a narrow range

can dramatically alter a cell's IL-2 responsiveness.

4.3   Results

Proliferative Responses to IL-2

Since naïve T-cells do not express the 'high affinity' IL-2 receptor, we generated CD4

and CD8 T-cell blasts from primary murine T-cells in order to compare IL-2 signaling in each cell

type. Upon stimulation with a physiologic dose of IL-2 (50 u/mL), both resting CD4 and CD8 T-

cell blasts enter S-phase and proliferate. However, CD8+ T-cell blasts enter S-phase sooner

and more synchronously than CD4+ T-cell blasts (Figure 4-1A. Consequently, CD8+ T-cell

blasts undergo more cell divisions in 72 hours following IL-2 stimulation (Figure 4-1B). This

increased proliferative response of CD8 vs. CD4 T cells to IL-2 has been seen before[16].

Furthermore, enhanced CD8 vs. CD4 proliferation has also been observed in response to

simultaneous TCR and IL-2 stimulation in vitro and in vivo[17,18].
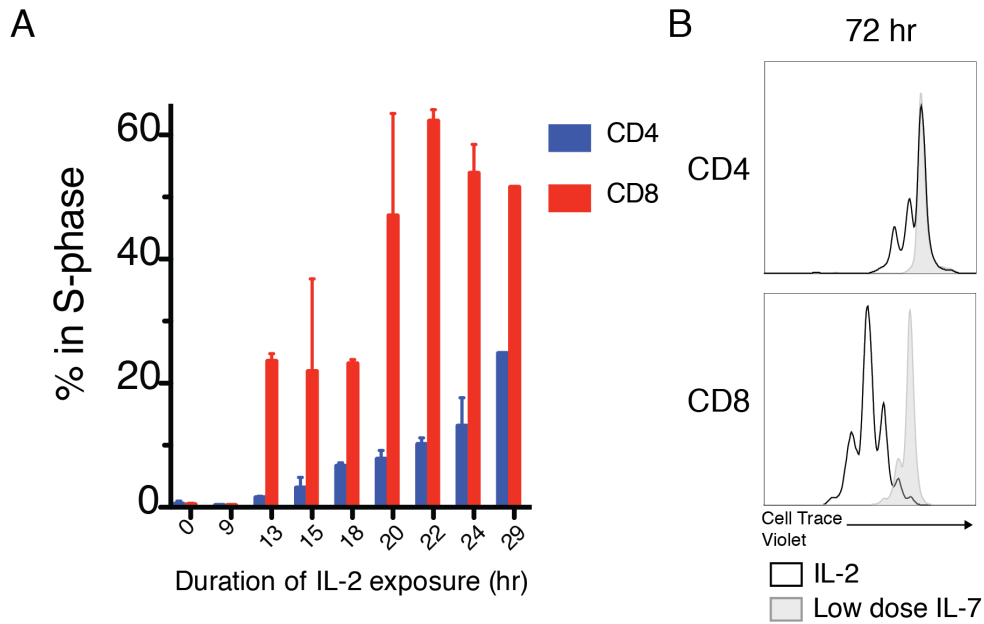
Figure 4-1 Proliferative Response of CD4 and CD8 T Cells to IL-2
(A) S-phase entry of rested CD4 and CD8 T cell blasts was assessed with a 1-hr pulse of ethynyl deoxyuridine (EdU) after the indicated duration of IL-2 stimulation. (B) Cell proliferation after 72 hours of IL-2 stimulation was assessed by dye dilution (Cell Trace Violet) compared to undivided cells sustained with low dose IL-7. Pooled results from 7 independent experiments plotted as mean +/- SEM (A) or representative of 3 independent experiments (B).

Distinct IL-2 Signaling Dynamics

To understand the signaling basis for this enhanced response observed in CD8 T-cell blasts, we first assessed the immediate (t=15 min) phosphorylation of STAT5, which is essential for IL-2 driven proliferation [2]. In response to a wide titration of IL-2 concentrations, CD4 and CD8 T-cell blasts displayed nearly identical dose responses (EC$_{50}$ 0.25 u/mL and 0.24 u/mL respectively, Figure 4-2A, B). At high concentrations, the magnitude of the response (i.e. the mean fluorescence intensity of the responding population) was approximately 25% higher in CD8 T-cells compared to CD4 T-cells (Figure 4-3A, B). While it was tempting to attribute the enhanced proliferation of CD8 T-cells to this increase in maximal pSTAT5, prior work showing that T-cell proliferation requires hours of continuous IL-2 exposure led us to suspect a more complicated mechanism [4,5].
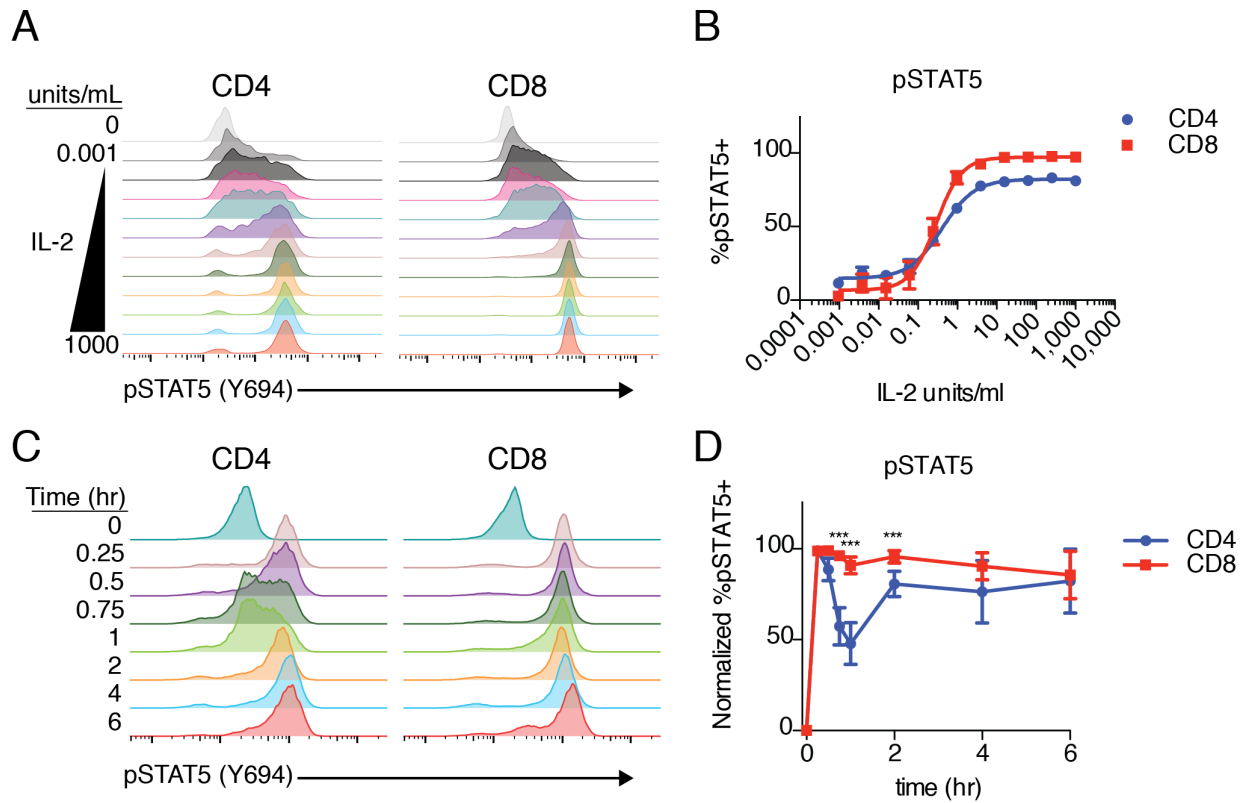
Figure 4-2 Distinct IL-2 Signaling Dynamics in CD4 and CD8 T Cells

Rested T cell blasts were stimulated with a 4-fold titration of IL-2 from 1000 to 0.001 units/mL and pSTAT5 was assessed by phosphoflow cytometry. (B) Fraction of responding (pSTAT5+) cells at each concentration of IL-2. (C) Time course of pSTAT5 following IL-2 stimulation. (D) quantification of pSTAT5 over time. Representative histograms from 3 (A) or 11 (C) independent experiments. Plotted as mean +/- SEM from 3 independent experiments (B) or mean with 95% confidence interval from 11 independent experiments (D). *** $p < 0.001$ by one-way ANOVA with Bonferroni multiple comparison test.
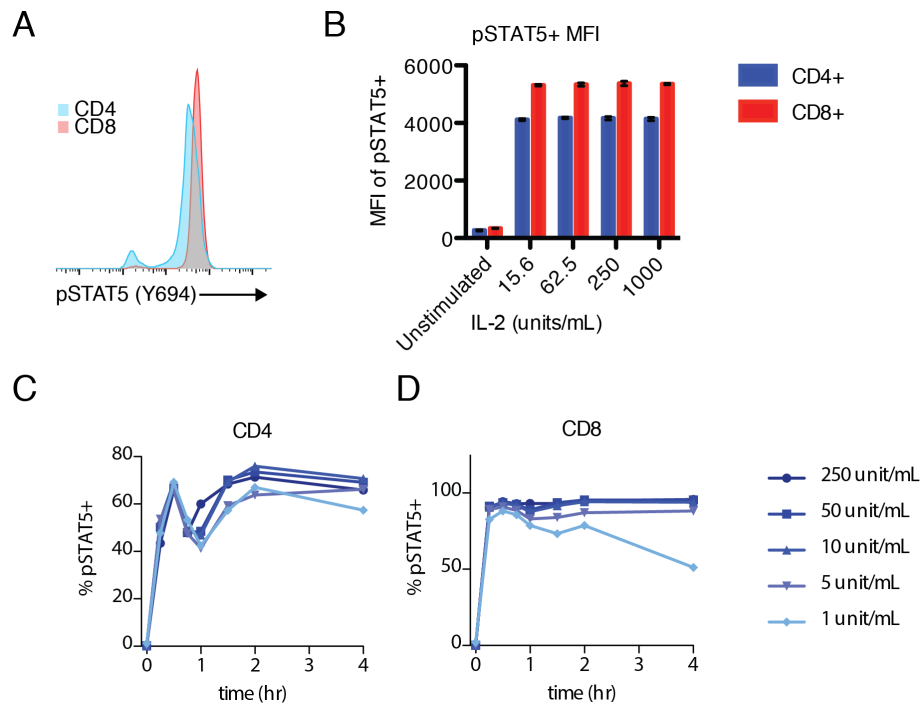
Figure 4-3 IL-2 Signaling in CD4 and CD8 T Cells
(a) Overlay of pSTAT5 histograms from 62.5 units/mL dose of IL-2 for CD4 and CD8 T cells. (b) Quantification of mean fluorescence intensity (MFI) of pSTAT5+ peak at each dose of IL-2. (c) and (d) pSTAT5 time course at range of IL-2 doses in CD4 (c) and CD8 (d) T cells.

In CD4 T-cells, IL-2 triggers a biphasic STAT5 phosphorylation response, with an initial peak of phosphorylation 15-30 minutes after IL-2 stimulation and a second peak 2-12 hours after stimulation [5]. Given this result, we next asked whether CD8 T cells displayed a similar pattern of STAT5 phosphorylation (pSTAT5). To our surprise, CD8 and CD4 T cells exhibited very different signaling dynamics reflected by pSTAT5 (Figure 4-2C, D). Unlike CD4 T cells, there was a single, sustained peak of pSTAT5 in CD8 T cells without the characteristic decrease in phosphorylation seen at 1 hr in CD4 T cells. The fraction of pSTAT5+ cells was significantly higher in CD8 T cells 45 minutes, 1 hr and 2 hrs after IL-2 stimulation, but similar before and after those time points. These patterns persisted at a range of physiologic IL-2 concentrations from 1 unit/mL to 250 units/mL (Figure 4-3 C, D).

IL-2-dependent proliferation in T-cell blasts also requires activation of PI3K & mTOR signaling (although not ERK/MAPK) [5]. As a proxy for mTOR activity, phosphorylated ribosomal protein S6 (pS6) was monitored over time in CD4 and CD8 T-cell blasts. While CD4 T cells

required ~2 hours before a majority of cells had activated pS6, almost all CD8 T cells activated

S6 immediately after stimulation. The mean fluorescence intensity of pS6 also increased

throughout the time course for CD8 T cells (Figure 4-4).
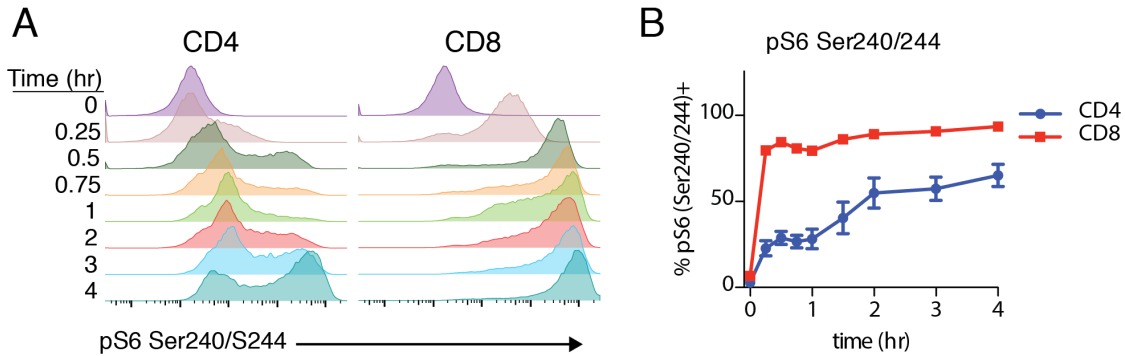
Figure 4-4 PI3K/mTOR Signaling
(A) Induction of pS6 Ser240/244 over time following IL-2 stimulation, assessed by phosphoflow cytometry. (B) quantification of pS6+ cells over time. Plotted as mean +/- SEM of 4 independent experiments.

Requirements for Sustained pSTAT5

These striking results led us to ask whether these distinct signaling dynamics could

explain the difference in proliferative responses to IL-2. To address this question, we first

needed to understand the mechanistic basis for these patterns. Washout experiments

suggested that both the second wave of pSTAT5 in CD4 T cells and sustained signaling in

CD8s required the continued presence of IL-2, perhaps to initiate new signaling complexes

between IL-2 and unoccupied receptors (Figure 4-5 A-B). To assess possible differences in the

negative regulation of the IL-2 pathway in CD4 and CD8 T cells, we monitored the decay of

pSTAT5. Cells were stimulated with IL-2 for 15 minutes and then a high dose of JAK3i was

added to shut off signaling. In both cell types, pSTAT5 was abolished within 30 minutes of

adding JAK3i and the decay was roughly similar (Figure 4-5 C-D).

The washout and inhibitor studies led us to suspect a difference in the signal generation

capacity of CD4 and CD8 T cells. At a minimum, STAT5 phosphorylation requires the IL-2Rβ

and IL-2Rγ chains and the cytoplasmic kinases JAK1 and JAK3. Upon IL-2 binding, the IL-2

receptor complex is rapidly internalized [13,14], potentially creating a shortage of receptors to generate new signal. To test whether sustained signaling required new receptor chains to traffic to the surface from intracellular pools, we treated cells simultaneously with IL-2 and brefeldin A, a Arf-GEF inhibitor that blocks vesicular transport. In the presence of brefeldin A, Both CD4 and CD8 T cells reached the maximum pSTAT5 after 15 minutes and then rapidly returned to basal levels, indicating that vesicular transport was essential to sustain pSTAT5 (Figure 4-5 E-F). Given the apparent short half-life of signaling-competent receptors, we wondered whether differences in receptor abundance could underlay the distinct signaling dynamics in CD4 and CD8 T cells.
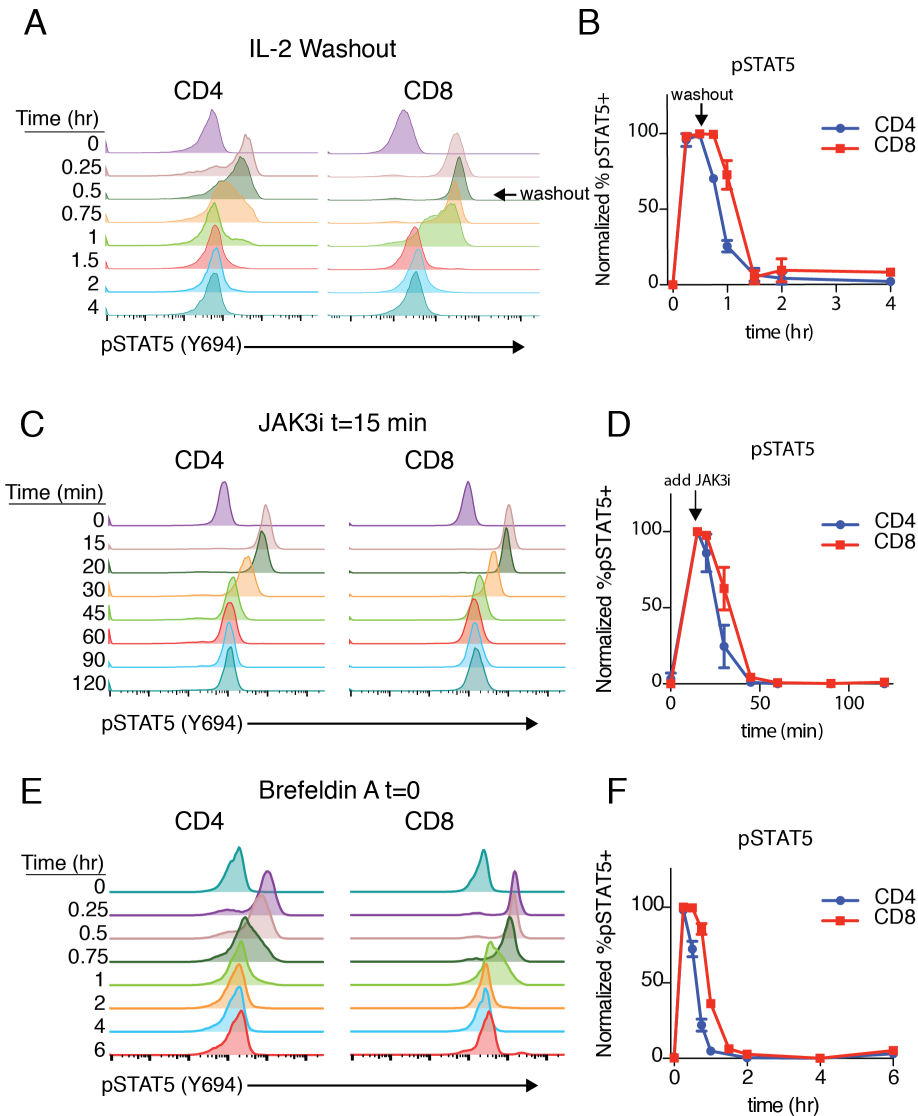
Figure 4-5 Requirements for Sustained IL-2 Signaling
(a) Cells were stimulated for 30 minutes and then IL-2 was washed out (3 washes with 1 mL of warm media) and pSTAT5 monitored by phosphoflow. (b) quantification of washout. (c) Cells were stimulated with IL-2 and then high dose JAK3i (500 nM) was added at t=15 minutes and signal decay was monitored, quantified in (d). Cells were stimulated simultaneously with IL-2 and brefeldin A and pSTAT5 was monitored over time. Data are plotted as mean +/- SEM of 3 independent experiments.

IL-2 Receptor Abundance

Staining of surface IL-2 receptor chains revealed that CD8 T cells have approximately

twice as much IL-2Rβ and IL-2Rγ as CD4 T-cells, but no significant difference in IL-2Rα

abundance (Figure 4-6A, B). To probe the intracellular pool specifically, we bound surface

receptors with unlabeled antibodies prior to fixation and membrane permeabilization and then

stained for each receptor with the same fluorophore-antibody conjugate as used in the surface

only experiments. Using this method, we observed that intracellular IL-2Rα staining was much weaker than surface staining, suggesting a predominantly surface localization, and was not significantly different in CD4 and CD8 T cells (Figure 4-6C, D). In contrast to IL-2Rα, there was strong intracellular staining for IL-2Rβ and IL-2Rγ, which indicated substantial intracellular pools, and that these pools were significantly larger in CD8 T cells, by approximately 2-fold and 1.5-fold respectively (Figure 4-6C, D). For IL-2Rβ, this difference appeared to be encoded at the mRNA level. mRNA did not correlate with protein for either IL-2Rα or IL-2Rγ (Figure 4-6E).
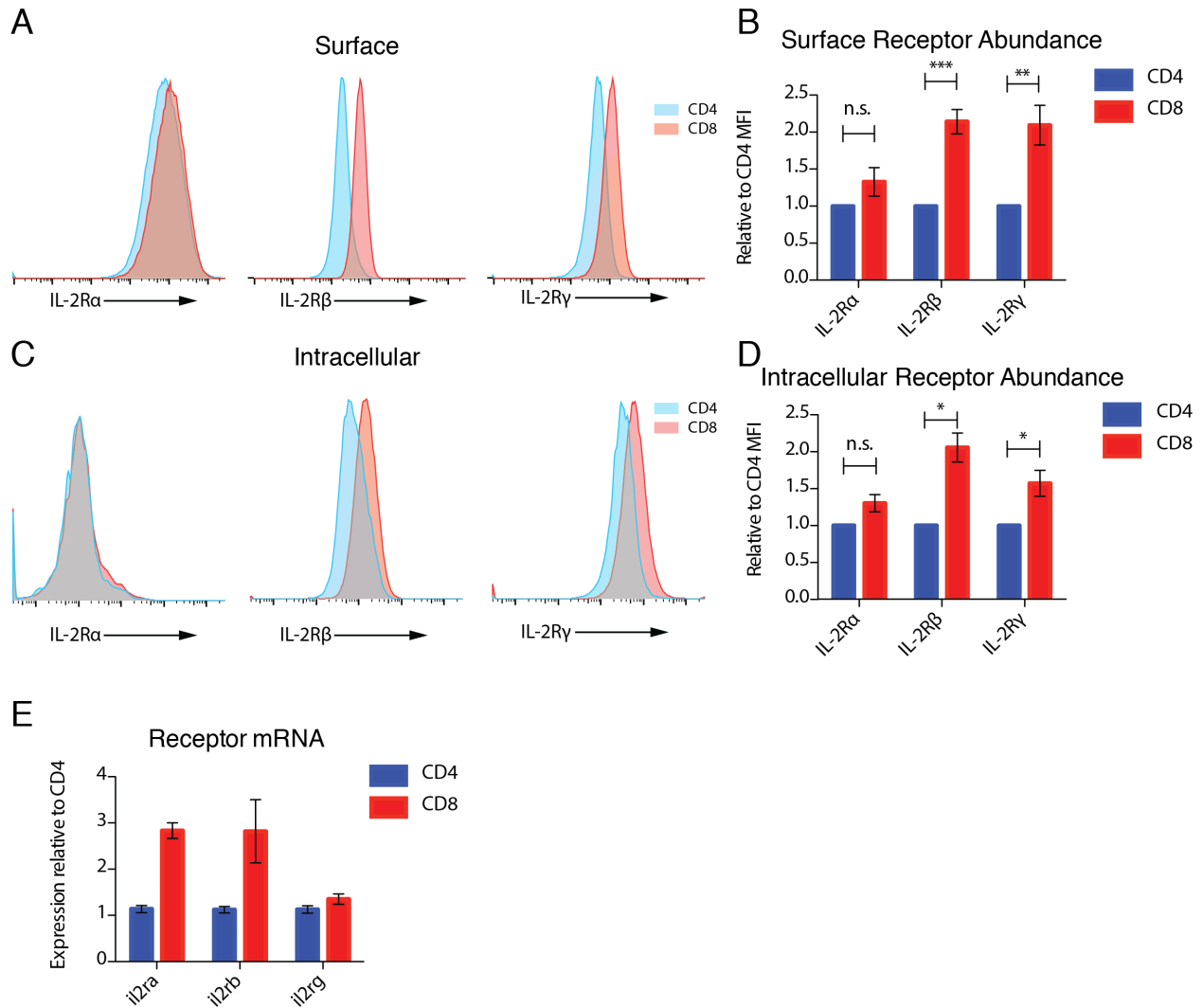
Figure 4-6 IL-2R Subunit Abundance
(A) Representative histograms of IL-2Ra, IL-2Rb and IL-2Ry staining on the surface of CD4 and CD8 T cells. (B) Quantification of receptor abundance relative to MFI on CD4 T cells in each experiment. (C) Intracellular receptor pools were assessed by binding surface receptor with unlabeled antibody and subsequent fixation and permeabilization prior to staining with the same antibody-fluorophore conjugates as in (A). (D) Quantification of intracellular receptor abundance relative to MFI on CD4 T cells in each experiment. (E) qPCR of mRNA levels for each receptor chain in resting CD4 and CD8 T cell blasts. Representative of 7 (A) and 3 (C) independent experiments. Pooled data from 7 (B) and 3 (D) independent experiments, plotted +/- SEM. Student's T Test: n.s. not significant; * $p<0.05$, **$p<0.01$, ***$p<0.001$. mRNA from 3 biological replicates plotted with 95% confidence interval.

IL-7 and IL-15 Signaling Dynamics

The increased abundance of IL-2Rβ and IL-2Rγ on CD8 T cells suggested that either or both receptor chains could explain the distinct signaling dynamics observed in response to IL-2. Internalization and degradation of a limiting number of IL-2Rβ or IL-2Rγ could lead to the loss of signal between 45 minutes and 2 hours in CD4 but not CD8 T cells. Within the common γ-chain

family of cytokines (γ_c), two cytokines (IL-2 and IL-15) utilize the IL-2Rβ chain, while others have a unique chain that pairs with IL-2Rγ (Figure 4-7A). To test the respective roles of IL-2Rβ and IL-2Rγ, we compared IL-7 (IL-7Rα & IL-2Rγ) and IL-15 (IL-2Rβ & IL-2Rγ) signaling. If IL-2Rγ was limiting, IL-2, IL-7 and IL-15 would all exhibit biphasic signaling, whereas limiting amounts of IL-2Rβ would only impact IL-2 and IL-15. Following stimulation of CD4 T cells with IL-7, pSTAT5 was strong and sustained, with no loss of signal until 5 hr after IL-2 addition (Figure 4-7B, C). In striking contrast, stimulation with IL-15 produced a biphasic response, with a significant loss of signal at 1 hr and subsequent partial recovery (Figure 4B, C). When CD8 T cells were stimulated with either cytokine, pSTAT5 was strong and sustained (Figure 4-7D, E). Taken together, these results were most consistent with a limiting pool of IL-2Rβ in CD4 T cells causing a drop in IL-2 and IL-15 driven STAT5 phosphorylation.
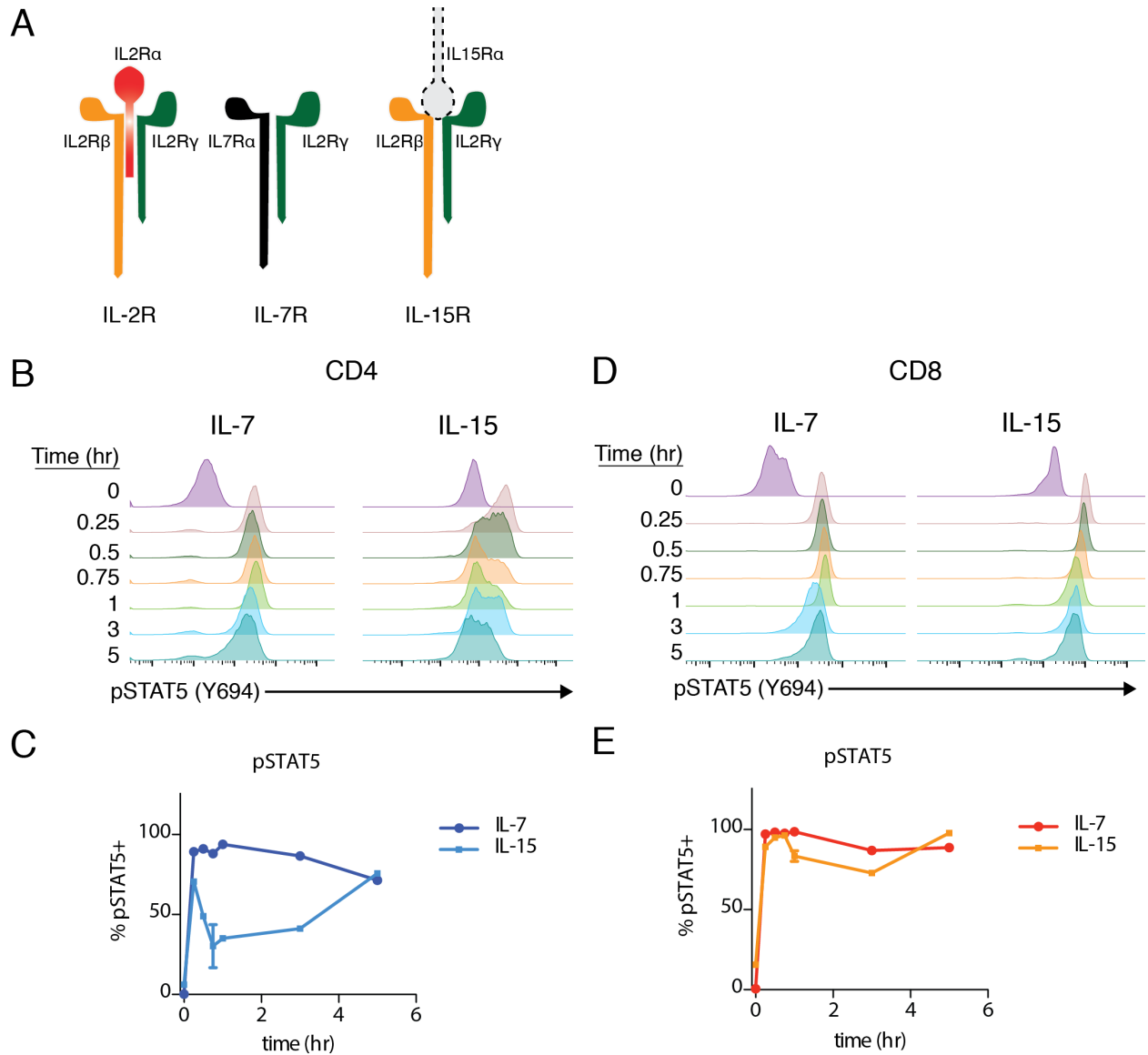
Figure 4-7 Comparative dynamics of IL-7 and IL-15
(A) Schematic of IL-2, IL-7 and IL-15 receptor components. Note IL-15 usually presented in trans from IL-15Ra on neighboring cell. (B) Representative time course histograms of IL-7 and IL-15 in CD4 T cells. (C) quantification of fraction pSTAT5 in response to IL-7 and IL-15. (D) Representative time course histograms of IL-7 and IL-15 in CD8 T cells, quantified in (E). Representative of (B, D) or pooled from (C, E) 3 independent experiments. Plotted +/- SEM in (C, E).

Knockdown of IL-2Rβ

The data in Fig. 4-7 suggest a model in which the dynamics of STAT5 phosphorylation can be tuned by IL-2Rβ abundance. This model predicts that reducing IL-2Rβ levels in CD8 T cells would result in a CD4-like signaling pattern. To test this, we transduced primary CD8 T cell blasts with lentiviruses expressing GFP and one of a panel of 4 small hairpin RNAs (shRNA) targeting *il2rb*. These hairpins gave a range of knockdown efficiencies from 22-77% based on surface staining (Figure 4-8A & Figure 4-9A). Reduction of IL-2Rβ in CD8 T cells by ~50% with IL2RB shRNA #2 or #3 resulted in a biphasic CD4-like signaling pattern, with a loss of pSTAT5 at 1 hr, followed by rapid recovery (Figure 4-8B, C & Figure 4-9B). Scrambled shRNA or a marginal reduction with IL2RB shRNA #4 had minimal effect on signaling dynamics (Figure 4-8B, C and Figure 4-9B). Knockdown to below 25% of WT levels with IL2RB #1 markedly impaired signaling, producing a very weak pSTAT5 response at all time points (Figure 4-8C and Figure 4-9B). Two-fold reduction in IL-2Rβ (with shRNA #2) had only a small effect on the maximal pSTAT5 response observed at 15 minutes (Figure 4-8C and Figure 4-9C), which was comparable to the difference observed between CD4 and CD8 T cells (Figure 4-3).

We next asked whether this reduction in IL-2Rβ abundance contributed to the weaker proliferative response of CD4 T cells (Figure 4-1). Sustaining primary CD8 T cells in culture was challenging in the context of impaired IL-2 signaling. After culture for 3 days in IL-2, the frequency of cells expressing IL2RB shRNA #1 and #2 had decreased by 6 and 3-fold, respectively, while there was no significant change in the frequency of scrambled shRNA expressing cells (Figure 4-9D). This result could be explained by either proliferative or survival signaling defects, so we next assessed S-phase entry in cells that were activated for 3 days, rested overnight and stimulated with IL-2 for 13 hours. Here, a significantly smaller fraction of IL2RB shRNA expressing cells entered S-phase compared to untransduced cells in the same

sample (Figure 4-8D). Together, these results suggest that even a modest 50% reduction in IL-2Rβ abundance greatly impacts IL-2 driven proliferation.
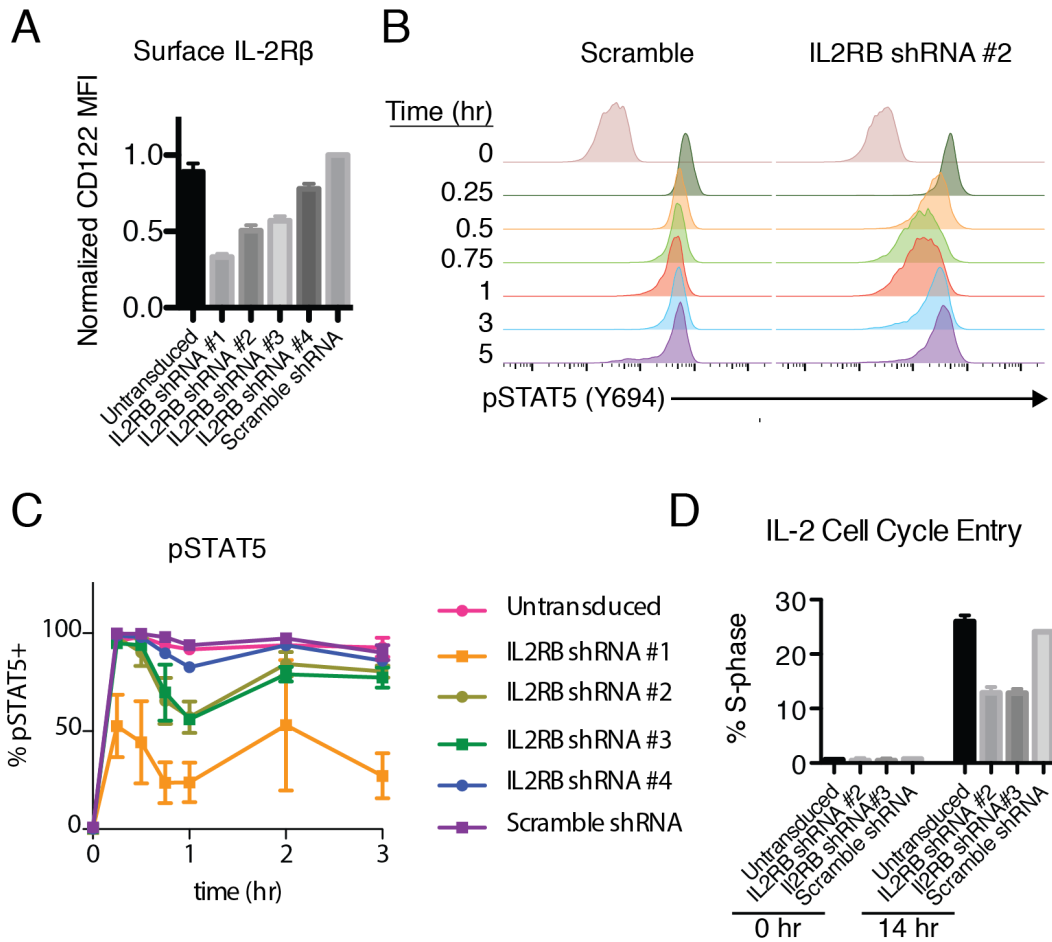
Figure 4-8 Knockdown of IL2RB in CD8 T Cell blasts.
(A) Effect of panel of shRNAs targeting IL2RB relative to scramble shRNA on surface IL-2Rβ abundance, assessed by FACS. (B) IL-2 signaling time course showing pSTAT5 in scramble and IL2RB shRNA #2. (C) Quantification of pSTAT5+ fraction over time. (D) S-phase entry, assessed by EdU incorporation, after 13 hours of IL-2 stimulation in briefly rested CD8 T cell blasts transduced with shRNA (GFP+) or untransduced (GFP-). Data are representative of (B) or pooled from 4 (A) or 3 (B, C, D) independent experiments. Plotted as mean +/- SEM.
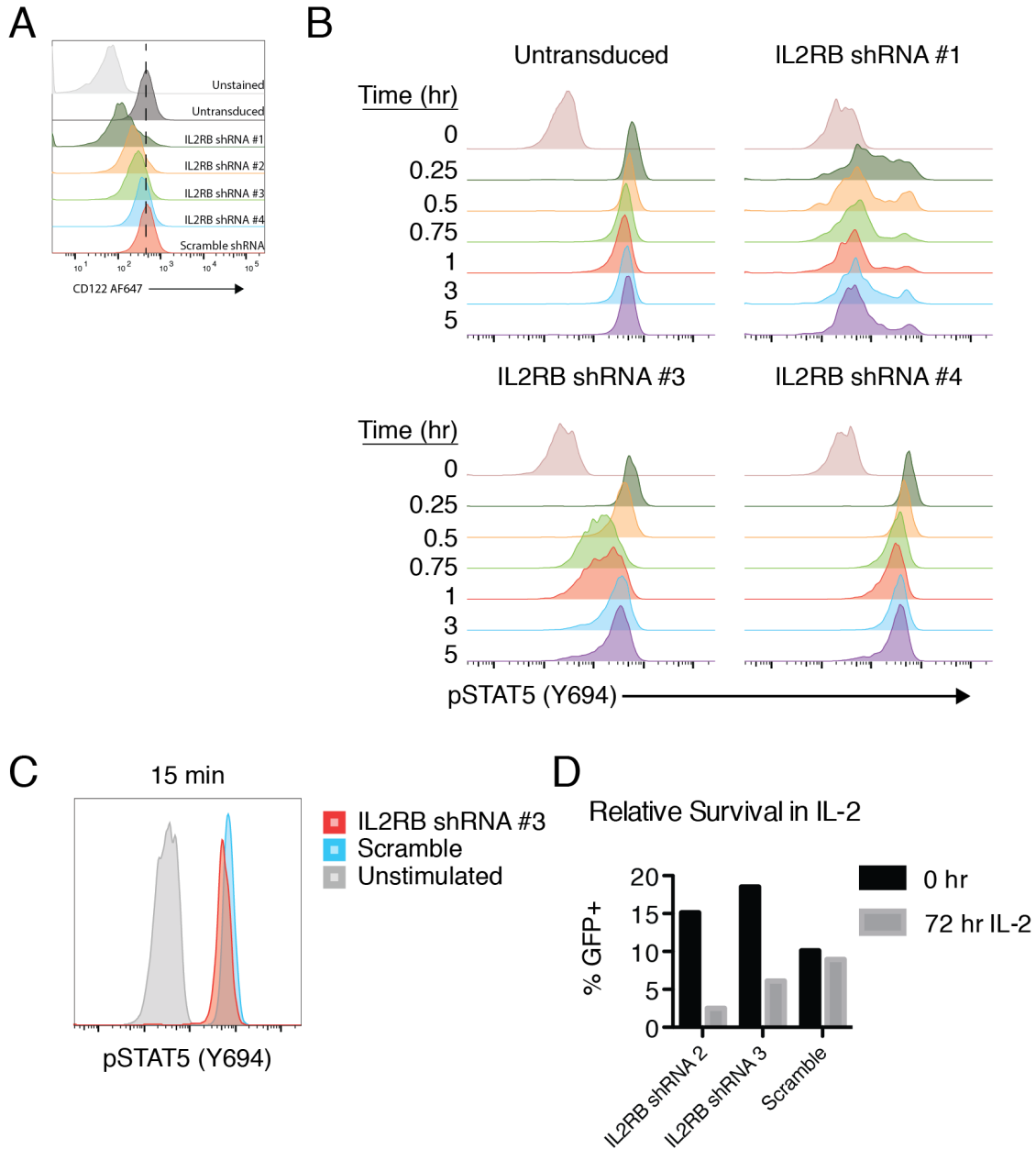
Figure 4-9 Supplementary Figure to IL2RB shRNA Figure
(A) Representative histograms of IL-2Rβ surface abundance with each shRNA. (B) pSTAT5 time course for other shRNAs and untransduced cells. Data quantified in Figure 5C. (C) Overlay of pSTAT5 after 15 minutes of IL-2 stimulation. (D) Fraction of shRNA expressing (GFP+) cells was assessed immediately after TCR activation (0 hr) and after 72 hours of IL-2 stimulation.

IL-2 Signaling Dynamics in Tregs

To extend our model, we examined regulatory T-cells (Tregs), which are highly dependent on IL-2 signaling for development, survival and function. Comparing the intracellular pool of IL-2Rβ on freshly isolated Tregs to CD4 and CD8 T-cell blasts, we found that Tregs have roughly similar amounts of receptor to CD8 T cells, or roughly than twice the amount found in CD4 T cells (Figure 4-10A, B). Unlike naïve T cells, Tregs express high basal levels of IL-2Rα and respond to physiologic doses of IL-2 without pre-activation. Splenocytes were stimulated ex-vivo with IL-2 and pSTAT5 in Foxp3+ Tregs was monitored over time. As predicted by the significant intracellular pool of IL-2Rβ, we observed a strong and sustained pattern of pSTAT5 similar to that observed in CD8 T cells (Figure 4-9C, D).
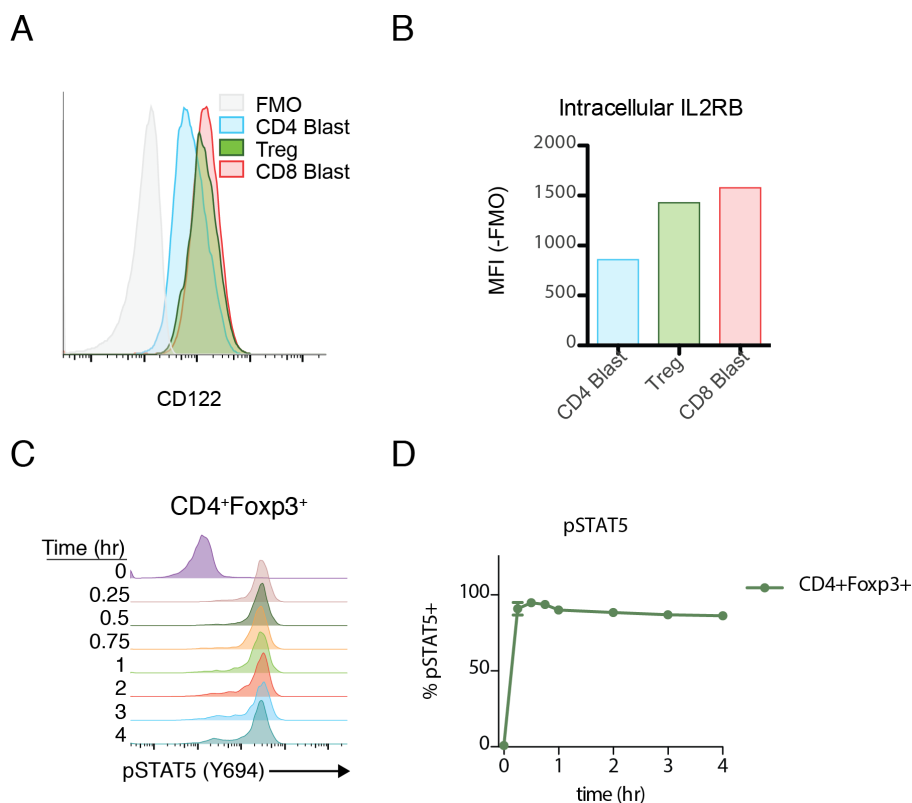
Figure 4-10 Treg IL-2 Signaling Dynamics
(A) Representative histogram comparing intracellular pool of IL-2Rb in Tregs, CD4 and CD8 T-cell blasts. (B) Quantification of IL-2Rb abundance by MFI minus fluorescence minus one (FMO) control. (D) pSTAT5 time course in Tregs, quantified in (D) as fraction of responding cells. Representative of 2 independent experiments (A) and (B). Pooled data from two experiments +/- SEM in (D).

4.4 Discussion

Recent work has recognized the important role that signaling dynamics play in quantitatively altering cell proliferative responses, as shown in the case of EGF and TNFα signaling [19,20]. In these latter studies, the authors altered signaling dynamics by modulating the stimulus. Here, we observe different signaling dynamics in two closely related cell types in response to the same stimulus. A 50% lower abundance of one component of the IL-2R, IL-2Rβ, appears to explain the altered dynamics and contribute to the decreased proliferative response of CD4 T cells to IL-2. In the context of receptor assembly, this is the logical step to specifically regulate the pro-proliferative & growth signals of IL-2 and IL-15 without impacting other γ_c-cytokines. Although there is some debate as to whether IL-2 first binds a preformed IL-2Rα/IL-2Rβ heterodimer [21,22] or first to IL-2Rα and then IL-2Rβ [6,23], there is consensus between both the structural and biochemical studies that a tertiary complex of IL-2/IL-2Rα/IL-2Rβ forms prior to binding of IL-2Rγ. In either model, a shortage of IL-2Rβ would disfavor the formation of the final tertiary complex, required for signaling [22]. On CD4 T cells, there appears to be sufficient IL-2Rβ to maximally phosphorylate STAT5 initially. However, our data suggest that internalization and degradation between 15 minutes and 1 hour reduces surface abundance such that the number of competent signaling complexes falls below the threshold needed to outpace phosphatase activity and maintain sufficient pSTAT5. By contrast, the total pool of IL-2Rβ on CD8 T cells seems to be large enough to sustain signaling above this threshold.

Why are these two cell types programmed to respond to IL-2 with distinct signaling dynamics? We speculate that this may serve as an additional check against the unintentional or mis-localized expansion of CD4 T cells in response to IL-2. Since IL-2 has a very short effective range in vivo (<20 μm)[24,25], only a T cell that maintains close proximity with an IL-2 producing source (such as a peptide-APC-bound T cell) would receive sufficient exposure for a first and

second wave of pSTAT5. This would prevent the expansion of a CD4 T cell that once saw antigen (perhaps self-antigen) and by chance circulated through an area of active infection. CD4 T cells respond to infections by recruiting and activating other immune cells, many of which are non-specific and have the potential to cause harmful inflammation. This mechanism both necessitates tight control over CD4 expansion to prevent autoimmunity and minimizes the need for massive expansion since other cells will amplify the response. By contrast, CD8 T cells primarily respond by directly killing virally infected cells with lytic granules. Unlike the non-specific effectors downstream of CD4 T cells, CD8 killing requires recognition of the correct peptide-MHC on target cells, which mitigates the need for tightly regulated IL-2 responses. In fact, this direct killing mechanism necessitates the opposite: a rapid and large expansion of CD8 T cells is required since there is little amplification by other effector cells.

In order to focus on the consequences of IL-2 signaling specifically, we studied pre-activated T-cell blasts that were no longer receiving TCR stimulation. Recent work from our lab suggests that IL-2Rβ abundance correlates with responses in the context of simultaneous TCR and IL-2 signals[11]. We and others have found that T cells integrate both of these signals at the level of Myc when deciding whether or how much to proliferate[11,26]. However, IL-2 augments TCR-driven Myc induction only in CD8 T cells[11]. This enables CD8, but not CD4, T cells to proliferate in response to suboptimal TCR stimulation. Even 24 hours after T cell activation, CD4 T cells have a very minimal pSTAT5 response to IL-2 (similar to 75% knockdown of IL-2Rβ in Fig. 5c). These CD4 T cells express very little IL-2Rβ and may represent a physiologic example of the IL-2Rβ tuning described here.

Cell fate decisions in response to cytokines and other stimuli require sustainted signaling. Our results highlight how a focus on immediate signaling can be deceptive when attempting to understand events that occur hours later. Here, distinct dynamics in two cell types contribute to quantitatively different proliferative outcomes.

4.5 Material and Methods

Mice. C57BL/6J mice, B6.Cg-*Gpi1*[a]*Thy1*[a]*Igh*[a]/J and B6.SJL-*Ptprc*[a] *Pepc*[b]/BoyJ (Jackson) used in this study were housed in the specific pathogen–free facilities at the University of California, San Francisco, and were treated according to protocols approved by the Institutional Animal Care and Use Committee in accordance with US National Institutes of Health guidelines. Both male and female mice were used as a source of primary T cells, all aged 6-12 weeks.

Reagents. JAK3i was synthesized as previously[5]. Recombinant human IL-2 was from the NIH AIDS Reagent Program, Division of AIDS, National Institute of Allergy and Infectious Diseases, NIH: Maurice Gately (Hoffmann-La Roche). Recombinant murine IL-7 was purchased from Peprotech.

Primary T-Cell Culture. T cells were purified from single-cell suspensions of spleen and lymph nodes from male and female mice aged 6-12 weeks by negative selection with biotinylated antibodies (CD8 or CD4, CD19, B220, CD11b, CD11c, DX5, Ter119 and CD24, UCSF Monoclonal Antibody Core) and magnetic anti-Biotin beads (MACSi Beads, Miltenyi Biotec). For IL-2 stimulation, purified T cells were pre-activated on 6-well plates coated with anti-CD3 (2C11) and anti-CD28 (37.51) for 72 hours, removed and cultured with rhIL-2 (100 u/mL, Roche) for 36 hours, and then cultured without rhIL-2 for the 36 hours prior to all experiments.

T-Cell Proliferation. Pre-activated T cells were cultured in 24-well plates for 10-30 hours with IL-2 and then pulsed with 10 μM 5-ethynyl-2'-deoxyuridine for 1 hour and assayed per the manufacturer's procedure (Click-IT Plus EdU, Life Technologies). Alternatively, cells were loaded with Cell Trace Violet (Life Technologies), plated into 96-well plates and stimulated with IL-2 for 72 hours. To maintain viability in the undivided population, control (non IL-2 stimulated) cells were treated with low dose IL-7 (0.1 ng/mL). Division was then analyzed by flow cytometry.

Flow Cytometry. Cells were live/dead stained using the Live/Dead Fixable Near IR Dead Cell

Stain Kit or Live/Dead Fixable Violet Dead Cell Stain Kit (Life Technologies). For surface stains,

cells were stained for 30 minutes on ice with indicated antibodies. Clones, sources & dilutions

can be found in the **Supplementary Table 1**. For intracellular stains, samples were fixed at the

indicated time after stimulation in 2% paraformaldehyde, surface stained with CD8a-BUV737

and CD4-BUV395, fixed again and permeabilized with ice cold 90% methanol at -20 °C

overnight. Samples were then barcoded using Pacific Orange-NHS ester (0.33 or 5 μg/mL),

Pacific Blue-NHS Ester (0.67 or 10 μg/mL), and AlexaFluor (AF) 488-NHS Ester (0.26 or 2

μg/mL) (Life Technologies), as previously described[5]. Intracellular antigens were then stained

for 30 minutes at 23 °C with antibodies indicated in **Supplementary Table 1**.   Samples were

acquired on a BD LSR Fortessa SORP and analyzed in FlowJo (Tree Star).

qPCR: RNA was isolated from 1-2 $\times$ 10^6 CD4+ T-cell blasts per condition using RNAeasy kit

(Qiagen) and cDNA was synthesized using qScript (Quanta Biosciences). mRNA was detected

by Primetime (IDT) or Taqman (Life Technologies) predesigned qPCR assays. Primer & probe

sequences can be found in **Supplementary Table 2**. Data are from 3 replicates collected on a

QuantStudio 12k (Life Technologies), plotted with 95% confidence intervals as calculated by

Quantstudio (Life Technologies).

IL2RB Knockdown: Four shRNAs targeting IL2RB and one scramble were purchased

(pLKO1.0, The RNAi Consortium / Sigma Aldrich). Sequences can be found in **Supplementary

Table 3.** The puromycin selection cassette was replaced with eGFP by restriction enzyme

cloning. Lentivirus was produced in HEK293T cells in 10 cm dishes transfected with pCMV-

dr8.91 (9 μg), pMD2.G (0.9 μg), and pLKO (9 μg) in the presence of Viral Boost (Alstem). CD8+

T cells were isolated as described above and incubated for 1 day on TCR coated plates prior to spin transduction (1 hr, 2200 RPM, RT) with viral supe in the presence of IL-2 (100 u/mL). Cells were left on TCR plates through day 3 and treated as per culture conditions described above. Assays were conducted as described above, except anti-GFP-AF488 was used to detect GFP in the saponin based perm for S-phase entry.

Supplementary Table 1 | FACS Antibody Information

Target	Fluor	Clone	Source	Dilution
CD4	BUV395	GK1.5	BD	1:200
CD8α	BUV737	53-6.7	BD	1:200
	FITC	53-6.7	Biolegend	1:200
CD25	BUV395	PC61.5	BD	1:200
	APC			
CD122	AF647	TM-$\beta 1$	AB-Direct	1:50
	PE	TM-$\beta 1$	Biolegend	1:50
	Biotin	TM-$\beta 1$	Biolegend	1:50
CD132	PE	TUGm2	BD	1:50
	Biotin	TUGm2	BD	1:50
Streptavidin	AF647	n/a	Life Technologies	1:800
STAT5 pY694	AlexaFluor647	47/STAT5(pY694)	BD	1:5
pS6 S240/244	Unconjugated	D68F8	Cell Signaling	1:200
GFP	AF488	FM264G	Biolegend	1:100
Anti-rabbit	PE		Jackson Immuno	1:200

Supplementary Table 2 | qPCR Assays

IDT Primetime Assays		
Target		**Sequence**
il2rb	Probe	/56-FAM/CCC TCA TTC /ZEN/CCT CCA AGT TCT GCA /3IABkFQ/
	Primer 1	GTA AAG ACC TGC GAC TTC CAT
	Primer 2	ACC TTC CAG CTT ATG TTA CAT CT
il2rg	Probe	/56-FAM/TCA CTA TTA /ZEN/GTT CCG TCC AGC TTC GAT CT/3IABkFQ/
	Primer 1	ACA ATA CTT GGT GCA GTA CCG
	Primer 2	GAA CCC GAA ATG TGT ACC GT
Life Technologies Taqman Assays		
Target	**Exons Targeted**	**Assay ID**
il2ra	2-3	Mm01340213_m1
b2m	1-2	Mm00437762_m1

Supplementary Table 3 | IL2RB shRNA

Paper ID	RNAi Consortium Clone ID	Target Sequence	Forward Oligo
IL2RB shRNA #1	TRCN00000068072	GCCTATCTGTCTCTTCAAGAA	CCGGGCCTATCTGTCTCTTCAAGAACTCGAGTTCTTGAAGAGACAGATAGGCTTTTTG
IL2RB shRNA #2	TRCN00000068071	GCTGATCCCTAGTACCTCATA	CCGGGCTGATCCCTAGTACCTCATACTCGAGTATGAGGTACTAGGGATCAGCTTTTTG
IL2RB shRNA #3	TRCN00000068069	CCCAAGATTCAGTCCACCTAA	CCGGCCCAAGATTCAGTCCACCTAACTCGAGTTAGGTGGACTGAATCTTGGGTTTTTG
IL2RB shRNA #4	TRCN00000068070	CCATCTTGAATGCTTCTACAA	CCGGCCATCTTGAATGCTTCTACAACTCGAGTTGTAGAAGCATTCAAGATGGTTTTTG

4.6 References

1. Rochman, Y., Spolski, R. & Leonard, W. J. New insights into the regulation of T cells by γc family cytokines. *Nature Reviews Immunology* **9,** 480–490 (2009).

2. Lin, J.-X. *et al.* Critical Role of STAT5 transcription factor tetramerization for cytokine responses and normal immune function. *Immunity* **36,** 586–599 (2012).

3. Weist, B. M., Kurd, N., Boussier, J., Chan, S. W. & Robey, E. A. Thymic regulatory T cell niche size is dictated by limiting IL-2 from antigen-bearing dendritic cells and feedback competition. *Nature Immunol.* **16,** 635–641 (2015).

4. Cantrell, D. A. & Smith, K. A. The Interleukin-2 T-cell system: a new cell growth model. *Science* **224,** 1312–1316 (1984).

5. Smith, G. A., Uchida, K., Weiss, A. & Taunton, J. Essential biphasic role for JAK3 catalytic activity in IL-2 receptor signaling. *Nat. Chem. Bio.* **12,** 373–379 (2016).

6. Wang, X., Rickert, M. & Garcia, K. C. Structure of the quaternary complex of Interleukin-2 with its alpha, beta, and gammac receptors. *Science* **310,** 1159–1163 (2005).

7. Boyman, O. & Sprent, J. The role of Interleukin-2 during homeostasis and activation of the immune system. *Nature Reviews Immunology* (2012). doi:10.1038/nri3156

8. Balaji M Rao, Ian Driver, Douglas A Lauffenburger, A.K Dane Wittrup. *High-Affinity CD25-Binding IL-2 Mutants Potently Stimulate Persistent T Cell Growth†. Biochemistry* **44,** 10696–10701 (American Chemical Society, 2005).

9. Damjanovich, S. *et al.* Preassembly of Interleukin 2 (IL-2) receptor subunits on resting Kit 225 K6 T cells and their modulation by IL-2, IL-7, and IL-15: a fluorescence resonance energy transfer study. *Proc. Natl Acad. Sci. USA* **94,** 13134–13139 (1997).

10. Pillet, A.-H. *et al.* IL-2 Induces Conformational Changes in Its Preassembled Receptor Core, Which Then Migrates in Lipid Raft and Binds to the Cytoskeleton Meshwork. *J. Mol. Biol.* **403,** 671–692 (2010).

11. Au-Yeung, B. B. *et al.* IL-2 Modulates the TCR Signaling Threshold for CD8 but Not CD4

T Cell Proliferation on a Single-Cell Level. *J. Immunol.* 1601453 (2017). doi:10.4049/jimmunol.1601453

12. Cho, J.-H. *et al.* Unique Features of Naive CD8+ T Cell Activation by IL-2. *J. Immunol.* (2013). doi:10.4049/jimmunol.1302293

13. Hémar, A. *et al.* Endocytosis of Interleukin 2 receptors in human T lymphocytes: distinct intracellular localization and fate of the receptor alpha, beta, and gamma chains. *J Cell Biol* **129,** 55–64 (1995).

14. Lamaze, C. *et al.* Interleukin 2 Receptors and Detergent-Resistant Membrane Domains Define a Clathrin-Independent Endocytic Pathway. *Mol Cell* **7,** 661–671 (2001).

15. Kalia, V. *et al.* Prolonged Interleukin-2Ra Expression on Virus-Specific CD8. *Immunity* **32,** 91–103 (2010).

16. Gesbert, F., Moreau, J.-L. & Thèze, J. IL-2 responsiveness of CD4 and CD8 lymphocytes: further investigations with human IL-2Rbeta transgenic mice. *Int Immunol* **17,** 1093–1102 (2005).

17. Foulds, K. E. *et al.* Cutting Edge: CD4 and CD8 T Cells Are Intrinsically Different in Their Proliferative Responses. *J. Immunol.* **168,** 1528–1532 (2002).

18. de Boer, R. J., Homann, D. & Perelson, A. S. Different dynamics of CD4+ and CD8+ T cell responses during and after acute lymphocytic choriomeningitis virus infection. *J. Immunol.* **171,** 3928–3935 (2003).

19. Albeck, J. G., Mills, G. B. & Brugge, J. S. Frequency-Modulated Pulses of ERK Activity Transmit Quantitative Proliferation Signals. *Mol Cell* **49,** 249–261 (2013).

20. Kellogg, R. A. *et al.* Digital signaling decouples activation probability and population heterogeneity. *eLife* **4,** e08931 (2015).

21. Wu, Z., Johnson, K. W., Choi, Y. & Ciardelli, T. L. Ligand binding analysis of soluble Interleukin-2 receptor complexes by surface plasmon resonance. *J. Biol. Chem.* **270,** 16045–16051 (1995).

22. Stefano F Liparoto *et al.* Analysis of the Role of the Interleukin-2 Receptor γ Chain in Ligand Binding†. *Biochemistry* **41,** 2543–2551 (2002).

23. Stauber, D. J. Crystal structure of the IL-2 signaling complex: Paradigm for a heterotrimeric cytokine receptor. *Proc. Natl Acad. Sci. USA* **103,** 2788–2793 (2006).

24. Busse, D. *et al.* Competing feedback loops shape IL-2 signaling between helper and regulatory T lymphocytes in cellular microenvironments. *Proc. Natl Acad. Sci. USA* **107,** 3058–3063 (2010).

25. Thurley, K., Gerecht, D., Friedmann, E. & Höfer, T. Three-Dimensional Gradients of Cytokine Signaling between T Cells. *PLoS Comput Biol* **11,** e1004206 (2015).

26. Heinzel, S. *et al.* A Myc-dependent division timer complements a cell-death timer to regulate T cell and B cell responses. *Nature Immunol.* **18,** 96–103 (2017).

Chapter 5   Conclusions and Future Directions

To understand the consequences of inhibiting JAK3 in physiologic and pathologic settings, we sought a highly selective chemical probe. This would enable us to bypass the developmental defects associated with JAK3 deficiency and address the temporal elements of signaling. To this end, we identified a highly selective JAK3 inhibitor (JAK3i) with efficacy in animals. Together with the drug resistant C905S allele, it forms a chemical genetic toolkit that allows the specific interrogation of JAK3 catalytic function in cells and in vivo.

In our hands, JAK3i extended the life of mice with acute graft-versus-host disease following a MHC-mismatched bone marrow transplant. This is only the beginning of interesting questions that can be addressed in vivo. Currently, collaborators are exploring JAK3 inhibition to treat T-cell malignancies (T-Cell Acute Lymphoblastic Leukemia (T-ALL) and Smoldering/Chronic Adult T-cell Leukemia), with some initial success in re-sensitizing T-ALL cells to corticosteroids. In the setting of autoimmunity, JAK3i could be used in more complicated models of T-cell driven disease, such as the SKG model of CD4 T cell-mediated arthritis. Studying the inhibitor in these models would also address more fundamental biological questions: how does JAK3 inhibition shift the balance between IL-2-dependent Tregs and Teffector cells? What are the consequences of JAK3 inhibition in the context of TCR stimulation?

The drug resistant C905S JAK3 mutant allowed us to demonstrate that biological effects required covalent drug binding to JAK3. Using the same retrovirus system, we were also able to extend this to an in vivo setting, where JAK3i was able to selectively block wild type but not C905S JAK3 cells in the same mouse. These chemical genetic studies suggest the development of an even more powerful tool for studying JAK3 biology in vivo: a mouse with inducible sensitivity to the JAK3 inhibitor. A FLOX-STOP-FLOX system with both sensitive and resistant JAK3 kinase domains would enable one to ask whether specific cell types require JAK3 activity for pathology or for therapeutic drug effects. Given the many cell types that respond to γ_c-cytokines, these are important questions for understanding the mechanism(s) of action of JAK3 inhibition and the underlying biology.

JAK3i potently inhibited CD4+ T-cell blast proliferation in response to IL-2 but had little effect on immediate signaling readouts at the same doses. Resolving this paradox led us to focus on IL-2R signaling dynamics over time rather than immediately after stimulation. In doing so, we identified a previously unappreciated second wave of signaling that was more JAK3-dependent than the first, which explained the potent anti-proliferative effects of JAK3i. Since many signaling events require long exposure to stimuli before a cell commits to a new fate (i.e. dividing, differentiating etc.), this paradigm likely has broad applicability to other signaling systems.

Comparing CD4 and CD8 IL-2R signaling dynamics revealed that these patterns could be determined by cell type as well as stimuli. Unlike CD4 T cells, CD8 T cells expressed a higher level of IL-2Rβ, which allowed them to sustain signaling throughout a 6-hour time course. This translated into an earlier and stronger proliferative response to IL-2. Although we were able to convert CD8 T cells to a CD4-like phenotype in cell culture, the consequences of this remain to be seen in vivo. Are CD4 T cells that respond to IL-2 similarly to CD8 T cells more prone to harmful, potentially autoimmune expansion? Are CD8 T cells with CD4-like IL-2 responses unable to mount a sufficient response to viruses?

The differences between CD4 and CD8 signaling dynamics and responses also raise a more fundamental question: how do we relate signal input over time to specific outcomes? For instance, what occurs during the first two hours of signaling transcriptionally that enables the faster CD8 response? Given that S-phase entry is a binary event on a single cell level, there is likely a threshold of signal that must be accumulated. Quantifying this threshold for proliferation, as well as other IL-2-dependent events like induction of anti-apoptotic proteins or cytokine production will further our understanding of the pleotropic effects of IL-2. Extending these results to the in vivo settings will likely necessitate the development of new tools. Currently, monitoring STAT5 phosphorylation requires fixation and methanol permeabilization. A live-cell reporter of

JAK3 kinase activity or STAT5 nuclear localization would allow us to assess dynamics in real time and potentially in animals via imaging.

Studying temporal requirements for cell signaling is greatly enabled by high quality chemical probes. While new genetic tools can turn off signaling on the timescale of hours, only chemical probes allow the rapid inactivation of a physiological signal. Here, our chemical genetic toolkit provides a way to rapidly and specifically interrupt JAK3 activity that we hope will be useful to groups beyond our own. This project highlights a strategy for rapidly generating covalent probes based on existing reversible scaffolds that is likely applicable to other targets. Efforts are underway to expand this approach to nucleophilic residues other than cysteine as well as non-kinase targets. The continued development of new chemical probes, especially with the genetic controls inherent in covalent inhibitors, will further our understanding of signaling biology and help validate new targets in many disease areas.
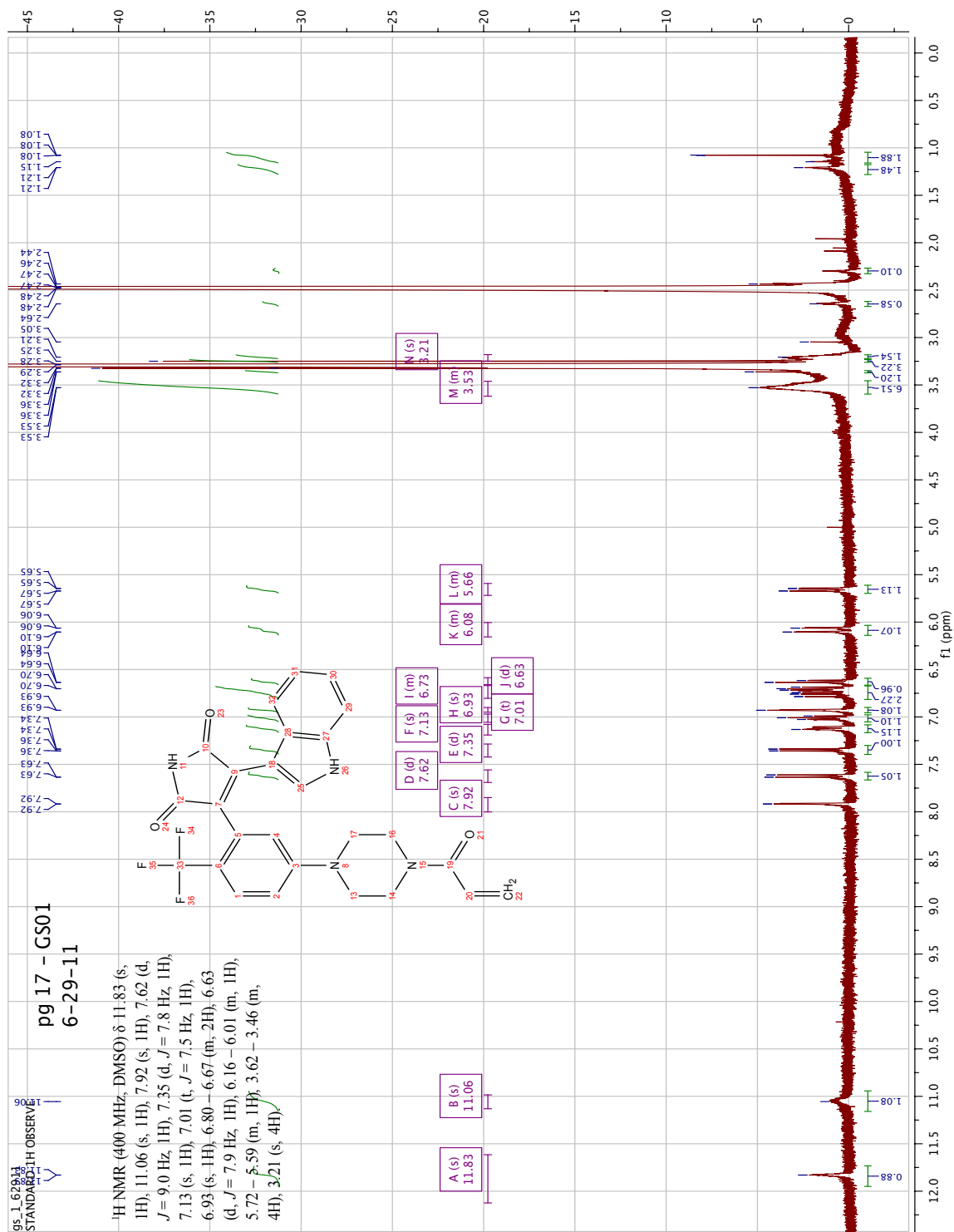
Appendix A – Compound ID Cross Reference

Chapter 2 Compound #	Lab Compound Identifier	Notebook Page Reference
7	GS01	GS I-17
8	GS02	GS I-19
9	GS03	GS I-45
10	GS04	GS I-47
11	GS05	GS I-95
12	GS06	GS I-97
13	GS07	GS II-31
16	GS11	GSCI-25
17	GS9	GSCI-14
18	GS12	GSCI-32
19	AC2	AC-83
20	GS13	GSCI-50
21	GS15	GSCI-63
22	AC1	AC-44
23	GS10	GSCI-21
24	KU1	KU1-19
25	AC3	AC-93
26	KU3	KU1-30
27	GS16	GSCI-65
28	GS14	GSCI-58
29	KU6	KU1-42
30 (JAK3i)	KU2	KU1-28

Chapter 2 Compound #	Lab Compound Identifier	Notebook Page Reference
31	KU28	KU2-85
32	KU5	KU1-40
33	KU4	KU1-32
34	KU29	KU2-89
35	KU30	KU2-99
36	KU31	KU2-100
37	KU39	KU3-36
38	KU40	KU3-38
39	KU7	KU1-53
40	KU17	KU1-97

Appendix B – NMR Spectra

Compound 7

pg 17 - GS01
6-29-11

gs_1_629a14
STANDARD 1H OBSERVE

¹H NMR (400 MHz, DMSO) δ 11.83 (s, 1H), 11.06 (s, 1H), 7.92 (s, 1H), 7.62 (d, J = 9.0 Hz, 1H), 7.35 (d, J = 7.8 Hz, 1H), 7.13 (s, 1H), 7.01 (t, J = 7.5 Hz, 1H), 6.93 (s, 1H), 6.80 − 6.67 (m, 2H), 6.63 (d, J = 7.9 Hz, 1H), 6.16 − 6.01 (m, 1H), 5.72 − 5.59 (m, 1H), 3.62 − 3.46 (m, 4H), 3.21 (s, 4H).

156

Compound 8

¹H NMR (400 MHz, DMSO) δ 11.83 (s, 1H), 11.05 (s, 1H), 7.92 (s, 1H), 7.62 (d, *J* = 8.9 Hz, 1H), 7.35 (d, *J* = 8.1 Hz, 1H), 7.11 (d, *J* = 8.7 Hz, 1H), 7.05 – 6.97 (m, 1H), 6.91 (s, 1H), 6.78 – 6.65 (m, 1H), 6.62 (d, *J* = 8.3 Hz, 1H), 3.41 (s, 4H), 3.23 – 3.12 (m, 4H), 2.27 (dd, *J* = 14.8, 7.6 Hz, 2H), 1.08 (d, *J* = 1.0 Hz, 1H), 0.94 (t, *J* = 7.4 Hz, 3H).

gs19_1h_62911
STANDARD 1H OBSERVE

Compound 9

¹H NMR (400 MHz, DMSO) δ 11.84 (s, 1H), 11.01 (s, 1H), 7.99 (d, *J* = 20.0 Hz, 1H), 7.56 (d, *J* = 9.0 Hz, 1H), 7.36 (d, *J* = 8.1 Hz, 1H), 7.00 (t, *J* = 7.5 Hz, 1H), 6.92 (t, *J* = 8.6 Hz, 1H), 6.60 (dddd, *J* = 37.8, 29.4, 14.6, 5.9 Hz, 3H), 6.04 (ddd, *J* = 44.0, 16.6, 2.3 Hz, 1H), 5.58 (ddd, *J* = 31.6, 10.4, 2.2 Hz, 1H).

GS_45_f_1h
STANDARD 1H OBSERVE

Compound 10

¹H NMR (400 MHz, DMSO) δ 11.87 (s, 1H), 11.03 (s, 1H), 8.02 (dd, J = 16.4, 2.4 Hz, 1H), 7.59 (d, J = 8.9 Hz, 1H), 7.38 (d, J = 7.7 Hz, 1H), 7.03 (t, J = 7.5 Hz, 1H), 6.93 (d, J = 8.9 Hz, 1H), 6.69 (t, J = 7.1 Hz, 1H), 6.63 (s, 1H), 6.52 (dd, J = 21.7, 8.2 Hz, 1H), 3.66 (d, J = 15.1 Hz, 1H), 3.45 (dd, J = 20.6, 11.7 Hz, 3H), 3.21 (s, 1H), 2.83 (dd, J = 29.0, 21.0 Hz, 2H), 2.28 – 2.12 (m, 2H), 1.72 – 1.48 (m, 1H), 1.47 – 1.20 (m, 2H), 0.90 (dt, J = 21.9, 7.3 Hz, 3H).
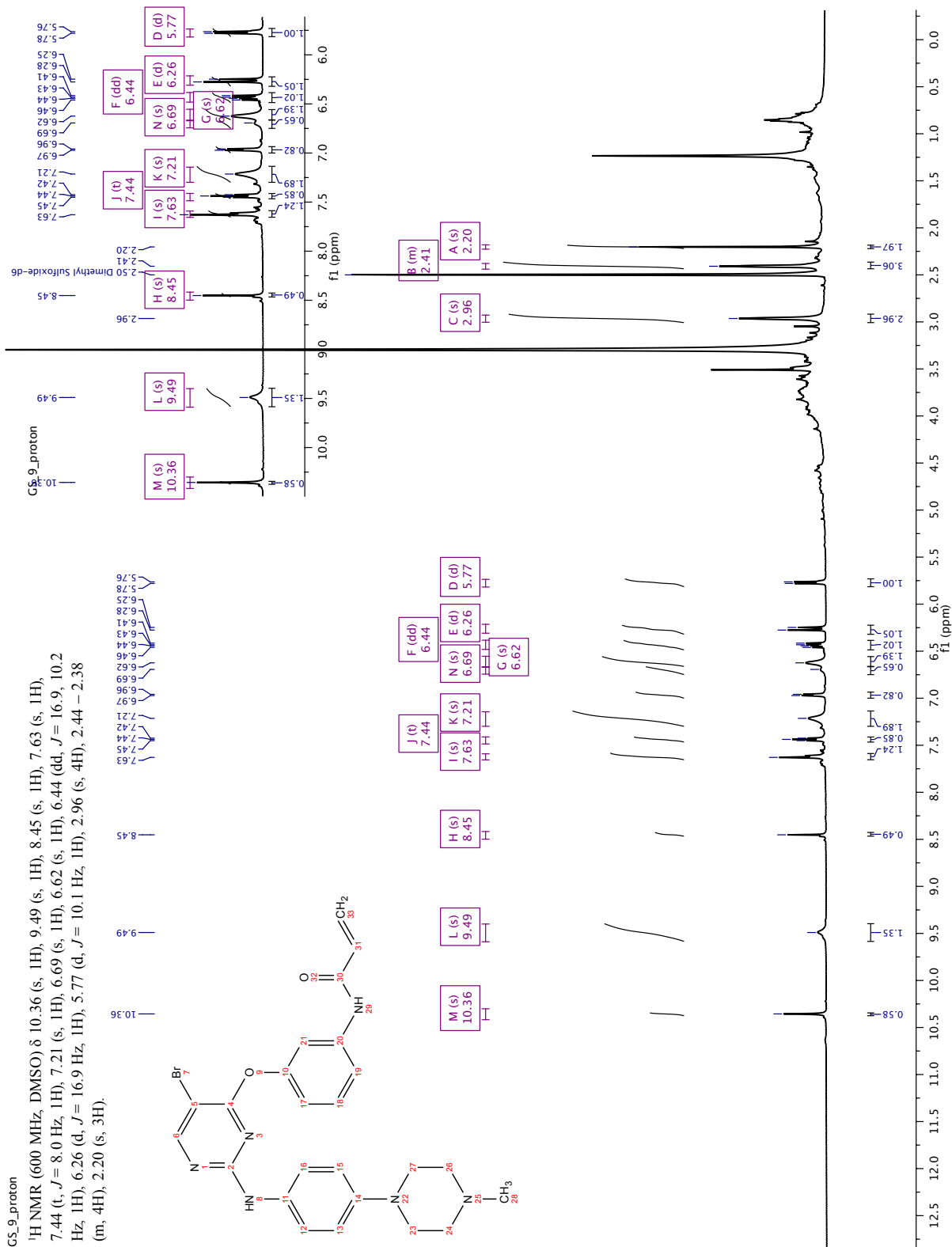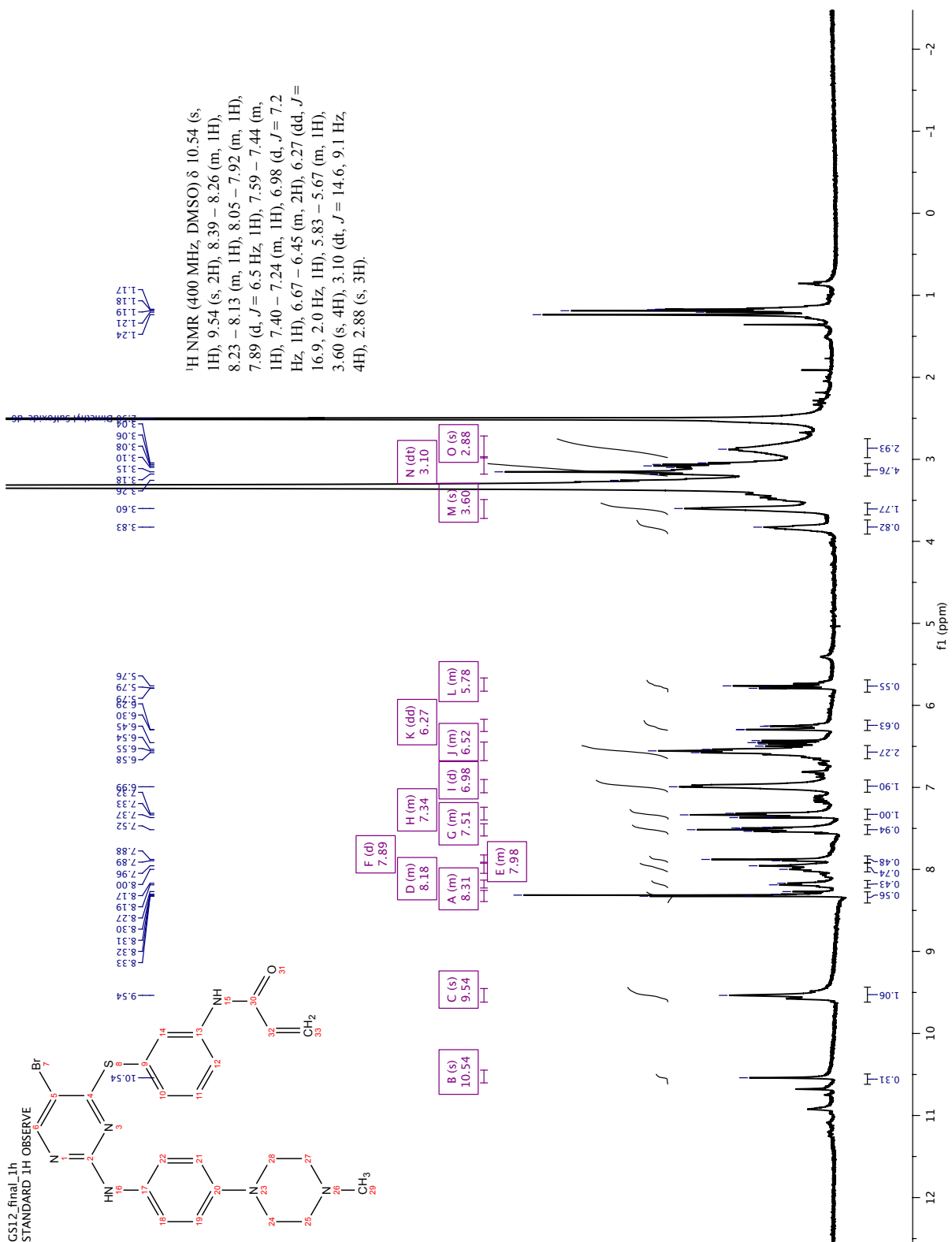
Compound 11

Compound 12

Compound 13

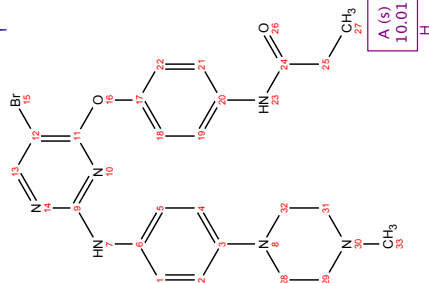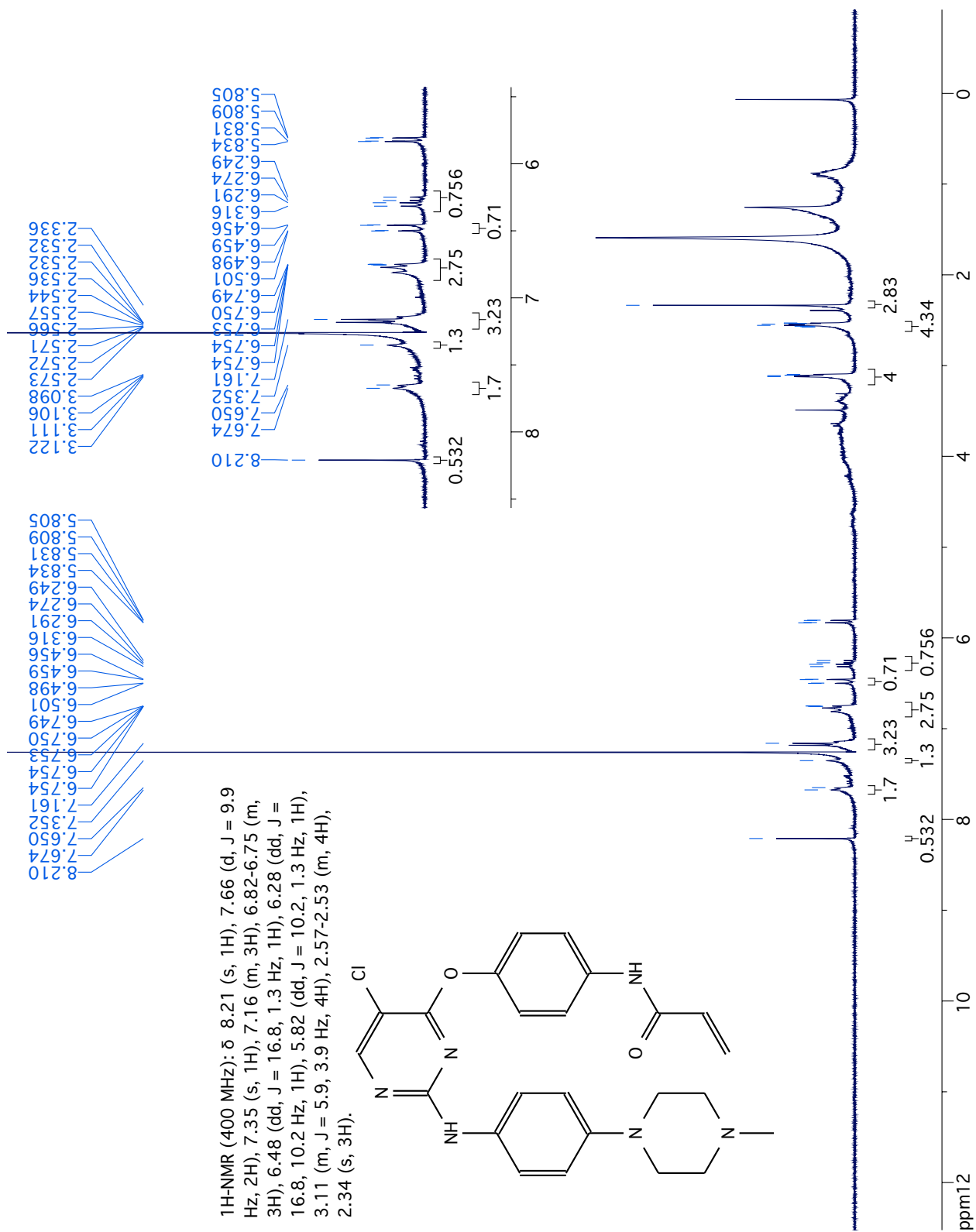^{1}H NMR (400 MHz, DMSO) δ 11.86 (s, 1H), 11.04 (s, 1H), 8.08 (dd, J = 9.2, 2.3 Hz, 1H), 7.95 (dd, J = 28.8, 3.2 Hz, 1H), 7.69 (m, 1H), 7.37 (d, J = 8.5 Hz, 1H), 7.14 (dd, J = 6.3, 3.8 Hz, 1H), 7.08 (dd, J = 24.7 Hz, 1H), 6.93 (d, J = 24.7 Hz, 1H), 6.78 – 6.68 (m, 1H), 6.58 (d, J = 8.7 Hz, 1H), 6.21 (dd, J = 17.3, 9.3 Hz, 1H), 6.16 – 6.00 (m, 1H), 5.58 (d, J = 11.1 Hz, 1H), 3.92 – 3.54 (m, 2H), 2.97 – 2.75 (m, 1H), 2.76 – 2.61 (m, 1H), 1.87 – 1.60 (m, 2H), 1.46 (ddd, J = 8.6, 15.2, 5.6 Hz, 2H), 1.29 – 1.08 (m, 1H).

Compound 16

GS11_proton

¹H NMR (600 MHz, DMSO) δ 10.46 (s, 1H), 9.52 (s, 1H), 8.27 (s, 1H), 8.17 (d, J = 7.3 Hz, 1H), 7.87 (s, 1H), 7.52 (t, J = 8.0 Hz, 1H), 7.34 – 7.32 (m, 1H), 6.99 (s, 2H), 6.53 (d, J = 8.1 Hz, 2H), 6.43 (dd, J = 16.9, 10.2 Hz, 1H), 6.27 (dd, J = 17.0, 1.9 Hz, 1H), 5.78 (dd, J = 10.1, 1.9 Hz, 1H), 3.02 (s, 4H), 2.62 (s, J = 1.8 Hz, 4H), 2.44 – 2.32 (m, 3H).

Compound 17

GS_9_proton

^{1}H NMR (600 MHz, DMSO) δ 10.36 (s, 1H), 9.49 (s, 1H), 8.45 (s, 1H), 7.63 (s, 1H), 7.44 (t, J = 8.0 Hz, 1H), 7.21 (s, 1H), 6.69 (s, 1H), 6.62 (s, 1H), 6.44 (dd, J = 16.9, 10.2 Hz, 1H), 6.26 (d, J = 16.9 Hz, 1H), 5.77 (d, J = 10.1 Hz, 1H), 2.96 (s, 4H), 2.44 – 2.38 (m, 4H), 2.20 (s, 3H).

Compound 18

GS12_final_1h
STANDARD 1H OBSERVE

¹H NMR (400 MHz, DMSO) δ 10.54 (s, 1H), 9.54 (s, 2H), 8.39 – 8.26 (m, 1H), 8.23 – 8.13 (m, 1H), 8.05 – 7.92 (m, 1H), 7.89 (d, *J* = 6.5 Hz, 1H), 7.59 – 7.44 (m, 1H), 7.40 – 7.24 (m, 1H), 6.98 (d, *J* = 7.2 Hz, 1H), 6.67 – 6.45 (m, 2H), 6.27 (dd, *J* = 16.9, 2.0 Hz, 1H), 5.83 – 5.67 (m, 1H), 3.60 (s, 4H), 3.10 (dt, *J* = 14.6, 9.1 Hz, 4H), 2.88 (s, 3H).

Compound 19

1H-NMR (400 MHz; DMSO-d6): δ 10.35 (s, 1H), 9.52 (s, 1H), 8.41 (s, 1H), 7.65-7.61 (m, 2H), 7.45 (t, J = 8.1 Hz, 1H), 7.25 (s, 2H), 6.99 (ddd, J = 8.1, 2.3, 0.9 Hz, 1H), 6.65 (s, 2H), 6.43 (dd, J = 17.0, 10.1 Hz, 1H), 6.26 (dd, J = 17.0, 2.0 Hz, 1H), 5.78 (dd, J = 10.1, 2.0 Hz, 1H), 3.70 (t, J = 4.7 Hz, 4H), 2.95-2.93 (m, 4H).

Compound 20

Compound 21

GS15_final
STANDARD 1H OBSERVE

^{1}H NMR (400 MHz, DMSO) δ 10.01 (s, 1H), 9.48 (s, 1H), 8.42 (s, 1H), 7.68 (d, J = 8.9 Hz, 2H), 7.21 – 7.09 (m, 4H), 6.62 (s, 2H), 3.02 – 2.93 (m, 4H), 2.44 – 2.39 (m, 4H), 2.35 (q, J = 7.5 Hz, 2H), 2.20 (s, 3H), 1.12 (t, J = 7.6 Hz, 3H).

168

Compound 22

1H-NMR (400 MHz): δ 8.21 (s, 1H), 7.66 (d, J = 9.9 Hz, 2H), 7.35 (s, 1H), 7.16 (m, 3H), 6.82-6.75 (m, 3H), 6.48 (dd, J = 16.8, 1.3 Hz, 1H), 6.28 (dd, J = 16.8, 10.2 Hz, 1H), 5.82 (dd, J = 10.2, 1.3 Hz, 1H), 3.11 (m, J = 5.9, 3.9 Hz, 4H), 2.57-2.53 (m, 4H), 2.34 (s, 3H).
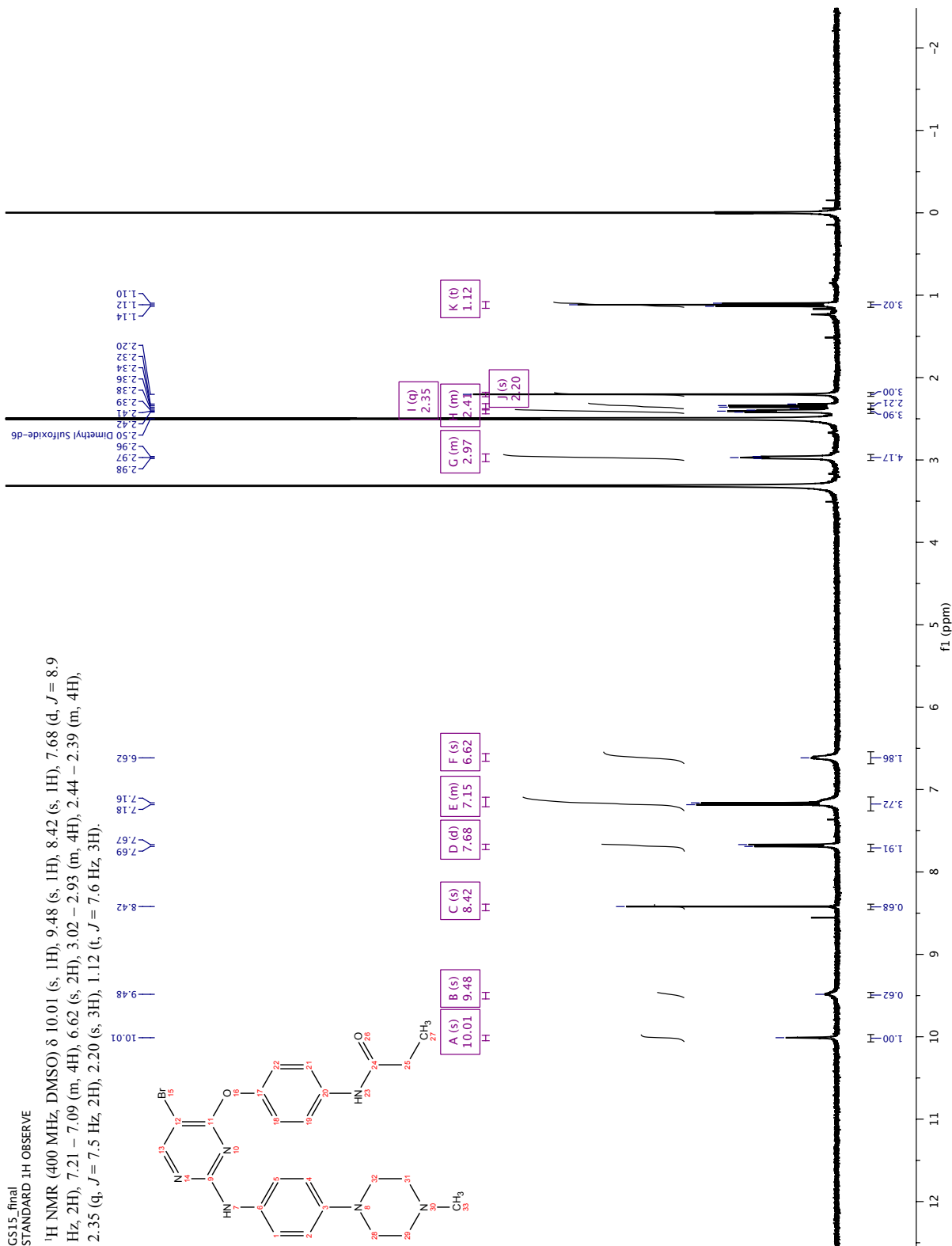
Compound 23

GS10_final_1h
STANDARD 1H OBSERVE

^{1}H NMR (400 MHz, CDCl$_3$) δ 8.30 (s, 1H), 7.66 (d, J = 8.3 Hz, 2H), 7.49 (s, 1H), 7.19 – 7.08 (m, 4H), 6.84 (s, 1H), 6.76 (s, J = 8.6 Hz, 2H), 6.48 (dd, J = 16.8, 1.3 Hz, 1H), 6.30 (dd, J = 16.9, 10.2 Hz, 1H), 5.81 (dd, J = 10.2, 1.3 Hz, 1H), 3.18 – 3.09 (m, 4H), 2.66 – 2.57 (m, 4H), 2.38 (s, 3H).

Compound 24

Compound 26

Acquisition Time (sec)	3.7440	Comment	STANDARD 1H OBSERVE		Date	Dec 10 2013	Date Stamp	Dec 10 2013
File Name	D:¥USERS¥B067043¥DESKTOP¥NMR¥KU-1-030.FID¥FID				Frequency (MHz)	399.56	Nucleus	1H
Number of Transients	16	Original Points Count	22466		Pulse Sequence	s2pul	Receiver Gain	36.00
Solvent	DMSO-d6	Spectrum Offset (Hz)	2009.3591	Points Count	65536	Spectrum Type	STANDARD	Temperature (degree C)	25.000
				Sweep Width (Hz)	6000.60			

KU-1-030.esp

VerticalScaleFactor = 1

No.	(ppm)	Value	Absolute Value	Non-Negative Value
1	0959 .. 2.252	.99930573	4.54360360e+7	2.99930573
2	3154 .. 2.434	.17418432	6.32341000e+7	4.17418432
3	3520 .. 3.074	.16449833	6.30873680e+7	4.16449833
4	3032 .. 4.460	.62023622	9.39586600e+6	0.62023622
5	5935 .. 5.871	.26175523	1.91141420e+7	1.26175523
6	1873 .. 6.824	.79044485	7.25697360e+7	4.79044485
7	9497 .. 7.324	.10232210	6.21454680e+7	4.10232210
8	5448 .. 7.852	.26421380	3.43002400e+7	2.26421380
9	3155 .. 8.510	.78506172	1.18927830e+7	0.78506172
10	1327 .. 10.41	.15548670	1.75042960e+7	1.15548670

172

Compound 29

Acquisition Time (sec)	3.7440	Comment	STANDARD 1H OBSERVE	Date	Dec 23 2013
Date Stamp	Dec 23 2013	File Name	D:¥USERS¥B067043¥DESKTOP¥NMR¥KU-1-042-2.FID¥FID		
Frequency (MHz)	399.56	Nucleus	1H	Number of Transients	16	Original Points Count	22466
Points Count	65536	Pulse Sequence	s2pul	Receiver Gain	32.00	Solvent	DMSO-d6
Spectrum Offset (Hz)	2008.9929	Spectrum Type	STANDARD	Sweep Width (Hz)	6000.60	Temperature (degree C)	AMBIENT TEMPERATURE

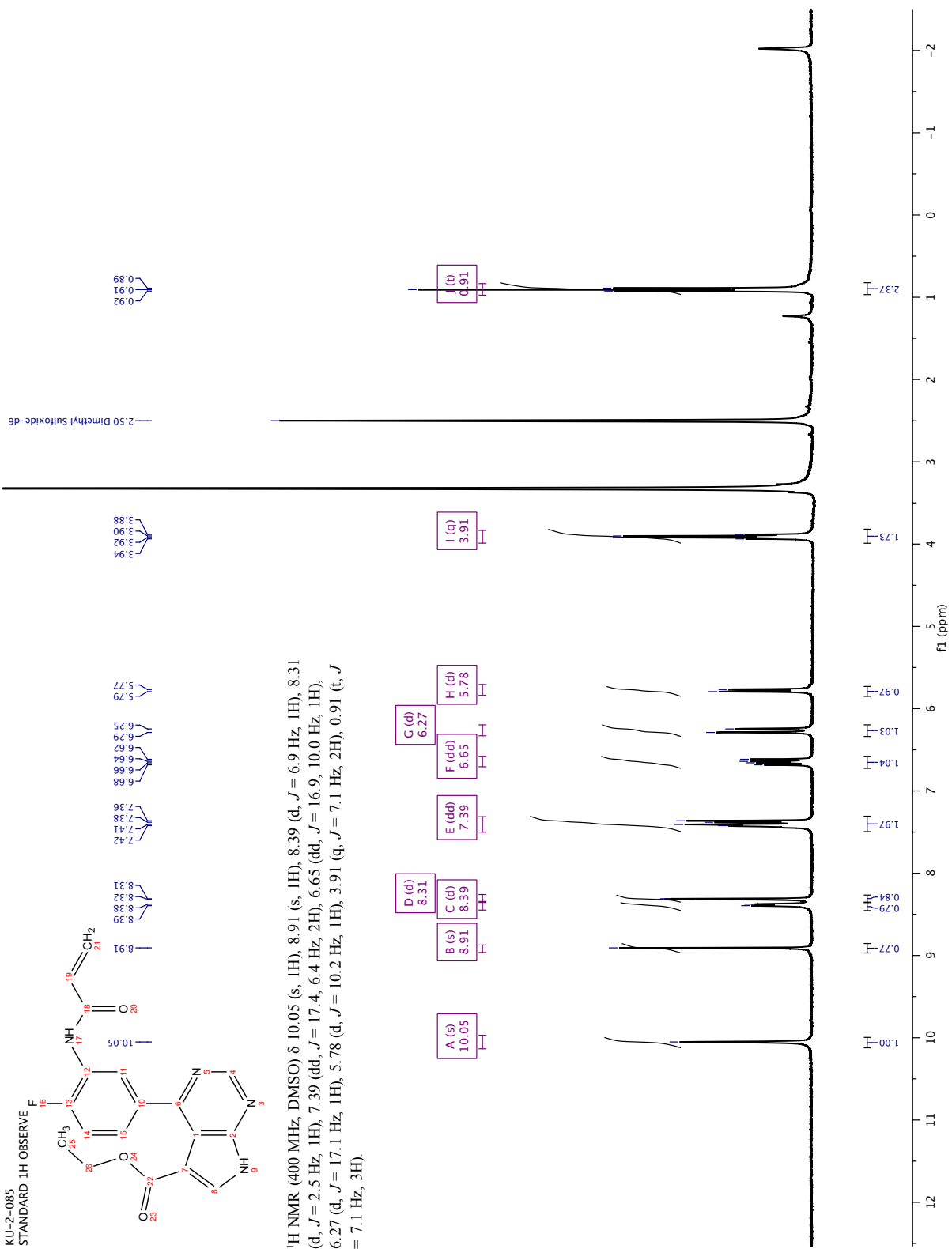KU-1-042-2.ESP   VerticalScaleFactor = 1

2013/12/23 16:15:11
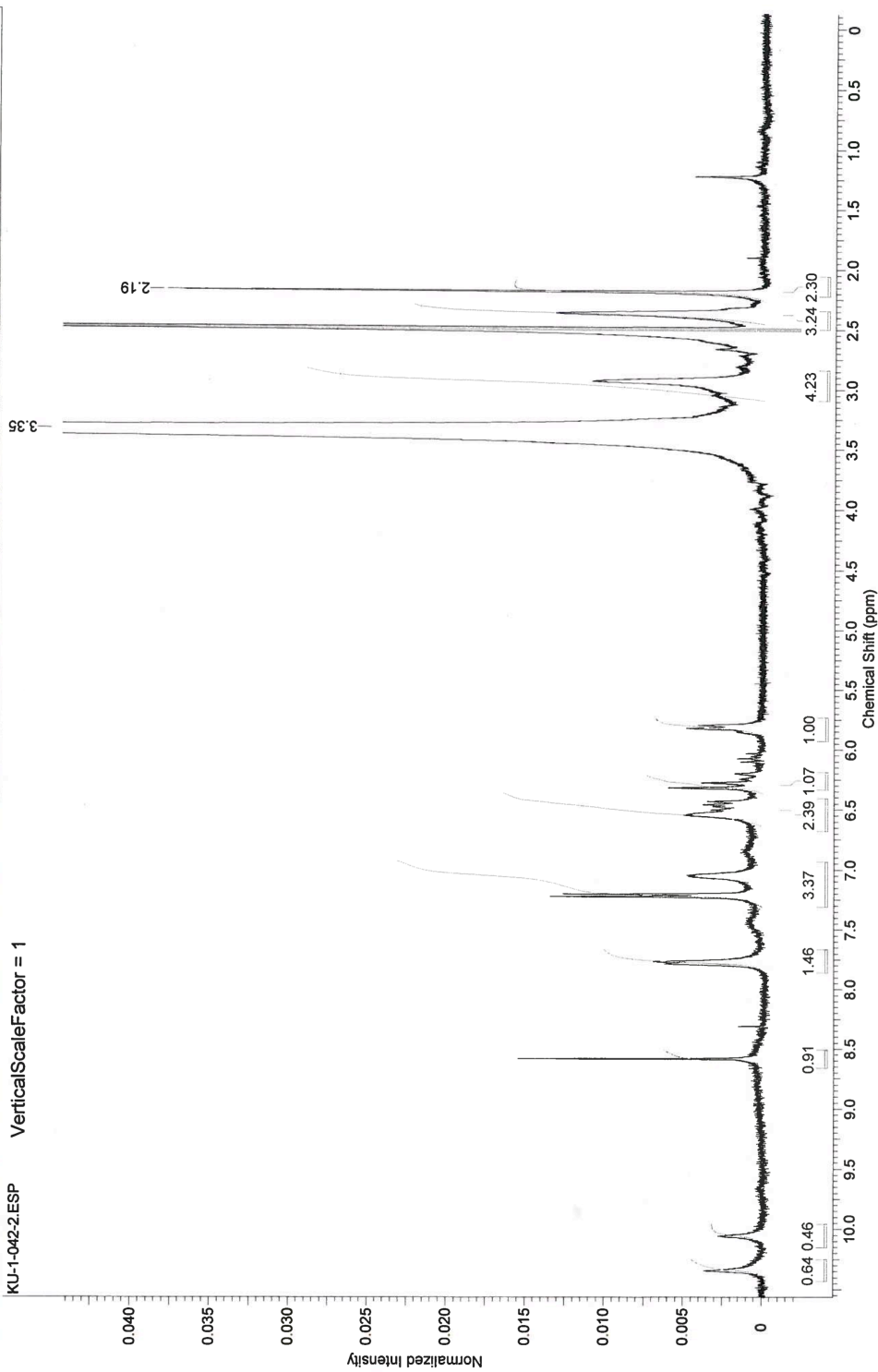
Compound 30

GSCI-123
GSCI_123_crude

¹H NMR (400 MHz, DMSO) δ 13.02 (s, 1H), 10.32 (s, 1H), 8.96 (d, J = 5.3 Hz, 1H), 8.33 (d, J = 2.9 Hz, 1H), 8.05 (dd, J = 6.5, 2.7 Hz, 1H), 7.82 (ddd, J = 8.9, 4.5, 2.8 Hz, 1H), 7.22 (dd, J = 10.0, 9.0 Hz, 1H), 6.43 (dd, J = 17.0, 10.1 Hz, 1H), 6.27 (dd, J = 17.0, 2.0 Hz, 1H), 5.78 (dd, J = 10.1, 2.0 Hz, 1H), 3.94 (br, 2H), 0.94 (t, J = 7.1 Hz, 3H).
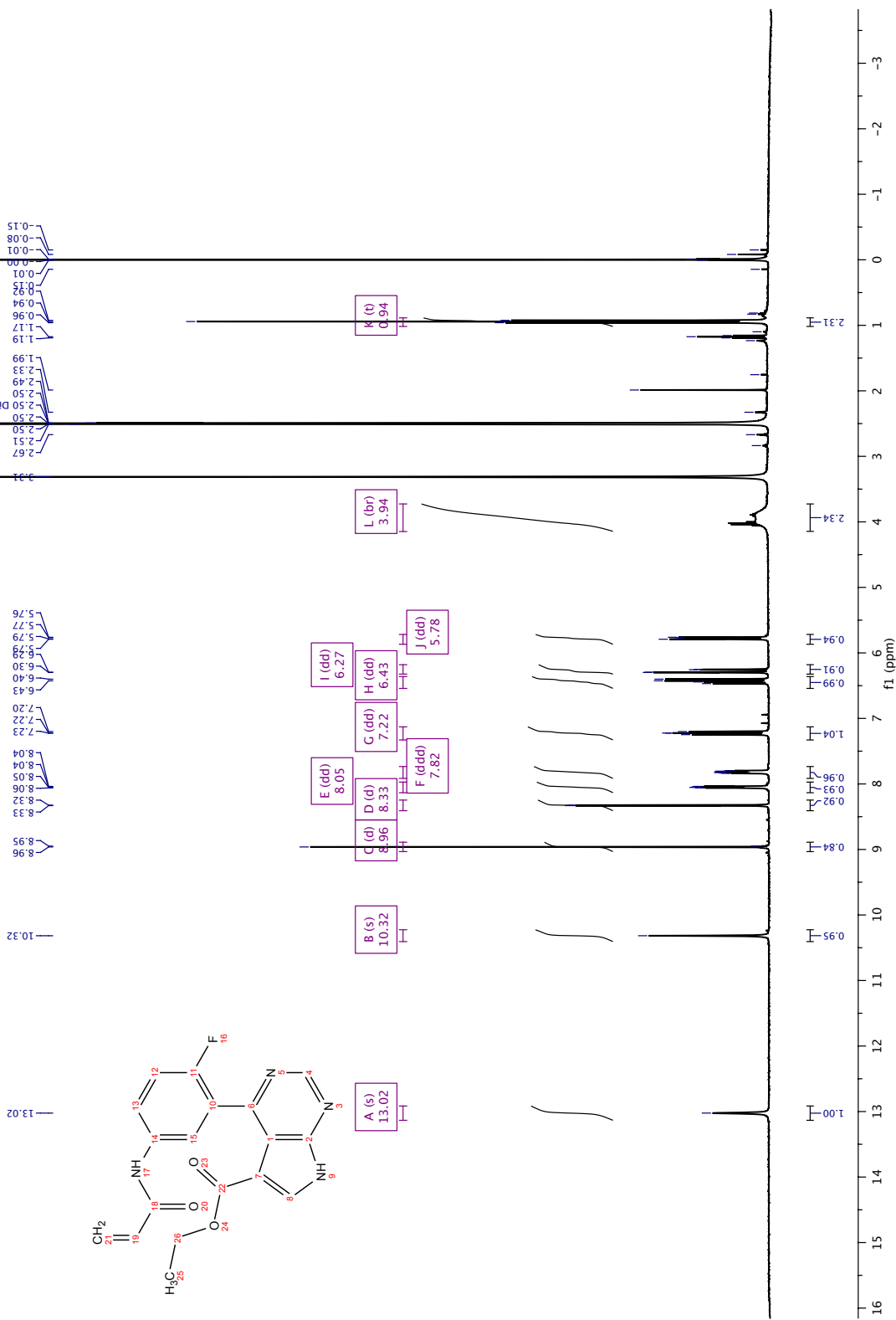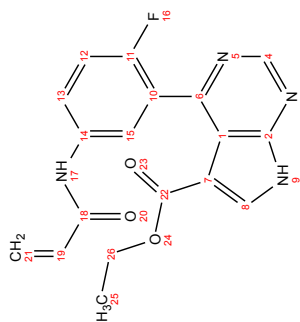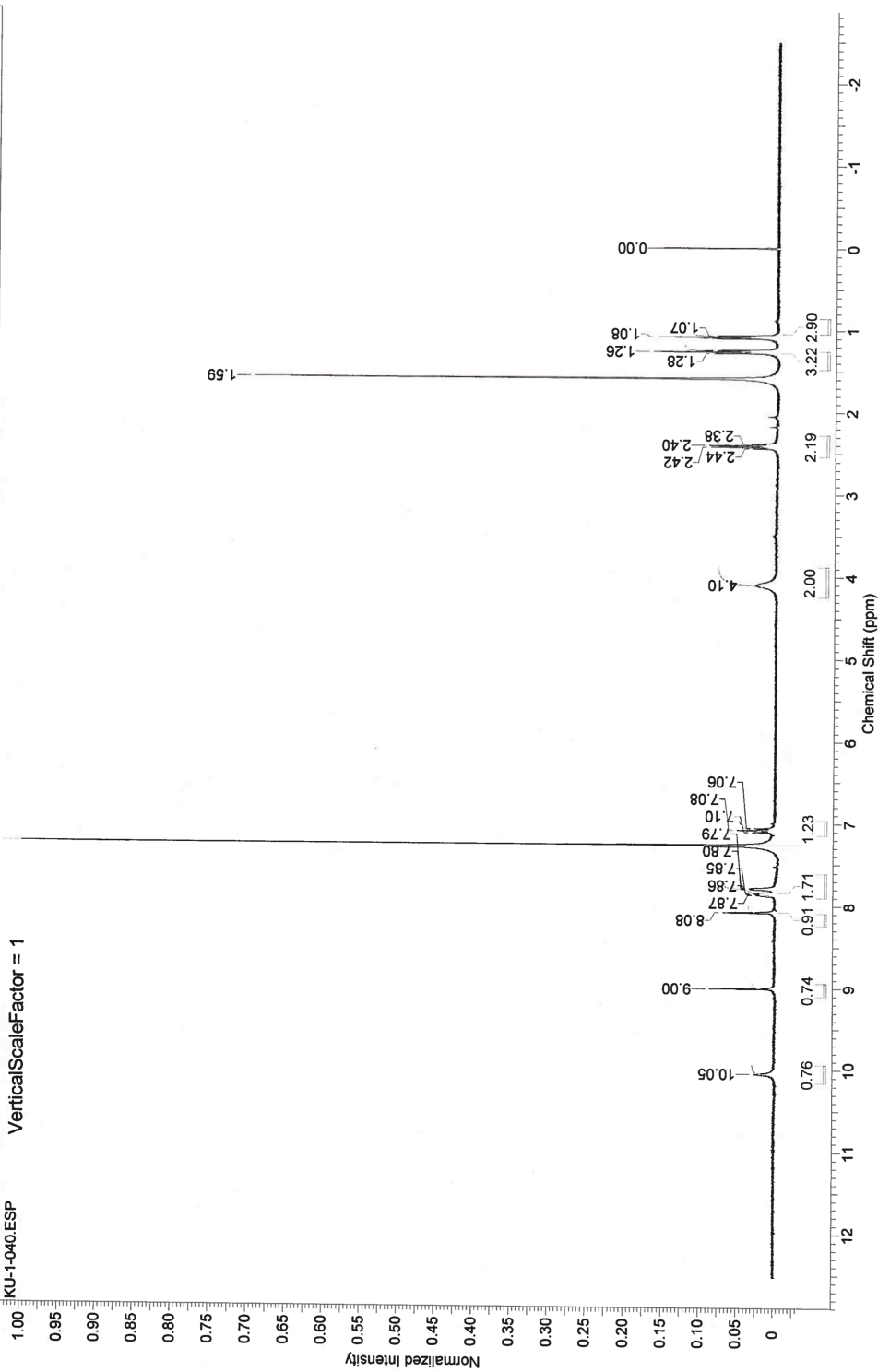
Compound 31

KU-2-085
STANDARD 1H OBSERVE

¹H NMR (400 MHz, DMSO) δ 10.05 (s, 1H), 8.91 (s, 1H), 8.39 (d, *J* = 6.9 Hz, 1H), 8.31 (d, *J* = 2.5 Hz, 1H), 7.39 (dd, *J* = 17.4, 6.4 Hz, 2H), 6.65 (dd, *J* = 16.9, 10.0 Hz, 1H), 6.27 (d, *J* = 17.1 Hz, 1H), 5.78 (d, *J* = 10.2 Hz, 1H), 3.91 (q, *J* = 7.1 Hz, 2H), 0.91 (t, *J* = 7.1 Hz, 3H).

175

Compound 32

Acquisition Time (sec)	3.7440	Comment	STANDARD 1H OBSERVE	Date	Dec 23 2013
Date Stamp	Dec 23 2013	File Name	D:¥USERS¥B067043¥DESKTOP¥NMR¥KU-1-040.FID¥FID	Frequency (MHz)	399.56
Nucleus	1H	Number of Transients	16	Original Points Count	22466	Points Count	65536
Pulse Sequence	s2pul	Receiver Gain	32.00	Solvent	CHLOROFORM-d
Spectrum Offset (Hz)	2004.5493	Spectrum Type	STANDARD	Sweep Width (Hz)	6000.60	Temperature (degree C)	AMBIENT TEMPERATURE

KU-1-040.ESP

VerticalScaleFactor = 1

2014/01/05 16:46:41

176

Compound 33

Acquisition Time (sec)	3.7440	Comment	STANDARD 1H OBSERVE		Date	Dec 11 2013	Date Stamp	Dec 11 2013
File Name	D:\USERS\WB067043\DESKTOP\NMR\KU-1-032.FID\FID				Frequency (MHz)	399.56	Nucleus	1H
Number of Transients	16	Original Points Count	22466	Points Count	65536	Pulse Sequence	s2pul	Receiver Gain	36.00
Solvent	DMSO-d6	Spectrum Offset (Hz)	2009.5422	Spectrum Type	STANDARD	Sweep Width (Hz)	6000.60	Temperature (degree C)	25.000
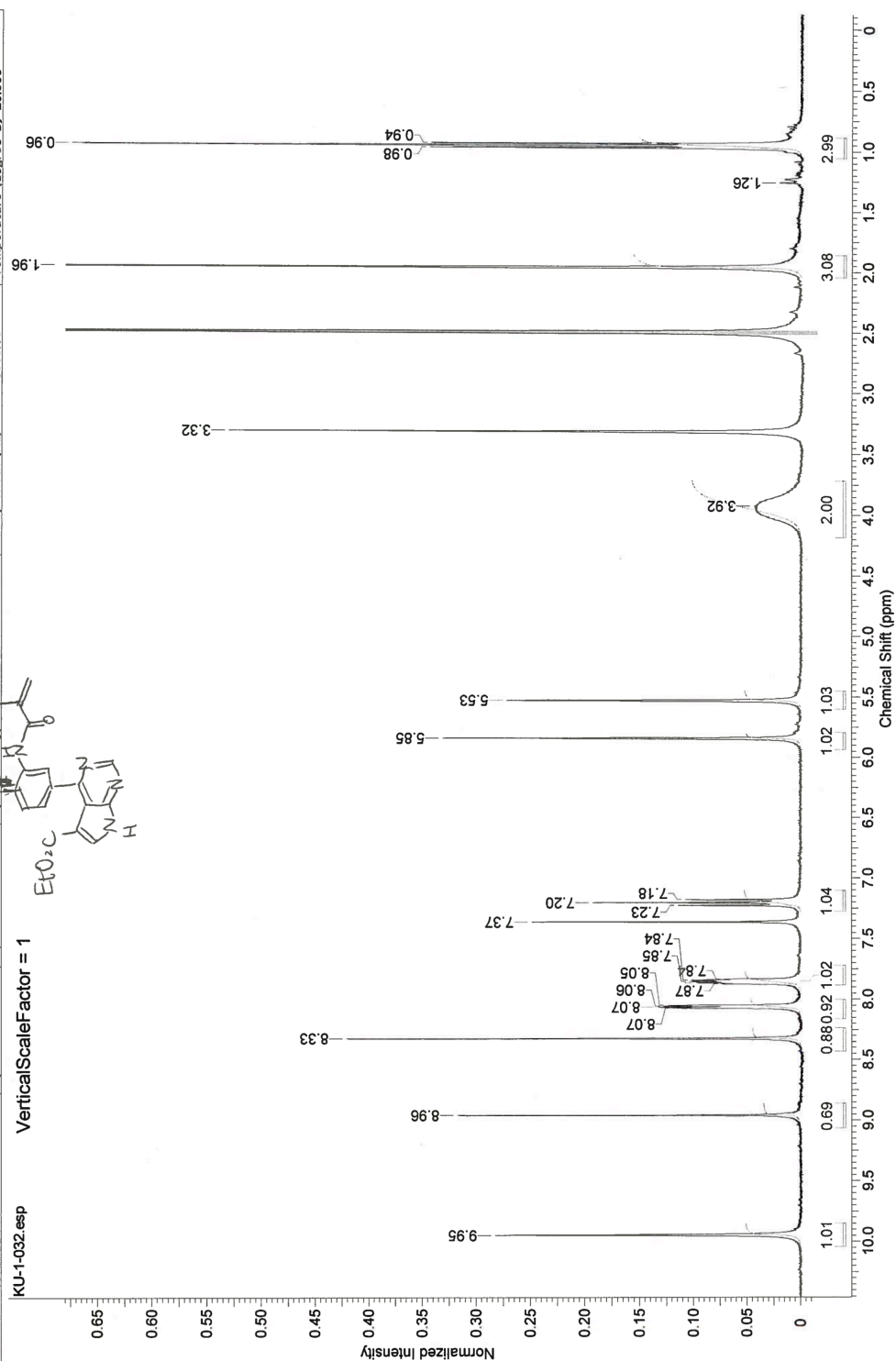
KU-1-032.esp

VerticalScaleFactor = 1

2013/12/11 8:50:52

Compound 34

^{1}H NMR (400 MHz, DMSO-d_6) δ ppm 0.88 - 0.93 (m, 12 H) 1.92 - 1.96 (m, 12 H) 3.87 - 3.96 (m, 9 H) 5.52 - 5.55 (m, 4 H) 5.86 - 5.88 (m, 4 H) 8.29 - 8.31 (m, 4 H) 9.66 (s, 4 H)

2014/07/31 1:44:42

Acquisition Time (sec)	3.7440	Comment	STANDARD 1H OBSERVE	Date	Jul 31 2014
Date Stamp	Jul 31 2014	File Name	D:¥USERS¥B067043¥DESKTOP¥NMR¥KU-2-089.FID¥FID	Frequency (MHz)	399.55
Nucleus	1H	Number of Transients	16	Original Points Count	22466	Points Count	131072
Pulse Sequence	s2pul	Receiver Gain	32.00	Solvent	DMSO-d6	Spectrum Offset (Hz)	1998.0544
Spectrum Type	STANDARD	Sweep Width (Hz)	6000.60	Temperature (degree C)	AMBIENT TEMPERATURE

KU-2-089.esp   VerticalScaleFactor = 1
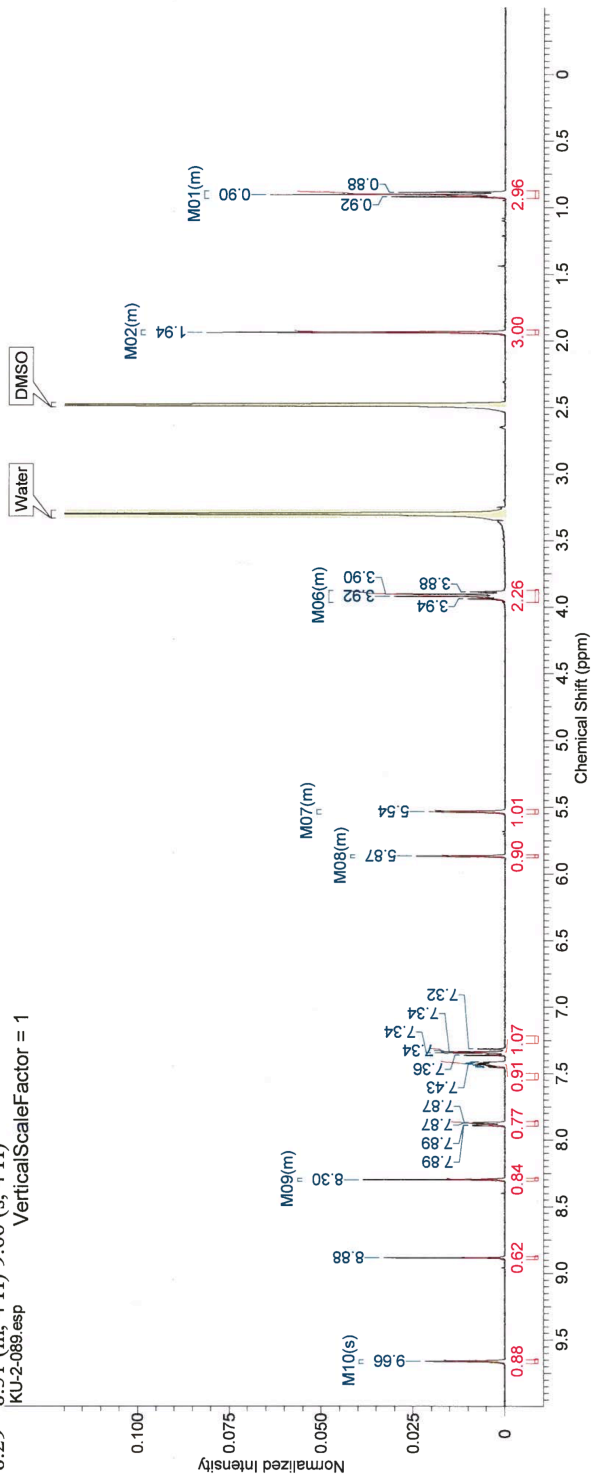
No.	(ppm)	Annotation	Layer No.	Created By	Created At	Modified By	Modified At
1	[2.46 .. 2.50]	DMSO	1	B067043	-∅ 2014/07/31 1:43:39		
2	[3.27 .. 3.33]	Water	1	B067043	-∅ 2014/07/31 1:43:39		

178

Compound 35

2014/08/09 19:38:16

Acquisition Time (sec)	3.7440	Comment	STANDARD 1H OBSERVE		Date	Aug 9 2014
Date Stamp	Aug 9 2014	File Name	D:¥USERS¥B067043¥DESKTOP¥NMR¥NMR¥KU-2-099.FID¥FID		Frequency (MHz)	399.55
Nucleus	1H	Number of Transients	16	Original Points Count	22466	Points Count	32768
Pulse Sequence	s2pul	Receiver Gain	32.00	Solvent	DMSO-d6	Spectrum Offset (Hz)	1998.0544
Spectrum Type	STANDARD	Sweep Width (Hz)	6000.60	Temperature (degree C)	AMBIENT TEMPERATURE		

KU-2-099.esp

VerticalScaleFactor = 1
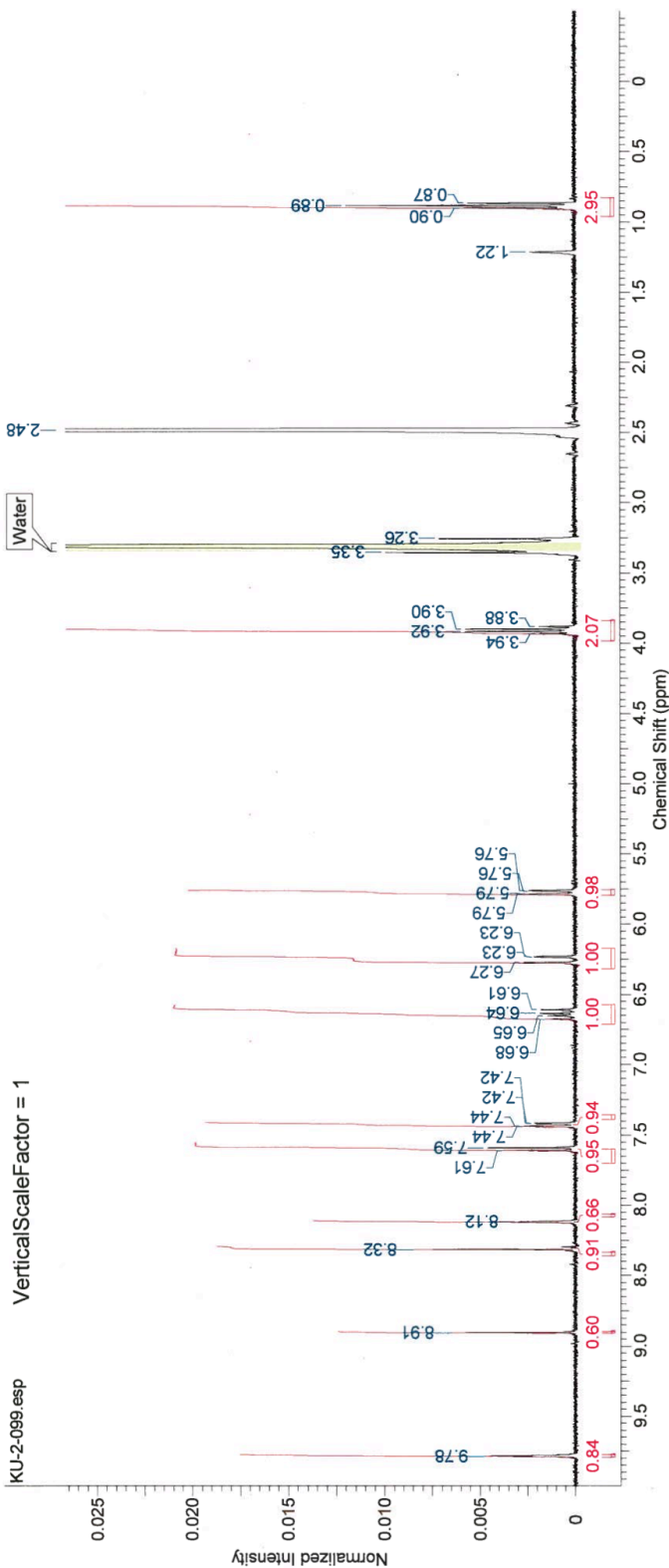
No.	(ppm)	Annotation	Layer No.	Created By	Created At	Modified By	Modified At
1	[3.29 .. 3.35]	Water	1	B067043	*y 2014/08/09 19:36:36		

179

Compound 36

Acquisition Time (sec)	3.7440	Comment	STANDARD 1H OBSERVE	Date	Aug 9 2014
Date Stamp	Aug 9 2014	File Name	D:¥USERS¥B067043¥DESKTOP¥NMR¥KU-2-100.FID¥FID	Frequency (MHz)	399.55
Nucleus	1H	Number of Transients	16	Points Count	131072
Pulse Sequence	s2pul	Receiver Gain	32.00	Solvent	DMSO-d6	Spectrum Offset (Hz)	2005.0424
Spectrum Type	STANDARD	Sweep Width (Hz)	6000.60	Temperature (degree C)	AMBIENT TEMPERATURE

^{1}H NMR (400 MHz, DMSO-d_6) δ ppm 0.90 - 0.98 (m, 3 H) 1.96 - 2.03 (m, 3 H) 2.48 - 2.54 (m, 5 H) 3.27 - 3.35 (m, 24 H) 3.38 (s, 1 H) 3.91 - 3.99 (m, 2 H) 5.54 - 5.58 (m, 1 H) 5.91 - 5.94 (m, 1 H) 7.44 - 7.48 (m, 1 H) 7.59 - 7.64 (m, 1 H) 7.89 - 7.92 (m, 1 H) 8.31 - 8.35 (m, 1 H) 8.91 - 8.94 (m, 1 H) 9.51 - 9.55 (m, 1 H)

Compound 37

KU-3-036
STANDARD 1H OBSERVE

^{1}H NMR (400 MHz, DMSO) δ 10.20 (s, 1H), 9.01 (s, 1H), 8.94 (d, J = 7.5 Hz, 1H), 8.06 − 7.98 (m, 1H), 7.50 (dd, J = 10.8, 8.6 Hz, 2H), 6.68 (dd, J = 17.1, 10.1 Hz, 1H), 6.34 (dd, J = 17.0, 1.8 Hz, 1H), 5.83 (dd, J = 10.2, 1.7 Hz, 1H).
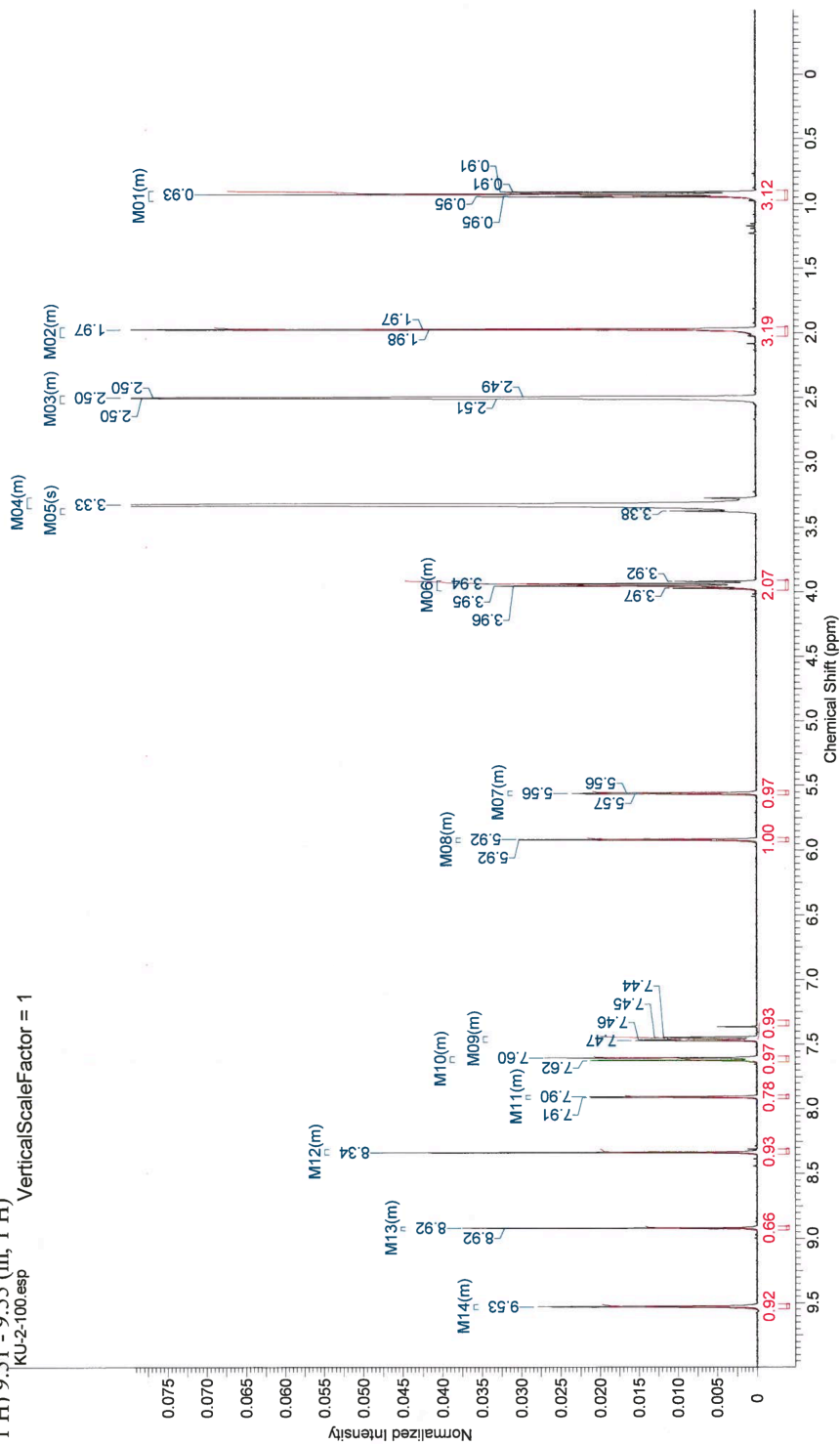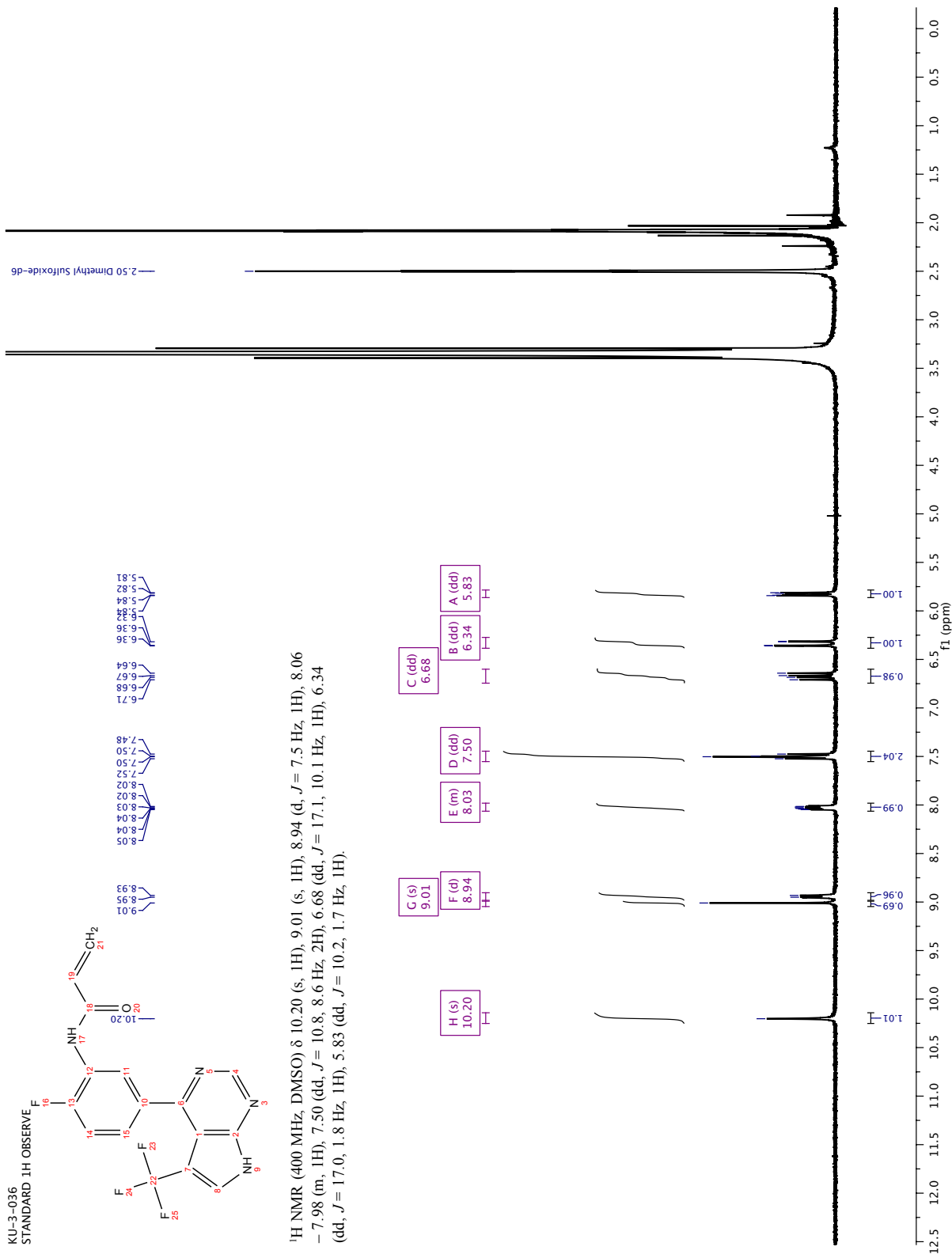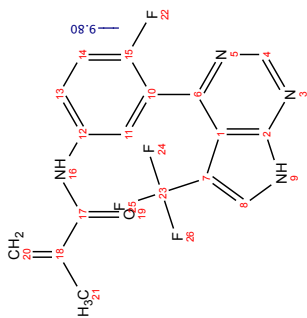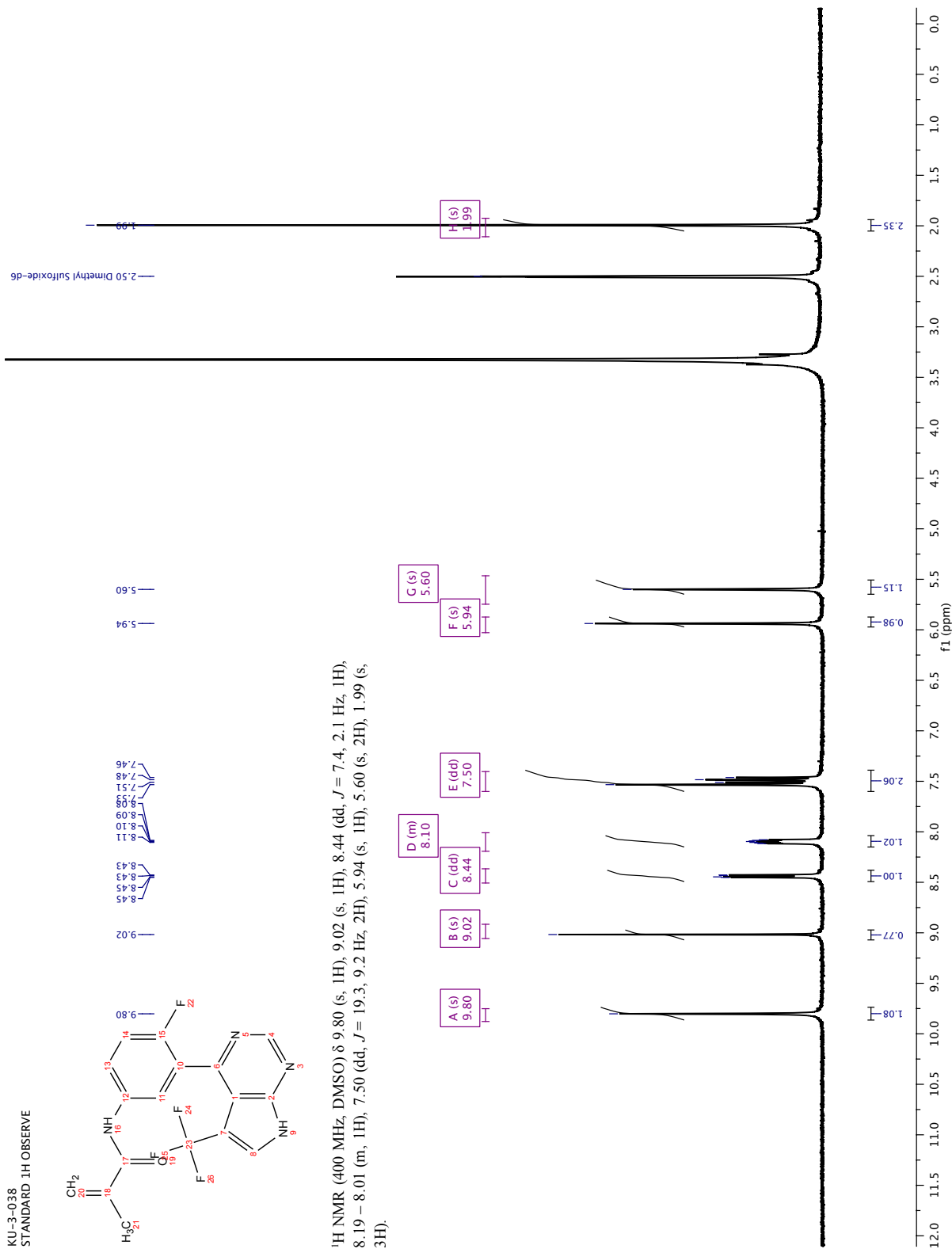
Compound 38

KU-3-038
STANDARD 1H OBSERVE

^{1}H NMR (400 MHz, DMSO) δ 9.80 (s, 1H), 9.02 (s, 1H), 8.44 (dd, J = 7.4, 2.1 Hz, 1H), 8.19 – 8.01 (m, 1H), 7.50 (dd, J = 19.3, 9.2 Hz, 2H), 5.94 (s, 1H), 5.60 (s, 2H), 1.99 (s, 3H).
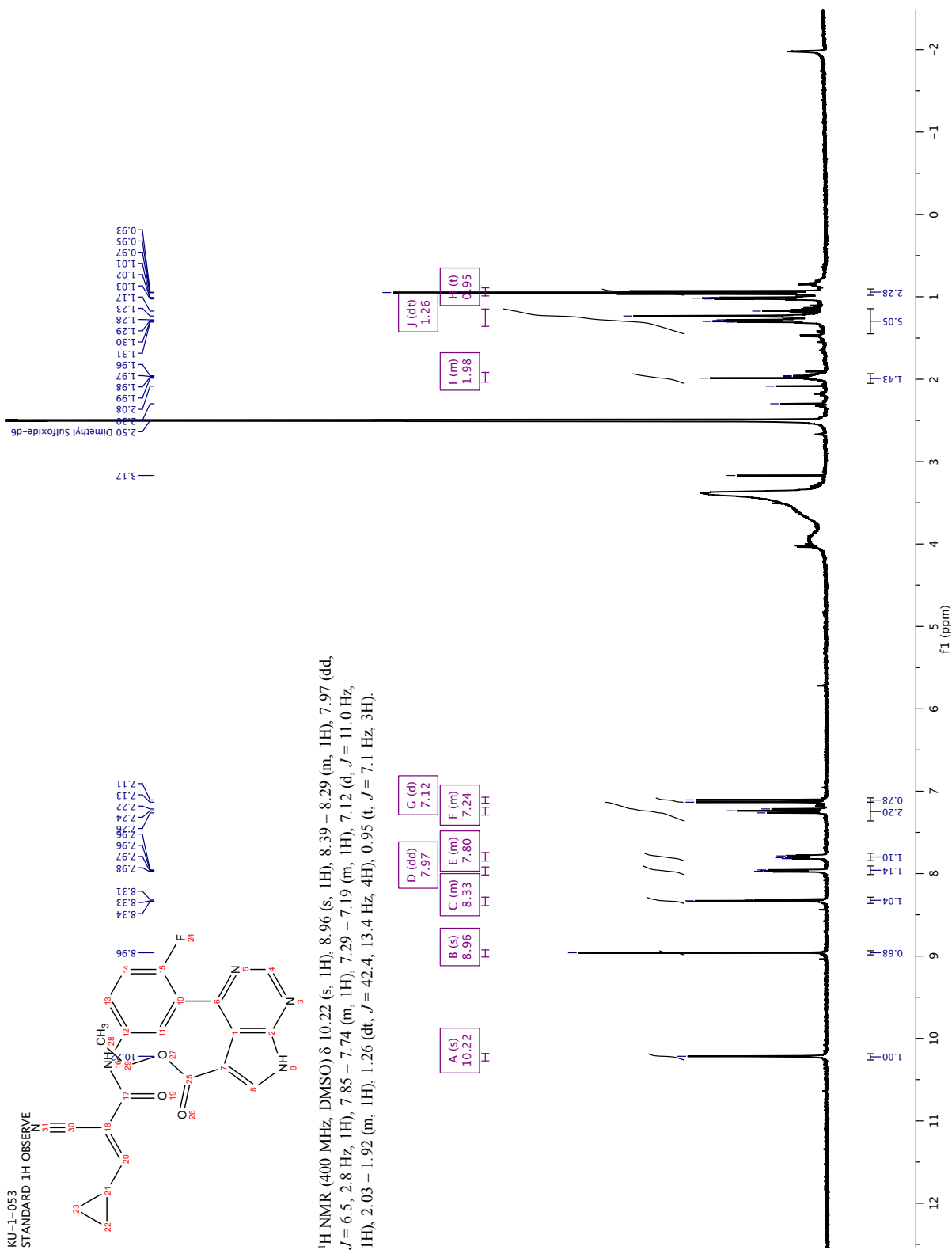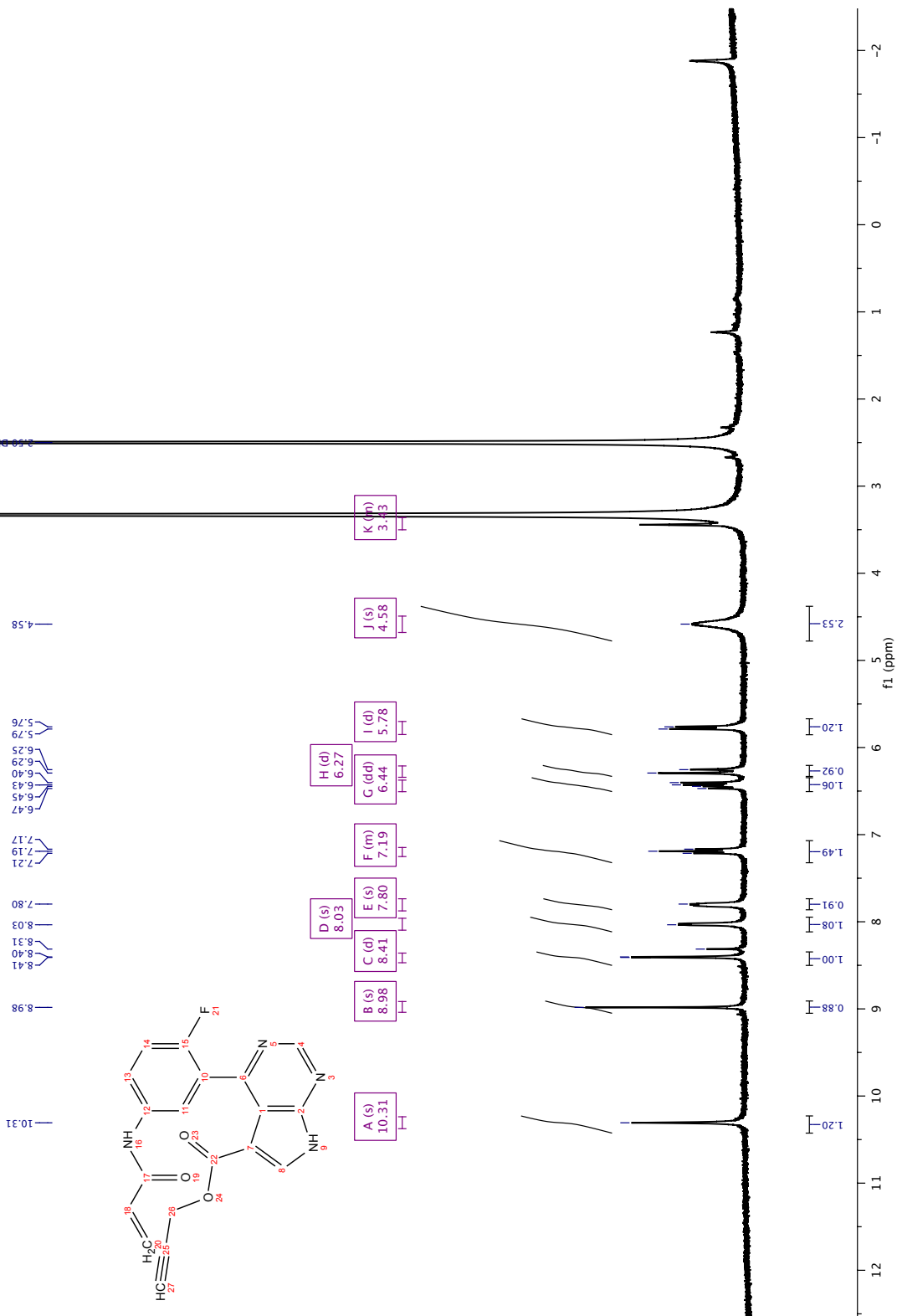
Compound 39

KU–1–053
STANDARD 1H OBSERVE
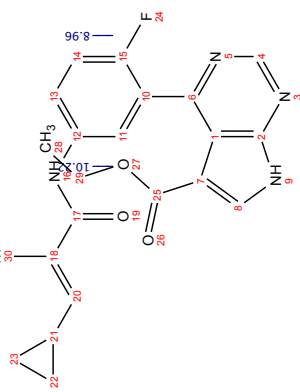
^{1}H NMR (400 MHz, DMSO) δ 10.22 (s, 1H), 8.96 (s, 1H), 8.39 – 8.29 (m, 1H), 7.97 (dd, J = 6.5, 2.8 Hz, 1H), 7.85 – 7.74 (m, 1H), 7.29 – 7.19 (m, 1H), 7.12 (d, J = 11.0 Hz, 1H), 2.03 – 1.92 (m, 1H), 1.26 (dt, J = 42.4, 13.4 Hz, 4H), 0.95 (t, J = 7.1 Hz, 3H).

Compound 40

KU-1-097
STANDARD 1H OBSERVE

¹H NMR (400 MHz, DMSO) δ 10.31 (s, 1H), 8.98 (s, 1H), 8.41 (d, J = 2.4 Hz, 1H), 8.03 (s, 1H), 7.80 (s, 1H), 7.25 – 7.15 (m, 1H), 6.44 (dd, J = 16.9, 10.2 Hz, 1H), 6.27 (d, J = 15.6 Hz, 1H), 5.78 (d, J = 10.0 Hz, 1H), 4.58 (s, 1H), 3.50 – 3.36 (m, 2H).

Publishing Agreement

It is the policy of the University to encourage the distribution of all theses, dissertations, and manuscripts. Copies of all UCSF theses, dissertations, and manuscripts will be routed to the library via the Graduate Division. The library will make all theses, dissertations, and manuscripts accessible to the public and will preserve these to the best of their abilities, in perpetuity.

I hereby grant permission to the Graduate Division of the University of California, San Francisco to release copies of my thesis, dissertation, or manuscript to the Campus Library to provide access and preservation, in whole or in part, in perpetuity.

Author Signature _____ Date 3/24/17